AN INFRARED STUDY OF DISTANT GALAXY CLUSTERS

by

Adam Virgil Muzzin

A thesis submitted in conformity with the requirements
for the degree of Doctor of Philosophy
Graduate Department of Astronomy and Astrophysics
University of Toronto

Abstract

An Infrared Study of Distant Galaxy Clusters

Adam Virgil Muzzin

Doctor of Philosophy

Graduate Department of Astronomy and Astrophysics

University of Toronto

2008

We present a study of the infrared properties distant galaxy clusters and their constituent galaxies covering the wavelength range $2.2\mu m$ - $24\mu m$. In the first part of the thesis we use ground-based K-band ($2.2\mu m$) data to study the scaling relations and luminosity functions (LFs) of 15 moderate redshift ($0.2 < z < 0.5$), X-ray luminous galaxy clusters. We find that the IR-selected density profiles, IR LFs, and the IR richness/light vs. mass scaling relations for these clusters are nearly identical to their local ($z < 0.1$) counterparts. The only notable change in the cluster NIR properties with redshift is the shallowing of the faint-end slope of the early-type LF with increasing redshift, which is attributed to "downsizing" in the cluster population.

In the second part of the thesis we combine the R-band and [$3.6\mu m$] photometry from the 3.8 deg^2 *Spitzer* First Look Survey and use the cluster red-sequence method to discover a set of 99 clusters at $0.1 < z < 1.3$. Using this cluster sample we make the first measurement of the suite of IRAC cluster LFs ([$3.6\mu m$], [$4.5\mu m$], [$5.8\mu m$], [$8.0\mu m$]) from $0.1 < z < 1.0$. Similar to the K-band study we find that for the bands that trace stellar mass at these redshifts ([$3.6\mu m$], [$4.5\mu m$]) the evolution in M* is consistent with a passively evolving population of galaxies with a high formation redshift ($z_f > 1.5$). The MIR ([$5.8\mu m$] & [$8.0\mu m$]) cluster LFs show that at $z < 0.4$ the bright-end of the cluster LF is well-described by a composite population of quiescent galaxies and regular star forming galaxies with a mix consistent with typical cluster blue fractions; however, at $z > 0.4$, an additional population of dusty starburst galaxies is required

to properly model these LFs.

In the final part of the thesis we present the results of a spectroscopic survey of cluster galaxies detected at $24\mu m$. We use the optical spectroscopy to classify the galaxies and find that the majority of cluster MIR galaxies are star forming galaxies ($\sim$ 80%), although their specific classes make them a very heterogeneous subset of galaxies. By comparing the equivalent widths of nebular emission lines we show that there is a non-negligible population of dusty star forming galaxies in clusters which have optical - IR colors redder than the cluster red-sequence.

Contents

List of Tables

List of Figures

Chapter 1

Introduction

1.1 Things in Perspective

In his controversial book "The Structure of Scientific Revolutions" published in 1962, Thomas Kuhn argued that the process of scientific discovery happens as continuous cycle of destructive "revolutions". Each revolution shakes the foundation of the current scientific common sense, or "paradigm"; obsoleting it and replacing it with a new, better one. In Kuhn's theory, revolutions always occur after paradigms have been faced with a period of "crisis" during which they cannot explain the current experimental data or the disconnects in accepted theoretical predictions. During the crisis period, paradigms are not discarded, but are modified in *ad hoc* ways in an attempt to reconcile the inconsistencies. In time the tension builds, until finally it is released following a scientific revolution or "paradigm shift". Once the old paradigm has been discarded, scientists proceed with a period of research that Kuhn defined as "normal science". This phase involves filling in the minutiae of the new paradigm, and performing detailed experiments which look for holes, inconsistencies, or "chinks in the armour" of the new paradigm. The period of normal science continues until new crises begin to accumulate. Thereafter, the process repeats itself.

About the period of normal science Kuhn wrote: "The study of paradigms ... is what mainly prepares the student for membership in the particular scientific community with which he will later practice. Because he there joins men who learned the basics of their field from the same concrete models, his subsequent practice will seldom evoke overt disagreement over fundamentals. Men whose research is based on shared paradigms are committed to the same rules and standards for scientific practice. That commitment and the apparent consensus it produces are the requirement

for *normal science*, i.e., for the genesis and continuation of a particular research tradition." (Kuhn 1962, pg. 11).

Remarkably, the study of galaxy evolution appears to have been in a period of normal science for more than 80 years. The most recent major paradigm shift came in December of 1925 with the publication of the paper "NGC 6822. A Remote Stellar System" by Edwin Hubble (Hubble 1925). The discovery of 11 Cepheid variables in NGC 6822 allowed Hubble to compute the distance to this "nebula" as 214 000 pc. In Hubble's own words "Familiar relations such as those connecting the periods and luminosities of Cepheids ... are consistent when applied to NGC 6822, *the first object definitely assigned to a region outside the galactic system*" (my italics). Hubble had already determined the distance to M31 as early as 1923; however, that work remained unpublished until 1929. The 1925 paper on NGC 6822 would inevitably settle the "great debate" about the nature of the spiral nebulae that had gained notoriety 5 years earlier in 1920 with the much popularized debate between Harlow Shapley and Herber Curtis. Hubble would prove that Curtis' arguments were correct and that the spiral nebulae were in fact "island universes" much like our own Milky Way.

Hubble's 1925 paper caused a major paradigm shift in the way we think about the universe and launched what was to become the modern-day study of galaxy evolution. In the 80 years since that paper we have continued in a period of normal science, "filling in the blanks" of Hubble's revolution and trying to understand the specifics of galaxies: How do they form? How old are they? What are they made of? How many are there? What "flavors" do they come in, and why? Of course, during this process there have been smaller paradigm shifts. Important unexpected discoveries such as dark matter and quasars have certainly changed the way we think about galaxies. Still, those discoveries can not compare to the revolution in perspective that occurred 80 years ago.

It is unlikely that there will be a major paradigm shift in our understanding of galaxy evolution in the near future. After all, according to Kuhn, paradigm shifts only occur after intense periods of "crisis", which we do not appear to be in at the moment. Indeed, at present there are few seriously contentious issues in the study of galaxy evolution. Observers in the field have much of their effort focused on basic surveys of galaxies in the local universe such as 2MASS (Skrutskie et al. 2006), 2dFRS (Colless et al. 2001), and the SDSS (Adelman-McCarthy et al. 2007), as well as surveys of the high-redshift universe such as DEEP2 (Davis et al. 2003), GOODS (Giavalisco et al. 2004), COSMOS (Koekemoer & Scoville 2005), AEGIS (Davis et al. 2007), SWIRE (Lonsdale

et al. 2003), and GDDS (Abraham et al. 2004). At the moment we are mostly invested in spotting trends and correlations in the galaxy population such as the morphology-density relation (e.g., Dressler 1980; Dressler et al. 1997), color-density relation (e.g., Hogg et al. 2003, 2004, Blanton et al. 2005, Cooper et al. 2007), space density evolution of galaxies (e.g., Hogg et al. 2002; Faber et al. 2005; Marchesini & van Dokkum 2007), star formation rate evolution (e.g., Madau et al. 1996; Lilly et al. 1996; Steidel et al. 1999; Juneau et al. 2005; Schminovich et al. 2005; Pérez-González et al. 2005), and the spatial distribution of galaxies (e.g., Zehavi et al.2005a, 2005b; Eisenstein et al. 2005), more than truely understanding the physics behind these correlations. Of course, the absence of understanding is not for lack of trying, but is almost certainly because the physics behind galaxy formation and evolution are highly complex and, despite the monumental observational efforts mentioned above, there is still not enough quality data to make heroic efforts towards physically motivated models of galaxy evolution worthwhile. As a result, there are currently no "working theories" of galaxy formation or evolution.

Semi-analytic models of galaxy evolution have dramatically increased in quality in the last decade. Still, these simulations use "prescriptions" for the important physics such as star formation and feedback. The interplay between the prescriptions can be so complicated that the primary objective of most simulations is simply to be able to reproduce the current observational data. If that can be done, the hope is that details of the prescriptions that were used will give insight into the processes involved in galaxy formation. Although unsophisticated from a pure physics point of view, semi-analytics have been extremely valuable in our effort to build a working theory of galaxy formation. For example, it was semi-analytics that first raised awareness of the "over-merging" problem. An abundance of blue, star forming galaxies in massive halos seen in simulations that is not seen the real universe was the first real "proof" that quenching and feedback are essential ingredients in galaxy formation. This discovery has in turn motivated a flurry of observational attention to these issues.

This bottom line is, despite monumental effort in the field, especially recently, we are more than 80 years in from the last major paradigm shift, and *we are still in a basic data gathering and modeling stage in the study of galaxy evolution*. This means it is unlikely we will see a significant paradigm shift in the near future and we are most probably in for many more years of normal science. That may sound a bit disheartening for young, enthusiastic scientists who are looking for the next big shift (and looking to be the ones who make it happen), but it shouldn't be. For Kuhn, normal science was as

important of a part of scientific discovery of as was the revolution or the paradigm shift. In many ways, the period of normal science may be the most enjoyable collaborative scientific environment to work in. During periods of normal science scientific careers need not be influenced by which "camp" a scientist belongs to. Right now we can all agree to disagree until we get more data!

The goal of this thesis is to add in just a very very small part to the collaborative effort of astronomers to understand the formation and evolution of structure in the universe. This thesis, like the vast multitude before it, are clearly part of the realm of normal science. Still, it is a part of a process. The focus of this thesis is to study some of the basic infrared (IR; the part of the electromagnetic spectrum from $\sim 1\mu m$ - $1000\mu m$) properties of galaxy clusters and their constituent galaxies in order to better understand how these large structures are formed, and how the evolve with cosmic time.

Of course, galaxy clusters and their constituent galaxies have been studied for almost 100 years, so what remains to be done? One of the ways that new scientific advances are made is to open up new windows on old problems. Although the very first IR detectors were introduced almost 30 years ago, the field is only reaching its renaissance now. Current near-IR (NIR) detectors are orders of magnitude larger and more sensitive than the early ones and allow us to perform imaging with nearly the same ease as CCD detectors. Furthermore, with the launch of satellites such as *ISO*, *AKARI*, and especially *Spitzer*, mid-IR (MIR) observations have increased orders of magnitude in sensitivity and angular resolution over the *IRAS* satellite.

The thesis comprises several different studies of IR observations of distant (which for this thesis we will define as $z > 0.1$, i.e., anything other than the local universe) galaxy clusters. IR observations provide information that is not easily obtained using optical photometry (In § 1.1.1 below we describe the role of different IR observations) and thus far IR studies of clusters are still in their infancy.

In the first two chapters of the thesis we study the IR scaling relations and luminosity functions of clusters at moderate ($0.2 < z < 0.5$) redshift. These scaling relations allow us to understand how the baryonic matter in the form of stars is distributed in these structures relative to the underlying dark matter distribution. Given that there are now comprehensive studies of the IR properties and scaling relations of local ($z \sim 0$) clusters (e.g., Lin et al. 2004; Rines et al. 2004), we can use those as a baseline to look for evolution in the scaling relations, which should gives clues about the growth of these structures.

In the fourth chapter we make use of new observations from the *Spitzer* telescope and make the first attempt to identify clusters with the red-sequence method (Gladders & Yee 2000) using IR data. Using the clusters discovered with this method we make the first large study of the evolution of the MIR cluster luminosity functions. This allows us to make a preliminary examination of the evolution of dusty star formation in cluster galaxies.

In the fifth chapter we present a spectroscopic study of some of the MIR galaxies detected in the clusters discovered in chapter three. Using the spectroscopy we classify these galaxies as well as measure some of the emission line properties. The purpose of this is to get a first-look understanding of what type of galaxies the cluster MIR population is composed of.

The chapters in this thesis are a series of four papers that have been written throughout the course of my graduate studies. Each chapter is self-contained and has its own introduction and conclusion. Given this, there is no need for a comprehensive introduction to clusters and cluster galaxy evolution in this chapter. Instead, the remainder of this introductory chapter is devoted to a short introduction on IR observations and the type of information they supply, as well as a quick synopsis of the work on clusters that has been done in the IR thus far.

1.1.1 The Role of IR observations

Observations in the IR are often classified into three general wavelength regimes, the near-, mid- and far- infrared (NIR, MIR, FIR). There is no official definition for the precise division of these wavelength ranges; however, they are only used as colloquial indicators of the wavelength range of interest. In general, the NIR is defined as the wavelength range of about $1\mu m$ - $5\mu m$, the MIR is considered to be the range $5\mu m$ - $60\mu m$, and the far IR around $60\mu m$ - $1000\mu m$. Subdividing the regions of the IR electromagnetic spectrum may seem pedantic; however it is usually done because the emission sources in the different regimes are not the same. Emission in the NIR tends to be dominated by relatively hot objects (T > 1000K) such as photospheres of lower mass stars. The Raleigh-Jeans tail of stellar emission becomes at the MIR range, and MIR emission typically emanates from warm dust (T > 100K) continuum (often heated to these temperatures by an AGN, or very active star formation) or the Polycyclic Aromatic Hydrocarbon features (PAHs, e.g., Gillett et al. 1973; Willner et al. 1977), which in the past were frequently referred to as the Unidentified Infrared Bands (UIBs). FIR

emission generally comes from the cool dust (T < 100K) in star forming regions.

Given the various emission sources in the NIR, MIR, and FIR, observations at these wavelengths are used to study very different physics. NIR observations have become the essential data for the measurement of galaxy stellar masses (e.g., Brinchmann & Ellis 2000; Bell et al. 2003; Bundy et al. 2006). NIR data are superb for this purpose for the following reasons. Firstly, it is the wavelength range where the spectral energy distributions (SEDs) of lower mass stars peak. Low mass stars dominate the overall stellar mass of galaxies and have long lifetimes. Their abundance is a metric of the integrated history of star formation within the galaxy. By contrast, massive stars emit the majority of their light in the bluer optical bandpasses. They have much shorter lifetimes and are therefore a better tracer of recent star formation. The second advantage of NIR for measuring stellar masses is that attenuation by dust is very weak in the NIR as compared to optical bandpasses, which means that there is no need for sophisticated models of galactic dust extinction when measuring stellar masses.

MIR observations primarily detect warm dust continuum and PAH emission, both of which tend to be found in dusty star forming regions (although warm dust is also found in AGN). Many studies have shown that the MIR emission from star forming regions/galaxies is directly proportional to the SFR (e.g., Elbaz et al. 2002; Wu et al. 2005; Calzetti et al. 2005). Furthermore, MIR emission is almost certainly the best diagnostic of ongoing star formation in dusty galaxies, where nebular emission lines can be completely extincted. Recent advances in space-based MIR imaging (e.g., *ISO* and *Spitzer*) are ushering in a new era for MIR astronomy and the study of dusty star formation, particularly at high redshift.

FIR observations are also probes of star formation and AGN activity. FIR observations have been primarily used for the study high-redshift galaxies ($z > 2$; e.g., Blain et al. 2002) because of the famous "negative k-correction" for dusty galaxies. The k-correction is so negative at high redshift in the FIR that almost all cosmological dimming is offset by the increase in flux due to band shifting. Therefore, FIR-luminous galaxies change minimally in apparent brightness between $2 < z < 4$.

1.1.2   NIR Observations of Galaxy Clusters

Although good-quality, array-style NIR cameras have been available for ~ 15 years, the literature on NIR studies of distant clusters is far from overwhelming. In part the lack of comprehensive data has been because until recently, there were few distant

clusters known. One of the first studies of cluster galaxies at $z > 0$ in the NIR was done by Lilly (1987) who used a single element detector to study 53 galaxies in 5 clusters at $z \sim 0.45$. Surprisingly, he found that the majority of the galaxies in his sample were 0.1 mag *redder* in rest-frame V-H colors than the early-type galaxies in Coma. These results are difficult to reconcile with later work, and may have been spurious due to the very early stages of the NIR detector technology.

By the early 90s, NIR arrays became available and these made the study of clusters (and all galaxies for that matter) much easier. Early work in the field concentrated on studying the optical-NIR color-magnitude relations (CMRs) in order to measure the aging of the stellar populations in cluster galaxies with redshift (e.g., Aragón-Salamanca et al. 1991; Bower et al. 1992; Aragón-Salamanca et al. 1993; Stanford et al. 1995; Ellis et al. 1997; Kodama et al. 1998; Stanford et al. 1998). These early studies obtained remarkably consistent results. They found that the rest-frame color of the CMR became consistently bluer with increasing redshift. This color evolution followed the predictions of a passively evolving population of galaxies formed at high-redshift and demonstrated that the majority of the stars in cluster early-type galaxies are formed at high redshift and have passively evolved since then. These studies also showed that the CMR remained remarkably tight out to $z \sim 1$, which was further evidence that the stellar populations in cluster early-types were extremely old.

Early attempts were also made to study the NIR LFs of clusters; however, these did not fare as well. Aragón-Salamanca et al. (1993) published K-band LFs for 10 clusters $0.5 < z < 0.9$ and detected no luminosity evolution in the bright cluster galaxies. Unfortunately the K-band data for these clusters was very shallow, not even reaching M*, which made interpretation of the data difficult. Barger et al. (1998) also published LFs for 13 clusters at $0.17 < z < 0.56$ and found no luminosity evolution in the sample. Although it is not entirely clear how that result arose, part of the lack of evolution is certainly explained by the fact that Barger et al. (1998) used an $\Omega_m = 1$ cosmology to determine their absolute magnitudes.

The first robust study of the evolution of the NIR cluster luminosity function did not come until De Propris et al. (1999). They used the Stanford et al. (1998) and Stanford et al. (2002) NIR data to show that the luminosity evolution in the cluster population was consistent with the passive evolution of an old stellar population, thus reconciling the previously inconsistent luminosity evolution and color evolution. The result also showed that the majority of the stellar mass in cluster galaxies must have been assembled into massive galaxies at high redshift.

Since those pioneering NIR studies of cluster galaxy evolution, NIR cluster work has returned to nearby ($z < 0.1$) clusters. The re-emergence of lower redshift studies has primarily been driven by the release of the Two Micron All Sky Survey (2MASS, Skrutskie et al. 2006). The high-quality, homogeneous 2MASS data now permit detailed studies of large samples of clusters. The focus of these studies has been to understand the scaling relations between NIR light (which traces the abundance and location of baryons in the form of stars) and dark matter. These studies have shown that there is a strong correlation between the total integrated K-band light ($L_{200,K}$) of clusters and their dark matter mass (Lin et al. 2003; Kochanek et al. 2003; Lin et al. 2004; Ramella et al. 2004; Rines et al. 2004) although the scatter in these correlations is significant ($\sim 30\text{-}50\%$). Lin et al. (2004) and Rines et al. (2004) also showed that the K-band luminosity and galaxy density profiles are consistent with NFW (Navarro et al. 1997) profiles with concentration parameters of c ~ 3. This is slightly less concentrated than the dark matter profiles which typically have c ~ 5, suggesting that the baryons are more widely dispersed than the dark matter.

Another important result from these studies was the discovery that the K-band mass-to-light ratios (M/L) are an increasing function of the cluster mass. This contrasted with earlier optical studies which found that the cluster M/L ratio was independent of mass (e.g., Carlberg et al. 1997; Girardi et al. 2002, although see Bahcall & Comerford 2002). Even though we have yet to completely assimilate the reasons for this, it suggests that either the conversion of baryons into stars is less efficient in more massive halos, or if this is not the case, that disruptions and mergers may be more efficient in more massive halos which would lead to larger fraction of the stars being in the form of intra-cluster light which is too faint to be included in the M/L ratios.

These detailed 2MASS studies of nearby clusters have provided the framework for understanding the evolution of cluster baryons in the form of stars. At the time of the undertaking of this thesis there were no good constraints on the redshift evolution of the NIR scaling relations of clusters[1]. Measuring the evolution in the cluster scaling relations provides critical constraints for modeling the assembly of clusters and the evolution of cluster galaxies. Motivated by this lack of data, the first two chapters of this thesis are dedicated to a study of the evolution of the NIR cluster scaling relations up to $z \sim 0.5$.

---

[1]Subsequently, Lin et al. (2006) published a letter with a brief synopsis of the evolution of these properties for 27 clusters $0 < z < 0.9$

1.1.3 MIR Observations of Galaxy Clusters

The launch of the *IRAS* satellite almost single-handedly created the field of MIR astronomy. Early *IRAS* observations of cluster galaxies showed that clusters tend to have very few MIR-luminous galaxies. The first major work on the subject was by Bicay & Giovanelli (1987) who examined a sample of ~ 200 galaxies detected at $60\mu m$ in seven local clusters. They showed that there were no examples of luminous infrared galaxies (LIRG, $L_{IR} > 10^{11}$ $L_{\odot}$) in these clusters and that the mean L_{IR} of the sample was $10^{9.8}$ $L_{\odot}$. By contrast, field galaxies showed a much higher percentage of LIRGs ($\sim 20\%$ of all MIR-detected field galaxies were LIRGs), and that field galaxies had a higher average luminosity $<L_{IR}> = 10^{10.2}$ $L_{\odot}$. These results reinforced what was already generally known about clusters, namely that they have fewer star forming galaxies relative to the field, and that they have lower star formation rates.

With the launch of *ISO* in 1995, the first good quality MIR observations of clusters at $z > 0.1$ were obtained. An excellent review of both *IRAS* and *ISO* observations of clusters is presented in Metcalfe et al. (2005). *ISO* also observed local clusters such as Virgo (e.g., Boselli et al. 1997a,b; Boselli et al. 1998, Tufts et al. 2002; Popescu et al. 2002a,b) and Coma (e.g., Boselli et al. 1998; Contursi et al. 2001); however, the major step forward was the observations of more distant clusters. In total *ISO* observed eight clusters at $z > 0.1$ (Fadda et al. 2000; Duc et al. 2002, 2004; Metcalfe et al. 2003; Biviano et al. 2004; Coia et al. 2005a,b) detecting a total of 48 cluster galaxies at $15\mu m$. Of these 48 galaxies, almost half came from the clusters Abell 1689 ($z = 0.17$) and CL0024+1654 ($z = 0.39$). There were two significant results from these studies. The first was the discovery that the lower redshift clusters ($z < 0.2$) tended to have very few LIRGs, but that the frequency of LIRGs in clusters increased with increasing redshift. The highest redshift cluster in the sample (CL0024+1654, $z = 0.39$) had the largest number of LIRGs of all clusters (10, see Coia et al. 2005). The second significant result was the discovery of a population of dusty star forming galaxies in Abell 1689 that had no obvious signs of star formation in their optical spectra by Duc et al. (2002). This population constituted $\sim 30\%$ of the MIR cluster members. They also showed that the SFR inferred from L_{IR} were between 10-100 times larger than the SFR rates inferred from [OII] and suggested that $> 90\%$ of the star formation in the cluster was hidden by dust.

The extraordinary sensitivity of *Spitzer* over *ISO* promises to push our understanding of MIR cluster galaxies significantly further. Thus far there are only three

published studies of *Spitzer* observations of galaxy clusters (Geach et al. 2006; Marcillac et al. 2007; Bai et al. 2007). In total, these studies comprise only two clusters at $z \sim$ 0.5 (Geach et al. 2006), and two clusters at $z \sim 0.8$ (Marcillac et al. 2007; Bai et al. 2007). These studies show an increase in both the average luminosity and frequency of MIR clusters galaxies at higher redshift and are in good agreement with the *ISO* results. Still, four clusters is far from a comprehensive look at this issue. Again, motivated by the lack of data, in this thesis we undertook the first large statistical study of MIR sources in clusters using a sample of ~ 100 clusters observed by *Spitzer*. This sample is about an order of magnitude larger than all previous work combined, and allows us to study how the MIR galaxies in the average cluster are evolving with redshift. In chapter four of the thesis we study the evolution of the $[5.8 \mu m]$ and $[8.0 \mu m]$ LFs of clusters $0.1 < z < 1.0$. In chapter five we look at the redshift evolution in the number of cluster galaxies detected at $[24 \mu m]$. These studies allow us to make the first comprehensive study of the evolution of dusty star formation in clusters galaxies over a large range in redshift ($0.1 < z < 1.0$).

In addition to the measurement of the evolution in the abundance of MIR cluster galaxies, in chapter five we also use optical spectroscopy to classify a subsample of these galaxies an attempt to understand the nature of these sources. Although the assumption has been that the majority of cluster $[24 \mu m]$ galaxies will be dusty star forming galaxies, the optical spectroscopy allow us to test this hypothesis.

Chapter 2

Near-Infrared Luminosity Functions and Density Profiles

2.1   Abstract

We present K-band imaging for 15 of the Canadian Network for Observational Cosmology (CNOC1) clusters. The extensive spectroscopic dataset available for these clusters allows us to determine the cluster K-band luminosity function and density profile without the need for statistical background subtraction. The luminosity density and number density profiles can be described by NFW models with concentration parameters of c_l = 4.28 $\pm$ 0.70 and c_g = 4.13 $\pm$ 0.57 respectively. Comparing these to the dynamical mass analysis of the same clusters shows that the galaxy luminosity and number density profiles are similar to the dark matter profile, and are not less concentrated like in local clusters. The luminosity functions show that the evolution of K^* over the redshift range $0.2 < z < 0.5$ is consistent with a scenario where the majority of stars in cluster galaxies form at high-redshift ($z_f > 1.5$) and evolve passively thereafter. The best-fit for the faint-end slope of the luminosity function is α = -0.84 $\pm$ 0.08, which indicates that it does not evolve between $z = 0$ and $z = 0.3$. Using Principal Component Analysis of the spectra we classify cluster galax-

ies as either star-forming/recently-star-forming (EM+BAL) or non-starforming (ELL) and compute their respective luminosity functions. The faint-end slope of the ELL luminosity function is much shallower than for the EM+BAL galaxies at $z = 0.3$, and suggests the number of faint ELL galaxies in clusters decreases by a factor of ~ 3 from $z = 0$ to $z = 0.3$. The redshift evolution of K^* for both EM+BAL and ELL types is consistent with a passively evolving stellar population formed at high-redshift. Passive evolution in both classes, as well as the total cluster luminosity function, demonstrates that the bulk of the stellar population in all bright cluster galaxies is formed at high-redshift and subsequent transformations in morphology/color/spectral-type have little effect on the total stellar mass.

2.2   Introduction

Galaxy clusters are fundamental tools in the study of galaxy evolution because they are unique locations in the universe, where the high-density environment produces a population of galaxies that is different from the general field. The ability to predict how and when cluster galaxies are assembled, and their subsequent evolution is an important test for any model of galaxy formation. Unfortunately, the cluster population transforms significantly in morphology, color, and star-formation properties over the redshift range $0 < z < 0.5$ and thus far, our understanding of this evolution is incomplete. At low redshift ($z < 0.2$), clusters are primarily composed of a population of quiescent early-type galaxies which obey a tight color-magnitude relation (CMR, e.g., Bower et al. 1992; Lopez-Cruz et al. 2004), morphology-density relation (Dressler 1980; Goto et al. 2003a), and spectral type-density relation (Tanaka et al. 2004; Gomez et al. 2003; Lewis et al. 2002).

At higher redshifts ($0.2 < z < 0.5$) the cluster galaxy population is no longer completely dominated by early-types. The number of blue galaxies in clusters increases (the Butcher-Oemler effect, e.g., Butcher & Oemler 1984; Ellingson et al. 2001; Andreon et al. 2004) and the morphological mix of galaxies also changes as the proportion of spiral galaxies increases at the expense of the early-type (primarily S0) population (e.g., Dressler et al. 1997; Postman et al. 2005; Smith et al. 2005). Despite these major changes in star-formation properties and morphology, studies of the fundamental plane (e.g., van Dokkum et al. 1998; van Dokkum & Stanford 2003; Holden et al. 2005) and the CMR (e.g., Stanford et al. 1998; Gladders et al. 1998; Holden et al.

2004) of early-type galaxies (both of which include S0 galaxies) show that their stellar populations are extremely old and consistent with a passively evolving population formed at high redshift ($z_f > 2$-3). The differences in the star-formation history of cluster galaxies and the average age of their stellar populations could be reconciled by postulating that the predecessors of low-redshift early-types are high-redshift late-types which form the bulk of their stars at high-redshift (van Dokkum et al. 2001). If transformations in color and morphology are primarily passive (i.e., from the truncation of star formation by strangulation; e.g., Balogh et al. 1999; Abraham et al. 1996; Treu et al. 2003; Goto et al. 2003b) then they should leave little imprint on the overall stellar population. The prediction that the majority of evolution in cluster galaxies from $z \sim 0.5$ to the present is simply the passive transformation of late-type galaxies into early-type galaxies is in good qualitative agreement with the data; however, it is possibly too simplistic a picture.

Recent work suggests that galaxy-galaxy mergers may play a significant role in driving cluster galaxy evolution at high redshift. Lin et al. (2004, hereafter L04) compared the Halo Occupation Distribution (HOD, the number of galaxies in a dark matter halo of a given mass) of $0.2 < z < 0.9$ clusters to that of $z < 0.1$ clusters and showed that it is *larger* by a factor of ~ 2 in the high-redshift clusters. This result implies that numerous mergers or tidal disruptions in the cluster environment at moderate to high redshift are required to reduce the number of bright cluster galaxies, and match the local HOD. The prediction of a large merger fraction is consistent with observations of MS1054-03 at $z = 0.83$ by Tran et al. (2005) and van Dokkum et al. (1999) who show that 16% of the cluster galaxies are currently undergoing major mergers. Understanding how the merger rate interplays with the transformation in color, spectral-type, and morphological-type of the cluster population without significantly altering the overall stellar population remains a challenge.

The K-band luminosity function (LF) of clusters at this redshift can provide useful information on this problem. K-band light suffers little contamination from recent star formation and dust; furthermore, the k-corrections are small, negative, and nearly independent of galaxy type (e.g., Poggianti 1997; Mannucci et al. 2001). These advantageous properties mean that K-band light is closely related to the total stellar mass of a galaxy (Brinchmann & Ellis 2000; Rix & Rieke 1993) and therefore, the K-band LF is nearly analogous to the galaxy stellar mass function. The dependence on the stellar mass contained in galaxies makes the K-band LF a useful check on the merger rate, because its evolution will proceed quite differently depending on the number of major

mergers. Furthermore, the K-band LF is also sensitive to the age of the stellar populations in cluster galaxies because it puts constraints on luminosity evolution of the stellar population. Most commonly, luminosity functions are fit to a Schechter (1976) function of the form:

$$\phi(K) = (0.4\ln 10)\phi^*(10^{0.4(K^*-K)})^{1+\alpha}\exp(-10^{0.4(K^*-K)}), \qquad (2.1)$$

where α is the faint-end slope; ϕ^*, the normalization; and K^* is the "characteristic" magnitude, which indicates the transition between the power-law behavior of the faint-end and the exponential behavior of the bright-end.

The advent of the Two Micron All-Sky Survey (2MASS, Skrutskie et al. 2006) has facilitated a considerable number of studies of the Near Infrared (NIR) LF of clusters in the local universe (i.e., $z < 0.1$) using a very homogeneous set of data. These studies now provide a crucial comparison sample for higher-redshift NIR cluster LFs. Balogh et al. (2001, hereafter B01), Kochanek et al. (2003), Lin et al. (2003), L04, Rines et al. (2004, hereafter R04) and Ramella et al. (2004) have all investigated the K-band LF of local clusters and groups using 2MASS data. The LFs vary somewhat from sample to sample; however, it appears that the overall shape of the K-band LF in local clusters is similar to the local field. The only notable difference being that K^* is slightly (~ 0.2 - 0.4 magnitudes) brighter in clusters, and K^* in groups is closer to, if not equal, the field value (Ramella et al. 2004; L04).

At higher redshift, the K-band LF of clusters is not as well constrained. Thus far, the best measurement of the evolution of the cluster K-band LF comes from the study of De Propris et al. (1999, hereafter dP99). Using a heterogeneous set of 38 clusters with $0.1 < z < 1.0$, they show that the brightening of K^* with increasing redshift is consistent with a passively evolving stellar population with a formation redshift (z_f) of $\sim$ 2-3. Subsequent measurements of the K-band LF in a handful of $z > 1$ clusters have been made (Kodama & Bower 2003; Ellis & Jones 2004; Toft et al. 2004; Strazzullo et al. 2006) and those data further confirm the passive evolution scenario. The interpretation of these results has been that the majority of the stellar mass in bright cluster galaxies is already assembled into IR-bright (and therefore massive) galaxies by $z \sim 1$. It is difficult to reconcile these data with the prediction of a significant number of mergers in the cluster environment.

We have obtained wide-field K-band imaging for 15 of the 16 CNOC1 clusters (Yee et al. 1996a) to a depth of $\sim K^* + 2$. With these data we examine the redshift evolution of the K-band cluster LF, the difference between the field and cluster LFs, the LFs of

clusters of different mass, and the K-band luminosity and number density profile of clusters at $0.19 < z < 0.54$ using a homogeneous, X-ray-selected cluster sample. We have IR-imaging and spectroscopy to $R \sim 1.5R_{200}$ for most clusters and this radial coverage allows us to compute the LFs for the entire virialized region without the need for statistical background subtraction. Furthermore, the spectroscopy also allows us to classify the galaxies into star-forming, and non-star-forming types and determine how the LFs of these classes differ.

This paper is the first in a series of three which examine the NIR properties of moderate redshift clusters. The HOD, mass-to-light ratios and correlation between the cluster physical properties and K-band luminosity/richness are presented in Muzzin et al. (2006, hereafter Paper II). The evolution of the color-magnitude relation and the K-band selected Butcher-Oemler effect will be presented in a third paper (Yee et al. in-prep, hereafter Paper III).

The structure of this paper is as follows: In §2 we describe our observations, and in §3 the data reduction and calibration. Section 4 discusses the weighting scheme based on the spectroscopic catalogue that is used to construct both the density profiles and luminosity functions. In §5 we compute the K-band luminosity and number density profile of the clusters and compare with the dark matter profile. In §6 we determine the cluster K-band LF for all cluster galaxies as a function of redshift and cluster mass and compare to field LFs in the literature. In §7 we divide the galaxies into two spectral classes and show the dependence of these LFs on redshift and cluster mass. We conclude with a summary in §8. When computing magnitudes and angular sizes we adopt an $\Omega_m = 0.3$, $\Omega_\Lambda = 0.7$, $H_0 = 70$ km s^{-1} Mpc $^{-1}$ cosmology. All magnitudes quoted throughout the paper are on the Vega system.

2.3   Observations

The CNOC1 clusters are an X-ray selected sample of 16 intermediate ($0.19 < z < 0.54$) redshift clusters (Yee et al. 1996a), and are likely the most well-studied clusters in this redshift range. The masses (Carlberg et al. 1996, Borgani et al. 1999), mass-profiles (Carlberg et al. 1997a, 1997b; van der Marel et al. 2000), X-ray temperatures (Mushotzky & Scharf 1997; Henry 2000; Lewis et al. 1999; Hicks et al. 2006), X-ray luminosities (Ellis & Jones 2002), richnesses (Yee & Ellingson 2003), and stellar populations (Abraham et al. 1996; Balogh et al. 1999; Diaferio et al. 2001; Ellingson et

al. 2001) have all been examined in detail. For our sample we selected 15 of the 16 CNOC1 clusters for K-band imaging. The cluster MS0906+11 was not observed because it is was shown to be a strong binary in redshift-space by Carlberg et al. (1996) and therefore the cluster dynamical mass measurement is unreliable.

2.3.1 Optical Photometry and Spectroscopy

Gunn g and r band imaging data were obtained at the 3.6m Canada-France-Hawaii-Telescope (CFHT) as part of the original CNOC1 project (Yee et al. 1996a) using the Multi-Object Spectrograph (MOS) camera in imaging mode. The 5σ depth of the optical photometry varies from cluster-to-cluster but is typically 23.7 - 24.3 mag in g, and 23.5 - 24.0 mag in r. The CNOC1 project also acquired > 2500 spectroscopic redshifts in the fields of the 15 clusters. The spectroscopy was obtained using 1-10 masks of $\sim$ 100 slits per cluster. Of the 2500 redshifts, approximately half are cluster members. The spectroscopic catalogues were chosen as an r-band magnitude-limited, complete sample, but are sparsely sampled. The spectroscopic magnitude limits are r = 20.5, 21.5, and 22.0 for clusters at $z < 0.3$, $0.3 < z < 0.45$, and $z > 0.45$ respectively. Using the passive evolution color-redshift model for an early-type galaxy from Kodama et al. (1998), these spectroscopic completeness limits correspond to K-band limits of $\sim$ 17.0, 17.5, and 18.0 mag for the same redshift bins. The definition of the completeness limiting magnitude is that all galaxies brighter than the limit, *that had slits placed on them*, have reliably determined redshifts. However, the sparse sampling means that not all galaxies in the field brighter than the completeness limit had slits placed on them. Therefore, use of the redshift catalogues requires a selection function that corrects for the sparse sampling of the data (§4).

Complete details of the optical observations, reductions, photometry and redshift determination of these data can be found in Yee et al. (1996a). Our analysis is based on the original photometric and spectroscopic catalogues (Ellingson et al. 1998, 1997; Abraham et al. 1998; Yee et al. 1998, 1996b) and additional unpublished spectroscopy for $z < 0.3$ clusters.

2.3.2 Near Infrared Observations

K-band imaging for 14 of the 15 clusters was obtained at the Kitt Peak National Observatory (KPNO) 2.1m telescope using the Ohio State / NOAO Infrared Imaging

Spectrograph (ONIS). The ONIS detector is a 1024×1024 InSb array with 2 working quadrants which makes it effectively a 1024×512 imager with a pixel scale of $0\rlap{.}''288$/pixel. The observations were made on UT 1999 February 3-4 and 1999 June 3, and were taken in a Mauna Kea Observatory filter set version of the K_s filter (Tokunaga et al. 2002), which is nearly identical to the 2MASS K_s filter. Hereafter we treat them as identical and refer to the filter simply as the "K-band". All three nights were photometric and standard stars were observed at different airmasses for photometric calibration. The seeing in the images is typically around $1\rlap{.}''0$, but ranges from $0\rlap{.}''8$ to $1\rlap{.}''2$. Because of time constraints, we were unable to obtain data for one cluster (MS0440+02) during the February run. K-band imaging of MS0440+02 was instead obtained using the PISCES camera on the KPNO 2.5m telescope on UT 1999 February 27 during an imaging run for CNOC2 fields. The PISCES camera is a 1024×1024 HAWAII array with a pixel scale of $0\rlap{.}''495$/pixel. The PISCES imaging was done using the K_s filter. Table 1 summarizes our observational data.

2.3.3 Pointing Strategy and Field Coverage

The goal of the original CNOC1 observations was to obtain photometry and spectroscopic redshifts of cluster members beyond the cluster virial radius (R_{vir}), in order to determine the cluster dynamical mass-to-light ratio. For the massive, lower-redshift clusters, the angular size of R_{vir} was larger than the CFHT-MOS Field-of-View (FOV) ($\sim 10' \times 10'$) and several MOS pointings were required. For these clusters, either a north-south or east-west strip through the cluster center was observed. Column 8 of Table 1 lists the configuration of the MOS pointings. The first number in the column is the number of east-west pointings and the second is the number of north-south pointings. A 1×1 pointing is the cluster center. Column 9 lists what percentage of the area of a circle with radius R_{200}, the radius at which the mean density of the cluster exceeds the critical density by a factor of 200 (see Paper II for updated values of R_{200} for the CNOC1 clusters using a ΛCDM cosmology), is covered by the optical imaging data. Column 3 of Table 1 lists the number of cluster members (see Carlberg et al. 1996 for membership criteria) with spectroscopic redshifts within R_{200}.

In order to overlap as much of the optical imaging and spectroscopic data as possible, we designed a pointing strategy for the ONIS observations based on the locations of the CFHT MOS fields. To obtain images with similar coverage as the $\sim 10' \times 10'$ CFHT MOS (although only $\sim 8' \times 8'$ are useful for photometry and spectroscopy due

Table 2.1. Summary of Observational Data for the CNOC1 Cluster Sample

Cluster	z	N_{spec} ($R \leq R_{200}$)	K_{lim} (mag)	Seeing ($''$)	g/r area ($\square'$)	K area ($\square'$)	MOS Fields	% R_{200} Obs
(1)	(2)	(3)	(4)	(5)	(6)	(7)	(8)	(9)
A2390	0.2279	140	18.08	1.2	269.56	249.01	5×1	60.9
MS0016+16	0.5466	52	18.57	1.1	57.58	57.58	1×1	100.0
MS0302+16	0.4246	26	19.12	0.9	63.27	62.62	1×1	100.0
MS0440+02	0.1965	33	19.01	1.4	182.02	168.46	3×1	89.0
MS0451+02	0.2010	76	18.66	0.9	253.41	173.75	4×1	53.6
MS0451-03	0.5392	64	18.69	0.9	61.22	61.22	1×1	100.0
MS0839+29	0.1928	39	18.70	0.9	176.35	167.47	3×1	68.3
MS1006+12	0.2605	29	18.14	0.9	59.13	57.51	1×1	81.0
MS1008-12	0.3062	61	17.89	1.0	63.01	45.29	1×1	73.1
MS1224+20	0.3255	29	18.05	0.8	57.07	71.72	1×1	93.5
MS1231+15	0.2350	67	18.66	0.9	181.35	181.35	1×3	100.0
MS1358+62	0.3290	136	17.93	1.2	193.71	185.14	1×3	100.0
MS1455+22	0.2570	57	18.22	0.9	58.69	56.39	1×1	77.3
MS1512+36	0.3726	23	18.75	1.0	207.61	181.45	3×1	100.0
MS1621+26	0.4274	59	18.85	1.1	72.44	67.72	1×1	100.0

Note. — (3) Number of spectroscopic clusters members with $R \leq R_{200}$, (4) 5σ limiting magnitude of observations, (6) Total area with g and r band data, (7) Total area with both K-band and g/r data (9) Percentage of a circle with radius R_{200} with K-band imaging

to a significant radial distortion and vignetting) using the $\sim 2.5' \times 5'$ FOV of ONIS we used a 3×2 pointing pattern for each MOS field. This gives us an ONIS mosaic with a FOV of $\sim 7.5' \times 7.5'$, which is similar to the usable portion of the MOS. Each pointing consists of ~ 4 dithers of $\sim 6''$ to $10''$, and each dither consists of 1-3 internal coadds with exposure times of 25-45 seconds. The nature of the mosaicking is such that there is significant overlap of the pointings in the north-south direction and a strip in the center of each field has a higher signal-to-noise than the rest of the mosaic. The depth of the images at the lower signal-to-noise parts still reaches the limit of the spectroscopic observations, so we make no correction for the slightly uneven depth of the images. The PISCES camera has a FOV of $8' \times 8'$, nearly the same size as the MOS, and therefore we made a single PISCES pointing for each MOS pointing in MS0440+02. The PISCES pointings consist of 5 dithers of $\sim 5''$ with a 40 second exposure time.

2.4   Data Reduction

Reduction of the ONIS data was done using the IRAF packages PHIIRS and PHAT (see Hall, Green, & Cohen, 1998). Reduction of the PISCES data was done with a modified version of the ipipe reduction package (Gilbank et al., 2003). Both of these packages employ the standard techniques for reducing NIR imaging, and here we summarize only the most important steps in the process.

The first step in the reduction is to make a first-pass dark subtraction, flat-fielding, and sky estimate for all frames. Frames are then registered and coadded into a first-pass mosaic of the cluster. Object finding is performed on this mosaic, and from this an "object mask" is made. Flat-fielding and sky subtraction are then redone using only pixels that do not appear in the the object mask. This step ensures that faint galaxies not detected in a single frame do not cause the sky level to be overestimated.

All ONIS images are flattened with dome flats (for the PISCES images we use the value of the sky itself to flat-field). Whenever possible, sky subtraction is done using a "running sky". This procedure involves calculating the sky from a fixed number of frames taken before and after the frame for which the sky is being subtracted. Determining the sky from a small number of frames improves the photometric accuracy of the data because the moderate-duration sky variations (of the order 10 minutes in the NIR) can be removed accurately. Unfortunately, using a small number of frames

to compute the sky also results in a larger Root-Mean-Squared (RMS) background in the final mosaic because shot noise is significant when using only a few frames. Our criteria for choosing the best number of frames for sky subtraction was as follows: The sky was first computed using all the frames from a cluster (we termed this a "quick sky"). The quick sky was subtracted from all frames, and the final mosaic made. The RMS noise and standard deviation of that image are then recorded. We then repeat sky subtraction using the running sky technique. The final sky we adopt is the one that uses the fewest number of frames and gets an RMS background for the final image that is within 1σ of the quick sky image. For most clusters this results in a sky computed from $\sim$ 16-32 frames (i.e., approximately 5 - 10 minutes before and after each frame was observed). Once the final sky has been subtracted from each frame, we adopt an airmass extinction term of -0.08 mag for the K-band, and all frames are rescaled by $1.08 \times$ <airmass> of the observation. As an example of the data quality, we show a portion of the final mosaics of one of the highest-redshift (MS0016+16) and lowest-redshift (Abell 2390) clusters in the sample in Figures 1 & 2.

2.4.1   ONIS Pattern Removal

All frames obtained using the ONIS instrument have a lined pattern that appears in the bottom-half of the image. This pattern is probably caused by extra noise generated when the camera is read out. The pattern is well-fit by a variable-amplitude sinusoid curve with a period 6 times the width of the chip. We remove the pattern by fitting each original frame (before flat-fielding and sky subtraction) with a sinusoid and then subtracting the fit from the image. In all cases the fits are good and all images are subsequently eye-checked to make sure nothing which might significantly alter the photometry is subtracted. The final mosaic for each cluster is made from the final sky-subtracted, pattern-removed frames.

2.4.2   PISCES Distortion Correction

The PISCES camera has a radial distortion in the focal plane. The pattern is different each time the camera is mounted on the telescope and therefore must be corrected using stars in the science images. We correct this pattern using code developed by McCarthy et al. (2001). Comparing the positions of objects on the optical images with the distortion-corrected PISCES images shows that this correction works extremely
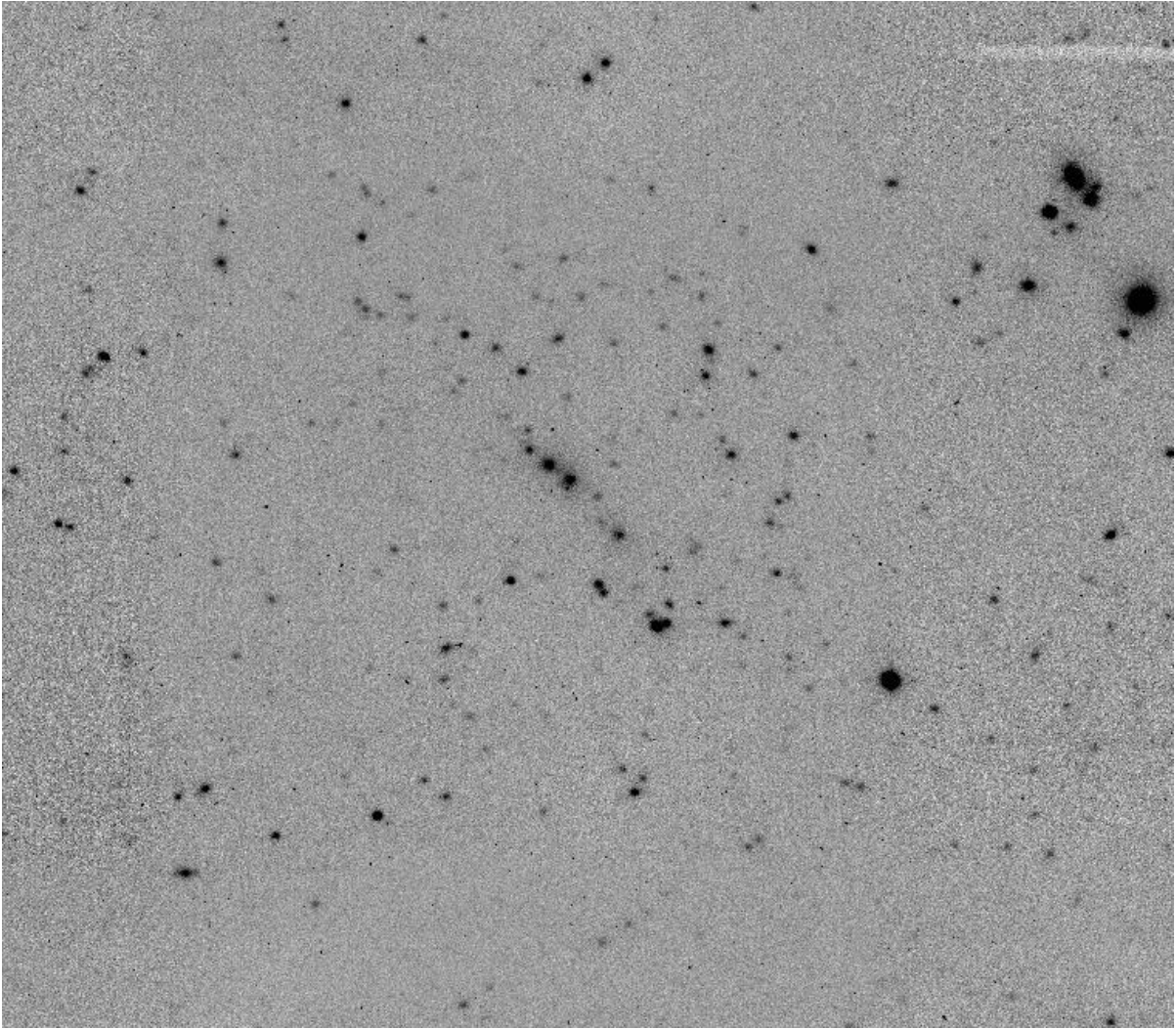
Figure 2.1 K-band image of the central region of MS0016+16 (z = 0.55), one of the highest-redshift clusters in the sample. The image has a FOV of 3.5 × 3.0 arcmin, and seeing of $1''\!.1$. North is to the top, east is to the left.

well.

2.4.3 Object Finding and Photometry

The g and r-band optical images are significantly deeper than the K-band images for every cluster. Therefore we match the optical catalogue positions to the K-band images using the IRAF task *xyxymatch*. The significant pincushion of the CFHT-MOS is corrected using tabulated data supplied by CFHT. In most cases this allows for excellent matches of the whole optical catalogue. In the few cases where a slight offset remains, a higher order correction is computed and then eye checked. A final eye
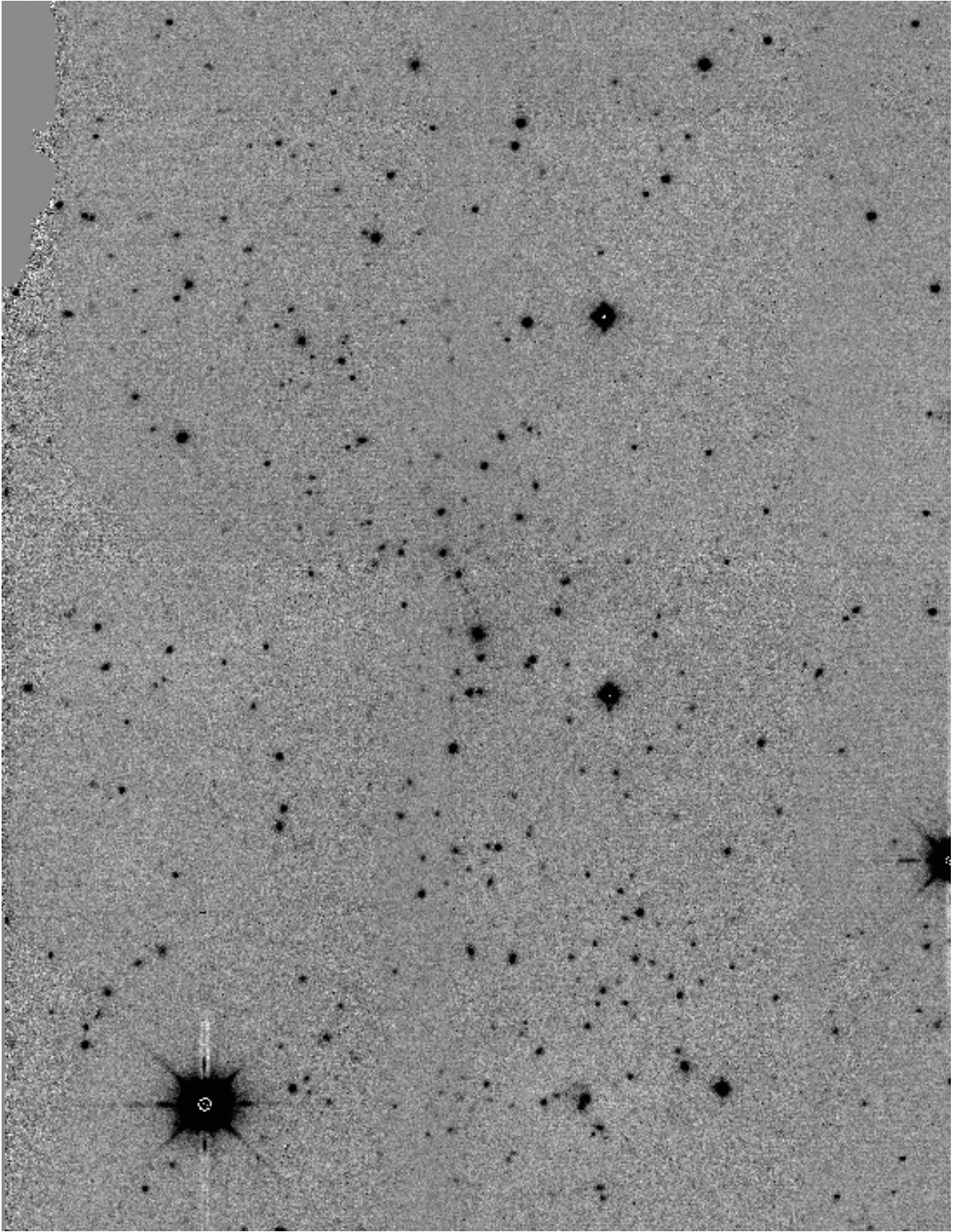
Figure 2.2 K-band image of the central region of Abell 2390 ($z = 0.22$), one of the lowest-redshift clusters in the sample. The image has a FOV of $\sim 2.5 \times 3.5$ arcmin, and seeing of $1{''}2$. North is to the left, east is to the bottom.

check is made for objects that may have been so red as to be apparent only in the K-band images. Very few such objects were found ($\sim$ 1-2 per MOS field). Those that are found are not faint Extremely Red Objects (EROs); they tend to be objects undetected in the optical image because they are obscured by the bleeding of charge from a saturated star. No attempt is made to account for these objects because there are so few. Furthermore, these galaxies do not have redshifts and therefore will have negligible impact on the results of the study.

Photometry and star-galaxy classification are done on all objects using Picture Processing Package (PPP, Yee 1991). PPP identifies objects as either stars or galaxies based on analysis of their growth curve. The r-band images are the deepest for all clusters and therefore the object classification is based exclusively on the r-band images.

Galaxy colors are nominally computed using a $3''$ diameter aperture magnitude. However, PPP determines whether this aperture is appropriate based on the object's growth curve. If the growth curve appears "normal" (i.e., it is monotonically increasing, but has a monotonically decreasing derivative) then an actual $3''$ aperture is used; however, if the growth curve is abnormal (due to, e.g., crowding from another object, or a cosmic ray hit) PPP uses the largest, non-contaminated aperture to compute the color (we refer to this diameter as the optimal aperture, d_{opt}). Computing colors using this technique is particularly useful for avoiding the crowding problems which can be significant in the dense, central parts of galaxy clusters.

Galaxy total magnitudes are determined by analyzing the shape of the growth curve. For faint small galaxies ($r > 19$) the magnitudes are extrapolated to a diameter of $8.5''$ to account for seeing effects. The extrapolation is done using a reference Point Spread Function (PSF), determined from several bright stars in the field. For brighter galaxies ($r < 19$), variable apertures up to a maximum of $25.5''$ are used. The size of the aperture is determined from the growth curve of the object. This step is primarily employed to account for bright galaxies with large angular diameters (i.e., foreground galaxies). A thorough discussion of photometry using PPP and a comparison with simulations can be found in Yee (1991).

2.4.4 Photometric Calibration and Comparison with Previous Photometry

Photometric standards from Persson et al. (1998) were observed throughout all nights, at different airmasses. There are not enough standards to solve for the atmospheric

extinction coefficient; however, comparing observations of the same standard at different air masses shows that they are consistent with -0.08 value assumed for the science frames. Standards taken throughout the night were extremely stable, so photometric zeropoints are determined for each night based on an average of all standards for that night. The standard deviations in the zeropoint calibration for the three ONIS nights are 0.022, 0.014, and 0.035 mag, and are determined from 3, 10, and 6 standard stars respectively. The PISCES photometric zeropoint has a standard deviation of 0.022 mag and is determined from 4 standard stars.

The cluster imaging is sufficiently wide that it contains enough bright stars per cluster field to check the consistency of the photometry with the 2MASS point-source catalogue (Skrutskie et al. 2006). The 2MASS photometric calibration is excellent, having zeropoint variations that are less than 0.02 mag across the entire survey. For the purpose of determining any differences in zeropoint, we compare the photometry of objects $13.5 < K_s < 15.0$ classified as stars by PPP in the cluster fields to the same objects in the 2MASS Point Source Catalogue. We adopt a faint limit of $K_s < 15.0$ because the mean photometric uncertainty for an individual star at $K_s \sim 15$ becomes fairly large in the 2MASS catalogue (~ 0.1 mag). We choose a bright limit of $K_s > 13.5$ because stars begin to saturate at this magnitude on the ONIS detector (the PISCES potential well is slightly deeper and therefore a bright limit of $K_s = 12.5$ is adopted for MS0440+02). The number of stars available for comparison in the fields of the clusters varies from from 6 in MS1008-12 and MS1455+22 to 70 in Abell 2390. In general, the agreement between our photometry and the 2MASS photometry is good. Eight of 15 clusters have median photometric differences of < 0.05 mag, and 12 of 15 have differences of < 0.1 mag. The cluster with the largest offset is MS0016+16, which is fainter than the 2MASS photometry by 0.18 mag. We noted the possibility of light cirrus in the logbook when observing this cluster, and assume that this is the explanation for the difference in zeropoint. Table 2 lists the clusters, the number of stars, and the mean difference between our photometry and the 2MASS photometry. Although the offsets between our calibration and the 2MASS calibration are small, we have chosen to recalibrate our photometry to the 2MASS photometry, rather than use the solutions from the standard stars. This provides consistent photometric zeropoint for the entire cluster sample. Once recalibration is complete, the magnitudes of all galaxies are corrected for Galactic reddening using the dust maps of Schlegel et al. (1998).

Three of the CNOC1 clusters (MS1358+62, MS0451-03, and MS1008-12) were also observed in the study of Stanford et al. (1998, 2002; hereafter SED02). As an addi-

tional check on the consistency of our photometry, we compare the magnitudes of all galaxies brighter than the 5σ limiting depth of the shallowest observation (in all three cases our data is shallower by ~ 0.1 mag). The top panels of Figures 3, 4, and 5 show plots which compare our total magnitudes with the SED02 total magnitudes. The solid line in the plot has a slope of unity. The bottom panel of the plots shows the residuals. Overall, the agreement between our photometry and the SED02 photometry is poor. The median offset for MS1008-12, MS1358+62, and MS0451-03 is 0.089, 0.223, and 0.305 mag respectively, with our photometry being fainter in all cases. Objects which are extreme outliers (> 1 mag) are likely to be bad matches, as we use a relatively simple matching technique.

The systematic differences in the photometry are much larger than the zeropoint uncertainties (~ 0.02 mag for 2MASS, and ~ 0.03 mag for the SED02 data) and they are also larger than the even the largest difference between our own photometric calibration and the 2MASS calibration (0.18 mag). This makes it difficult to understand the cause of the discrepancy. The data reduction procedure employed by SED02 is nearly identical to our own, and therefore it is unlikely that this causes any systematics between the datasets. The most notable difference between the SED02 datasets and our own is that the SED02 observations were done with different cameras on different telescopes: OSIRIS on KPNO 1.3m for MS1008-12, IRIM on KPNO 2.1m for MS1358+62, and IRIM on KPNO 4m for MS0451-03 whereas ours were done with the same instrument/telescope configuration. In our program, the observations for MS1008-12 and MS1358+62 were taken consecutively on February 3. If there were some systematic change during the observations (e.g., cirrus) it most likely would have affected both of these clusters, yet the photometric calibration from the standard stars matches the 2MASS calibration for both these clusters very well ($<\Delta m>$ = -0.003 and -0.039, for MS1008-12 and MS1368+62, respectively).

It is interesting to note that the photometry for objects brighter than K ~ 15.0 agrees somewhat better than for objects fainter than K ~ 15. Given that our zeropoints are determined using stars brighter than this, it suggests that the SED02 photometry could be as consistent with the 2MASS photometry as our own, and that the relative offset is not a zeropointing problem, but may be a systematic due to the different way magnitudes are measured. The cameras used by SED02 have a much larger pixel scale than ONIS ($0\!''\!95$/pixel, $1\!''\!09$/pixel, $0\!''\!65$/pixel for OSIRIS, IRIM-2.1m, and IRIM-4m, respectively, compared to $0\!''\!288$/pixel for ONIS). Such a large pixel size means that the some of their observations may be significantly undersampled if the seeing was

close to $1''0$ or better. This could pose a problem because the SED02 magnitudes were measured using the FOCAS (Valdes, 1982) code, which determines magnitudes using isophotes. SED02 then correct the FOCAS magnitudes because FOCAS tends to produce total magnitudes which are too faint. It is possible that determining isophotal magnitudes using undersampled data may result in a significant scatter, because the location of the isophote is difficult to determine. We cannot be certain that this is the source of the discrepancy over such a small area; however, because we use primarily a single instrument, and our photometry agrees well with 2MASS photometry, we are confident of the photometric accuracy of our own data.
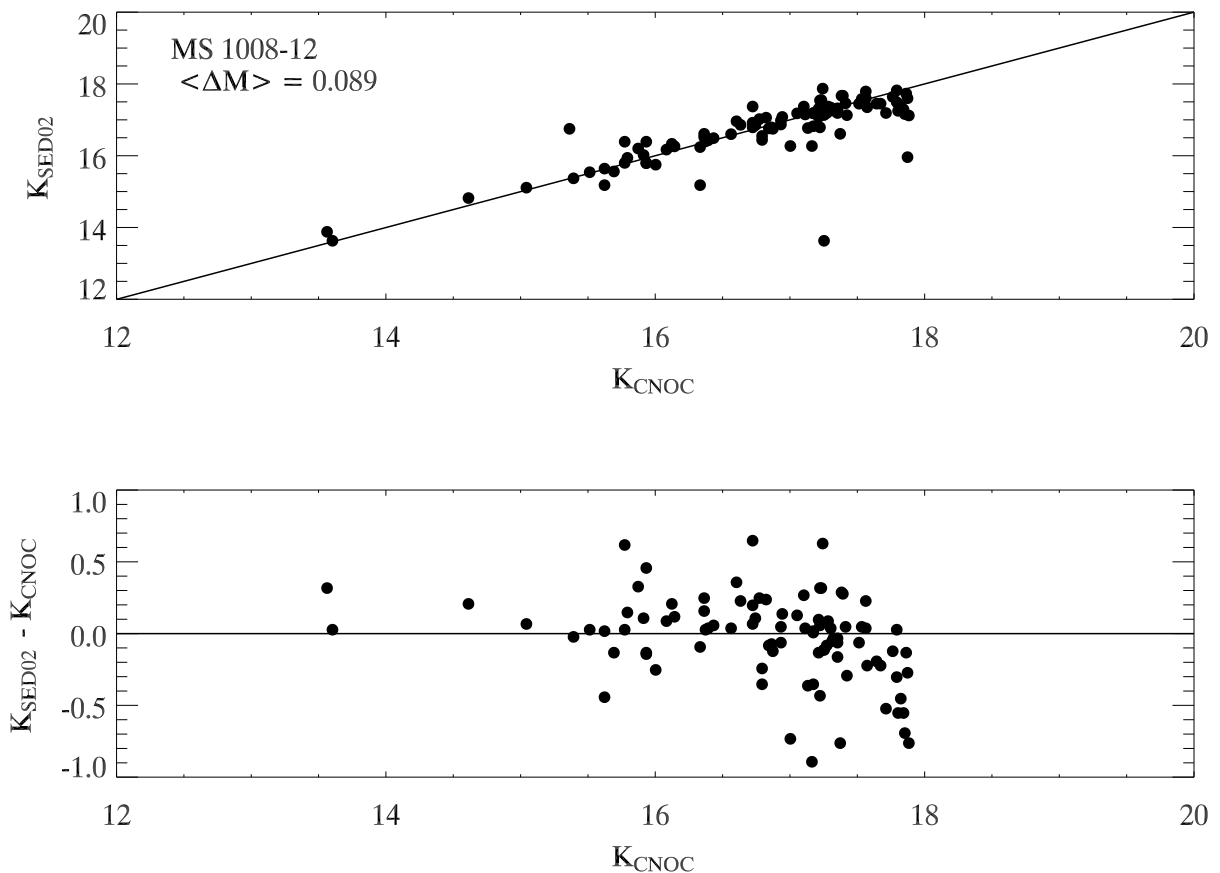
Figure 2.3 Top Panel: Total magnitudes from the SED02 photometry vs. total magnitudes from this photometry for the cluster MS1008-12. The solid line has a slope of unity and intercept of zero. Bottom Panel: Residuals from the top panel.
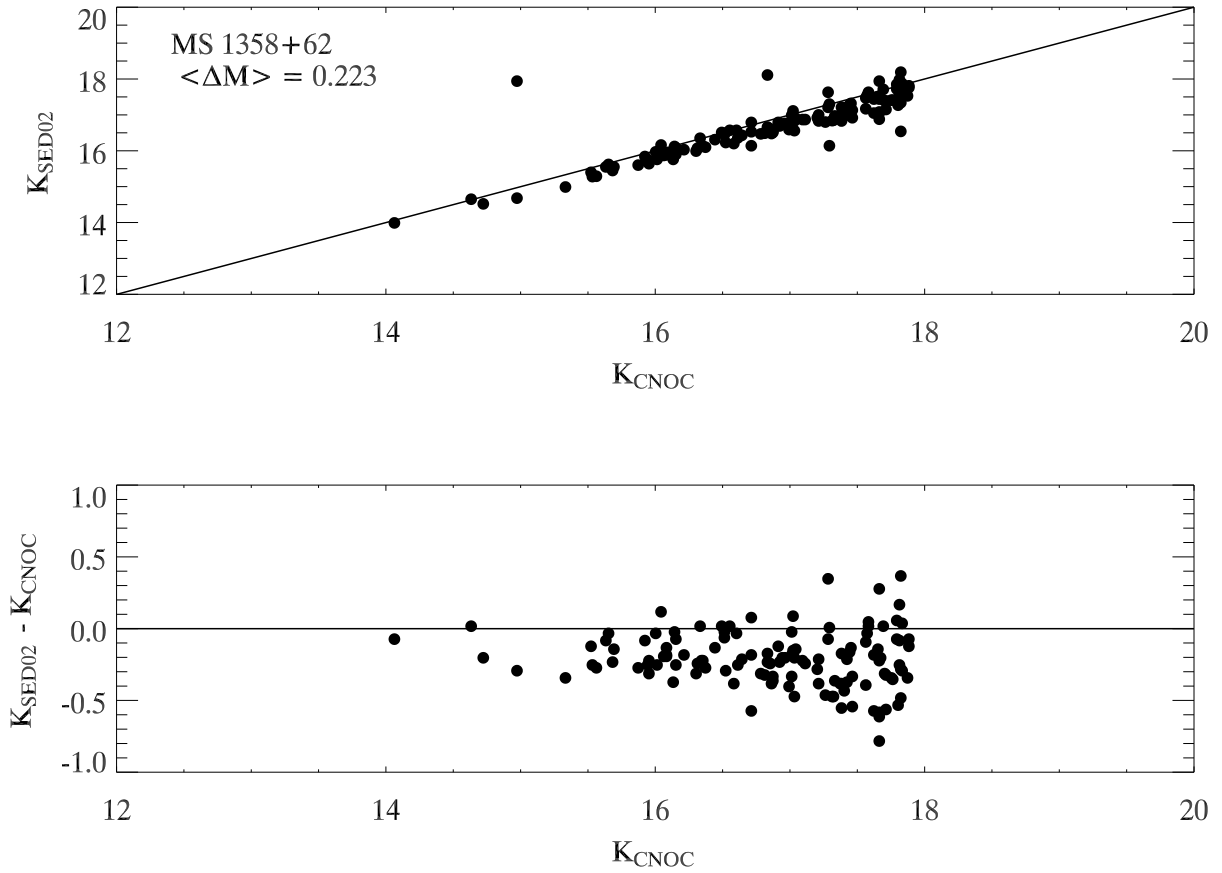
Figure 2.4 As Figure 3 for the cluster MS1358+62. Objects that are significant outliers may be poorly matched.
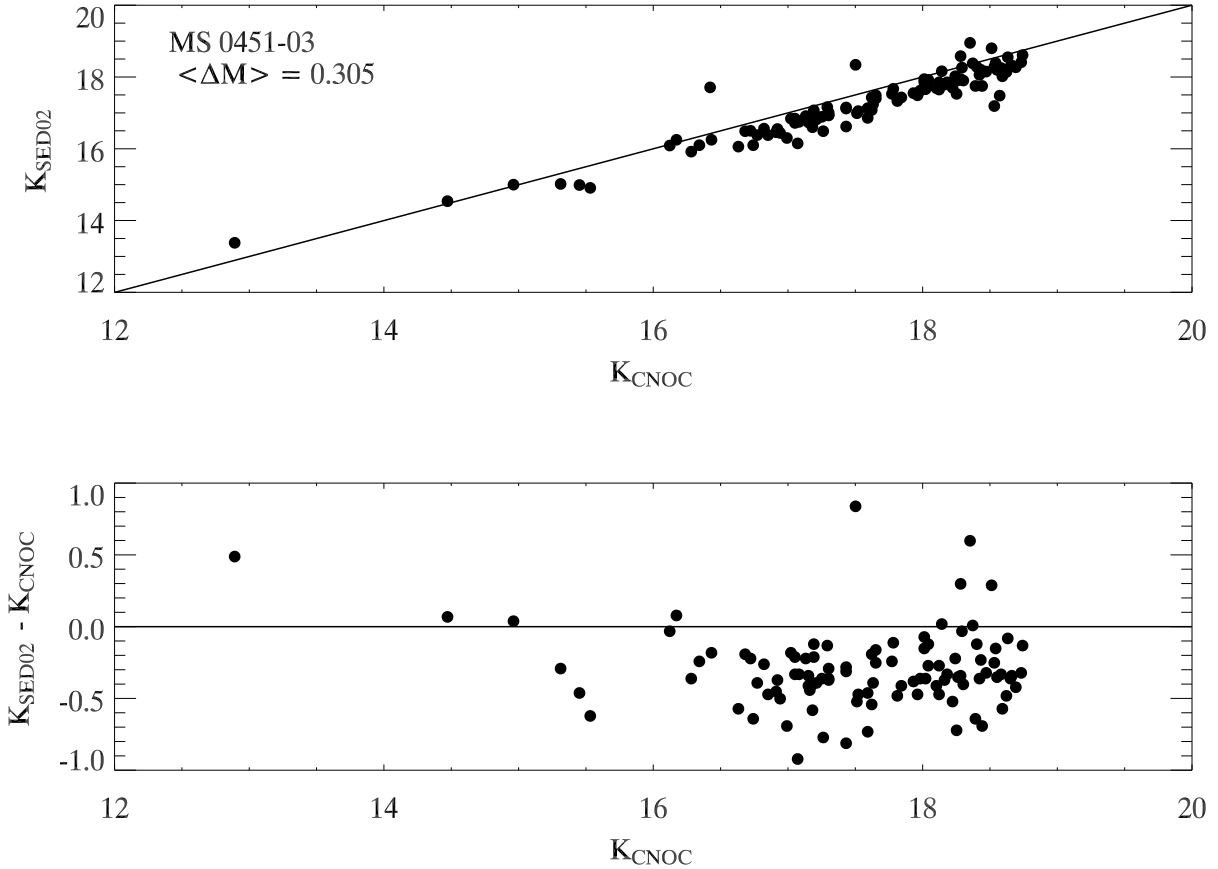
Figure 2.5 As Figure 3 for the cluster MS0451-03. Objects that are significant outliers may be poorly matched.

2.5   Spectroscopic Selection Function

The large number of spectroscopic redshifts available from the CNOC1 project allows us to measure the K-band LF and density profiles with more confidence than by statistical background subtraction; however, the cluster redshift catalogues are sparsely sampled and a weighting scheme is required to correct for the spectroscopic selection function. Galaxies may preferentially have a measured redshift depending on their magnitude, color, position in the cluster, or z; and the galaxy weights are a function of these four parameters.

The weighting scheme that is employed is based on the one derived by the CNOC1 and CNOC2 collaborations and is discussed thoroughly in the respective papers (Yee et al. 1996a, Yee et al. 2000). The basic philosophy behind the weighting scheme is that the distribution of galaxies with redshifts is representative of the ones without

Table 2.2.   Comparison of 2MASS and CNOC1 Photometric Zeropoints

Cluster	N_{stars}	K_{CNOC}-K_{2MASS}
(1)	(2)	(3)
A2390	70	0.042 ± 0.045
MS0016+16	7	0.180 ± 0.038
MS0302+16	9	0.003 ± 0.052
MS0440+02	62	0.064 ± 0.015
MS0451+02	43	0.005 ± 0.030
MS0451-03	15	0.058 ± 0.038
MS0839+29	27	0.025 ± 0.028
MS1006+12	7	0.048 ± 0.058
MS1008-12	6	-0.003 ± 0.080
MS1224+20	7	0.009 ± 0.043
MS1231+15	9	-0.068 ± 0.079
MS1358+62	23	-0.043 ± 0.043
MS1455+22	6	0.117 ± 0.079
MS1512+36	18	-0.097 ± 0.051
MS1621+26	20	0.114 ± 0.084

redshifts in terms of the primary selection biases. The magnitude selection function (i.e., a brighter galaxy is more likely to have a spectroscopic redshift) is overwhelmingly dominant over the other 3 possible selection effects, which can be considered "secondary effects" (Yee et al. 1996a). Incorporating the full set of weights in our computations has little effect on the final results and for simplicity of interpretation we ignore the secondary biases and use only the magnitude weights when computing the cluster LFs.

The spectroscopic weights are computed as follows. Galaxies with redshifts are compared to the total number of galaxies in running bins of ± 0.25 mag for galaxies fainter than $K^* + 1.5$, and in running bins of ± 0.50 mag for galaxies brighter than $K^* +$ 1.5. K^* for each cluster is estimated using a passive evolution model (§6.3). The weight

for a galaxy is then the inverse ratio of galaxies with redshifts to the total number of galaxies in its magnitude bin. The weights for the brightest cluster galaxies (BCGs) are sometimes not equal to 1, even though the spectroscopy for the BCGs is 100% complete. This occurs because there are bright field galaxies within the cluster field. In order to avoid overestimating the contribution from bright galaxies, the spectroscopic weight of the BCG in each cluster is set equal to 1.

All galaxies within the cluster field are used to compute the weights when we measure the cluster density profiles. For the LFs, only galaxies within R_{200} are used to determine the weights. We adopt this approach for the LFs because the K-band imaging does not have the same coverage as the optical imaging/spectroscopy in all clusters. A few clusters have K-band data to only $R \sim R_{200}$ whereas others have coverage well beyond R_{200} and therefore have a larger proportion of field galaxies with redshifts. Throughout the analysis in this paper, the determination of cluster membership is done using the cluster redshift-space bounds calculated by Carlberg et al. (1996).

One potentially serious problem with the spectroscopic catalogue is that it is r-band selected, yet it is being used to determine the abundance of K-band selected galaxies. If a cluster or field contains a significant number of EROs which are redder than the cluster red-sequence then they will be missing from the spectroscopic sample, and could artificially inflate the K-band spectroscopic weights. Although we already verified qualitatively that there is not a significant number of EROs in the cluster field (§3.3), one way to further confirm there is no bias in the r-band selected spectroscopic catalogue is to compare the weights computed for the r-band data to the K-band weights. Figures 6 and 7 show plots of the r-band weights and K-band weights for the clusters MS1358+62 and MS0302+16. MS1358+62 has the best spectroscopic completeness of the sample, while MS0302+16 has the worst. The weight functions show the characteristic dip at bright magnitudes ($r < 20$, $K < 16$) and the gradual fall-off at fainter magnitudes. The dip at bright magnitudes occurs because most of the bright galaxies are close together in the cluster core and getting slits on all of them is difficult, even with the multiple-mask strategy of CNOC1. The weight functions are similar between the K-band and r-band for both clusters, and this behavior is similar for all clusters in the sample. Therefore, we conclude that the r-selected spectroscopy is still representative of the K-band sample of galaxies.
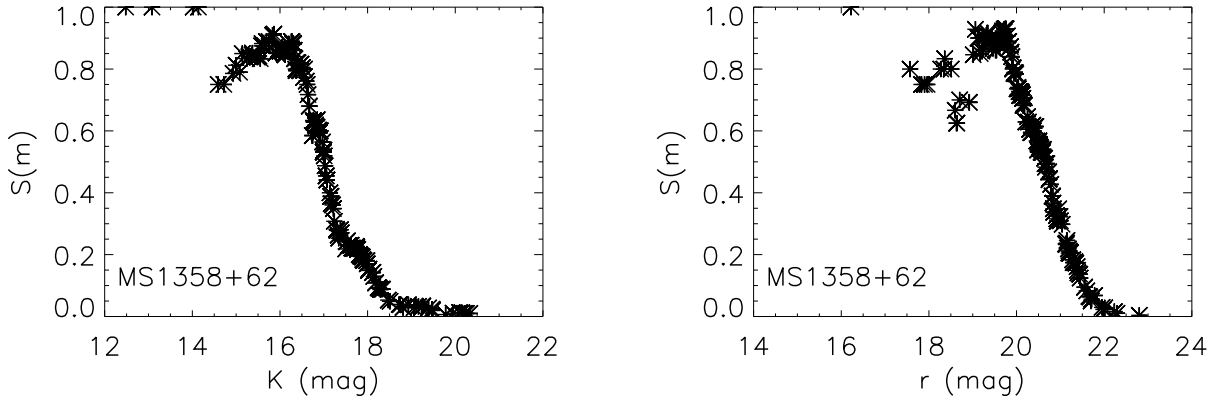
Figure 2.6 An example of the inverse of the magnitude weights (S(m)) for the galaxies in MS1358+62. Spectroscopic coverage of this cluster is very complete and the distribution of K-band weights is similar to the *r*-band weights.
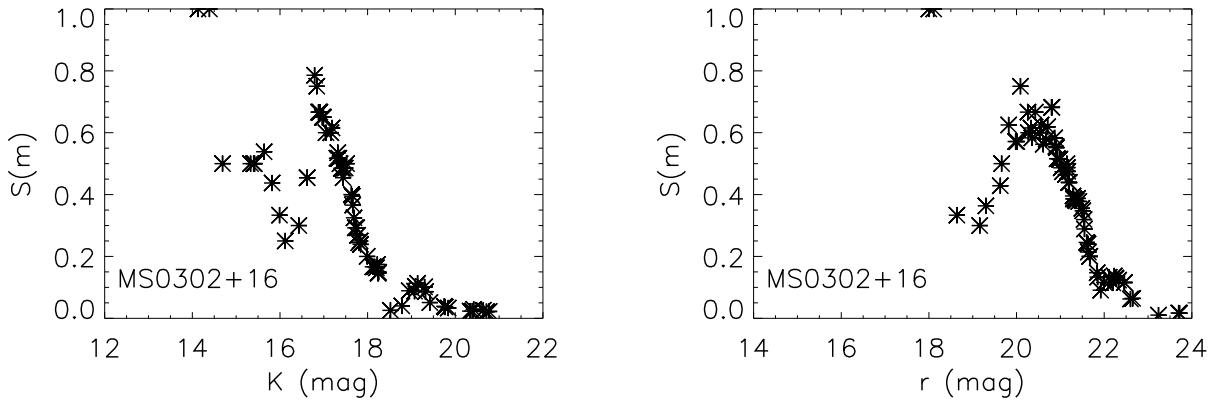
Figure 2.7 As Figure 6 for the cluster MS0302+16. Spectroscopic coverage of MS0302+16 is somewhat poor, however the distribution of K-band weights is still similar to the *r*-band weights.

2.6 Cluster Density Profiles

The mass density profiles and *r*-band number density profiles for the CNOC1 clusters have already been measured using the spectroscopic dataset by several authors (Carlberg et al. 1997a, 1997b; van der Marel et al. 2000). Here we compute the K-band selected luminosity and number density profiles as a comparison to check whether K-band selected galaxies (which better trace stellar mass) produce profiles that are different from *r*-selected galaxies. Computing the luminosity and number density profiles also allows us to compare the K-band density profiles of the higher-redshift CNOC1 clusters to the K-band density profiles of lower-redshift clusters (e.g., L04, R04).

The density profiles are constructed by stacking all 15 clusters into an ensemble cluster. Before adding galaxies to the ensemble cluster the radius of each cluster is normalized by its R_{200}. The number density profile is calculated by totaling the number of cluster galaxies with $K < K^* + 1$ in circular shells, scaling each galaxy by its spectroscopic weight (§4). The luminosity profile is computed in the same manner using the K-corrected, and evolution corrected (see §6.1) luminosity of galaxies with $K < K^* + 1$.

The clusters do not have homogeneous radial coverage and most are observed in a strip running through the cluster center. Therefore, the total counts or total luminosity in each shell is multiplied by the relative coverage of the shell before converting to a surface density. Some clusters also have coverage that extends to a larger R than others. To reduce the noise at large R from poorly sampled clusters, the contribution from individual clusters is truncated at the radius where the actual coverage of the shell is less than 10% and each data point in the ensemble cluster is weighted by the number of clusters that contribute to it. The data for the ensemble cluster extends to $1.5R_{200}$.

In the top panel of Figure 8 we plot the cluster number density profile (including the BCGs) and in the bottom panel we plot the luminosity density profile (excluding the BCGs). The data are fit to a projected NFW (Navarro et al. 1997) profile of the form derived by Lokas & Mamon (2001)

$$\Sigma(R) = Ac^2 g(c) \frac{1 - |x^2 - 1|^{-1/2} C^{-1}(1/x)}{(x^2 - 1)^2}, \tag{2.2}$$

where c is the concentration parameter, $x \equiv R/r_s$ and

$$g(c) = [\ln(1+c) - c/(1+c)]^{-1}, \tag{2.3}$$

$$C^{-1}(x) = \begin{cases} \cos^{-1}(x) & \text{if } R > r_s \\ \cosh^{-1}(x) & \text{if } R < r_s. \end{cases} \tag{2.4}$$

The parameters A and c are fit using the Levenberg-Marquardt least-squares technique for χ^2-minimization (Press et al. 1992). The best fit concentration parameter for the galaxy number density profile is $c_g = 4.13 \pm 0.57$. This agrees well with the $c_g = 3.7$ calculated by Carlberg et al. (1997b) using the r-band photometry. It is also similar to the best-fit concentration of the K-band luminosity profile, $c_l = 4.23 \pm 0.70$.

Interestingly, a good fit for the luminosity profile can only be obtained when the luminosity of the BCGs is excluded. The asterisk in the bottom panel of Figure 8 shows the value of the central point in the luminosity density with the BCGs included. This

central part is better described by a power-law fit (dashed line) with an index of n = -1.38 ± 0.03. The power-law can describe the luminosity profile with BCGs included approximately as well as the NFW profile does with the BCGs removed (reduced-χ^2 = 2.97 and 2.79 respectively). It is perhaps surprising that the *number* density profile can be described by an NFW profile when the BCGs are included, but the *luminosity* density profile can only be fit when the BCGs are removed. This illustrates the unique nature of the BCG luminosity in the context of the formation of large-scale structure. The distribution of K-band light closely follows the distribution of K-band-selected halos throughout the cluster which suggests the average luminosity per halo is roughly constant for cluster galaxies, except the central galaxy which is by far the brightest galaxy residing in a single halo. This is also intuitively supported by the cluster LFs (§6 & §7) where the luminosity distribution of cluster galaxies is well-fit by a Schechter function, except for the BCGs which are much brighter than the rest of the population and are more abundant than a Schechter function would predict.

How do the luminosity and number density profiles compare to the cluster mass profiles? van der Marel et al. (2000) computed the mass profile of the CNOC1 clusters with detailed Jeans equation analysis. They showed that a variety of generalized density profiles fit these data well, with the best-fitting NFW model having c_{DM} = 4.17 (unfortunately, no error-bar is quoted for this value). This is nearly identical to the concentration of the K-band number and luminosity density profiles and suggests that both the stellar mass contained in galaxies (excluding the BCGs) and the stellar-mass selected subhalo population, tightly trace the dark matter mass. The same conclusion was made by both Carlberg et al. (1997b) and van der Marel et al. (2000) using the r-band selected number density. However, if the BCGs are included in the luminosity profile, it appears that stellar mass may dominate over dark matter in the cluster core. The same trend is seen by Sand et al. (2004) using a sample of 6 clusters in the same redshift range ($0.17 < z < 0.44$) selected for having radial arcs. Sand et al. (2004) use a combination of strong-lensing, BCG velocity distribution and BCG luminosity to model the ratio of luminous and dark matter in cluster cores. Unfortunately, the K-band photometry and the van der Marel et al. (2000) velocity dispersion profile do not reach the resolution of the Sand et al. (2004) sample at small radii and therefore we can only remark that the CNOC1 profiles appear to be consistent with their result.

A comparison of the cluster number density profiles to those measured at lower redshift shows that the K-band light in the somewhat more massive, higher-redshift, CNOC1 clusters is more concentrated, at the 2σ level. L04 find $c_g = 2.88^{+0.21}_{-0.10}$ for an

ensemble of 93 $z < 0.1$ clusters using K-band photometry from 2MASS. Similarly, R04 measure $<c_g> = 2.83 \pm 0.56$ in the K-band for the 9 CAIRNS clusters. Unfortunately, because these samples and the CNOC1 clusters have different masses and are at different redshifts, understanding why their concentrations differ is not entirely straightforward.

N-body simulations show that c (for dark matter) is: 1) higher in lower-mass halos; 2) higher in halos which collapse first; and 3) for virialized halos becomes higher with decreasing redshift as the halo accretes mass (e.g., Navarro et al. 1997; Wechsler et al. 2002). However, the simulations show that the dependence of c on 1) and 3) is relatively weak, especially for cluster-mass halos. Given that the concentration parameter is most strongly dependent on the collapse epoch of the halo, the factor of $\sim$ 1.5 difference between the concentrations of these samples suggests an earlier collapse time for the CNOC1 clusters. Furthermore, the fact that the CNOC1 clusters are more massive and observed at an earlier epoch than the L04 and CAIRNS clusters would seem to support this interpretation. Nonetheless, these simulations are for dark matter only, and do not measure the concentration of stellar light. Therefore, it remains possible that the difference in concentrations between the samples could be caused by a redshift evolution in the concentration of stellar light, rather than different collapse epochs for the two samples.

Interestingly, the concentration of galaxy number density and dark matter are the same in the CNOC1 clusters (within the precision of our data), yet this is not seen in the local clusters. Both L04 and R04 find that the K-band selected c_g is smaller than c_{DM} for their clusters. Their results also agree with the simulations of Nagai & Kravtsov (2005) who find $c_{DM} > c_g$ for a set of 8 clusters in a full hydrodynamical simulation. Five of the simulated clusters have c_{DM} which is a factor of ~ 2 larger than c_g, while 2 clusters have $c_{DM} \approx c_g$. The 8th cluster has $c_g > c_{DM}$. These ratios are similar to the CAIRNS clusters, where the mean ratio between c_{DM} and c_g (for the NFW model) is 2.3 ± 0.67. While the errors in c_g and c_l for the CNOC1 clusters are somewhat large, they still exclude the possibility that the number density of K-band-selected galaxies is less concentrated than the matter by a factor of 2 at the 3σ level ($c_g/c_{DM} = 0.99 \pm 0.14$ and $c_l/c_{DM} = 1.01 \pm 0.17$), suggesting a real difference between the moderate and low-redshift cluster samples.

If we assume that the ratio of $c_{DM}/c_g \approx 2$ at $z = 0$ seen by R04 and L04 is universal for galaxy clusters, then this suggests the possibility of an evolution in the relative c_g and c_{DM} with redshift. For c_{DM} to increase faster than c_l or c_g would require a pref-

erential radial segregation of dark matter and light during the accretion process. One consideration is that such a segregation could be mimicked by a redshift evolution in the radial distribution of cluster galaxy stellar populations. While possible, this is unlikely to be the case for our profiles which are computed using K-band light, which is fairly insensitive to star-formation properties or dust. Furthermore, they are computed using a cut of $K < K^* + 1.0$ where K^* is very well determined and consistent with simple passive evolution (§6.3).

The simulations of Nagai & Kravtsov (2005) show that accreted galaxies near the cluster core have had $\sim 70\%$ of their total halo mass stripped since being accreted by the cluster, whereas those near the virial radius have lost only $\sim 30\%$. Since stellar mass tends to be tightly bound within a dark matter halo, the process of tidal stripping of dark matter subhalos could plausibly cause a differential evolution in c_{DM} and c_g for galaxy clusters. The tidally stripped dark matter of the infalling galaxies may sink to the center of the cluster halo and increase c_{DM}, while the stellar mass will remain bound to the subhalo and continue to orbit within the cluster halo, where it preferentially spends more time at the perimeter.

While this is a possibility, we note that with the current dataset it is impossible to untangle whether the difference in the relative concentrations of dark matter and stellar mass between the moderate and low-redshift samples is caused by such an evolution or simply because the ratio of c_{DM} to c_g is not universal for all cluster masses at all epochs. It would be interesting to compare these results with simulations that trace the redshift evolution of the cluster c_{DM} and c_g. It would also be useful to compare to simulations that have the same c_{DM} as the CNOC1 clusters. We note that all of the Nagai & Kravstov (2005) clusters have higher concentrations than the CNOC1 clusters and that the two clusters with the lowest concentrations (which are similar to the CNOC1 clusters) have a ratio of $c_{DM}/c_g \approx 1$.

2.7   Cluster Luminosity Functions

In this section we compute the K-band LFs for cluster galaxies. Our technique for creating stacked, k-corrected LFs using clusters at different redshifts and correcting for imaging of varying depths is discussed in §6.1. The method outlined there is used to create all LFs in the remainder of the paper (§6 and §7). In §6.2 we construct an ensemble cluster LF using all 15 clusters centered at $z \sim 0.3$. This allows us to fit the
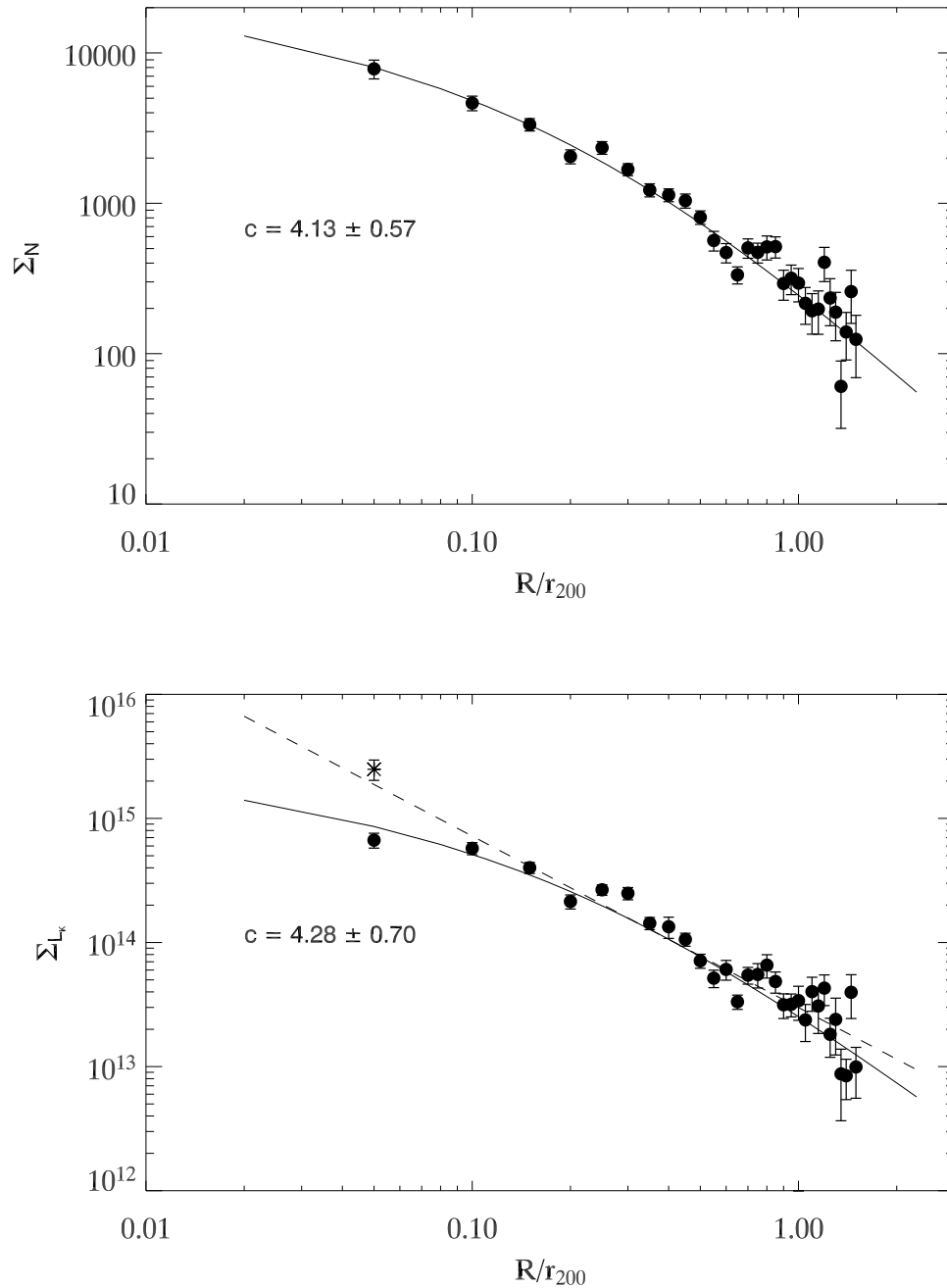
Figure 2.8 Top Panel: Surface number density per virial area of K-band selected galaxies vs. radius. The solid line is the best-fit NFW profile. Bottom Panel: Surface K-band luminosity density per viral area vs. radius. The asterisk is the luminosity density calculated when the BCGs are included. The solid line is the best-fit NFW profile excluding the BCGs. The dashed line is the best-fit power-law (γ = -1.38 $\pm$ 0.03) including the BCGs.

faint-end slope of cluster LF (α) as well as compare it to field LFs at the same redshift. In §6.3 and §6.4 we examine the redshift evolution of K^* as well as its dependence on cluster mass using a fixed value of α.

2.7.1 Technique for Constructing Luminosity Functions

LFs are constructed by stacking the sample of 15 clusters into either a single cluster (§6.2, §7.2) or else into 3 redshift (§6.3, §7.3) or mass (§6.4, §7.4) bins with 5 clusters per bin. Many clusters have enough spectroscopy to determine their individual LFs reasonably well; however, stacking the clusters improves the statistical errors. The LFs are constructed by counting the number of cluster galaxies (multiplied by their spectroscopic magnitude weights) within R_{200} in bins of 0.25 mag. Most clusters have some galaxies that lie outside the projected R_{200} but have velocities consistent with cluster membership; these galaxies are excluded from the LFs. R04 showed that the K-band cluster LF becomes fainter by ~ 0.5 magnitudes from the virialized to infall regions in local clusters. There is insufficient coverage of the infall region to compute a separate LF and therefore the LFs are constructed using only galaxies within the virialized region.

The cluster BCGs are not removed when computing the luminosity functions. The inclusion of the BCGs results in inflated reduced-χ^2's for the fits (because the BCGs do not follow a Schechter function); however, similar to the optical cluster LFs of de Propris et al. (2003), we find that removing the BCGs has no significant effect on the fitted value of K^* (~ 0.01 mag). Therefore, the BCGs are included as an indication of their abundance relative to other cluster galaxies. In the determination of all LFs (§6 and §7) no attempt is made to account for the incomplete coverage of R_{200} in some clusters. Most clusters have full coverage of R_{200}, and those that do not have a strip of observations across the cluster which provides reasonably equal sampling of the cluster center and the periphery.

The clusters are at different redshifts and therefore stacking them requires that the magnitudes of galaxies within each cluster be "redshifted" to a common redshift. For the ensemble LFs (§6.2, §7.2) and the LFs for clusters of different masses (§6.4, §7.4) we use absolute magnitudes at a common redshift of $z = 0.296$, the median redshift of the sample. This requires the computation of a distance modulus, k-correction and differential evolution correction for each galaxy. When we compute the redshift evolution of the LFs (§6.3, §7.3) we keep the conventions of the literature and use appar-

ent magnitudes. This requires only a differential distance modulus and differential k-correction.

k-Corrections

The k-corrections are taken from the models of Poggianti (1997) who list corrections for E, E1 (an early-type with longer duration episode of star-formation, which we consider an S0), Sa, and Sc types. The K-band k-corrections are fairly independent of spectral type; however, there are small differences, and therefore determining a spectral type for each galaxy is preferable. The availability of the optical photometry allows us to compute g - r colors and estimate the spectral type of each galaxy using a simple model for how the colors of different spectral types evolve with redshift. We have fit the g - r vs. r color-magnitude relation of each cluster (Paper III) using the biweight estimator (Beers et al. 1990). For the purpose of spectral classification of the galaxies, we assume that all cluster galaxies that are < 0.1 magnitudes bluer than the cluster red-sequence are early-type galaxies. The redshift/color models of Fukugita, Shimasaku, & Ichikawa (1995) are then used as template colors for the remaining galaxies. Rather than directly using the colors in their models, the color of an early-type galaxy at the appropriate redshift is determined empirically from the cluster color-magnitude relation, and then the *differential* colors from the models are used to determine whether galaxies are S0, Sa, or Sc types. This approach minimizes any systematics which might be caused by incorrect normalization of the models. Furthermore, because the colors between the 4 spectral types are significantly different, it implies an error of ±1 spectral type at most. This is fairly inconsequential as the k-corrections differ by only 0.02 - 0.05 mag across all spectral-types for galaxies at $0.2 < z < 0.55$.

Evolution Correction

Previous studies have shown that there is strong luminosity evolution with redshift in the K-band for both field (Drory et al. 2003, Feulner et al. 2003, Pozzetti et al. 2003) and cluster (dP99) galaxies. Therefore, a differential evolution correction must be included in the LFs to "evolve" higher and lower redshift clusters to the appropriate redshift. We use the evolution corrections listed in Poggianti (1997). The Poggianti models consist of 15 Gyr old galaxies in a $q_0 = 0.225$, $H_0 = 50$ km s^{-1} cosmology. We have adjusted the evolution corrections by assuming the galaxies are 13.7 Gyr old at the

present, and then mapped the $q_0 = 0.225$ cosmology on to our own by comparing lookback times. Once this correction is made, the Poggianti evolution corrections are in excellent agreement with our own measurement of the luminosity evolution for cluster galaxies (see §6.3). Computing the LF at the median redshift of the clusters, rather than correcting to $z = 0$ allows smaller evolution corrections (which are of order 0.08 to 0.18 mag depending on spectral-type and cluster redshift) and therefore, the choice of evolution model does not strongly affect the results from the LFs.

Completeness

Not all clusters have photometry which is complete to the same absolute magnitude; hence, to maximize the depth of the stacked LFs we adopt the approach of Schechter (1976). The clusters are ranked by limiting absolute magnitude, and the limiting magnitude of the stacked LFs is set by the depth of the deepest cluster. Clusters are then added to the stacked LF in the order of deepest to shallowest. The counts at magnitudes fainter than the completeness limit for a shallower cluster are extrapolated from the stacked LF of the deeper clusters. Using this technique means that the faintest bins in the stacked LF are scaled versions of the faint-end of the deepest clusters, whereas the bright end is determined from all clusters. While not strictly correct, it maximizes the information on the bright-end of the LF, where the statistics are poorest. Furthermore, most of the clusters are complete to approximately the same depth ($\sim K_* + 2$) with only the two highest redshift clusters (MS0016+16 and MS0451-03) being notably shallower ($\sim K_* + 1$); hence, only the faintest bins are affected by this approach. Because we do not use statistical background subtraction we assume the errors in each bin of the LF to simply be Poisson errors. The errors are computed *before* the faint-end of the LF is scaled.

The fitting of all LFs is done using the Levenberg-Marquardt algorithm for χ^2 minimization (Press et al. 1992). Errors for the parameters are estimated from the covariance matrix.

2.7.2 Ensemble Luminosity Function and Comparison of the Cluster and Field Luminosity Function at Moderate Redshift

Here we construct a composite LF from all 15 CNOC1 clusters. By stacking the clusters we reduce the statistical errors and are able to make a good measurement of both K^*

and α using imaging of only moderate depth.

Figure 9 shows the composite LF for all clusters centered at $z = 0.296$, the median redshift of the sample. The best-fit Schechter function parameters are $K^* = -24.53 \pm 0.15$ and $\alpha = -0.84 \pm 0.08$. The fit parameters for this LF as well as all other LFs computed in this paper are listed in Table 3. If we compare this LF to the local K-band cluster LF measured by L04 we find the following. 1) The faint-end of the LF has not evolved from $z = 0$, to $z = 0.3$. L04 find that the best-fit α for their LF is $\alpha = -0.84 \pm 0.02$, which is identical to the best-fit for the CNOC1 clusters. 2) The evolution in K^* is consistent with a passive luminosity evolution of the stellar population. L04 measure $K^* = -24.02 \pm 0.02$ for their clusters, which implies K^* for the CNOC1 clusters is 0.51 ± 0.15 mag brighter at $z = 0.3$. The Poggianti evolution model (adapted to our cosmology, §6.1) predicts 0.31 magnitudes of luminosity evolution from $z = 0$ to $z = 0.3$ for an early-type galaxy, which is smaller, but consistent with the observed evolution. A more detailed investigation and discussion of the redshift evolution of K^* is presented in §6.3.

The cluster LF shows no significant change (other than the passive aging of the stellar populations) with redshift between $z = 0$ and $z = 0.3$; however, it is worthwhile to consider whether it depends on environment at $z = 0.3$. In the local universe the K-band LFs of the field and cluster environments are different. B01, Lin et al. (2003), L04, R04, Ramella et al. (2004), and Kochanek et al. (2003) have all shown that the field and cluster have similar faint-end slopes, but that K^* is brighter (by $\sim 0.2 - 0.4$ mag) in clusters. Recently, several $z > 0.1$ field K-band LFs have become available in the literature, and we can now compare the cluster and field LFs at $z = 0.3$.

Pozzetti et al. (2003) use the K20 survey with a set of ~ 500 spectroscopic redshifts to determine the evolution of the K-band field LF from $z = 0.2$ to $z = 1.5$. They find that the evolution of K^* to $z \sim 1$ is consistent with a luminosity evolution of $\Delta K^* = -0.54 \pm 0.12$. The MUNICS survey group combined their K-band photometry with spectroscopic (Feulner et al. 2003) and photometric (Drory et al. 2003) redshifts to determine the evolution of the K-band field LF from $z = 0$ to $z \sim 1$. Feulner et al. (2003) find that the K-band field galaxy LF evolves by $\Delta K^* = -0.70 \pm 0.30$ magnitudes from $z = 0$ to $z \sim 1$, while Drory et al. (2003) find similar ($\Delta K^* \sim -0.5$ to -0.7 mag) results.

The faint-end slopes of the field LFs are steeper than the $\alpha = -0.84 \pm 0.08$ measured for the CNOC1 clusters. In their $z = 0.2 - 0.65$ redshift bin, Pozzetti et al. (2003) find that $\alpha = -1.25^{+0.25}_{-0.20}$, and Feulner et al. (2003) assume that $\alpha = -1.1$ in their $z = 0.1 - 0.3$

and z = 0.3 - 0.6 redshift bins. Unfortunately, the correlation between K* and α makes the comparison of K* from LFs that use different values of α difficult to interpret. Therefore, we refit the cluster LF forcing α to be fixed at -1.1. This fit is shown as the dashed line in Figure 9. With α fixed at -1.1, the best-fit value for the cluster LF is K* = -24.93 $\pm$ 0.04 (the smaller error bar arises because α is held fixed).

The field LFs have coarse redshift bins, and therefore we can only compare the cluster and field LFs as an average over a broad redshift range. For example, the lowest redshift bin in the Pozzetti et al. (2003) study is $0.2 < z < 0.65$, which spans the entire redshift range of the CNOC1 clusters. The mean redshift of the CNOC1 clusters is similar to the mean redshift of the two lowest bins from Feulner et al. (2003), so we average those values to K* = -24.68 $\pm$ 0.26 at $z \sim$ 0.3. Comparing this to our value shows that K* is 0.25 $\pm$ 0.26 magnitudes brighter in clusters than the field at $z \sim$ 0.3. If we compare our LF to the z = 0.2 - 0.6 redshift bin of Pozzetti et al. (2003) who obtain K* = -24.87$^{+0.54}_{-0.77}$ we find that K* in clusters is 0.05$^{+0.54}_{-0.77}$ magnitudes brighter than in the field. Both these values agree within the large error bars; however, the error bar on the Feulner et al. (2003) value is significantly smaller, and consistent with the results from the much larger photometric redshift study of Drory et al. (2003). Therefore, we adopt ΔK* = -0.25 $\pm$ 0.26 between field and cluster at $z \sim$ 0.3 as our best result.

Unfortunately, the errors bars on the field values of K* are quite large, and clearly any difference between the cluster and field at moderate redshift is of the order of the error bars or less. Despite the large error bars, it is interesting to note that the difference in K* between cluster and field galaxies at z = 0.3 is similar to that at $z \sim$ 0. This suggests that the processes which cause the K-band luminosity function, and by corollary the stellar mass function, to be brighter in clusters (e.g., hierarchical growth of cluster galaxies from mergers) probably have already occurred by $z \sim$ 0.3, and that there is little differential evolution since then. A larger field K-band study, with finer redshift bins and better constraints on K* would be useful for investigating this further.

2.7.3 Redshift Evolution of the Cluster Luminosity Function

In §6.2 we showed that the composite LF for all 15 CNOC1 clusters, when compared with $z \sim$ 0 clusters, is consistent with no evolution in the faint-end slope and passive evolution of the stellar populations. Here we make a more detailed examination of the redshift evolution of K* by separating the clusters into 3 redshift bins with 5 clus-
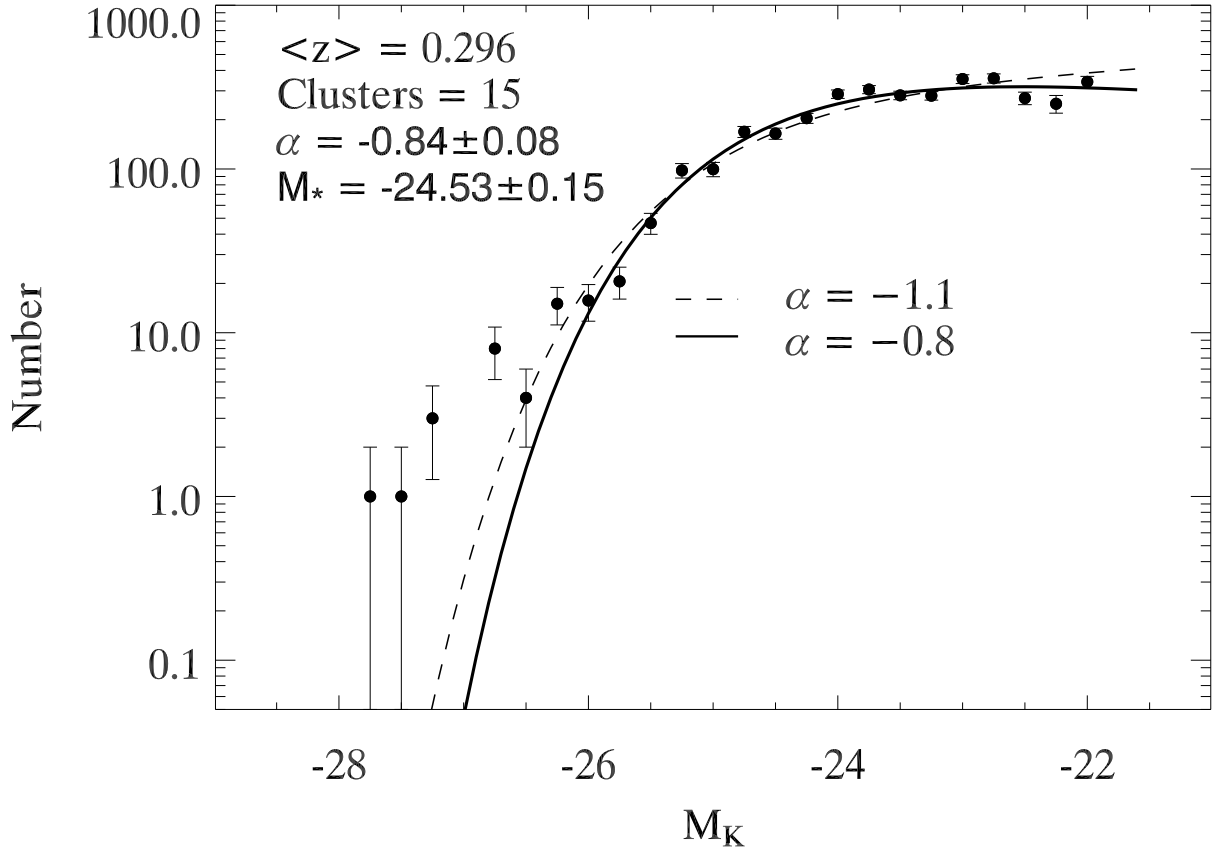
Figure 2.9 Stacked LF for all 15 clusters, corrected to a redshift of $z = 0.296$. The solid line is the best-fit Schechter function ($K^* = -24.53 \pm 0.15$, $\alpha = -0.84 \pm 0.08$). The dashed line is the best-fit Schechter function with a fixed $\alpha = -1.1$ ($K^* = -24.93 \pm 0.04$). The bright end of the LF diverges from a Schechter function because the BCGs are included.

ters per bin. The LFs are computed at the mean redshift of the 5 clusters within each bin. This corresponds to redshift bins of $z = 0.21, 0.29$, and 0.46. For these LFs we use apparent rather than absolute magnitudes so that we can make a direct comparison to the LFs of dP99.

When the LFs are separated into redshift bins, they do not have enough depth to obtain meaningful constraints on both K^* and α (especially in the highest redshift bin). Therefore, we hold α constant and fit only K^* and ϕ^*. Rather than assume $\alpha = -0.84$, the best-fit value for the ensemble LF, we adopt the value of $\alpha = -0.9$ assumed by dP99, which is consistent with our best-fit. Because of the strong correlation between K^* and α, assuming the same faint-end slope also allows for a straightforward comparison of K^*'s from different studies. We note that given that there is a $\sim 10\%$ uncertainty in

α from the combined LF (§6.2), the error on K* for a given α is an underestimate of the total error budget. To obtain an estimate of the total error budget for K* which includes the uncertainty in α, we refit the LFs with values of α that range from -0.76 to -0.92 (i.e., enclosing the 1σ error bar in α from §6.2). This refitting results in values of K* that are +0.15 magnitudes fainter when α = 0.76 and -0.05 magnitudes brighter when α = 0.92. These additional deviations are comparable to the fitting errors with fixed αs (see Table 3).

In Figure 10 we plot the LFs and the Schechter function fits for the 3 redshift bins. The redshift evolution of K* for the CNOC1 clusters is compared with the dP99 values in Figure 11. The lines in the figure are models of single-burst populations with a z_f = 1.0, 1.5, 2.0, 2.8, and 5.0 constructed using the Bruzual & Charlot (2003) code. The model is a 0.1 Gyr duration single-burst with solar metallicity followed by an exponentially declining star-formation rate with τ = 0.1 Gyr. The model is normalized to K* = -24.02 at z = 0, the L04 value which was measured using a faint-end slope (α = -0.84) that is similar to the α = -0.9 assumed for our clusters and the dP99 clusters. Figure 11 demonstrates that the stellar populations in CNOC1 clusters are consistent with a passively evolving population formed at z > 1.5; however, the values of K* for the CNOC1 clusters are significantly fainter than those of the dP99 clusters. If we compare the z = 0.21, 0.29, and 0.46 bins of the CNOC1 clusters to the z = 0.20, 0.32, and 0.46 bins of dP99, K* for the CNOC1 clusters is fainter by 0.36, 0.19, and 0.76 mag, respectively, and are 0.44 mag fainter on average.

We have considered several possible explanations for the very different values of K* between the studies, the most likely of which is the systematic differences in the photometry. In §3.4 we noted that for the 3 clusters that overlap our sample and the SED02 sample (the data used to compute the dP99 LFs), our photometry is systematically fainter by 0.21 mag. If the entire datasets differ by this much, then this accounts for approximately half of the discrepancy in K*.

It is possible that the different radial coverage in the two samples is partially responsible for the difference in K*. R04 showed that the K-band cluster LF becomes fainter from the virial to infall region. If a such radial dependence also exists within the virial region, then this may partially explain the discrepancy because the dP99 data cover only the central region of the clusters ($\sim$ 0.5 - 1 Mpc) whereas our observations cover out to R$_{200}$ ($\sim$ 1 - 2 Mpc) for most clusters. We test this possibility by recomputing the LFs using only galaxies within 0.5 Mpc of the cluster center. K* from those luminosity functions is brighter; however, by only $\sim$ 0.1 magnitudes, which is

smaller than the discrepancy, even if photometry accounts for a portion of it. We also consider the possibility that the size of the magnitude bins used for the LFs may influence the value of K^*. dP99 use larger bins (0.5 mag) which might bias the value of K^* to brighter values because of the poor statistics at the bright-end of the LF. When we recompute our LFs using 0.5 mag bins instead of 0.25 mag bins we find that this has no effect on K^*.

Perhaps the most significant difference in the methods used to derive the luminosity functions is that we use spectroscopic redshifts, whereas dP99 use statistical background subtraction. In principle, both methods work equally well, however, the statistical method requires the stacking of a large number of clusters, because cosmic variance in the background can cause large errors in the LFs. Two of the three dP99 redshift bins that compare with ours have only a few clusters in each bin (3, 9, and 2 respectively). A higher than average background in the cluster field might result in an overestimate of the number of cluster galaxies. We cannot be conclusive as to why the value of K^* in the CNOC1 clusters is significantly fainter than in the dP99 sample; however, our simple comparisons suggest that the size of the magnitude bins and the different radial coverage between the samples has little effect on K^*. Most likely, the difference is caused by differences in the photometry (§3.4), and possibly because of the different techniques used for background subtraction.

Comparing the LFs to the $K^* = -24.02$, $\alpha = -0.84$ LF of L04 shows there is an evolution of $\Delta K^* = -0.35 \pm 0.06$ mag from $z = 0$ to $z = 0.46$. This agrees well with the passive evolution predicted from the Bruzual & Charlot single burst, $z_f = 2.8$ model ($\Delta K^* = -0.40$) and the passive evolution from the Poggianti (1997) model ($\Delta K^* = -0.39$). We conclude that the CNOC1 clusters agree well with the scenario where the bulk of the stars in galaxies are formed at high-redshift and evolve passively thereafter. Furthermore, the close relation between the K-band light and stellar mass of a galaxy suggest that the stellar mass function of $K < K^* + 2$ cluster galaxies is unchanged up to $z = 0.3$.

It is difficult to understand how no evolution in α (§6.2) and purely passive evolution of K^* is compatible with the L04 HOD data which suggest a significant number of mergers in this redshift range. Even if mergers populate all parts of the LF appropriately as to maintain the overall shape, K^* would have to be fainter than passive evolution at higher-redshift to account for the breakup of galaxies into their progenitors. It is possible that the reduction in luminosity of galaxies at high redshift due to breakup could be offset by increased amounts of star-formation which correspond-

ingly brighten the galaxy, and therefore mimic passive evolution; however, such a scenario seems contrived, and the most reasonable interpretation of the data is that galaxies in massive, relaxed, X-ray-selected clusters do not experience a significant number of mergers between $0 < z < 0.3$. This may not be a surprising result, as the high velocity dispersion of galaxies in the cluster environment makes merging diffi- cult. The passive evolution of the LFs at moderate redshift does not rule out the pos- sibility that mergers play a role in cluster galaxy evolution; however, it suggests that if they are important, they most likely occur in higher-redshift systems that are in the process of relaxing (e.g., MS1054+03, Tran et al. 2005), rather than massive virialized clusters at $z \sim 0.3$.
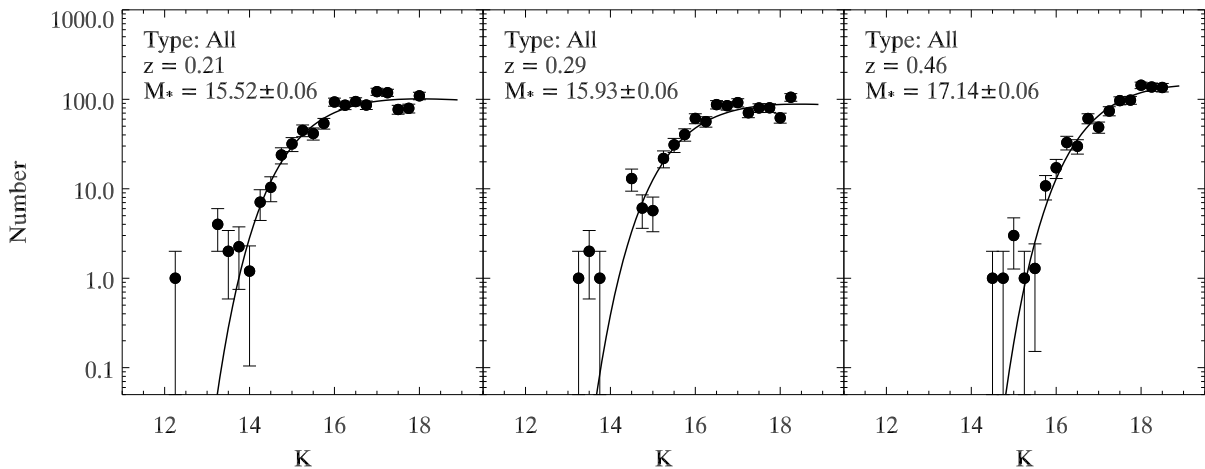
Figure 2.10 Stacked LF for clusters in three different redshift bins. Each LF is composed from a stack of 5 clusters that have been corrected to the mean redshift listed in each panel. The solid-line is the best-fit Schechter function assuming α = -0.9. The bright- end of the LFs sometimes diverge from a Schecheter function because the BCGs are included.
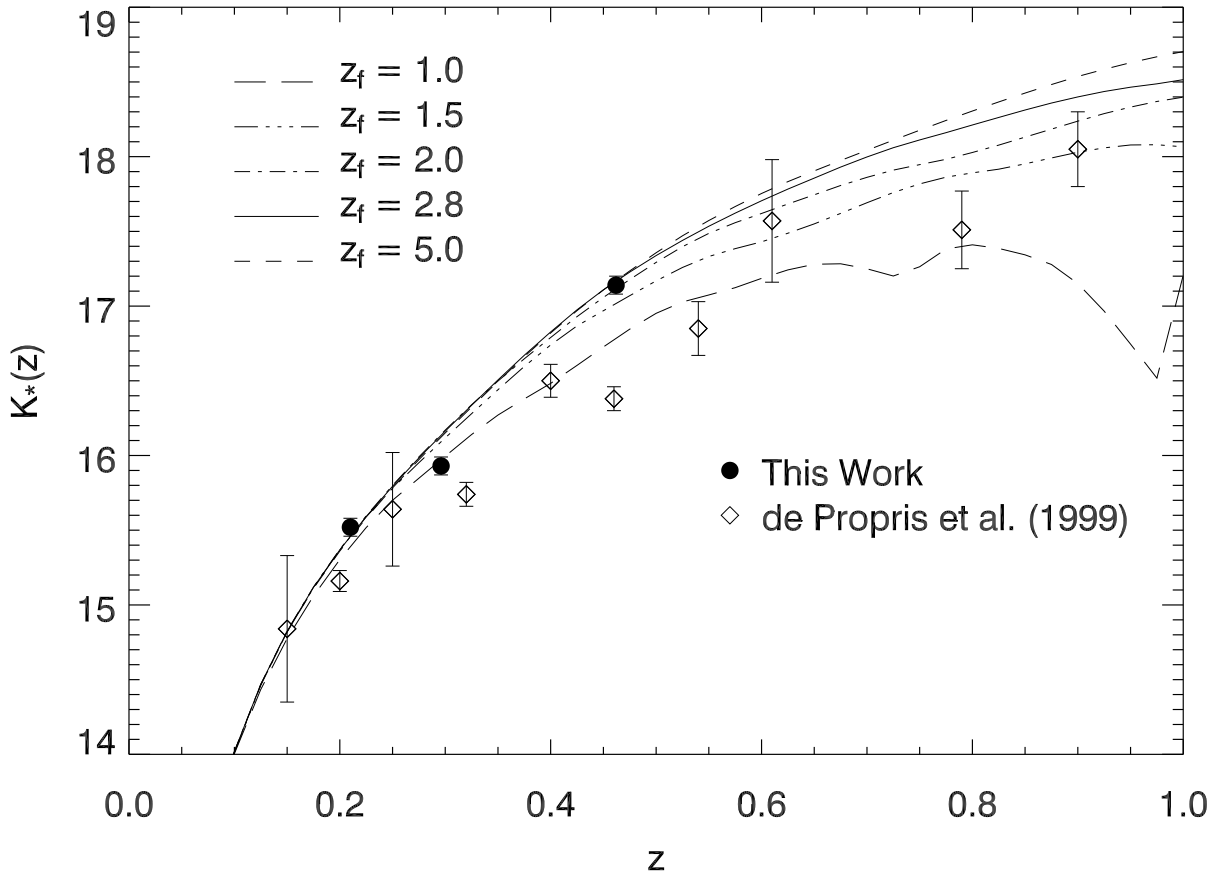
Figure 2.11 Evolution of K* as a function of redshift. Solid points are the CNOC1 cluster LFs (Figure 10) and the open diamonds are clusters from dP99. The long-dashed, triple-dot-dashed, dot-dashed, solid, and dashed lines are single burst models with z_f = 1.0, 1.5, 2.0, 2.8, 5.0 respectively. The models have been normalized to the low-redshift value of K* from the L04 study (see text). The bright galaxies in the CNOC1 clusters are consistent with a scenario where the bulk of the stellar mass is formed at high redshift and evolves passively thereafter.

2.7.4 Luminosity Functions of Different Mass Clusters

Here we separate the CNOC1 sample into 3 mass bins using cluster dynamical masses determined from the velocity dispersions of Carlberg et al. (1997a, see Paper II for values of M_{200} computed using a ΛCDM cosmology) and investigate the dependence of the K-band LF on cluster mass. The mean masses of the three bins are $<M_{200}>$ = 2.73 $\times 10^{14}$ $M_{\odot}$, 5.96 $\times 10^{14}$ $M_{\odot}$, and 1.34 $\times 10^{15}$ $M_{\odot}$, and we designate these low, mid, and high-mass bins, respectively.

Figure 12 shows the LFs for the 3 mass bins, as well as the best Schechter function fits, again using a fixed α = -0.9. The values of K* for the three mass bins are K* = -24.51 $\pm$ 0.08, -24.59 $\pm$ 0.06, -24.52 $\pm$ 0.05 for the low, mid and high mass bins respectively. This shows that there is no significant dependence of K* on cluster mass over the one order-of-magnitude range in mass covered by the CNOC1 clusters.

Interestingly, L04 do not find the same result in local clusters. They divide their sample of 93 clusters into high and low-mass subgroups (using masses determined from X-ray temperatures) and find that α is similar between the two groups (α = -0.84 $\pm$ 0.03 and -0.81 $\pm$ 0.04 for high-mass and low-mass clusters, respectively); however, K* is brighter by 0.16 $\pm$ 0.07 mag in high-mass clusters (K* = -24.10$\pm$ 0.04 in high-mass clusters vs. K* = -23.94 $\pm$ 0.06 in low-mass clusters). The L04 high-mass clusters have a mean M$_{200}$ similar to the mid-mass CNOC1 clusters, while their low-mass clusters have a mean M$_{200}$ similar to the low-mass CNOC1 clusters, and therefore the corresponding difference between those mass bins in the CNOC1 sample is ΔK* = -0.08 $\pm$ 0.10 mag.

The dP99 clusters have a similar redshift range as the CNOC1 clusters, and similarly, they do not show a dependence of K* on cluster mass. Although masses for their clusters were unavailable at the time, dP99 divided their sample into high and low optical richness and high and low X-ray luminosity (L$_x$) subgroups. Both optical richness and L$_x$ are correlated with cluster mass (Yee & Ellingson 2003; although there is some scatter) and therefore these subgroups can be considered roughly as high and low-mass subgroups. Similar to our result, dP99 find that within the errors, K* is the same between high and low richness and high and low L$_x$ clusters from z = 0.15 to z $\sim$ 1.0.

Given the uncertainty of our measurement of the difference in K* between different mass bins, our result is consistent at $< 1\,\sigma$ with both no dependence of K* on cluster mass (dP99) or a very weak ($\sim$ 0.1 mag) dependence of K* on cluster mass (L04).

2.8   Luminosity Functions of Different Spectral-Types

The analysis in §6 demonstrated that the K-band cluster LF shows no evolution in α and only passive evolution in K* from z = 0 to z = 0.3. Because of the close correlation between K-band light and stellar mass it also suggests no strong evolution in the stellar mass function of cluster galaxies over this redshift range. However, stud-
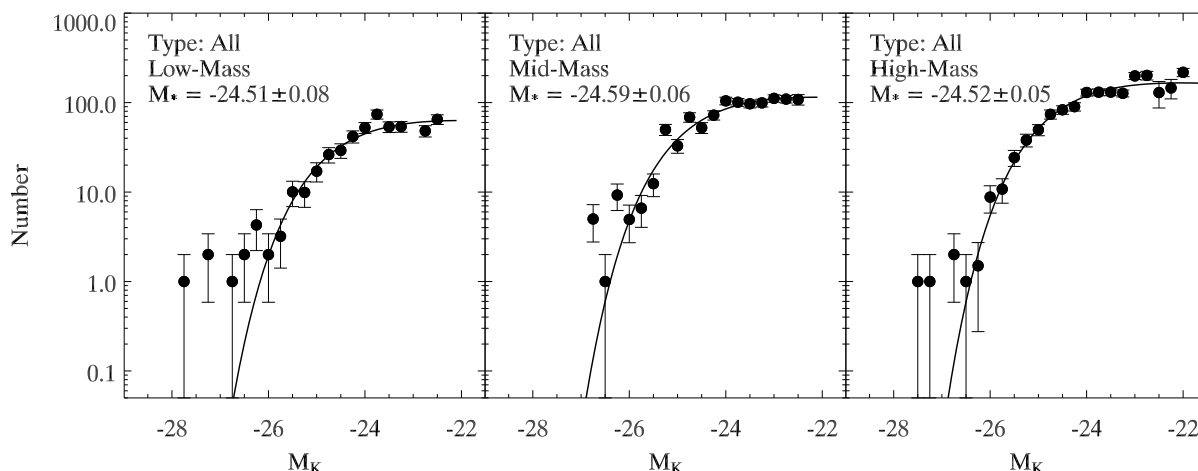
Figure 2.12 Stacked LF for clusters in three different mass bins. Each LF is composed from a stack of 5 clusters. The solid-line is the best-fit Schechter function assuming α = -0.9. The bright-end of the LFs sometimes diverge from a Schechter function because the BCGs are included. There appears to be no correlation between K^* and mass for over the mass range covered by the CNOC1 clusters.

ies of the evolution of morphology-density relation (Postman et al. 2005, Smith et al., 2005, Dressler et al., 1997), as well as the star-formation rate in clusters (e.g., Balogh et al. 1999, Poggianti et al. 1999), and the Butcher-Oemler effect (Ellingson et al. 2001) suggest that there is significant evolution in the morphological and star-formation properties of the cluster galaxy population over the same redshift range. Therefore, it seems likely that that the LFs of the early and late-type populations will evolve differently over this redshift range, even though the combined LF of cluster galaxies shows only passive evolution.

This possibility can be addressed directly within the CNOC1 sample using the spectroscopy. Ellingson et al. (2001) performed Principal Component Analysis (PCA) on the spectroscopic data and classified galaxies into three broad spectral-types. In this section we use the PCA analysis and examine the K-band LF of these spectral-types. In §7.1 we briefly summarize the PCA decomposition. In §7.2 we construct a composite LF for the spectral types using all 15 clusters so that we can fit α. Using the best-fit values of α we study the redshift evolution of K^* and its dependence on cluster mass for the different spectral types in §7.3 and §7.4.

2.8.1   PCA Decomposition

Here we present a brief discussion of the PCA analysis. A thorough explanation of the fitting method and reliability of the spectral-typing is presented in Ellingson et al. (2001). The principal components of a galaxy's spectrum are determined by decomposing it using three galaxy types as eigenvectors: Elliptical, Emission-line, and Balmer-line. The template spectra used for these types are composite spectra drawn from the Las Campanas Redshift survey (Shectman et al. 1996). In the PCA analysis, each eigenvector is assigned an amplitude from 0 to 1, based on how well it represents the spectrum being fit. The total amplitude of all three eigenvectors adds up to 1. While this analysis is simplistic, it is quite effective at providing a reasonable quantitative measurement of the principal component of a galaxy's spectrum. Using the amplitudes of the PCA decomposition we divide the galaxies into 2 broad spectral-types: Early (ELL), and Emission + Balmer (EM+BAL). Galaxies with ELL > 0.5 are considered ELL, and those with ELL < 0.5 are considered part of the EM+BAL class. This provides a simple way to identify star-forming or recently star-forming galaxies from those which are dominated by absorption-lines and are likely to have been quiescent for at least a few Gyr. It is important to note that this analysis is a spectral analysis, not a morphological one. Galaxies which have early-type morphologies may still be considered EM+BAL galaxies if they show the appropriate spectral features (in fact, the BCGs in the highest redshift clusters all show emission lines and therefore do not fall into the ELL category). Separating galaxies by spectral-type (rather than morphology) is similar to the analysis done by B01 for low-redshift clusters and groups (although they use line indices, not PCA), and therefore allows easy comparison between moderate and low-redshift clusters.

2.8.2   Ensemble Spectrally-Types Luminosity Functions

In Figure 13 we show the LFs for ELL and EL+BAL classes. Immediately obvious is the difference between the faint-end slopes of the two LFs. The best-fit faint-end slope for the EM+BAL galaxies is α = -0.95 $\pm$ 0.27, while for the ELL galaxies it is α = 0.17 $\pm$ 0.18. This difference indicates significant redshift evolution in the faint populations of these spectral-types because in the local field and local clusters their faint-end slopes are nearly identical.

In the local field, Kochanek et al. (2001) showed that for morphologically-typed galaxies, early and late-types have faint-end slopes of -0.92 $\pm$ 0.10 and -0.87 $\pm$ 0.09

respectively. Bell et al. (2003) performed the same analysis using spectral-types from Sloan Digital Sky Survey (SDSS) spectroscopy and 2MASS photometry and found that α was similar across the types, but that it was slightly shallower for the early-types. In local clusters B01 examined a set of galaxies in the field, group, and cluster environment using 2MASS photometry and spectroscopic redshifts from the Las Campanas Redshift Survey. They split their sample into emission-line (EL) and no-emission-line (NEL) types and although the error bars are large, they find that local cluster EL and NEL galaxies have comparable faint-end slopes (α = -1.18 $\pm$ 0.76 for EL and α = -1.28 $\pm$ 0.50 for NEL). They also find that these values of α are similar to their local field and group values for EL and NEL galaxies.

Our result suggests a strong decrease in the faint ELL population in clusters from $z = 0$ to $z = 0.3$, whereas the faint EM+BAL population remains mostly unchanged. We can make a rough estimate of the relative decrease of $K^* < K < K^* + 2$ ELL galaxies between $z = 0$ and $z = 0.3$ by integrating the LFs. Assuming the B01, $z = 0$ value of α in local clusters (α = -1.18 $\pm$ 0.76) and our own best-fit value for $z = 0.3$ clusters (α = 0.17 $\pm$ 0.18) and integrating the number of galaxies between $K^* < K < K^* + 2$ for these different values of α, we find that the number of ELL galaxies with $K^* < K < K^* + 2$ decreases by a factor of 3.8 over this redshift range. Considering the large error bar in the B01 value of α, we also compare to an α = -0.92 LF (the Kochanek et al. 2001 value for field early-types). If the local cluster early-type population has the same faint-end slope as the field, then the relative decrease in $K^* < K < K^* + 2$ galaxies is a factor of 2.6.

One potential concern with our ELL LF is that it may suffer from selection effects caused by difficulty obtaining successful redshifts for faint, absorption-line systems. Extensive tests on the completeness of the spectroscopy (Yee et al. 1996) and PCA analysis (Ellingson et al. 2001) show that the spectroscopy is complete to the adopted limits; however, given the implications it is worth exploring this result further. As a check that the measured decrease in α is not caused by selection effects in the faintest bins, we refit the ELL LF using galaxies more than a full magnitude brighter than the spectroscopic completeness limit. This LF has a slightly steeper slope and a larger error bar (α = -0.04 $\pm$ 0.24); however, it is $> 3\sigma$ different than the EM+BAL limit. Furthermore, within the error, it is completely consistent with the measurement using the full spectroscopic catalogue. From this we conclude that a significant difference in the number of faint ELL vs. EM+BAL galaxies does exist, and is not a selection effect.

A decreasing number of faint, non-starforming galaxies with increasing redshift is

expected in the "downsizing" scenario of galaxy formation (Cowie el al. 1996). More-over, the same decrease is predicted by studies of the fundamental plane in the local universe. Nelan et al. (2005) show that the typical age of the stellar populations of low-luminosity early-types is $\sim$ 4 Gyr. If these galaxies form in the monolithic collapse scenario, then this suggests that they would be star-forming galaxies at z > 0.3 and would not populate the faint-end of the ELL LF.

The same trend has also been observed as a decrease in the number of faint red-sequence galaxies at high redshift. Kodama et al. (2004), De Lucia et al. (2004), and Tanaka et al. (2005) all show that clusters at z > 0.7 have fewer faint red-sequence galaxies than their low-redshift counterparts.

Interestingly, the decrease in faint ELL galaxies in the CNOC1 clusters is not met with a corresponding increase in the number of EM+BAL galaxies. The faint-end slope measured from these galaxies is in good agreement with the local field and cluster values. This suggests that if the faint-end of the ELL LF is built-up between z = 0.3 and z = 0 from the quenching of star-formation in faint EM+BAL galaxies, that these galaxies must be replenished in order to maintain the faint-end slope. This could naturally be explained by a scenario where faint, star-forming galaxies are continuously accreted from the field and gradually transformed into quiescent galaxies.
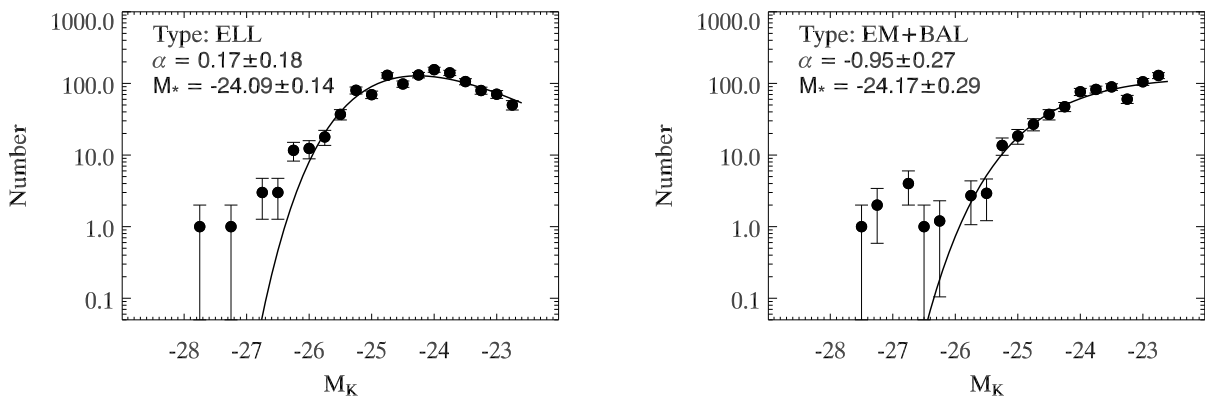
Figure 2.13 Left Panel: Ensemble LF for galaxies in all 15 clusters with spectra classified as ELL. The LF is corrected to z = 0.296. Right Panel: Same as the left panel for galaxies classified as EM+BAL. The bright-end of the LFs diverge from a Schechter function because the BCGs are included.

2.8.3 Redshift Evolution of Spectrally-Typed Luminosity Functions

It is also useful to test whether the value of K^* from the spectrally-typed LFs shows any differential evolution with redshift. Here we compute LFs for the spectral-types at different redshifts in the identical manner as §6.3. For these LFs we hold the faint-end fixed using the values measured in §7.2 (α = 0.2 for ELL galaxies and α = -0.9 for EM+BAL galaxies). Figure 14 shows the resulting LFs, and the Schechter function fits. Surprisingly, the ELL LFs have fainter values of K^* than the EM+BAL galaxies. The same result is not seen in local K-band cluster and field studies. B01 show that in local clusters the NEL galaxies are 0.60 mag brighter than the EL galaxies and Kochanek et al. (2001) show that they are 0.55 mag brighter in the local field. While K^* is brighter for the EM+BAL galaxies in the CNOC1 clusters, this does not mean that the average EM+BAL galaxy is brighter than the average ELL because K^* and α are correlated. Shallower values of α typically result in fainter values of K^*. As an example, if we re-fit the ELL galaxies using a much steeper faint-end slope α = -0.5 (the value measured for the stellar mass function of early-type galaxies in the local universe by Bell et al. 2003), then we find that K_* is brighter for the ELL galaxies by 0.51, 0.50, and 0.59 mag for the z = 0.21, 0.29, and 0.46 bins, and that, similar to the local K-band studies, the ELL galaxies have values of K_* which are brighter than the EM+BAL galaxies.

We can compare the evolution of K^* with some simple models of galaxy evolution. The left and right panels of Figure 15 shows a plot of K^* vs. z for the ELL and EM+BAL types, respectively. The solid-line in the right panel is a z_f = 2.8 single-burst model normalized to the B01 value of K^* = -23.31 for EL galaxies at z = 0. The dashed line in the right panel is a stellar population constructed with the Bruzual & Charlot (2003) code which forms half its stars in a single-burst at z = 2.8, and the other half with a constant star-formation rate of $5 M_\odot$ yr^{-1}. The solid line in the left panel shows the z_f = 2.8 single-burst model for the ELL galaxies. Unfortunately, the ELL passive evolution model can not be normalized to the K^* computed for the NEL LF by B01 because it is measured using α = -1.28 and this value is very different from the α = 0.2 that we use. Instead, the ELL single-burst model is normalized to pass through the z = 0.29 value of K^* for ELL galaxies.

While it is difficult to make robust conclusions from Figure 15, it is worth noting that both the ELL and EM+BAL types are consistent with single-burst, passive evolution models. This result, combined with the fact that the total cluster K^* evolves passively would be consistent with a scenario where the bulk of the stellar mass in

bright cluster galaxies is formed at high-redshift and the dominant evolution thereafter is the passive aging of the stellar populations, *regardless of spectral-type*. It also suggests there is no inconsistency between studies which find a significant change in the morphology, color and star-formation properties of the cluster galaxy population at $z > 0.1$, and studies which have shown that the evolution of the their stellar population is primarily passive (e.g., Stanford et al. 1998, van Dokkum et al. 1998). Even though the LFs of the ELL and EM+BAL galaxies at $z = 0.3$ change significantly by $z = 0$, there is no corresponding change the total cluster LF. This suggests that the transformations in morphology and color/spectral-type which occur to cluster galaxies over the same redshift range are "superficial" - they have little effect on the overall stellar mass of the galaxies which transform.
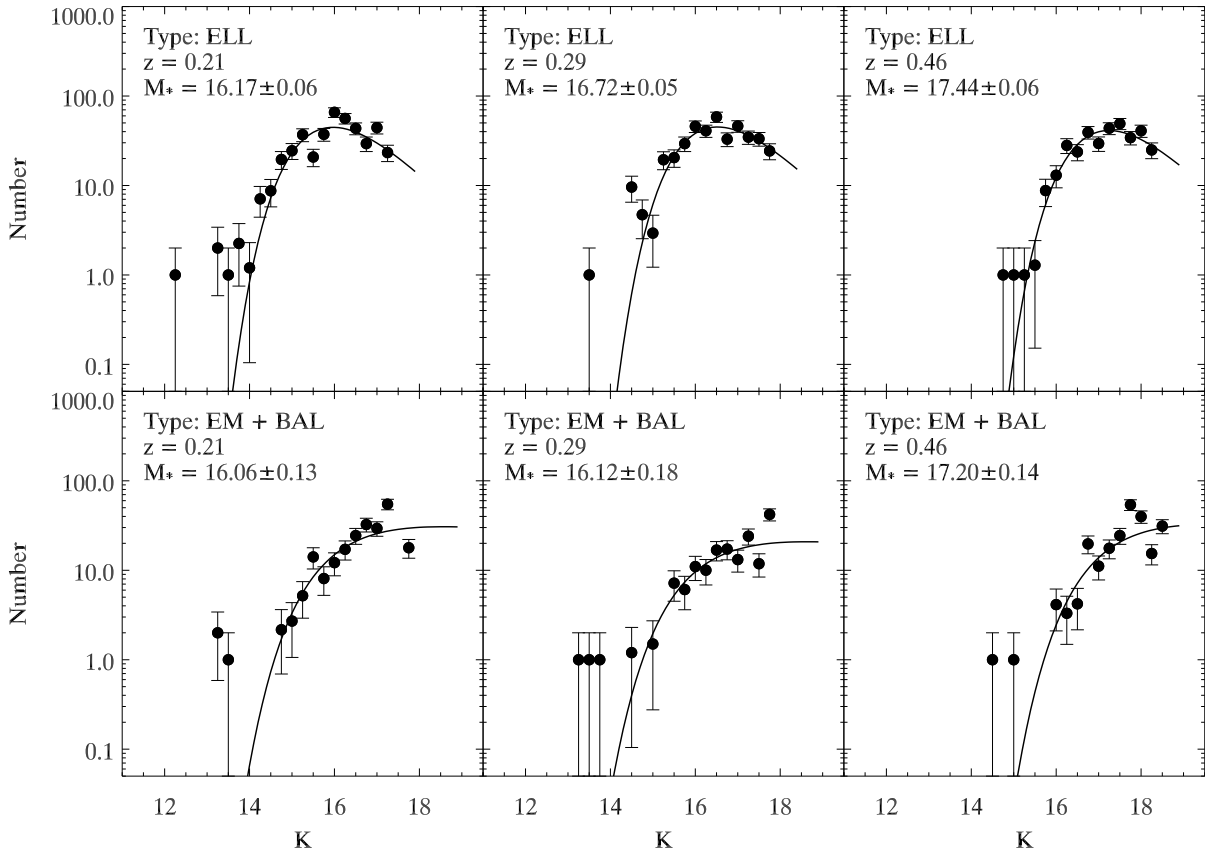
Figure 2.14 Top Row: LFs at increasing redshift for galaxies classified as ELL. Bottom Row: Luminosity functions at increasing redshift for galaxies classified as EM+BAL. Each LF is constructed from a stack of 5 clusters.
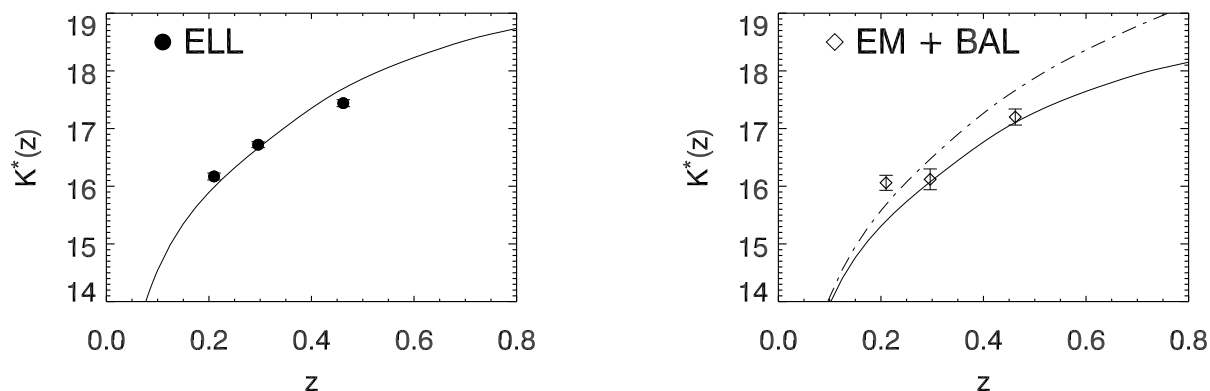
Figure 2.15 Left Panel: Redshift evolution in K* for ELL galaxies. The solid line is passive evolution model normalized to pass through the $z = 0.29$ point. Right Panel: Redshift evolution in K* for EM+BAL galaxies. The solid-line is a passive evolution model normalized to the B01 EL K*. The dot-dashed line is a single-burst + constant star-formation rate model with the same normalization.

2.8.4 Dependence of Spectrally-Typed Luminosity Functions on Cluster Mass

In §6.4 we showed that there was no dependence of the overall K-band LF on cluster mass for the mass range covered by the CNOC1 clusters. Here we test whether the LFs of galaxies of different spectral-types varies in clusters of different mass.

Figure 16 shows the LFs for the ELL and EM+BAL types in the 3 mass bins used in §6.4. The LFs are computed by again assuming $\alpha = 0.2$ for ELL galaxies and $\alpha = -0.9$ for EM+BAL galaxies. Figure 16 demonstrates that there is no significant change in K* for both spectral types across all three mass bins, with the possible exception of a slight trend (at $\sim 2\sigma$ level) with mass for the ELL galaxies. This suggests that any properties of the cluster environment that depend on the cluster mass (e.g., ram-pressure stripping efficiency, tidal forces) do not drastically alter the LF of different spectral types. It might be expected that there would be fewer faint, EM+BAL galaxies than bright EM+BAL galaxies in higher-mass clusters, as they would be more susceptible to having their star-formation truncated by tidal forces or ram-pressure stripping. However, to the depth of our LFs, we see no such reduction in the number of these galaxies.

Also, given that K* becomes brighter through the field, group, and cluster environment in the local universe (Kochanek et al. 2001, B01, Ramella et al. 2004, L04, R04) it is surprising that there is no significant difference for the spectral-types across the

cluster mass spectrum.
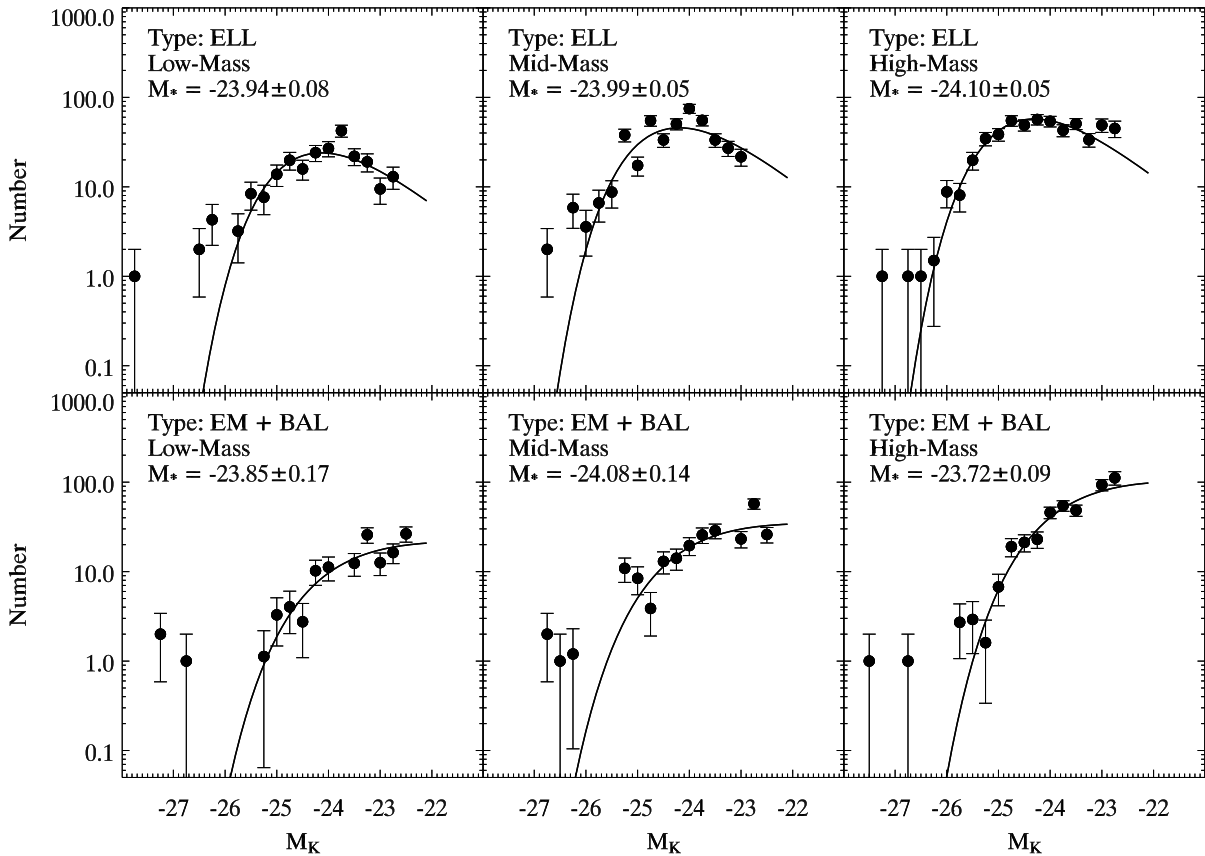
Figure 2.16 Top Row: LFs for galaxies classified as ELL in clusters of different mass. Bottom Row: Luminosity functions for galaxies classified as EM+BAL in the same clusters. Each LF is constructed from a stack of 5 clusters, and corrected to a mean redshift of $z = 0.296$

2.9 Summary

We have presented K-band photometry for 15 moderate-redshift CNOC1 clusters with extensive optical spectroscopy. Our results show that both the luminosity and number density profiles of the clusters are well-fit by NFW profiles with concentration parameters of $c \sim 4$. Furthermore, comparison with the dynamical mass analysis for the same clusters shows that for massive, moderate-redshift, X-ray selected clusters, K-band light closely traces the dark matter mass at $R < 1.5R_{200}$, except possibly in the cluster core. The galaxy number and luminosity densities of the CNOC1 clusters are more concentrated than local clusters, and this is likely caused by an earlier collapse

Table 2.3. Summary of LF Parameters

Redshift (1)	Type (2)	Environment (3)	K^* (4)	α (5)
0.296	all	-	-24.53±0.15	-0.84 ±0.08
"	all	-	-24.93±0.04	-1.1
"	ELL	-	-24.09±0.14	0.17 ± 0.18
"	EM+BAL	-	-24.27±0.27	-0.95 ± 0.27
0.210	all	-	15.52±0.06	-0.9
"	ELL	-	16.17±0.06	0.2
"	EM+BAL	-	16.06±0.12	-0.9
0.290	all	-	15.93±0.06	-0.9
"	ELL	-	16.72±0.07	0.2
"	EM+BAL	-	16.12±0.18	-0.9
0.462	all	-	17.14±0.06	-0.9
"	ELL	-	17.44±0.06	0.2
"	EM+BAL	-	17.20±0.14	-0.9
0.296	all	Cluster-Low Mass	-24.51±0.08	-0.9
"	ELL	"	-23.94±0.08	0.2
"	EM+BAL	"	-23.85±0.17	-0.9
"	all	Cluster-Mid Mass	-24.59±0.06	-0.9
"	ELL	"	-23.99±0.05	0.2
"	EM+BAL	"	-24.08±0.14	-0.9
"	all	Cluster-High Mass	-24.52±0.06	-0.9
"	ELL	"	-24.10±0.05	0.2
"	EM+BAL	"	-23.72±0.09	-0.9

epoch for the higher-mass, higher-redshift CNOC1 clusters. Furthermore, the ratio of c_{DM} to c_g for the CNOC1 clusters is less than in local clusters and we suggest that this is the product of either a non-universal ratio of c_{DM} to c_g for clusters, or else a relative evolution in c_{DM} and c_g with redshift.

Analysis of the cluster LFs show that the evolution of K* between $0.2 < z < 0.5$ is consistent with a scenario where the majority of the stellar mass in cluster galaxies forms at high redshift ($z_f > 1.5$) and evolves passively thereafter. The faint-end slope of the LF shows no evolution from the value measured in local clusters. These results imply that the stellar mass buildup of individual galaxies through major mergers is negligible in massive, X-ray selected clusters from $z = 0.3$ to $z = 0$.

We have also compared the K-band luminosity functions at moderate redshift in different environments ranging from the field to high-mass clusters. Our results suggest that K* may increase slightly in brightness from the field to the cluster environment at moderate-redshift; however, the error bars on the field K-band LFs are large and therefore, the data could also be consistent with no change. Unlike local clusters, it appears that for the CNOC1 clusters there is no correlation between K* and the dynamical mass of the cluster.

By dividing galaxies into star-forming/recently starforming (EM+BAL) and non-starforming (ELL) types we examined the individual LFs of these types. The faint-end slope of the ELL LF is significantly shallower than the faint-end slope for EM+BAL LF. Comparing the value of α for ELL galaxies to local field and cluster LFs suggest that the number of passive K* < K < K* + 2 galaxies in clusters decreases by a factor of $\sim$ 3 from $z = 0$ to $z = 0.3$. These results are consistent with "downsizing" in the cluster galaxy population.

The spectrally-typed LFs also show that K* for both ELL and EM+BAL galaxies is consistent with a passive evolution scenario and this, in tandem with the passive evolution of the combined cluster LF, suggests that the bulk of the stellar mass in both types of galaxies is formed at high-redshift, and that subsequent star-formation or changes in morphology do not affect the overall stellar mass of the galaxies. The spectrally-typed LFs also show that K* for both EM+BAL and ELL classes is independent of the mass of the cluster that they reside in.

Acknowledgements

Chapter 3

Halo Occupation Number, Mass-to-Light Ratios and Ω_m

3.1   Abstract

Using K-band imaging for 15 of the Canadian Network for Observational Cosmology (CNOC1) clusters we examine the near-infrared properties of moderate-redshift (0.19 $< z <$ 0.55) galaxy clusters. We find that the number of K-band selected cluster galaxies within R_{500} (the Halo Occupation Number, HON) is well-correlated with the the cluster dynamical mass (M_{500}) and X-ray Temperature (T_x); however, the intrinsic scatter in these scaling relations is 37% and 46% respectively. Comparison with clusters in the local universe shows that the HON-M_{500} relation does not evolve significantly between $z = 0$ and $z \sim 0.3$. This suggests that if dark matter halos are disrupted or undergo significant tidal-stripping in high-density regions as seen in numerical simulations, the stellar mass within the halos is tightly bound, and not removed during the process. The total K-band cluster light ($L_{200,K}$) and K-band selected richness (parameterized by $B_{gc,K}$) are also correlated with both the cluster T_x and M_{200}. The total (intrinsic) scatter in the $L_{200,K}$-M_{200} and $B_{gc,K}$-M_{200} relations are 43%(31%) and 35%(18%) respectively and indicates that for massive clusters both $L_{200,K}$ and $B_{gc,K}$

can predict M_{200} with similar accuracy as T_x, L_x or optical richness (B_{gc}). Examination of the mass-to-light ratios of the clusters shows that similar to local clusters, the K-band mass-to-light ratio is an increasing function of halo mass. Using the K-band mass-to-light ratios of the clusters, we apply the Oort technique and find $\Omega_{m,0} = 0.22 \pm 0.02$, which agrees well with recent combined concordance cosmology parameters, but, similar to previous cluster studies, is on the low-density end of preferred values.

3.2   Introduction

One of the principal objectives in modern cosmology is a good description of the physics that govern the formation of structure from the galactic through to the super-cluster scale. Recent theoretical and observational work in this area has concentrated on understanding the relationship between the dynamically dominant dark matter and the baryonic matter in the form of stars and gas. The major challenge has been that observables such as the galaxy correlation function (e.g., Zehavi et al. 2005a, 2005b; Eisenstein et al. 2005; Norberg et al. 2002, 2001), luminosity function (LF; e.g., Babbedge et al. 2006; Ilbert et al. 2005; Dahlen et al. 2005; Wolf et al. 2003; Blanton et al. 2003; Nakamura et al. 2003; Kochanek et al. 2001; Bell et al. 2003; Cole et al. 2001), and the Lyman-alpha forest (e.g., McDonald et al. 2006; Kim et al. 2002; Croft et al. 2002) constrain the distribution of stellar mass and gas in the universe, yet dark matter is the dominant gravitational component, and numerical simulations are more effective at predicting its distribution than that of baryonic mass..

Despite the difference between that which is easy to observe, and that which is easy to simulate, recent combined N-body + Smoothed Particle Hydrodynamics (SPH) simulations have suggested that dissipation from the baryonic component is relatively unimportant in the process of galaxy formation because the force of gravity from galactic dark matter halos is overwhelmingly dominant (e.g., Weinberg et al. 2006; Nagai & Kravtsov 2005). These results naturally explain why purely N-body simulations have been able to reproduce the correlation function (e.g., Colín et al. 1999; Berlind & Weinberg 2002; Kravtsov et al. 2004; Tinker et al. 2005; Nagai & Kravtsov 2005; Tasitsiomi et al. 2004) and the number of satellite galaxies per halo, the Halo Occupation Number (HON) or its probability distribution, the Halo Occupation Distribution, (HOD, e.g., Berlind & Weinberg 2002, see Cooray & Sheth 2002 for a review). Furthermore, full SPH simulations (e.g., Weinberg et al. 2006, 2004; Yoshikawa et al.

2001; Pearce et al. 2001) and semi-analytic models (e.g., Berlind et al. 2005, 2003; Cole et al. 2000; Zhu et al. 2006) which can be directly compared to observations, have also begun to enjoy a great deal of success at reproducing the LF, correlation function, and HON. These recent improvements in the quality of simulations and semi-analytic models as well as new observational datasets such as the SDSS and 2dFRS represent a major breakthrough in our understanding of the relative distribution of baryonic and dark matter in the universe and consequently, the formation of large-scale structure.

Detailed studies of galaxy clusters offer a complementary approach to the correlation function, Lyman-alpha forest, and simulations for studying the relationship between baryonic and dark matter. Clusters allow us to probe the distribution of baryons and dark matter in the most massive collapsed halos (which also happen to be the best-resolved objects in numerical simulations). The advantage of studying clusters is that the baryonic content in the form of stars and hot gas in the Intra-Cluster Medium (ICM) can be directly measured with observations, and in addition to this, cluster halos are sufficiently massive that their dark matter mass can be measured using either weak lensing, X-ray data, or the dynamics of cluster galaxies. This allows direct comparison between the baryonic and non-baryonic component on a halo-by-halo basis, whereas for galaxy-mass halos, the mass-to-light ratio (M/L), HON, or bias is usually measured statistically using either galaxy-galaxy lensing (e.g., Seljak et al. 2005; Sheldon et al. 2004; Hoekstra et al. 2005, 2002), or by stacking galaxies and studying the dynamics of satellite galaxies (e.g., Conroy et al. 2005, Brainerd et al. 2003), although recently strong-lensing analysis of a sample of individual systems has been done (Treu et al. 2006). The advantage of being able to study individual halos is that not only can the correlation between baryonic and dark matter be measured (via the HON or M/L ratio), but the relative *scatter* in the correlation can also be determined. Good constraints on the scatter are important because it is a direct measure of the stochasticity in the baryonic/dark matter bias.

In practice, the best way to measure the baryonic content of clusters in the form of stars is with detailed modeling of the stellar populations using either high-resolution spectroscopy, or multi-band photometric observations. As these observations are often difficult to obtain for large samples of galaxies, K-band light has frequently been adopted as a cheap and efficient proxy for the stellar mass of galaxies. K-band light is neither strongly affected by dust, nor strongly enhanced by starbursts, and is therefore a good tracer of underlying stellar mass of a galaxy (e.g., Brinchmann & Ellis 2000; Gavazzi et al. 1996; Rix & Rieke 1993). Furthermore, k-corrections are generally

small, and fairly independent of galaxy type (Poggianti 1997; Mannucci et al. 2001). Therefore, a study of the relative abundances of K-band light and mass in clusters is a good probe of the relationship between the cluster dark matter mass and the baryonic mass in the form of stars.

In addition to being useful for determining the relationship between dark matter and baryonic matter, a good understanding of the slope and scatter of the cluster K-band luminosity-mass correlation and K-band richness-mass correlation will be extremely valuable in the era of high-yield cluster surveys such as the Red-sequence Cluster Survey 2 (RCS-2, Yee et al. 2007), the South Pole Telescope (SPT, Ruhl et al. 2004), and the Atacama Cosmology Telescope (ACT, Kosowsky 2006). These projects will use the evolution of the cluster mass function, N(M, z) as a probe of cosmological parameters (see Mohr 2004 for a review); however, mass measurements for the thousands of clusters that will be detected in these surveys are unlikely to be available from traditional techniques such as L_x, T_x, weak-lensing, or dynamics and therefore new, observationally cheaper proxies for cluster mass will be required. Two candidates for this mass indicator are the integrated Sunyaev-Zeldovich Effect (SZE) y-parameter (e.g., Motl et al. 2005), as well as the total cluster K-band luminosity or K-band selected richness (e.g., Lin et al. 2004; Ramella et al. 2004; Rines et al. 2004). For the SZE surveys the y-parameter has significant potential as a mass indicator (e.g., Hallman et al. 2006, Motl et al. 2005) as it is a measure of the mass of cluster baryons in the form of hot gas. For optical/IR surveys, K-band richness/luminosity is an attractive alternative because it is a measure of the total mass of baryons in the form of stars in cluster galaxies. Gladders et al. (2006) have already shown that optical richness works well as a cluster mass proxy, and using the optically-selected RCS-1 survey and an empirical mass-richness calibration they determined cosmological parameters consistent with recent concordance values (e.g., Spergel et al. 2006), thus illustrating the potential for this technique. K-band light is a better tracer of stellar mass than optical light, and therefore it might be expected that the scatter in the K-band light/richness vs. mass relation will be smaller than the scatter in the optical light/richness vs. mass relation, or at least might have fewer catastrophic outliers. Using an observable with a smaller scatter, and fewer outliers could improve the accuracy in the measured cluster mass function (e.g., Lima & Hu 2005).

Since the advent of the 2-Micron All Sky Survey (2MASS, Skrutskie et al. 2006) several studies of the relationship between K-band light and dark matter in local ($z <$ 0.1) clusters have been done. Lin et al. (2003, 2004; hereafter L04), Rines et al. (2004),

Kochanek et al. (2003), and Ramella et al. (2004) all show that the K-band selected number counts and total cluster K-band light are indeed correlated with the dark matter mass, and have rms scatters of $\sim 40\%$. L04, Rines et al. (2004), and Ramella et al. (2004) also show that the slope of the L_K vs. M_{200} relation is shallower than unity for clusters, suggesting that the conversion of baryons into stellar mass proceeds less efficiently in higher-mass halos. Recently, Lin et al. (2006) presented an analysis of the K-band selected HON for a heterogeneous sample of 27 clusters at $0 < z < 0.9$ and found no significant evolution in the HON-Mass relation with redshift. Interestingly, this result was different from their original analysis using a subsample of ~ 20 clusters at $0.2 < z < 0.9$ where they found the HON at fixed mass increases by a factor of ~ 2 at $z > 0.2$.

The purpose of this paper is to extend the analysis of the local cluster K-band HON and M/L ratio to higher redshift using a well-defined sample of clusters with wide-field imaging and extensive spectroscopic data. Our sample consists of 15 massive, X-ray selected clusters that were part of the Canadian Network for Observational Cosmology (CNOC1, Yee et al. 1996) project. The K-band imaging, LF and density profiles for the clusters were presented in the first paper in this series (Muzzin et al. 2007a, hereafter Paper I). In addition to the K-band imaging, these clusters also have considerable optical spectroscopy and g and r photometry both of which extend to R $\sim R_{200}$ for each cluster.

The structure of this paper is as follows: In §2 we briefly describe the dataset, and in §3 present updated values for the cluster dynamical masses and X-ray temperatures. In §4 we present the cluster HON and discuss its redshift evolution. Section 5 shows that total K-band luminosity ($L_{200,K}$) and K-band selected richness (parameterized by $B_{gc,K}$) are correlated with the cluster halo mass, and can potentially be used as cheap proxies for this quantity in cluster abundance surveys. In §6 we present the K-band M/L ratios for the CNOC1 clusters and in §7 we present a measurement of Ω_m using the Oort (1958) technique. We conclude with a summary in §8. When computing magnitudes and angular sizes we adopt an $\Omega_m = 0.3$, $\Omega_\Lambda = 0.7$, $H_0 = 70$ km s^{-1} Mpc $^{-1}$ cosmology.

3.3   Data

The CNOC1 clusters are a set of 16 massive clusters with redshifts $0.17 < z < 0.54$. Fifteen of the clusters were detected in the Einstein Medium Sensitivity Survey (EMSS, Gioia et al. 1990). Abell 2390 was added as the 16th cluster and is also a massive cluster with strong X-ray emission. The clusters have extensive optical photometry and spectroscopy which were obtained as part of the CNOC1 project (Yee et al. 1996). Our sample is comprised of 15 of the 16 CNOC1 clusters. The cluster MS0906+11 is omitted because it was shown to be a strong binary in redshift-space by Carlberg et al. (1996) and therefore the mass measurement for the cluster is unreliable. The optical photometric and spectroscopic data as well as the K-band photometric data used in this paper were already presented in Paper I. We refer to that paper as well as the CNOC1 paper (Yee et al. 1996) for complete details of the observations, reductions and photometry and below present only a quick overview of the data.

3.3.1   Optical Photometry and Spectroscopy

Gunn g and r band imaging data were obtained at the 3.6m Canada-France-Hawaii-Telescope (CFHT) using the Multi-Object Spectrograph (MOS) camera. Photometry was performed on these data using the Picture Processing Package (PPP, Yee 1991). The photometry reaches a 5σ depth of $\sim \mathrm{M}^* + 3$ in both the g and r bands. The CNOC1 collaboration also obtained > 2500 spectroscopic redshifts in the fields of the 15 clusters using the CFHTMOS. Of these, approximately one-half are cluster members. The spectroscopy is sparsely sampled, but complete to a depth of $\mathrm{K}^* + 2$ for all but the two highest-redshift clusters (MS0016+16 and MS0451-03). The spectroscopy for those clusters is complete to $\sim \mathrm{K}^* + 1$.

3.3.2   Near Infrared Photometry

K-band imaging for 14 of the 15 clusters was obtained at the Kitt Peak National Observatory (KPNO) 2.1m telescope using the Ohio State / NOAO Infrared Imaging Spectrograph (ONIS). Observations were taken in a Mauna Kea filter set version of the K_s filter (Tokunaga K), which is nearly identical to the 2MASS K_s filter. For our analysis we treat the Tokunaga K filter as the K_s-band and hereafter refer to it as the "K-band". K_s-band imaging of MS0440+02 was obtained using the PISCES camera on the Steward Observatory $90''$ telescope. Photometry for the K-band data was also

performed using PPP. The K-band imaging is complete to a 5σ depth of $\sim K^* + 2$ for all clusters, except the two highest-redshift clusters where it is complete to $\sim K^* + 1$ (see Table 1 of Paper I for a summary of observations).

3.4   Cluster Physical Parameters

The masses of the CNOC1 clusters are without a doubt the most well-studied for clusters at moderate redshift. There are numerous measurements using X-ray temperatures (T_x, Hicks et al. 2006; Lewis et al. 1999; Henry 2000; Mushotzky & Scharf 1997), the dynamics of cluster galaxies (van der Marel et al. 2000; Borgani et al. 1999; Carlberg et al. 1996; 1997; Diaferio et al. 2005), and both strong (Fahlman et al. 1994; Luppino & Gioia 1995; Pierre et al. 1996, Wu 2000) and weak lensing (Allen 1998; Hoekstra et al. 1998; Smail et al 1995; 1997). In this section we discuss the masses and dynamical radii we adopt for comparing with the K-band properties.

3.4.1   Dynamical Masses

The first study of the dynamics of the CNOC1 clusters was done by Carlberg et al. (1996) who measured the line-of-sight velocity dispersion (σ_1) for each cluster. These velocity dispersions were used to calculate the virial mass (M_{vir}), the radius at which the cluster mass density exceeds the critical density of the universe by a factor of 200 (R_{200}), and the mass contained within that radius (M_{200}), by assuming the cluster had an isotropic velocity ellipsoid. In subsequent work, Carlberg et al. (1997) and van der Marel et al. (2000) examined in detail the velocity dispersion profiles, and velocity anisotropy of the clusters. van der Marel et al. (2000) verified that they are compatible with an isotropic velocity ellipsoid and that the cluster mass profile was consistent with an NFW (Navarro et al. 1997) profile. The cluster velocity dispersions were also determined by Borgani et al. (1999) using different background subtraction techniques. They found that the different techniques provide velocity dispersions that are self-similar to $\sim 10\%$, and that the velocity dispersions they derive are also consistent to $\sim 10\%$ with the Carlberg et al. (1997) velocity dispersions.

Unfortunately, the M_{200} and R_{200} values determined from these studies are now out of date because they were computed assuming cosmological parameters which are different from recent concordance values (e.g., Spergel et al. 2006). Fortunately, the velocity dispersions do not depend on cosmology and, given that the clusters are con-

sistent with an isotropic velocity ellipsoid, we have recomputed both R_{200} and M_{200} with a $\Omega_m = 0.3$, $\Omega_\Lambda = 0.7$, $H_0 = 70$ km s^{-1} Mpc^{-1} cosmology using the equations,

$$R_{200} = \frac{\sqrt{3}\sigma_1}{10H(z)},\tag{3.1}$$

and,

$$M_{200} = \frac{4}{3}\pi R_{200}^3 \cdot 200\rho_c,\tag{3.2}$$

where H(z) is the Hubble constant at redshift z, and ρ_c is the critical density for a flat universe. Equation 1 can be derived by assuming $M_{200} \approx M_{vir}$ and equating the virial theorem ($M_{vir} = \frac{3}{G}\sigma_1^2 R_{vir}$) and Equation 2. For all clusters the σ_1 values determined by Carlberg et al. (1997) are used to compute M_{200} and R_{200}. Errors in M_{200} are calculated by propagating the errors in σ_1 in the standard way. The new values of R_{200} and M_{200} are on average ~ 1.6 times larger than the Carlberg et al. (1997) values. We list the updated values in Table 1.

3.4.2   X-ray Temperatures

X-ray temperatures have been measured for the CNOC1 clusters by several authors. The clusters we originally discovered in the Einstein Medium Sensitivity Survey (EMSS, Gioia et al. 1990); however, only X-ray fluxes were computed using the original data. Subsequently, Lewis et al. (1999) measured T_x for 13 of the 15 clusters in our sample using data from the ROSAT satellite. They found that the average cluster masses determined from T_x were in good agreement with the updated dynamical masses, even though individual clusters could have discrepancies as large as a factor of 2. Recently, Hicks et al. (2006) used archival Chandra Advanced CCD Imaging Spectrometer (ACIS) data to determine accurate T_x values for 13 of the 15 clusters in our sample. They use single and double-β-model fits to determine the temperatures. Several clusters (A2390, MS0839+29, MS1358+62, MS1455+22) are also corrected for significant cooling flows. They find that the X-ray masses they compute agree well with the dynamical masses determined with the velocity dispersions of Carlberg et al. (1997) and Borgani et al. (1999). These new T_x values are superior to the older data and for comparisons with the HON (§4), $L_{200,K}$ (§5.1), and $B_{gc,K}$ (§5.2) we use these values. There are two clusters without a Chandra observation (MS1224+20, MS1231+15). For MS1224+20 we use the temperature listed in Lewis et al. (1999). MS1231+15 has no X-ray temperature available so we assume a temperature of 6 keV, which is appropriate

Table 3.1.   Physical Properties of the CNOC1 Clusters

Cluster	z	σ_1	R_{200}	M_{200}	T_x
		km s^{-1}	Mpc	M$_\odot \times 10^{14}$	keV
(1)	(2)	(3)	(4)	(5)	(6)
A2390	0.2279	1095 ± 61	2.00	20.1 ± 3.4	$10.3^{+0.6}_{-0.6}$
MS0016+16	0.5466	1243 ± 128	1.89	24.0 ± 7.5	$9.2^{+1.0}_{-0.9}$
MS0302+16	0.4246	656 ± 93	1.07	3.7 ± 1.6	4^{+3}_{-1}
MS0440+02	0.1965	611 ± 62	1.13	3.5 ± 1.1	8^{+2}_{-1}
MS0451+02	0.2010	979 ± 76	1.81	15.0 ± 3.5	$6.1^{+0.7}_{-0.6}$
MS0451-03	0.5392	1354 ± 105	2.06	33.3 ± 7.6	$10.2^{+1.0}_{-1.0}$
MS0839+29	0.1928	788 ± 104	1.46	6.6 ± 2.7	$4^{+0.3}_{-0.3}$
MS1006+12	0.2605	912 ± 101	1.63	11.2 ± 3.8	7^{+1}_{-1}
MS1008-12	0.3062	1059 ± 107	1.85	17.2 ± 5.3	$5.9^{+0.9}_{-0.7}$
MS1224+20	0.3255	798 ± 90	1.38	7.5 ± 2.5	$4.3^{+0.65}_{-0.65}$
MS1231+15	0.2350	662 ± 69	1.20	4.5 ± 1.4	6^{+1}_{-1}
MS1358+62	0.3290	910 ± 54	1.57	12.0 ± 2.1	$8.0^{+1.1}_{-0.9}$
MS1455+22	0.2570	1169 ± 140	2.10	22.0 ± 8.2	$4.4^{+0.1}_{-0.1}$
MS1512+36	0.3726	697 ± 96	1.17	4.7 ± 2.0	$3.4^{+0.8}_{-0.7}$
MS1621+26	0.4274	833 ± 55	1.36	6.8 ± 1.4	7^{+3}_{-2}

given the X-ray luminosity (Yee & Ellingson 2003). We list the X-ray temperatures and their associated errors in Table 1.

3.5   The Halo Occupation Number

Clusters are massive dark matter halos, and therefore computing their HON simply requires counting the total number of cluster members within some dynamical radius, typically R$_{200}$. The extensive spectroscopy for the CNOC1 clusters could be used to differentiate between field and cluster galaxies; however, we prefer to measure the

HON using statistical background subtraction. Using spectroscopic data to separate field and cluster galaxies is preferable when computing cluster properties that depend on the luminosity of cluster members (e.g., LFs, total luminosity §5.1, or M/L ratios §6.1) because these calculations require information on the membership of individual galaxies to compute distance moduli and k-corrections. However, unless the spectroscopy of a cluster field is quite complete, statistical background subtraction is better-suited for counting the overdensity of cluster galaxies. Furthermore, using statistical background subtraction provides a consistent technique for each cluster and avoids any biases from cluster-to-cluster that might be caused by poor determination of the spectroscopic selection function.

The background counts are measured from our own K-band imaging survey of CNOC2 fields (Yee et al. 2000). The data was taken using the PISCES camera on the Steward Observatory 90″ telescope and are reduced and photometered using the same techniques as for the CNOC1 dataset. The imaging consists of 23 ($8' \times 8'$) fields and covers a total area of 0.26 square degrees. Complete details of the observations, data reduction, and photometry will be presented in a future paper (Lin et al. in preparation). Figure 1 shows background counts from the CNOC2 fields with the number counts from the K20 Survey (Cimatti et al. 2002) and the MUNICS Survey (Drory et al. 2001) overplotted for comparison. The CNOC2 galaxy counts agree well with the counts from these surveys as well as various other K-band surveys in the literature (e.g., Elston et al. 2006; Maihara et al. 2001; Saracco et al. 2001; Gardner et al. 1993).

We measure the HON for the clusters within the radius R_{500} (the radius at which the cluster mass density exceeds the critical density of the universe by a factor of 500), rather than the more typical R_{200}. It would be preferable to use R_{200}, as it is similar to the cluster virial radius; however, some of the clusters are very sparsely sampled at R_{200}, and therefore require large corrections to compensate for the poor sampling. These corrections propagate as large uncertainties in the total number of galaxies. Conversely, the coverage at R_{500} is complete for all clusters (except MS1455+22) and therefore those measurements have much smaller uncertainties and should also be more robust. The cluster R_{500} is estimated from the R_{200} values assuming an NFW profile with c = 5. Hereafter we refer to the HON within R_{500} as N_{500} and the HON within R_{200} as N_{200}.

Thus far, the largest study of the cluster HON is the work of L04 who measured N_{500} and N_{200} for 93, X-ray selected, $z < 0.1$ clusters using 2MASS data. In order to make a direct comparison between our sample and their sample, we measure N_{500}

using the same limiting magnitude as L04. Their technique for measuring the HON involves determining the Schechter parameters K^* and ϕ^* for each cluster and then integrating the Schechter function to an absolute magnitude limit of M_K = -21 to find the total cluster counts. For their ensemble of 93 clusters, they measured K^* = -24.02 $\pm$ 0.02. Therefore, statistically speaking, their N_{500} values are measured at K^* + 3, although the depth varies from cluster-to-cluster. Our data does not reach K^* + 3 for most clusters, therefore galaxies are counted to K^* + 1 and then these counts are extrapolated to K^* + 3.

K^* evolves with redshift; however, we showed in Paper I that the evolution tightly follows the luminosity evolution of a single-burst population formed at high-redshift. The single-burst model from Paper I is used to infer K^* at the redshift of each cluster. The background subtracted, $K < K^*$ + 1 counts are scaled to the appropriate counts for K^* + 3 by extrapolating a Schechter function with a faint-end slope of α = -0.9. This value of α is consistent with the faint-end slope measured for the CNOC1 cluster LF in Paper I (α = -0.84 $\pm$ 0.08) and is similar to the faint-end slope measured for the L04 data (α = -0.84 $\pm$ 0.02).

We plot N_{500} vs. M_{500} for the clusters in the left panel of Figure 2, and N_{500} vs. T_x in right panel of Figure 2. In both cases there is a good correlation between the two parameters. The Spearman rank-correlation coefficients are 0.79 and 0.77 respectively, implying probabilities of $7.1 \times 10^{-4}, 8.5 \times 10^{-4}$ that the data are uncorrelated.

One cluster which has an extremely small N_{500} for its mass is MS1455+22. This cluster is also a significant outlier in the M_{200}-B_{gc} relation (B_{gc} is a measure of cluster richness, see §5.2) from Yee & Ellingson (2003, hereafter YE03). They suggest that the most logical interpretation is either that the mass has been significantly overestimated or else that the cluster is in a very advanced state of evolution, different from most clusters in this redshift range. Therefore, MS1455+22 is excluded when we fit both M_{500} vs. N_{500} and and T_x vs. N_{500} and is plotted in Figure 2 as an open triangle. Using a χ^2-minimization technique for errors in both parameters (Press et al. 1992) we find the best-fit relation for the N_{500} - M_{500} correlation is

$$Log(M_{500}) = (1.40 \pm 0.22)Log(N_{500}) + (11.58 \pm 0.54),\qquad(3.3)$$

and has a reduced-χ^2 of 1.60. For the N_{500} - T_x the best-fit relation is

$$Log(T_x) = (0.77 \pm 0.11)Log(N_{500}) + (-1.01 \pm 0.27),\qquad(3.4)$$

and has a reduced-χ^2 of 2.46. The correlations have Root-Mean Squared (rms) scatters of 51% and 50% respectively. For the remainder of the paper, the percentage rms scat-

ter in all correlations is computed using the same method as YE03. The rms deviation from the fit in terms of the dependent variable (in this case, M_{500}) is determined and then compared to its mean value from the entire sample.

The scatter in these correlations is larger than the 35% scatter in the local scaling relations measured by L04. However, the random errors in our data are larger than theirs, and clearly a portion of the scatter comes from these measurement errors. Given that the total scatter is the result of both the measurement errors in M_{500} and N_{500} as well as some intrinsic scatter, we estimate the intrinsic scatter by assuming that the measurement scatter is independent of the intrinsic scatter and then subtracting the mean measurement scatter of the dependent variable in quadrature from the total scatter. Using this simplistic method we estimate that the intrinsic scatter in N_{500} - M_{500} is 37% and for N_{500} - T_x it is 46%.

We compare the N_{500} values from the CNOC1 clusters with the L04 values in the top panel of Figure 3. L04 measured N_{500} by integrating the cluster LFs over an NFW spatial distribution and therefore it is the N_{500} within a spherical volume. Our N_{500} is measured using statistical background subtraction and is therefore the number of galaxies in a cylinder of radius R_{500}. We convert our N_{500} in cylinders to N_{500} in spheres by multiplying by a deprojection constant of 0.791, the value for the percentage difference in enclosed number of galaxies between spheres and cylinders at R_{500} for an NFW profile with c = 5. The dash-dot blue line in Figure 3 is the best-fit relation for the L04 clusters, and the solid red line is the best-fit relation for the CNOC1 clusters. The slope of the CNOC1 relations ($M_{500} \propto N_{500}^{0.71\pm0.11}$) is slightly shallower than the L04 relation that includes the BCGs ($M_{200} \propto N_{500}^{0.82\pm0.04}$), but is consistent within the errors. It is also consistent with the scaling relation found by Rines et al. (2004) for the CAIRNS clusters ($M_{200} \propto N_{200}^{0.70\pm0.09}$); however, their relation is measured using N_{200} and M_{200} and a different luminosity cut. The overall normalization of the CNOC1 N_{500} is nearly identical to the L04 normalization. As a comparison between the samples we plot the measured N_{500} values divided by those predicted from the local M_{500}-N_{500} relation in the bottom panel of Figure 3 . Figure 3 shows that the HON - mass correlation measured by L04 does not evolve between $z = 0$ and $z \sim 0.3$. The higher redshift CNOC1 clusters have N_{500} values which are only 4% $\pm$ 11% smaller than would be predicted by the local relation. The mean(median) $N_{500}/N_{500,fitlocal}$ is 0.96(0.90) $\pm$ 0.11, and is consistent with no evolution in the HON with redshift. As a comparison, the L04 clusters have a mean(median) $N_{500}/N_{500,fitlocal}$ of 1.04(1.01) $\pm$ 0.04.

The non-growth of the HON at a fixed mass with increasing redshift is different from the results of L04. In addition to their local clusters, L04 also computed the HON for a subset of clusters with $0.1 < z < 0.9$ (K-band imaging from De Propris et al. 1999) which had available X-ray temperatures and compared it to the local clusters. Their comparison showed that the HON was roughly a factor of 2 larger in the $z > 0.1$ clusters. From this they suggested that half of all cluster galaxies may be removed (via either merging or disruption) between $z \sim 0.6$ (all but two of their clusters are $z < 0.6$) and $z = 0$ in order to match the local HON.

It is unclear why the conclusions of our studies are so different. We did note in Paper I that it is challenging to reconcile the idea of a strong evolution of the cluster HON between $z \sim 0.6$ and $z = 0$ and the passive evolution of the K-band cluster LF. Paper I showed that the evolution of the cluster K^* tightly follows the prediction of a passive evolution model between $z \sim 0.5$ and $z = 0$ and those results reaffirmed the findings of the pioneering cluster K-band luminosity function study of de Propris et al. (1999), as well as recent K-band LFs of high-redshift clusters (e.g., Toft et al. 2003; Kodama & Bower 2003; Ellis & Jones 2002; Strazzullo et al. 2006). Interestingly, all of the $z > 0.1$ clusters used by L04 are part of the de Propris et al. (1999) sample. If 50% of cluster galaxies are either merged, or disrupted by tidal forces between $z \sim 0.6$ and $z = 0$, then it seems unlikely that the evolution of K^* could follow a passive evolution model, unless the probability of being merged or tidally disrupted was independent of galaxy K-band luminosity (i.e., stellar mass). While mass-independence may be plausible in the case of mergers, more massive galaxies are more difficult to disrupt. If a significant number of disruptions do occur, they should preferentially destroy galaxies on the faint-end of the luminosity function and therefore will change its overall shape.

L04 appeal to the N-body simulations of Kravtsov et al. (2004) for an explanation of the strong redshift evolution of the HON. Kravtsov et al. (2004) show that for dark matter halos, the HON at a given mass becomes approximately a factor of three larger from $z = 0$ to $z = 5$. They show that the dark matter HON at a given mass is smaller at lower redshift because low mass halos merge with high mass halos as well as become tidally truncated or disrupted by massive halos in high-density regions such as clusters.

More recent simulations which incorporate both dark matter as well as baryonic matter using Smoothed Particle Hydrodynamics (SPH, e.g., Nagai & Kravtsov 2005, Weinberg et al. 2006) show that when the baryonic component is included, the in-

terpretation of the HON derived by counting galaxies becomes more subtle. Nagai & Kravtsov (2005) simulated a set of 8 clusters and found that as subhalos enter the cluster R_{200} they are stripped of $\sim$30% of their total dark matter mass. Once they fall into the cluster they are further stripped until $\sim$70% of their original dark matter mass is removed. Their result confirms the earlier N-body simulations which showed the dark matter HON is depleted with decreasing redshift, especially in high-density environments; however, the SPH simulations also show that primarily the dark matter is stripped from the halos and very little of the baryonic mass (in the form of stars and gas) is lost during this process. The baryonic matter remains because it tends to cool, and fall to the center of the subhalo and is amongst the most tightly bound mass in the subhalo.

These simulations suggest that the HON, when selected by counting the number of massive dark matter subhalos is quickly depleted in high density regions such as clusters because of tidal stripping and merging of the subhalos. However, when the HON is selected by the baryonic mass of halos (i.e., using K-band number counts) there should be little evolution in the HON at a given halo mass, because the baryonic component of subhalos is tightly bound, and will only be depleted in the case of full disruption. This interpretation is consistent with our data and is also consistent with the observation that both K* (Paper I, L04, de Propris et al. 1999) and α (L04) for cluster galaxies are basically identical across more than an order-of magnitude in cluster mass (Paper I, L04, de Propris et al. 1999). Given that the efficiency of tidal stripping is correlated with cluster mass, it is hard to understand how the K-band LF of cluster galaxies could be independent of cluster mass unless the baryonic component is unaffected in the process.

In summary, we find that the K-band selected HON of clusters at a given mass does not evolve significantly between $z = 0$ and $z \sim 0.3$. This result is consistent with the more recent work of Lin et al. (2006) who measured the HON within R_{2000}, R_{1000} and R_{700} for a sample of 27 clusters $0 < z < 0.9$ (a few of which are included in L04) and also find no-evolution in the HON at fixed mass. We argue that the non-evolution of the HON is naturally explained by recent SPH simulations, which show that while dark matter halos encounter a significant amount of tidal stripping in high-density regions such as clusters, the baryonic component within remains mostly intact. Furthermore, this interpretation reconciles the strong tidal stripping with the purely passive evolution of the cluster K-band LF, and its invariance across the cluster mass spectrum.
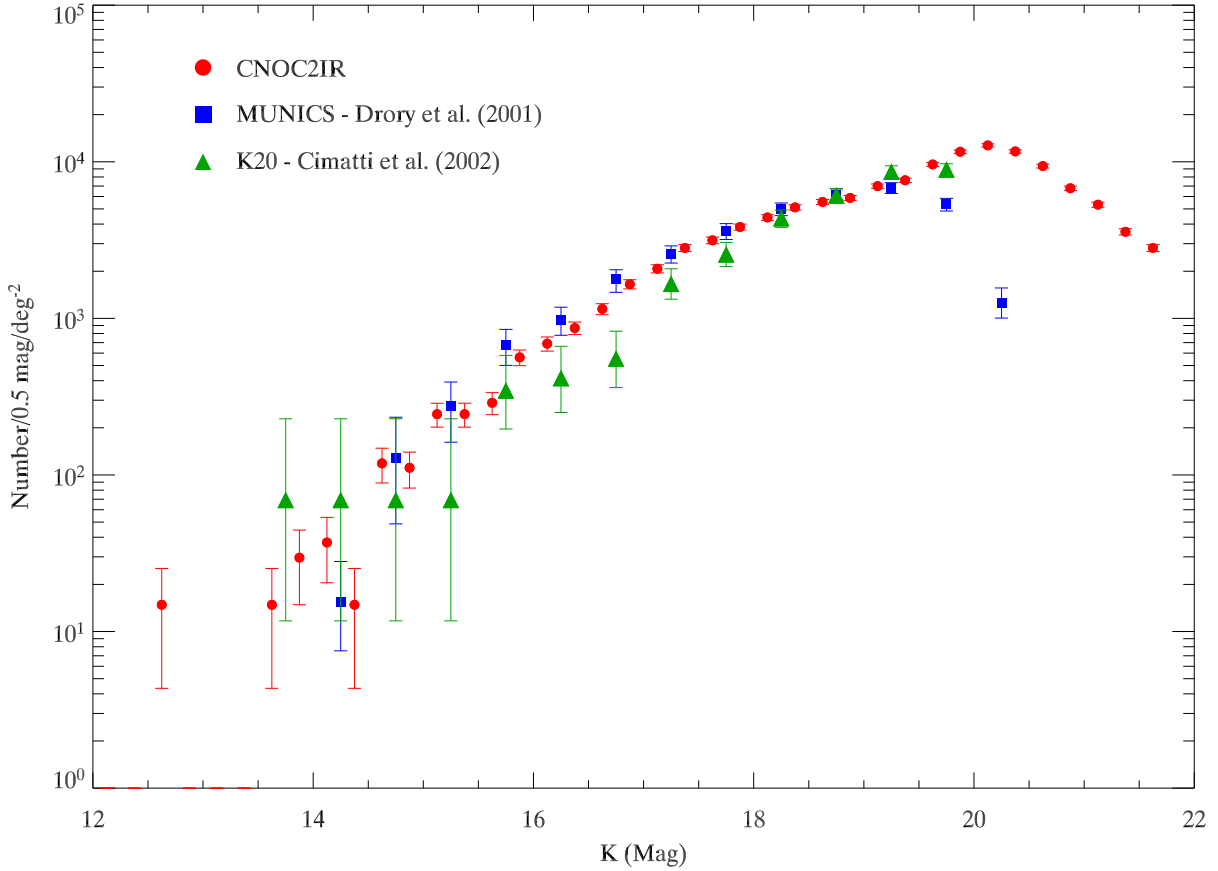
Figure 3.1 *Red Dots*: Number of galaxies per square degree per 0.5 magnitudes as a function of magnitude determined from 0.26 square degrees of CNOC2 K-band imaging data. *Green Triangles*: Number counts from the K20 Survey. *Blue Squares*: Number counts from the MUNICS Survey.

Our data cannot rule out the possibility that the simulations may over-exaggerate the tidal stripping and that similar to the baryonic component, the dark matter mass-selected HON at a fixed cluster mass also does not evolve within the same redshift range. A useful way to test this would be to compare the M/L ratios of cluster galaxies and field galaxies at large radii and look for evidence of truncated halos within the cluster population. Unfortunately, this is a challenging task, because there are few tracers of the dark matter potential at large radii for galaxies. There is now evidence from galaxy-galaxy lensing studies of massive clusters that supports the tidal-stripping scenario (Halkola et al. 2006, Natarajan et al. 2002); however, in lower-mass clusters (M $\sim$ 10^{13}-10^{14} M$_\odot$), the same trend is not observed (Mandelbaum et al. 2006). A more comprehensive study of galaxy-galaxy lensing in clusters in the range of M $\sim$ 10^{14}-10^{15} M$_\odot$ would be particularly useful for testing this interpretation.
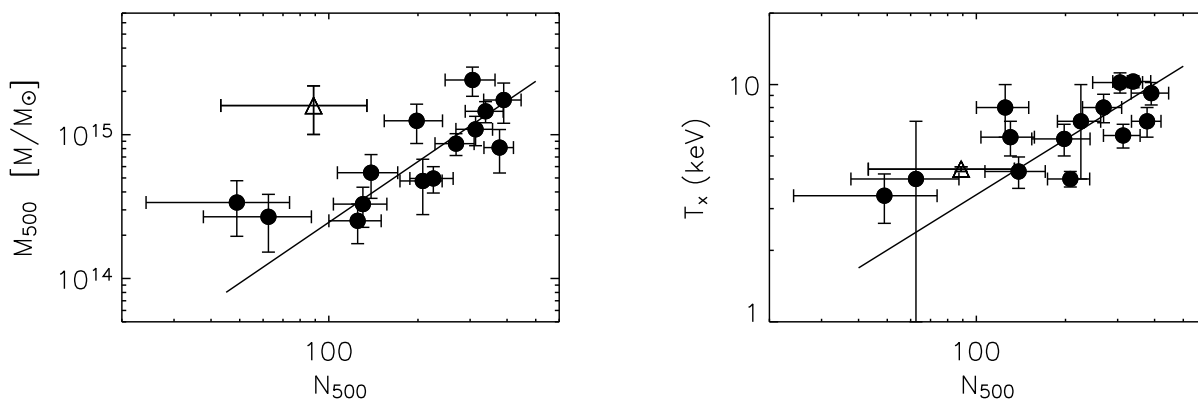
Figure 3.2 Left Panel: Plot of M_{500} vs. N_{500} for the CNOC1 clusters. The solid line is the best-fit linear relation and has an rms scatter of 50%. Right Panel: Plot of T_x vs. N_{500} for the same clusters. The solid line is the best-fit linear relation and has an rms scatter of 51%. MS1455+22 is plotted as an open triangle.

3.6 K-Band Light and Richness as an Indicator of Cluster Mass

In this section we measure the total K-band luminosity within R_{200} for the clusters ($L_{200,K}$) and examine its correlation with cluster mass. We also determine the correlation between K-band selected richness and cluster mass.

3.6.1 Total K-Band Luminosity

$L_{200,K}$ for a galaxy cluster is defined as the sum of the K-band luminosity of all cluster galaxies within R_{200} to a fixed absolute magnitude. In principle the measurement is straightforward; however, in practice, data are never homogeneous and additional corrections must be applied. In the case of the CNOC1 clusters, the clusters lie at a fairly large range of redshifts and therefore the light from each galaxy must be both k-corrected and evolution corrected to a common redshift. The need for these corrections means that the membership and approximate spectral-type for each galaxy in the cluster field must be determined. This is not as precise using statistical background subtraction and therefore we make use of the extensive spectroscopic catalogues. The spectroscopy is complete to $K^* + 1$ for all clusters, but is sparsely sampled. Therefore, a spectroscopic selection function is used to correct for the sampling. The method for determining the spectroscopic selection function was developed by the CNOC1 (Yee
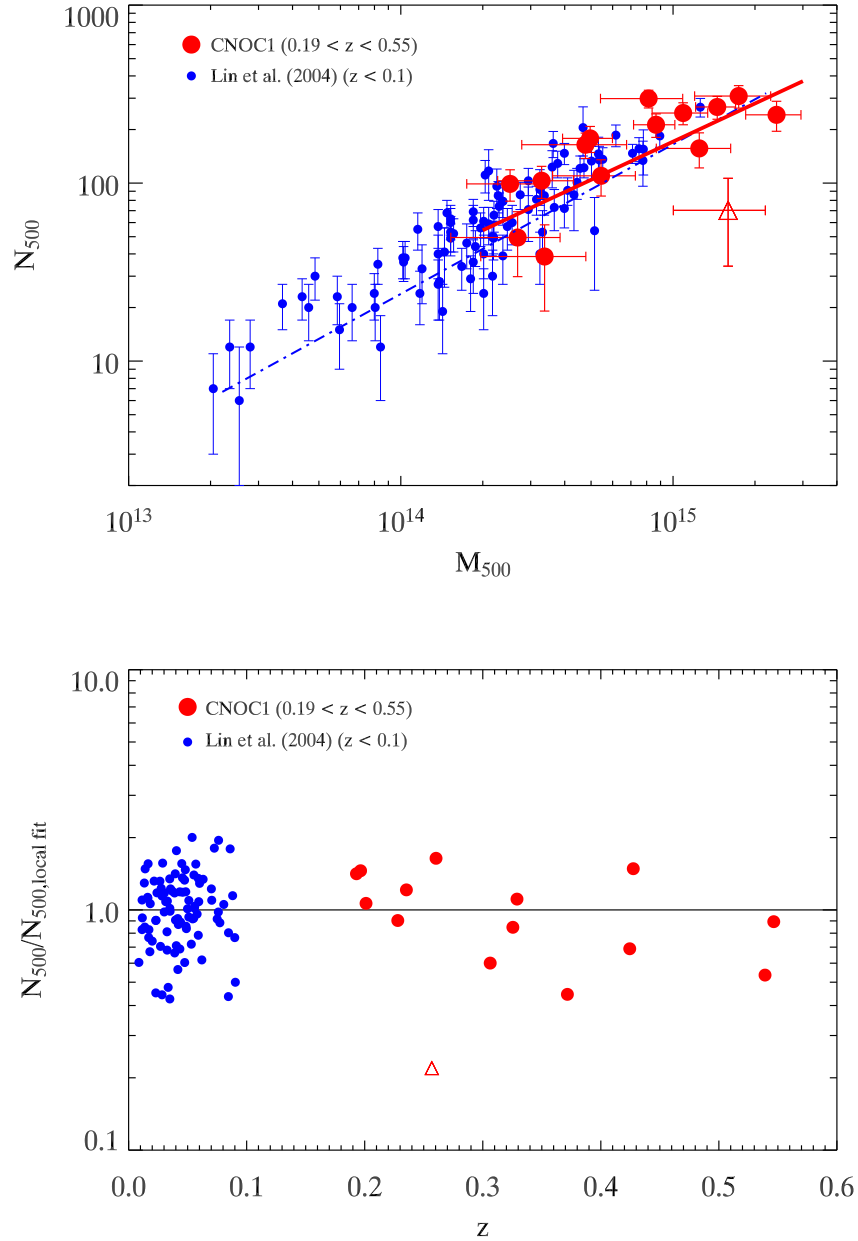
Figure 3.3 *Top Panel*: Plot of N_{500} vs. M_{500} for the CNOC1 clusters (large red points) and the L04 clusters (small blue points). MS1455+22 is plotted as an open triangle. The solid red line is the best-fit relation for the CNOC1 clusters, and the dash-dot blue line is the best-fit relation for the L04 clusters. The slope is the CNOC1 correlation is slightly shallower, but consistent with the L04 slope. *Bottom Panel*: Plot of the measured N_{500} divided by the value predicted by the L04 scaling relation as a function of redshift for the L04 clusters (blue points) and CNOC1 clusters (red points). The CNOC1 normalization is consistent with the L04 normalization suggesting no evolution in the HON with redshift.

et al. 1996) & CNOC2 (Yee et al. 2000) collaborations and is discussed in detail in those papers as well as Paper I. Similar to the analysis in Paper I, we ignore the "secondary" selection effects (color, position, and z) and use only the magnitude weights, which are the overwhelmingly dominant selection bias (Yee et al. 1996).

The k-correction for each galaxy is taken from the models of Poggianti (1997). The k-corrections depend only mildly on spectral-type and the color/spectral-type model discussed in Paper I is used to estimate a spectral-type for each galaxy. Also, the LFs from Paper I showed that the luminosity evolution in the clusters is passive, but significant (0.35 ± 0.06 magnitudes from $z = 0$ to $z \sim 0.5$). Therefore, an evolution correction from the Poggianti (1997) models is applied to each galaxy, where we have transformed the Poggianti (1997) evolution corrections to our cosmology (see Paper I, §6.1.2). By applying both k and evolutionary corrections the measured $L_{200,K}$ is corrected to $z = 0$, and therefore these values can be directly compared to local studies.

The $L_{200,K}$ for some clusters must also be corrected for the incomplete coverage of R_{200}. We noted that for the HON (§4) the coverage corrections propagate to large errors in the HON when it is computed within R_{200} and because of that, the HON was measured within R_{500}. The incomplete radial coverage is less problematic when computing $L_{200,K}$ because much of the total cluster luminosity comes from the BCG (~ 5 - 30%). Despite the fact that the number of cluster galaxies at $R_{500} < R < R_{200}$ is large, the most luminous galaxies tend to reside in the cluster core, and therefore galaxies at $R_{500} < R < R_{200}$ contribute less to the total luminosity than to the HON.

The clusters without complete coverage have been observed in a strip through the cluster core; therefore, the coverage problems are corrected by computing the luminosity in circular shells. The total luminosity of a shell is multiplied by the ratio of the total area of the shell, to the total area of the shell with imaging/spectroscopic data. Several of the clusters (MS0016+16, MS0451-02, MS1006+12, MS1008-12, and MS1455+22) have no coverage for a few of the outermost shells. For these clusters a correction based on the profile of clusters which have the best coverage in the outer regions is applied. This correction is small in four of the five cases (~ 5-10%), again because the majority of the cluster light comes from the core. MS1455+22 has a very large R_{200} (which is likely to be overestimated, see §4) and therefore the correction is much larger ($\sim 60\%$).

Once the selection function, k-correction and evolution corrections have been applied, and the sum of the luminosity of galaxies brighter than $K^* + 1$ has been tabulated, the "total" luminosity of the cluster is finalized by extrapolating the LF to a fixed

absolute magnitude. We choose to extrapolate to M_K = -21 (i.e., K* + 3 at z = 0), the same limiting absolute magnitude used by L04 and and effectively the same limiting magnitude of the HON. We evolution-correct the combined LF from all 15 clusters to z = 0 (K* = -24.14 ± 0.15 and α = -0.84 ± 0.08, see Paper I) and use this for extrapolation. This LF is consistent with the average LF found by L04 (K* = -24.02 ± 0.02 and α = -0.84 ± 0.02) and because our clusters have been evolution corrected to z = 0, extrapolating the luminosity to M_K = -21 results in a $L_{200,K}$ which can be directly compared between the samples. Before the correction is applied, the contribution from the BCGs is removed from the total cluster light. The BCGs contribute a significant, but variable, fraction of the total cluster light ($\sim$ 5-30% at K* + 1) and do not obey a Schechter function. Including them as part of the extrapolation of the Schechter function would overestimate the total cluster light. The light from the BCG galaxy is re-added to the total once the extrapolation has been done. Lastly, a bootstrap error for each cluster is computed by performing the entire analysis using 300 resamplings with replacement from the data. Table 2 lists the final $L_{200,K}$ values as well as the bootstrap errors.

We examine the correlation between the cluster mass and light by plotting Log(M_{200}) vs. Log($L_{200,K}$) in the first panel of Figure 4. The best-fit linear relation is

$$Log(M_{200}) = (1.20 \pm 0.16)Log(L_{200,K}) - (0.95 \pm 2.21), \qquad (3.5)$$

and the fit has a reduced-χ^2 of 2.65, where again we have ignored MS1455+22 because it is likely to have an incorrect M_{200}. The rms scatter in the M_{200} - $L_{200,K}$ relation is 43% and from this we estimate that the intrinsic scatter is 31%. The scatter in the correlation is about a factor of 1.3 larger than the 34% total, and 24% intrinsic scatter measured by L04 for local clusters. If we invert the axes, we find $L_{200,K} \propto M_{200}^{0.83\pm0.11}$. This agrees with the scaling relation for local clusters with the BCG included which is $L_{200,K} \propto M_{200}^{0.72\pm0.04}$ (L04), and somewhat less well with the scaling relation for local groups which is $L_{200,K} \propto M_{200}^{0.64\pm0.06}$ (Ramella et al. 2004). This shows that the slope, while slightly shallower for groups, does not change significantly over $\sim$ 2 orders of magnitude in cluster mass. Furthermore, the reasonable agreement between the slope and intrinsic scatter in the correlations at different redshifts suggests that whatever physical processes are responsible for building in the correlation have largely taken place by $z \sim 0.3$, and that there is little change in the L_{200} - M_{200} relation from $z \sim 0.3$ to z = 0, besides possibly a small decrease in the scatter.

In the second panel of Figure 4 we plot the correlation between the cluster X-ray

temperature and $L_{200,K}$. The best fit relation with MS1455+22 excluded is

$$Log(T_x) = (0.77 \pm 0.08)Log(L_{200,K}) + (-9.45 \pm 1.07), \qquad (3.6)$$

and has a reduced-χ^2 of 2.35. The rms scatter in the relation is 24% and this corresponds to an intrinsic scatter of 14%, notably better than the M_{200} - $L_{200,K}$ relation. As the CNOC1 clusters are all massive, relaxed X-ray systems, this may not be surprising. Using r-band data, YE03 found the correlation between B_{gc} and T_x for the CNOC1 clusters to have a smaller scatter (21%) than the B_{gc} - M_{200} relation (31%), although they used the T_x values determined by Lewis et al. (1999) rather than the Hicks et al. (2006) values.

If we compare the scatter in the M_{200} vs. $L_{200,K}$ relation to the scatter in the correlations of M_{200} vs. T_x, L_x, and B_{gc} (optical) determined by YE03 for these clusters, we find that the total K-band light is approximately as accurate as those parameters in inferring the dynamical mass. YE03 showed the scatter in the M_{200} vs. T_x, L_x, and B_{gc} (optical) for these clusters was 29%, 35%, and 31% respectively. This demonstrates that $L_{200,K}$ is as good as, but no more accurate than traditional mass indicators at inferring the cluster dynamical mass. It appears the fact that K-band light is a fairly clean tracer of an individual galaxy's stellar mass does not result in a smaller scatter for the $L_{200,K}$ - M_{200} scaling relation, suggesting that the amount of scatter measured in optical scaling relations is a real scatter in relative amounts of stellar mass and dark matter mass in clusters, and not enhanced due to a variance in star-formation properties or stellar populations from cluster-to-cluster.

It is possible that the scatter we measure is enhanced by systematics in the data analysis caused by the need for k-corrections, evolution corrections, spectroscopic selection functions, and coverage corrections; however, the level of scatter we find is of order that found by L04 in local clusters, which do not suffer from those uncertainties. Given that there is no reason to expect the scatter in the scaling relations to become *smaller* at higher-redshift, it would suggest that these corrections have been applied properly and do not significantly increase the overall scatter.

The correlations from Figure 4 are pleasing in the sense that total K-band light is observationally much cheaper to measure than L_x, T_x or M_{200} (via a velocity dispersion or weak lensing) for a given cluster. For clusters in this redshift range, a wide-field NIR camera on a 4m-class telescope can achieve a limiting magnitude of $M_K < K^* + 1$ with an integration time of only a few minutes. This means followup of many candidates in the generation of high-yield cluster cosmology projects is easily achievable.
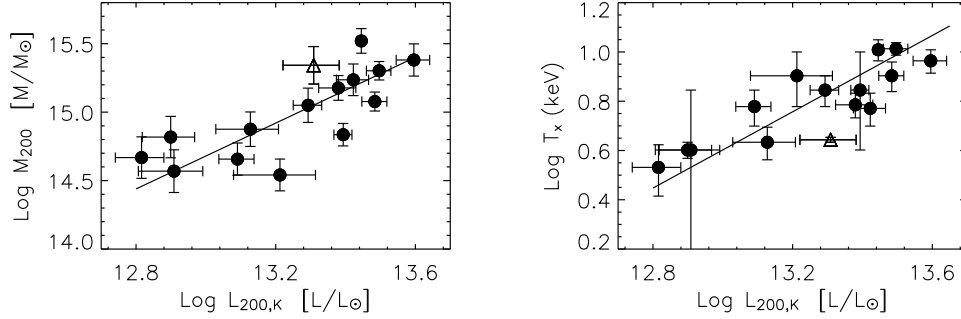
Figure 3.4 Left Panel: Plot of Log(M_{200}) vs. Log($L_{200,K}$) for the CNOC1 clusters. The solid line is the best-fit linear relation. The rms scatter around the relation is 43% (31% intrinsic). Right Panel: Plot of T_x vs. Log($L_{200,K}$). The solid line is the best-fit linear relation and as an rms scatter of 24% (14% intrinsic). MS1455+22 is plotted as an open triangle in both panels and is excluded in the fits.

Unfortunately, a major concern for cosmology projects is that although $L_{200,K}$ appears to be a good proxy for M_{200} or T_x it cannot be used in practice because it requires an *a priori* knowledge of R_{200}. In the next section we show that the NIR-selected richness in a fixed aperture is also well-correlated with the cluster mass and can be used as a mass proxy.

3.6.2 B_{gc} as an Indicator of Cluster Mass

The good correlation between $L_{200,K}$ and M_{200} found for the CNOC1 clusters, and by other authors (e.g. Lin et al. 2003; L04; Rines et al. 2004; Ramella et al. 2004) demonstrates that K-band light can be used as an efficient estimator of the cluster halo mass. Of course, measuring $L_{200,K}$ requires knowledge of R_{200}, which is generally an unknown, whereas the cluster richness, parameterized by B_{gc} does not require R_{200}. B_{gc} is the amplitude of the 3-dimensional, spatial correlation function between the cluster center and the cluster galaxies. If the shape of the 2-dimensional angular correlation function is assumed (i.e., $w(\theta) \propto \theta^{(1-\gamma)}$, with $\gamma \sim 1.8$), then its amplitude can be measured by counting galaxies in a fixed aperture around the cluster center. B_{gc} is then measured by deprojecting the angular correlation function via ($\xi(r) \propto r^{-\gamma}$) and scaling it by a luminosity function. A full derivation and motivation for B_{gc} is presented in Longair & Seldner (1979). The B_{gc} parameter is defined as:

$$B_{gc} = N_{net} \frac{(3-\gamma)D^{\gamma-3}\theta^{\gamma-1}}{2A_\theta I_\gamma \Psi[M(m_0, z)]},$$

(3.7)

Table 3.2. NIR Properties of the CNOC1 Clusters

Cluster	$L_{200,K}$ $L_\odot \times 10^{13}$	$\epsilon L_{200,K}$ $L_\odot \times 10^{13}$	$(M/L)_{200,K}$	$\epsilon (M/L)_{200,K}$	$B_{gc,K}$ $Mpc^{1.8}$	$\epsilon B_{gc,K}$ $Mpc^{1.8}$	N_{500}	ϵN_{500}
(1)	(2)	(3)	(4)	(5)	(6)	(7)	(8)	(9)
A2390	3.14	0.25	64	14	2302	303	338	50
MS0016+16	3.94	0.43	61	24	2298	311	389	56
MS0302+16	0.81	0.17	45	25	674	157	63	25
MS0440+02	1.63	0.43	21	8	1083	210	125	25
MS0451+02	2.40	0.29	63	18	1571	252	313	44
MS0451-03	2.79	0.08	119	34	2897	343	305	59
MS0839+29	0.79	0.14	83	43	1768	266	207	34
MS1006+12	1.96	0.18	57	24	2496	316	377	43
MS1008-12	2.64	0.28	65	28	1745	266	198	44
MS1224+20	1.34	0.27	56	24	733	169	139	32
MS1231+15	1.23	0.14	37	14	967	198	130	27
MS1358+62	3.05	0.25	39	8	1866	275	269	41
MS1455+22	2.03	0.37	108	50	982	199	89	46
MS1512+36	0.65	0.10	71	37	772	172	49	25
MS1621+26	2.47	0.15	27	7	1543	249	225	38

where N_{net} is the background corrected cluster galaxy counts, D is the angular diameter distance to the cluster redshift, θ is the angular size of the counting aperture, A_θ is the angular area of the counting aperture, I_γ is geometric deprojection constant which depends on γ ($I_\gamma = 3.78$ for $\gamma \sim 1.8$), and Ψ is the integrated cluster LF up to the apparent magnitude M, which corresponds to an absolute magnitude m_0 at the redshift z. The normalization of the LF (ϕ^*) is the universal normalization, and not the cluster normalization, so that B_{gc} is the overdensity of galaxies compared to the field density, not the average cluster density. This formula for B_{gc} is slightly different than formula presented in Yee & Lopez-Cruz (1999, their equation 3) in that it contains the A_θ term. We note that in their formula for B_{gc}, Yee & Lopez-Cruz (1999) had inadvertently left

out the A_θ term due to a transcribing error.

At first, B_{gc} may appear to be an unnecessarily complicated measure of the cluster richness; however, using it has some distinct advantages. As interest in an observationally cheap proxy for cluster mass has increased, so have the number of studies which have looked at the correlation between cluster richness and mass (e.g., Hansen et al. 2005; Miller et al. 2005; Gilbank et al. 2004; L04; Rines et al. 2004; Ramella et al. 2004; Lin et al. 2003; Kochanek et al. 2003; YE03). These studies define the cluster richness as the number of galaxies within a fixed aperture, to a fixed magnitude limit. However, because different authors use different apertures, and different magnitude limits, comparison between studies is extremely difficult. The advantage of the B_{gc} parameter is that it assumes a universal spatial distribution, and luminosity function for clusters. Therefore, aside from statistical fluctuations, *the value of B_{gc} is, in principle, identical regardless of what aperture is used to count galaxies, and which magnitude limit is chosen.*

Yee & Lopez-Cruz (1999) verified this was true, but showed that measuring B_{gc} from a fixed aperture with R = 500 kpc (using H_0 = 50 km s^{-1} Mpc^{-1}) produced the lowest statistical errors. Furthermore, they showed that counting galaxies to M < M$_*$ + 1 was all that was required for B_{gc} to be robust. Therefore, our values of $B_{gc,K}$ are computed using a fixed aperture of 500 kpc (although we use H_0 = 70 km s^{-1} Mpc^{-1}) and by counting galaxies to K* + 1.

Again, because B_{gc} requires counting the number of cluster members, we use statistical background subtraction, rather than the spectroscopic weights. YE03 demonstrated that B_{gc}'s computed using both techniques agree extremely well. In order to determine the integrated LF parameter ($\Psi[M(m_0,z)]$) a universal cluster luminosity function must be assumed. We showed in Paper I that besides the passive evolution of the stellar populations, this is a reasonable assumption for the CNOC1 clusters. When calculating $\Psi[M(m_0,z)]$ we assume passive evolution of the LF of our "average" cluster (K* = -24.14, α = -0.84). Unfortunately, we do not have a measurement of the universal ϕ^* in units of Number/Mpc^3. This cannot be determined from the cluster data alone because clusters are high-density regions in the universe, and not representative of the mean value of ϕ^*. Rather than using values from studies of the K-band field LF (which still have fairly large errors) we adopt the approach of Yee & Lopez-Cruz (1999) for determining ϕ^*. They showed that a self-consistent value of ϕ^* could be estimated by evolving the cluster LF assuming a simple model for the evolution of M$^*(z)$. The normalization (ϕ^*) is determined by requiring that the integrated

counts from the LF reproduce the background galaxy counts. We perform the same procedure using a $z_f = 5.0$ model passive evolution model (see Paper I) to parameterize the evolution of $M^*(z)$. By comparing the model background counts to the true background counts and using a χ^2-maximum-likelihood technique we determine $\phi^* = 4.34 \times 10^{-3}$ Mpc^{-3}. This value of ϕ^* is slightly larger than the $\phi^* = 3.40 \pm 0.29 \times 10^{-3}$ Mpc^{-3} determined locally (Kochanek et al. 2001), and about 3 times as large as the $\phi^* = 1.78^{+1.5}_{-0.9} \times 10^{-3}$ Mpc^{-3} measured at $0.2 < z < 0.65$ by Pozzetti et al. (2003). However, even if this value is incorrect it will be systematically incorrect for all clusters and will only affect the intercept in the correlation between $B_{gc,K}$ and other physical parameters. It will not affect the slope or scatter, which are of principle interest.

Column 6 of Table 2 lists the measured values of B_{gc} for the clusters. The errors have been computed using the prescription from Yee & Lopez-Cruz (1999),

$$\frac{\Delta B_{gc,K}}{B_{gc,K}} = \frac{(N_{net} + 1.3^2 N_{bg})^{1/2}}{N_{net}}, \tag{3.8}$$

where N_{bg} is the number of background counts within the 500 kpc and the 1.3^2 term is used to approximately account for the clustering of background galaxies.

In the left panel of Figure 5 we plot $Log(B_{gc,K})$ vs. $Log(M_{200})$ for the clusters. The best fit linear relation with MS1455+22 excluded is

$$Log(M_{200}) = (1.62 \pm 0.24)Log(B_{gc,K}) + (9.86 \pm 0.77). \tag{3.9}$$

The fit has a reduced-χ^2 of 1.29, and the rms scatter of the correlation is 35% (18% intrinsic). This implies that the K-band selected richness is slightly better than the total K-band light for predicting the mass of a galaxy cluster. The difference in total and (intrinsic) scatter between the two parameters is notable, 35%(18%) in M_{200} - $B_{gc,K}$ vs. 43%(31%) in M_{200} - $L_{200,K}$ and this may be because of the smaller aperture used to measure B_{gc}.

In the right panel of Figure 5 we plot $Log(B_{gc,K})$ vs. $Log(T_x)$. The best fit linear relation with MS1455+22 excluded is

$$Log(T_x) = (0.94 \pm 0.13)Log(B_{gc,K}) - (2.20 \pm 0.42), \tag{3.10}$$

and has a reduced-χ^2 of 2.00 and an rms scatter of 25% (16% intrinsic). This is very similar to the scatter seen in the $L_{200,K}$ - T_x relation and shows that the fixed-aperture richness is an excellent indicator of the cluster X-ray temperature at the $\sim$ 25% level.

If we compare the accuracy of $B_{gc,K}$ to the optical B_{gc} we find that they are almost
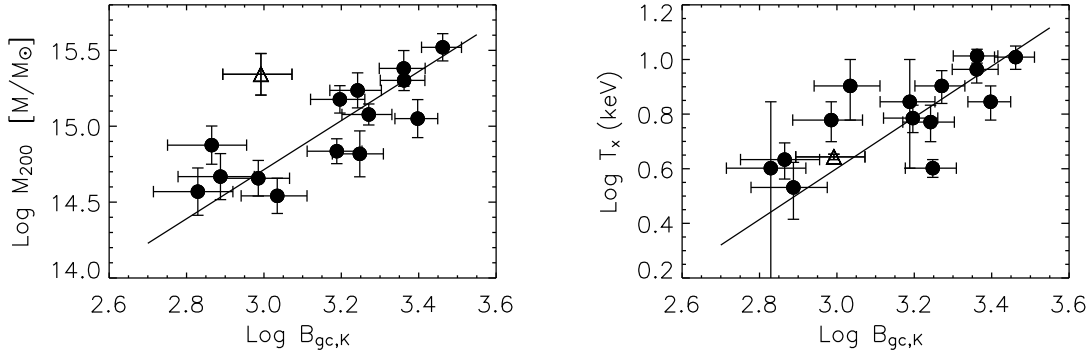
Figure 3.5 Left Panel: Plot of Log(M_{200}) vs. Log($B_{gc,K}$) for the CNOC1 clusters. The solid line is the best-fit linear relation and has an rms scatter of 35% (18% intrinsic). Right Panel: Plot of Log(T_x) vs. Log($B_{gc,K}$) for the same clusters. The solid line is the best-fit linear relation and has an rms scatter of 25% (16% intrinsic). MS1455+22 is plotted as an open triangle in both panels and is excluded in the fits.

identical at predicting M_{200} (scatters of 35%, and 31% respectively) as well as T_x (scatters of 25% and 21% respectively). $B_{gc,K}$ for the CNOC1 clusters also has a similar scatter to the fixed-aperture richnesses measured for local clusters in the K-band. L04 showed that the scatter in the number of galaxies within 0.75 Mpc vs. M_{500} was 43%, and estimated that ~ 24% of the scatter was intrinsic. The L04 cluster masses are measured using T_x and therefore the it is more relevant to compare the L04 intrinsic scatter to the intrinsic scatter in the CNOC1 B_{gc} - T_x relation. The scatter in the L04 relation is somewhat larger than the scatter from the CNOC1 relation, but this may be due to the fact that the CNOC1 clusters are generally more massive than the L04 clusters.

These results demonstrate that relatively cheap IR imaging can be used to determine cluster masses with good accuracy. Specifically, IR imaging of even higher redshift clusters ($z > 0.5$) will be valuable for determining masses in large optical cluster surveys. IR richnesses will likely be more robust than optical richnesses at predicting cluster masses at high-redshift because at high-redshift optical bandpassess probe bluer parts of a galaxy's spectrum where the star-formation properties can drastically alter a galaxy's luminosity.

It is also possible that in the case of large cluster surveys, $B_{gc,K}$ may prove to be as valuable for predicting the cluster halo mass as the cluster velocity dispersion or X-ray temperature. Determining the cluster mass from either the line-of-sight velocity dispersion or X-ray temperature require assumptions about the dynamical state of the cluster. Dynamical masses require that the cluster is in virial equilibrium and that that

the shape of the velocity ellipsoid is known (generally it is assumed to be isotropic). X-ray masses require the assumption of hydrostatic equilibrium, and spherical symmetry. They also require a correction if the cluster has a cooling flow. In cases where these assumptions do not apply (such as cluster-cluster mergers, or a collapsing system in the process of forming) the masses of the clusters may be poorly estimated, and these clusters will contaminate the measurement of the cluster mass function. The number of catastrophic outliers can have serious consequences on the measured cosmological parameters because they are particularly sensitive to the number of rare, massive clusters. On the other hand, if clusters which are unrelaxed, or currently undergoing a merger do not have the K-band light of their galaxies altered significantly, then using K-band richness as a mass indicator could potentially be a robust method for determining the masses of clusters that are not in dynamical or hydrostatic equilibrium.

One way to test this hypothesis is to use weak-lensing to measure the mass of clusters and compare those masses to B_{gc}, and $B_{gc,K}$. Weak-lensing does not require any assumptions about the dynamical state of the clusters and therefore it is an unbiased (although statistically noisy) measure of the cluster mass. Weak lensing masses for a subsample of the CNOC1 clusters have been measured and will be compared to $B_{gc,K}$ in a future paper.

3.7 The K band Mass-to-Light Ratio

Recent studies of the K-band M/L ratio in local clusters (Lin et al. 2003, L04, Rines et al. 2004, Ramalla et al. 2004) have shown that the K-band cluster M/L ratio is an increasing function of cluster mass (although Kochanek et al. 2003 find it is roughly constant with mass). These studies have also found that the M/L ratio is a slowly decreasing function of radius, with the integrated M/L ratio at R_{200} ($M_{200}/L_{200,K}$) being $\sim 15\%$ smaller than the M/L ratio at R_{500} (e.g., L04). Here we present the first K-band M/L ratios of massive, intermediate-redshift clusters.

We use the k and evolution corrected $L_{200,K}$ values to compute $M_{200}/L_{200,K}$ and therefore it is the $M_{200}/L_{200,K}$ ratio of clusters corrected to $z = 0$. The values are listed in Table 3 and the errors computed by propagating the M_{200} and L_{200} errors in quadrature. In Figure 6 we plot $\text{Log}(M_{200}/L_{200,K})$ vs $\text{Log}(M_{200})$. There is a clear correlation of M/L with M_{200} in the CNOC1 clusters. The Spearman rank-correlation coefficient for

these data is 0.60, which implies a probability of 0.017 that the variables are uncorrelated. The solid line in the plot is the best-fit linear relation with MS1455+22 excluded:

$$Log(M_{200}/L_{200,K}) = (0.57 \pm 0.13)Log(M_{200}) - (6.92 \pm 2.04). \qquad (3.11)$$

The fit has a reduced-χ^2 of 0.964 and implies that M/L $\propto$ M$^{0.57\pm0.13}$. Interestingly, this slope is about a factor of 3 steeper than the M/L $\propto$ M$^{0.17\pm0.11}$ that would be inferred using the $Log(M_{200})$ - $Log(L_{200,K})$ relation (Eqn 5) where the variables are less directly correlated (they still both depend on R$_{200}$). As a comparison, the inferred relation is plotted as the dashed line in Figure 6. The inferred relation, M/L $\propto$ M$^{0.17\pm0.11}$, agrees well with the relation from local clusters where M/L $\propto$ M$^\alpha$ with α = 0.26 $\pm$ 0.04 (L04), and α = 0.31 $\pm$ 0.09 (Rines et al. 2004), but does not agree well with the value for local groups, α = 0.56 $\pm$ 0.05 (Ramella et al. 2004). The Ramella et al. relation is similar to the correlation obtained by fitting $Log(M/L)$ vs. $Log(M_{200})$ directly.

It is likely that the inconsistent slopes from our own data, as well as between the local cluster and group M/L vs. M$_{200}$ are primarily caused by the large scatter in the M$_{200}$ - L$_{200,K}$ scaling relations and the difficulties associated in fitting to data with a larger scatter than is accounted for by the error bars. It is probably not caused by real differences in the M/L vs. M$_{200}$ scaling relations for the different cluster samples. In our own data the M$_{200}$ - L$_{200,K}$ relation has a large reduced-χ^2 (2.65). Examination of Figure 4 suggests that the inflated reduced-χ^2 is not caused by a linear fit being the incorrect model for these data, but is caused by a handful of significant outliers to the relation.

Another consideration is that the intrinsic correlation between M/L and M$_{200}$ (mass is in both parameters) can contribute to the discrepancy in slope. The Ramella et al. (2004) masses and our own masses are determined from the cluster velocity dispersion (σ_1) and equation 2, where M$_{200} \propto \sigma_1^3$. The L04 masses are determined from T$_x$ using the fit from Finoguenov et al. (2001) where M$_{200} \propto$ T$_x^{1.58}$. Given that M$_{200}$ depends on σ_1^3 but only on T$_x^{1.58}$, catastrophic errors in σ_1 will translate to larger errors in M$_{200}$ than catastrophic errors in T$_x$ will. Consequently, given that the $Log(M/L)$ vs. $Log(M_{200})$ slope is < 1, clusters which have their velocity dispersions incorrectly measured (and not properly accounted for by the errors, such as in the case of non-virialization) will steepen the slope of the M/L vs. M$_{200}$ correlation because the mass term is in both parameters.

As a test, we remove the highest and lowest mass CNOC1 clusters (MS0440+02 and MS0451-03, both of which are significant outliers in the M$_{200}$ - L$_{200}$ relation) and
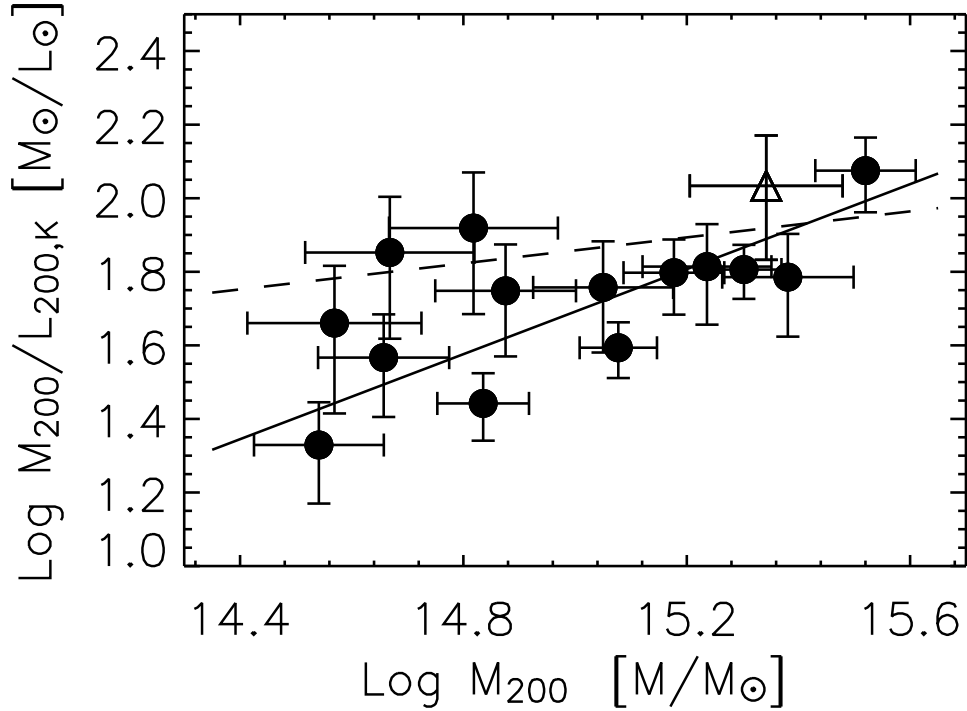
Figure 3.6 Plot of $\text{Log}(M_{200}/L_{200,K})$ vs $\text{Log}(M_{200})$ for the CNOC1 clusters. The solid line is the best-fit relation. The dashed line is the relation that is inferred from the $\text{Log}(M_{200})$ - $\text{Log}(L_{200,K})$ fit. MS1455+22 is plotted as an open triangle and is excluded in the fit.

refit. We find a slope of $\alpha = 0.44 \pm 0.15$, which is more consistent with the $\alpha = 0.17 \pm 0.11$ inferred directly from the M_{200} vs. $L_{200,K}$ relation. Unfortunately, this problem of outliers makes determining a robust slope for the M/L vs. M_{200} correlation difficult. The data are less directly correlated in the case of $\text{Log}(M_{200})$ vs. $\text{Log}(L_{200,K})$, and therefore we return to that relation and adopt $M_{200}/L_{200,K} \propto M^{0.17 \pm 0.11}$ as the best slope for M/L vs. M_{200} scaling relation for the CNOC1 clusters.

This slope, where M/L increases with increasing M_{200} supports the scenario proposed by both L04 and Rines et al. (2004), where either the star-formation efficiency of cluster galaxies is a decreasing function of cluster mass, or else that the amount of intra-cluster light is an increasing function of cluster mass. Interestingly, the slope of this scaling relation for the CNOC1 clusters is consistent with the the slope in local clusters and this shows that the M/L vs. M_{200} correlation is in place by at least $z \sim$ 0.3, roughly 4 Gyr in lookback time.

3.8 Ω_m from the Oort Technique

The original purpose of the CNOC1 project was to measure the cosmological density parameter $\Omega_{m,0} \equiv \rho_o/\rho_c$ using the Oort (1958) technique. The cluster M/L ratio, divided by the M/L ratio for closure $(\mathrm{M/L})_c \equiv \rho_c/j$, where j is the field luminosity density, provides a direct measure of $\Omega_{m,0}$ which is independent of the Hubble parameter. There has been some concern with this method because recent numerical simulations suggest that light is a biased tracer of dark matter, and that the M/L ratio of any region in the universe which contains galaxies automatically provides an underestimate of the universal M/L ratio, and an underestimate of $\Omega_{m,0}$ (e.g., Ostriker et al. 2003). However, this is only a significant concern for low-density regions in the universe (i.e., the group scale or less). Unlike those lower density regions, rich clusters are assembled from regions of > 10 Mpc across (Carlberg et al. 1997) and therefore, provided that observations extend to the entire volume of the cluster (i.e., $R \sim R_{200}$), clusters should contain a sufficient collapsed volume to provide a representative sample of the universal M/L ratio (e.g. Carlberg et al. 1996, Carlberg et al. 1997). This is yet to be verified in numerical simulations as, until recently, they lacked enough volume to contain rich clusters. The CNOC1 project was designed specifically with this biasing concern in mind and therefore is a wide-field study of a sample of rich clusters.

Although biasing is not a major concern for the cluster technique, we know that the stellar populations of galaxies in the cluster and field environments are different (e.g., Ellingson et al. 2001, Balogh et al. 1999, Poggianti et al. 1999, Dressler et al. 1997) and without a good understanding on how these differences affect the integrated luminosity of these regions, there arises the potential for a systematic error in $\Omega_{m,0}$.

Using the r-band data for the CNOC1 clusters, Carlberg et al. (1997) showed that $\Omega_{m,0} = 0.19 \pm 0.06$ (random) ± 0.04 (systematic). In their analysis they found that the r-band cluster galaxies were on average 0.11 ± 0.05 mag fainter than field galaxies at this redshift and hence they decreased the cluster M/L ratio accordingly. Given the need for this correction, it is advantageous to perform the same analysis with infrared data, because infrared light is a better tracer of total stellar mass than optical light. The infrared luminosity of galaxies does not depend strongly on the current star-formation properties of the stellar population and consequently, little or no correction is required to account for the varying star-formation properties of the field and cluster environment. The only potential correction required would be if the clus-

ter environment played a role in the star-formation *efficiency* of galaxies. A differing star-formation efficiency could manifest itself in two ways: 1) the stellar mass may be distributed differently in the cluster/field environment (i.e., the *shape* of the field and cluster LFs may be different); or 2) baryons may be converted into stars at a different rate than in the field (i.e., the ratio of the stellar mass to dark matter mass could be different between these environments).

In terms of problem 1), Paper I showed that the cluster K^* was brighter than, but consistent with the field value ($\Delta K^* = 0.25 \pm 0.26$ mag). Paper I also showed that α from the CNOC1 cluster LF was the same as α for local clusters as well as the local field. Those results agreed well with local measurements which showed the cluster K^* and α are roughly the same as the field (although we note that both L04 and Rines et al. 2004 find that the cluster K^* is ~ 0.2 mag brighter at the 2σ level). Given that both K^* and α for the cluster LF are similar to the field LF, the distribution of galaxies in terms of luminosity (and by corollary stellar mass) should be similar in both environments.

In terms of problem 2), it is important to note that the cluster M/L ratio continues to be an increasing function of cluster mass, even for objects as massive as the CNOC1 clusters. This shows that the overall rate of converting baryons to stars is a function of environment. The rich CNOC1 clusters have a K-band M/L ratio which is about an order of magnitude larger than the M/L ratio of groups (e.g., L04, Ramella et al. 2004), and in turn, the group M/L ratio is about an order of magnitude larger than for individual galaxies (e.g., Brinchmann & Ellis 2000). Remarkably, despite the fact that rich clusters are two orders of magnitude less efficient in converting baryons to stars than individual galaxies, their continually increasing M/L ratio with increasing mass suggests the possibility that they may still be slightly biased tracers of stellar mass in the universe. Unless the M/L vs. M_{200} relation flattens at the scale of $\sim 10^{15}$ $M_\odot$, the M/L ratio of clusters could be lower than the universal value. Unfortunately, there is no data for the K-band M/L ratio of superclusters to determine if the M/L ratio flattens at this size scale.

The mean M/L ratio for the clusters (corrected for passive evolution to $z = 0$) is 61.2 ± 1.8 $M_\odot/L_\odot$. Combining this with the luminosity density of the local universe measured by Kochanek et al. (2001) we find $\Omega_{m,0} = 0.22 \pm 0.02$ (random). This result is in good agreement with combined constraints from WMAP third-year results (WMAP3) and various other techniques (Spergel et al. 2006). The combined WMAP3 constraints on $\Omega_{m,0}$ range from a low-density of $\Omega_{m,0} = 0.226^{+0.030}_{-0.041}$ to a high-density

of $\Omega_{m,0} = 0.299^{+0.019}_{-0.025}$. Interestingly, the measurement from the clusters is closest to the lowest density of the of preferred values from combined constraints. Previous studies using K-band M/L ratios of local clusters have also found values of $\Omega_{m,0}$ on the low-end of preferred values.

Both Rines et al. (2004) and Lin et al. (2003) measured $\Omega_{m,0}$ using their local cluster samples. Rines et al. found that the result depended strongly on the location in the clusters where the M/L ratio was measured. The cluster infall region had a lower M/L ratio than the viralized region and therefore they found $\Omega_{m,0} = 0.18 \pm 0.04$ from the virial region and $\Omega_{m,0} = 0.13 \pm 0.03$ from the infall region. Lin et al. (2003) performed the same analysis with a larger sample of 27 clusters. They found $\Omega_{m,0} = 0.17 \pm 0.02$ using the mean M/L ratio of all clusters, and $\Omega_{m,0} = 0.19 \pm 0.03$ using a subsample of their most massive clusters.

Our analysis is in good agreement with both these studies, as well as the r-band measurement from the same clusters by Carlberg et al. (1997). Our results further confirm that $\Omega_{m,0}$ from clusters agrees well with concordance values but tends to be on the low-density end of preferred values. It is possible that the cluster measurements prefer lower $\Omega_{m,0}$ because their M/L ratios are still lower than the universal value. A measurement of the K-band M/L ratio on the supercluster scale would be a useful way to test this hypothesis. Regardless, the fact that the cluster $\Omega_{m,0}$ still agrees well with recent measurements of $\Omega_{m,0}$ using a variety of independent techniques, and combinations thereof suggests that the cluster M/L ratio is unlikely to be significantly lower than the universal value.

3.9   Summary

We have presented the K-band scaling relations for 15 moderate-redshift clusters with extensive optical spectroscopy and wide-field K-band imaging. The cluster HON is well-correlated with M_{500} and T_x; however, the intrinsic scatter in the scaling relations at $z \sim 0.3$ is fairly large (37% and 46% respectively). Comparing to local clusters we find that the HON is consistent with no evolution at fixed cluster mass out to $z \sim 0.5$. This result, in tandem with the purely passive evolution of the cluster LF, and the fact that the cluster LF does not depend on mass suggests that if the significant tidal stripping of galaxy halos in clusters seen in numerical simulation occurs, the stellar mass within the halo is tightly bound and remains intact. This interpretation is fur-

ther supported by recent SPH simulations which show that the baryonic matter is the amongst the most tightly bound mass within the halo.

Our data also show that both $L_{200,K}$ and $B_{gc,K}$ are well-correlated with the cluster dynamical mass and X-ray temperature. The slope of the L_{200} - M_{200} relation at $z \sim 0.3$ ($L_{200,K} \propto M_{200}^{0.83 \pm 0.11}$) is consistent with the slope measured for local clusters, suggesting that the cluster scaling relations are in place by at least $z \sim 0.3$. The good correlation, and relatively small scatter (intrinsic + measurement) in the $B_{gc,K}$ - M_{200} relation (35%) and $B_{gc,K}$ - T_x relation (25%) suggests that $B_{gc,K}$ would be useful mass indicator for upcoming cluster cosmology projects.

Our results from the M/L ratios of the clusters show that the moderate-redshift CNOC1 clusters are very similar to local clusters in that the M/L ratio is a slowly increasing function of cluster mass. By comparing the cluster M/L ratio to the local luminosity density we estimate that $\Omega_{m,0} = 0.22 \pm 0.02$, which agrees well with the original analysis of the CNOC1 clusters using optical data as well as with the local estimates using K-band photometry. The measured value is also in good agreement with recent WMAP third year joint constraints; however, similar to previous cluster studies the value is on the low-density end of preferred values.

The combined analysis of this paper and Paper I present a relatively simple picture of the evolution of the near-infrared properties of clusters from $z = 0$ to $z \sim 0.3$. The correlation between the cluster near-infrared properties (i.e., $L_{200,K}$, N_{500}, and $M_{200}/L_{200,K}$) and M_{200} shows no significant change between $z = 0$ and $z \sim 0.3$. Furthermore, the scatter in these scaling relations is similar at both redshifts. The cluster LF shows only passive evolution between $z = 0$ and $z \sim 0.3$ and does not depend on cluster mass. In addition to this, the (small) difference between the field and cluster LF at $z = 0$ is unchanged at $z \sim 0.3$. These results all show that there is little evolution in the the bulk of the stellar mass in cluster galaxies over this redshift range besides the passive aging of the stellar populations.

Specifically, it appears that 1) the significant tidal stripping of halo in high-density regions seen in N-body simulations does not affect the stellar mass contained in galaxies nor change the cluster scaling relations; 2) given passive evolution of the LF, and no-evolution in the HON, mergers and disruptions are unlikely to play a significant role in cluster galaxy evolution at $z < 0.3$; and 3) that the changes seen in the cluster stellar populations over the redshift interval $z = 0$ to $z \sim 0.3$ (i.e., the increase in blue-fraction/star-formation properties, and evolution of the morphology-density relation) are "superficial" - they result from changes in a small part of a galaxy's stellar mass,

while the majority of the stellar mass is already in place and passively evolving.

Overall, it appears that the bulk of the stellar mass in cluster galaxies is in place, and evolving passively with few mergers or disruptions between $z \sim 0.3$ and $z = 0$, and that the the cluster scaling relations are produced by processes that occur at higher redshifts.

Acknowledgements

Chapter 4

The $3.6\mu m$, $4.5\mu m$, $5.8\mu m$ and $8.0\mu m$ Cluster Luminosity Functions

To be published as:

"The Evolution of Dusty Star Formation and Stellar Mass Assembly in Clusters: Results from the IRAC $3.6\mu m$, $4.5\mu m$, $5.8\mu m$ and $8.0\mu m$ Cluster Luminosity Functions"

Muzzin, A., Wilson, G., Lacy, M., Yee, H.K.C. & Stanford S. A., 2007, ApJ, submitted August 2007

4.1 Abstract

We present a catalogue of 99 clusters and groups of galaxies in the redshift range $0.1 < z_{phot} < 1.3$ discovered in the *Spitzer* First Look Survey (FLS). The clusters are selected by their R_c - [$3.6\mu m$] galaxy color-magnitude relation using the cluster red-sequence algorithm. Spectroscopic redshifts from numerous FLS followup projects confirm the photometric redshifts of 29 clusters and demonstrate that the R_c - [$3.6\mu m$] red-sequence color provides photometric redshifts with an accuracy of $\Delta z = 0.04$ in the redshift range $0.1 < z < 1.0$. Using this cluster sample we compute the [$3.6\mu m$], [$4.5\mu m$], [$5.8\mu m$], & [$8.0\mu m$] cluster luminosity functions (LFs). Similar to previous studies, we find that for the bands that trace stellar mass at these redshifts ([$3.6\mu m$], [$4.5\mu m$]) the evolution in M^* is consistent with a passively evolving population of galaxies with a high formation redshift ($z_f > 1.5$). Using the [$3.6\mu m$] LF as a proxy for stellar luminosity we remove this component from the mid-IR ([$5.8\mu m$] & [$8.0\mu m$])

cluster LF and measure the LF of dusty star formation/AGN in clusters. We find that at $z < 0.4$ the bright-end of the cluster [8.0μm] LF is well-described by a composite population of quiescent galaxies and regular star forming galaxies with a mix consistent with typical cluster blue fractions; however, at $z > 0.4$, an additional population of dusty starburst galaxies is required to properly model the [8.0μm] LFs. Comparison to field studies at similar redshifts shows a strong differential evolution in the field and cluster [8.0μm] LFs with redshift. At $z \sim 0.65$ [8.0μm]-detected galaxies are more abundant in clusters compared to the field, but thereafter the number of [8.0μm] sources in clusters declines with decreasing redshift and by $z \sim 0.15$, clusters are underdense relative to the field by a factor of ~ 5. The rapid differential evolution between the cluster and field suggest a scenario where dusty starbursts are preferentially triggered in clusters at higher redshift, but quickly quenched thereafter by the high density environment.

4.2 Introduction

Since the compilation of the first large samples of galaxy clusters almost 50 years ago (Zwicky 1961; Abell 1958), clusters have been used as fundamental probes of the effect of environment on the evolution of galaxies. Over this time, our understanding of this phenomenon has grown significantly, and a basic picture of the formation and evolution of cluster galaxies between $0 < z < 1$ has emerged. Studies of the stellar populations of cluster galaxies via the fundamental plane (e.g., van Dokkum et al. 1998; van Dokkum & Stanford 2003; Holden et al. 2005) and the evolution of the cluster color-magnitude relation (e.g., Ellis et al. 1997; Stanford et al. 1998; Gladders et al. 1998; Blakeslee et al. 2003; Holden et al. 2004; Mei et al. 2006; Homeier et al. 2006; Tran et al. 2007) have shown that the majority of stars in cluster galaxies are formed at high-redshift ($z > 2$) and that most of the evolution thereafter is the passive aging of these stellar populations. Studies of the evolution of the near-infrared (NIR) luminosity functions (LFs) of clusters have shown that not only are the stellar populations old, but that the bulk of the stellar mass is already assembled into massive galaxies at high-redshift (e.g., De Propris et al. 1999; Toft et al. 2003; Strazullo et al. 2006; Lin et al. 2006; Muzzin et al. 2007a). Furthermore, it appears that the cluster scaling relations seen locally ($z < 0.1$, e.g., Lin et al. 2004; Rines et al. 2004; Lin et al. 2003), such as the Halo Occupation Distribution, Mass-to-Light ratio, and the galaxy num-

ber/luminosity density profile are already in place by at least $z \sim 0.5$ (e.g., Muzzin et al. 2007b; Lin et al. 2006).

These studies suggest a picture where the formation of the stars in cluster galaxies, as well as the assembly of the galaxies themselves occurs at a higher redshift than has yet been studied in detail; and that, other than the passive aging of the stellar populations, clusters and cluster galaxies have changed relatively little since $z \sim 1$. This picture appears to be a reasonable zeroth-order description of the evolution of cluster galaxies; however, there are still properties of the cluster population which cannot be explained within this context. In particular, there are significant changes in the morphology (Dressler et al. 1997; Postman et al. 2005, Smith et al., 2005), color (e.g., Butcher & Oemler 1984; Rakos & Schombert 1995; Smail et al. 1998; Ellingson et al. 2001; Margoniner et al. 2001) and star-formation properties (e.g., Balogh et al. 1999; Dressler et al. 1999; Poggianti et al. 1999; Dressler et al. 2004; Tran et al. 2005a; Poggianti et al. 2006, although see Kodama et al. 2004) of cluster galaxies since $z \sim 1$. The fraction of blue, star forming galaxies increases from almost zero at $z = 0$ to as much as 50% at $z \sim 0.5$ (the so-called Butcher-Oemler Effect), and correspondingly, the fraction of S0 galaxies in clusters drops by a factor of 2-3, with similar increase in the number of spiral/irregular galaxies over the same redshift range (Dressler et al. 1997). Naively, these results suggest that gas-rich, star-forming galaxies at high-redshift have their star-formation truncated by the cluster environment at moderate redshift and become the dominate S0 population seen locally. How such a transformation occurs, and how it avoids leaving a notable imprint on the stellar populations, is still not well-understood.

Citing an abundance of post-starburst (k+a) galaxies in clusters at $z \sim 0.4$, Poggianti et al. (1999) and Dressler et al. (2004) suggested that there may be an abundance of dusty starburst galaxies in clusters at moderate redshift, and that the dusty starburst and k+a galaxies may represent the intermediate stages between regular star forming late-type galaxies and S0 galaxies (e.g., Shioya et al. 2004; Bekki & Couch 2003). In particular, they suggested that the cluster e(a) galaxies would be the best candidates for dusty starburst galaxies because their inferred star formation rates appear larger from Hα emission than from [OII] emission. If the cluster environment excites a dusty starburst from harassment, tidal interaction, or ram-pressure stripping, then this may quickly deplete a star forming galaxy of its gas, transforming it first into a k+a galaxy, and then leaving it an S0. More detailed work on two $z \sim 0.5$ clusters by Moran et al. (2005) also showed an abundance of starbursting galaxies conspicuously near the

cluster virial radius, suggesting a environmental origin to their "rejuvenation". *ISO* observations of relatively nearby clusters have detected significant amounts of dust-obscured star formation (e.g., Fadda et al. 2000; Duc et al. 2002; Biviano et al. 2004; Coia et al. 2005), and this has recently been confirmed at even higher redshift ($z = $ 0.4 - 0.8) by *Spitzer* observations (Geach et al. 2006; Marcillac et al. 2007). Despite this, it is currently unclear whether there is a population of dusty starbursts which is sufficiently abundant to be the progenitors of the large number of cluster k+a galaxies.

Alternatively, there is evidence from other cluster samples that the S0 population may simply be the result of the truncation of star formation in infalling late-type galaxies via gas strangulation (e.g., Abraham et al. 1996; Balogh et al. 1999; Treu et al. 2003; Moran et al. 2006) and that no accompanying starburst occurs. Most likely, the star formation and morphology of galaxies are transformed both "actively" (as in a starburst triggered from merging/harassment/tidal forces) and "passively" (from gas strangulation or ram-pressure stripping), and that the magnitude of each effect varies significantly from cluster-to-cluster and possibly by epoch, which may explain why studies of small numbers of clusters have found discrepant results. Both processes can be active within massive clusters as was demonstrated by Cortese et al. (2007), who found two interesting galaxies in Abell 1689 and Abell 2667, one of which seems to be undergoing gas strangulation and ram-pressure stripping, while the other is experiencing an induced starburst. There is evidence that galaxies in clusters that are less dynamically relaxed have larger star formation rates (e.g., Owen et al. 1999; Metevier et al. 2000; Moss & Whittle 2000; Owen et al. 2005; Moran et al. 2005; Coia et al. 2005, and numerous others) and that the accretion of large substructures induces starbursts from harassment and tidal forces.

The most obvious way to understand whether dusty starbursts are important in the evolution of cluster galaxies is to observe their abundances directly in the mid-IR. In particular, differences in the mid-IR LFs of the cluster and field environments can be used to determine if dusty starbursts are more common in the cluster environment. If so, it would suggest that environmental processes may be responsible for triggering these events.

The InfraRed Array Camera (IRAC) onboard *Spitzer* provides a unique tool for studying this problem. IRAC images in 4 bands simultaneously ([$3.6\mu m$], [$4.5\mu m$], [$5.8\mu m$], [$8.0\mu m$]) and this is particularly advantageous because [$3.6\mu m$] and [$4.5\mu m$] observations are a good proxy for the stellar mass of cluster galaxies between $0 < z < 1$, and [$5.8\mu m$] and [$8.0\mu m$] are sensitive to emission from warm dust (i.e., from

dusty star forming regions) over the same redshift range. In particular, the Polycyclic Aromatic Hydrocarbons (PAHs) emit strong line emission at rest frame $3.3\mu m$, $6.2\mu m$, $7.7\mu m$, $8.6\mu m$, and $11.3\mu m$ (e.g., Gillett et al. 1973; Willner et al. 1977). These features, in addition to the warm dust continuum, are sensitive indicators of dusty star formation, and several studies have already shown a good correlation between [$8.0\mu m$] flux and star formation rate (SFR; e.g., Calzetti et al. 2005; Wu et al. 2005). Therefore, examining the suite of IRAC cluster LFs at redshifts $0 < z < 1$ shows both the evolution of the majority of stellar mass in cluster galaxies, as well as the evolution of dusty star formation in the same galaxies.

The obvious approach to measuring the presence of dusty star formation in clusters is to observe a handful of "canonical" galaxy clusters with IRAC. However, given that determining the LF from a single cluster suffers significantly from Poisson noise, and perhaps most importantly, *is not necessarily representative of the average cluster population at a given mass/epoch*, a better approach would be to stack large numbers of clusters in order to improve the statistical errors, and avoid peculiarities associated with individual clusters. This approach requires targeted observations of numerous clusters, which is time-consuming compared to other alternatives. For example, large-area *Spitzer* surveys such as the 50 deg^2 *Spitzer* Wide-area Infrared Extragalactic Survey (SWIRE[1], Lonsdale et al. 2003), the 8.5 deg^2 IRAC Shallow Survey (Eisenhardt et al. 2004), and the 3.8 deg^2 *Spitzer* First Look Survey (FLS[2], Lacy et al. 2005) are now, or soon-to-be, publically available and these fields already contain significant amounts of optical photometry. These wide optical-IRAC datasets can be employed to find clusters in the survey area itself using optical cluster detection methods such as the cluster red-sequence (CRS) technique (Gladders & Yee 2000, hereafter GY00), or photometric redshifts (e.g., Brodwin et al. 2006). Subsequently, the IRAC survey data can be used to study the LFs of clusters at a much larger range of masses and redshifts than could be reasonably followed up by *Spitzer*. Furthermore, these surveys also provide panoramic imaging of clusters out to many virial radii, something that has thus far rarely been attempted because it is time-consuming.

Finding clusters with the CRS algorithm is relatively straightforward with the ancillary data available from these surveys. The technique exploits the fact that the cluster population is dominated by early-type galaxies, and that these galaxies form a tight

---

[1]SWIRE data are publically available at http://swire.ipac.caltech.edu/swire/
[2]The FLS data are publically available at http://ssc.spitzer.caltech.edu/fls/

red-sequence in color-magnitude space. If two filters which span the 4000Å break are used to construct color-magnitude diagrams, early-types are always the brightest, reddest galaxies at any redshift (e.g., GY00) and therefore provide significant contrast from the field. The CRS technique is well-tested and provides photometric redshifts accurate to $\sim$ 5% (Gilbank et al. 2007a; Blindert et al. 2004) as well as a low false-positive rate (Gilbank et al. 2007a; Blindert et al. 2004; Gladders & Yee 2005). The method has been used for the 100 deg^2 Red-sequence Cluster Survey (RCS-1, Gladders & Yee 2005) and is also being used for the next generation, 1000 deg^2 RCS-2 survey (Yee et al. 2007). Variations of the red-sequence method have also been used to detect clusters in the Sloan Digital Sky Survey (the "BCGmax" algorithm, Koester et al. 2007; Bahcall et al. 2003) as well as in the fields of X-ray surveys (e.g. Gilbank et al. 2004; Barkhouse et al. 2006).

In this paper we combine the *Spitzer* FLS R$_c$-band and [3.6μm] photometry and use it to detect clusters with the CRS algorithm. Given the depth of the data, and that the R$_c$ - [3.6μm] filter combination spans the rest-frame 4000Å break to $z > 1$, we are capable of detecting a richness-limited sample of clusters out to $z \sim 1$. Using the sample of clusters discovered in the FLS we compute the [3.6μm], [4.5μm], [5.8μm], and [8.0μm] LFs of clusters $0.1 < z < 1.0$ and study the role of dusty star formation in cluster galaxy evolution. A second paper on the abundance of dusty starburst galaxies detected at [24μm] in the same clusters using the FLS MIPS data is currently in preparation by Muzzin et al. (2007).

The structure of this paper is as follows. In §2 we give a brief overview of the optical, IRAC, and spectroscopic data used in the paper. Section 3 describes the cluster-finding algorithm used to detect clusters and §4 contains the FLS cluster catalogue, and a basic description of its properties. In §5 we present the IRAC cluster LFs and §6 contains a discussion of these results as well as a comparison of the cluster and field LFs. We conclude with a summary in §7. Throughout this paper we assume an Ω_m = 0.3, Ω_Λ = 0.7, H$_0$ = 70 km s^{-1} Mpc $^{-1}$ cosmology. All magnitudes are on the Vega system.

4.3 Data Set

4.3.1 *Spitzer* IRAC Data and Photometry

The IRAC imaging data for this project was observed as part of the publically available, *Spitzer* First Look Survey (FLS; see Lacy et al. 2005 for details of the data acquisition and reduction). The FLS was the first science survey program undertaken after the telescope's in-orbit-checkout was completed. It covers 3.8 square degrees and has imaging in the four IRAC bandpasses ($[3.6\mu m]$, $[4.5\mu m]$, $[5.8\mu m]$, $[8.0\mu m]$). The FLS is a shallow survey with a total integration time of only 60 seconds per pixel. Because IRAC images all four channels simultaneously, the total integration time is identical in each channel. The resulting 5σ limiting flux densities are 20, 25, 100, and 100 μJy in the $[3.6\mu m]$, $[4.5\mu m]$, $[5.8\ \mu m]$, $[8.0\ \mu m]$ bandpasses, respectively. These flux densities correspond to Vega magnitudes of 18.0, 17.2, 15.2, and 14.6 mag, respectively. The 50% completeness limits for the 4 channels are 18.5, 18.0, 16.0, 15.4 mag and hereafter we use these limits for the cluster finding algorithm (§3) and computing the cluster LFs (§5). Completeness corrections are made to the data by fitting a third-order polynomial to the completeness tests provided in Lacy et al. (2005).

Photometry for the IRAC data was performed using the SExtractor (Bertin & Arnouts 1996) package. For each channel, four aperture magnitudes plus an isophotal magnitude are computed. The four apertures used are 3, 5, 10, and 20 pixels in diameter (3.66, 6.10, 12.20, and 24.40 arcseconds, respectively). The aperture magnitudes are corrected for the flux lost outside the aperture due to the large diffraction-limit of the telescope and the significant wings of the IRAC point spread function (PSF). The aperture corrections are computed from bright stars within the FLS field and are listed and discussed further in Lacy et al. (2005). The majority of galaxies with $[3.6\mu m] > 15.0$ mag are unresolved, or only slightly resolved at the resolution of the $[3.6\mu m]$ bandpass and therefore the 3 pixel aperture corrected magnitude provides the best total magnitude. For galaxies which are extended and resolved, this small aperture is an underestimate of their total magnitude. For these galaxies, a "best" total magnitude is measured by estimating an optimum photometric aperture using the isophotal magnitudes. The geometric mean radius of the isophote ($r_m = (A/\pi)^{0.5}$, where A is the isophotal area) is compared to the radius of each of the 4 apertures used for the aperture magnitudes (r_1, r_2, r_3, r_4). If $r_m < 1.1\ r_{ap}$, then that aperture magnitude is chosen as the best total magnitude. For objects with $r_m > 1.1\ r_4$ the isophotal magnitude is used

as the best total magnitude. When measuring the R_c - [$3.6\mu m$] colors, we always use the 3 pixel aperture-corrected magnitude, even for resolved galaxies (see discussion in §2.3).

Object detection was performed separately in all 4 channels and these catalogues were later merged using a 1.8″ search radius. Tests of this matching (Lacy et al. 2005) show that this radius provides the most reliably matched catalogues.

4.3.2 Optical Data

The ground-based Cousins R_c-band (hereafter "R-band") imaging used in this study was obtained as part of the FLS campaign and is also publically available. R-band imaging covering the entire FLS IRAC and MIPS fields was observed on the Kitt Peak 4m Mayall telescope using the MOSAIC-1 camera. MOSAIC-1 consists of eight 4096 × 2048 CCDs, and has a field-of-view of 36 × 36 arcmin with a pixel scale of 0.258 arcseconds per pixel. Data reduction was performed using the NOAO IRAF *mscred* package and procedures, and galaxy photometry was performed using the SExtractor (Bertin & Arnouts 1996) package. Typical seeing for the images was ∼ 1.1 arcseconds and the 5σ limiting magnitude in an aperture 1.35 × FWHM of the seeing is 25.5 mag (Vega). For apertures of 3 arcseconds the 50% completeness limit is 24.5 mag. A complete discussion of the data reduction, object finding, and photometry can be found in Fadda et al. (2004). For this study we performed additional photometry to that publically available in order to measure fluxes in a 3.66″ aperture which matches with the smallest aperture of the IRAC data (D. Fadda, private communication).

Astrometry from both the IRAC and R-band data is better than 0.1 arcseconds, and therefore the R-band catalogue was matched to the IRAC catalogue simply by looking for the closest object within 1.8″ of each IRAC detection. In approximately 4% of cases more than one R-band object was located within the search radius. In these cases, the object closest to the IRAC centroid was taken as the match. The space density of R-band sources is approximately 5 times higher than the number of IRAC sources at these respective depths. This suggests that at most, 20% of R-band sources have an IRAC counterpart at the respective depths.

When there are multiple R-band matches for an IRAC detection, the majority of cases will be where only one of the R-band detections is the counterpart of the IRAC detection, and our approach will provide correct colors. Nevertheless, a certain percentage of the multiple matches will be when two R-band objects, both of which have

IRAC counterparts, have these counterparts blended together into a single IRAC detection due to the large IRAC PSF. Because the IRAC source is a blend of two objects, but we use only one R-band counterpart, these objects will be cataloged as brighter and redder than they truly are. However, because only 4% of IRAC sources have multiple R-band matches, and the probability that both of those R-band sources have an IRAC counterpart is roughly, $20\%^2 = 4\%$, this suggests that only 4% x 4% = 0.16% of all IRAC sources are blended sources where only one R-band galaxy has been identified as the counterpart. This estimated contamination is very small, and because no single galaxy plays a crucial role in the detection of a cluster, nor the measurement of the LFs, no attempt is made to correct for blended objects.

The large IRAC PSF means that star-galaxy separation using these data is difficult and therefore the classification of each matched object is determined from the R-band data using the CLASS_STAR parameter from SExtractor. This is done using the criteria suggested in Fadda et al. (2004). All objects with $R < 23.5$ with CLASS_STAR < 0.9 are considered galaxies. For fainter objects with $R > 23.5$, those with CLASS_STAR < 0.85 are considered galaxies.

4.3.3 Galaxy Colors

The most important ingredient in the cluster red-sequence algorithm is the measurement of accurate colors. Excess noise in the colors causes scatter in the cluster red-sequence and reduces the probability that a cluster will be detected. For images with large differences in seeing, PSF shape, and pixel size such as the R-band and [$3.6\mu m$], measuring accurate colors can be problematic. To this end, significant effort was invested in finding the most appropriate way to measure colors with this filter combination.

Studies of the cluster red-sequence using telescopes/filters with equivalently large angular resolution differences (e.g., HST + ground based, Holden et al., 2004; Optical and low-resolution IR, Stanford et al., 1998) have typically measured colors by degrading the highest resolution images using the PSF of the lowest resolution images. This is certainly the most accurate way to measure a color, provided the PSFs are modeled correctly, and is feasible for small images the size of a single cluster; however, it is time consuming for a survey the size of the FLS that has more than a million sources detected in the R-band. More importantly, because there are so many more galaxies detected in R-band than in [$3.6\mu m$], degrading those images causes numerous un-

necessary blends of R-band galaxies resulting in an increased number of catastrophic color errors. Degrading the resolution also inhibits the potential for detecting distant clusters because the signal-to-noise ratio of the faintest R-band objects becomes much worse when they are smeared with a large PSF.

The compromise is to use a fixed aperture that provides accurate colors, yet is as large as possible for the IRAC data (to reduce the need for aperture corrections), and yet is as small is possible to reduce the excess sky noise in the R-band measurement. It is important to use the same diameter apertures for both [$3.6\mu m$] and R-band so that the colors of bright resolved galaxies are measured properly. Galaxies which are small and mostly unresolved require an aperture of only 2-3 times the seeing disk to measure a correct color. In principle, colors for such galaxies can be measured correctly using a different sized apertures for both [$3.6\mu m$] and R-band (i.e., optimized apertures). However, because measuring the color correctly for large galaxies that are resolved in both filters requires that the aperture must be the same size in both filters, we use the same aperture for all galaxies. After experimenting with apertures ranging in diameter between one to ten IRAC pixels (1.22″ to 12.2″) we determined that the three IRAC pixel diameter aperture (3.66″) was the smallest aperture that still measures the [$3.6\mu m$] flux correctly and provides acceptably small errors in the R-band magnitudes. Using this large fixed aperture means that the photometry of faintest R-band galaxies is not optimized because much of the aperture contains sky. As a result, some potential in discovering the most distant clusters is sacrificed because the faintest red galaxies (i.e., distant red-sequence galaxies) may have excessively large photometric errors. However, most importantly, accurate colors are determined for all galaxies, and overall the approach provides much better photometry than degrading the entire survey data.

As an illustration of the quality of colors achievable with this approach we show the color-magnitude diagram of FLS J171648+5838.6, the richest cluster in the survey, in Figure 1. The typical intrinsic scatter of the red-sequence at the redshift of this cluster ($z_{spec} = 0.573$) is ~ 0.075 (Stanford et al. 1998; Holden et al. 2004). As a comparison we measure the intrinsic scatter for FLS J171648+5838.6 by subtracting the mean photometric error from the total scatter in quadrature. This is slightly less rigorous than the Monte-Carlo methods used by other authors, but provides a reasonable estimate of the scatter. For galaxies with [$3.6\mu m$] < 17 mag ([$3.6\mu m$] > 17 mag) the observed scatter of the red-sequence is 0.149(0.225) mag, and the mean photometric color error is 0.118(0.167) mag, resulting in an intrinsic scatter of 0.091(0.151) mag. This is is
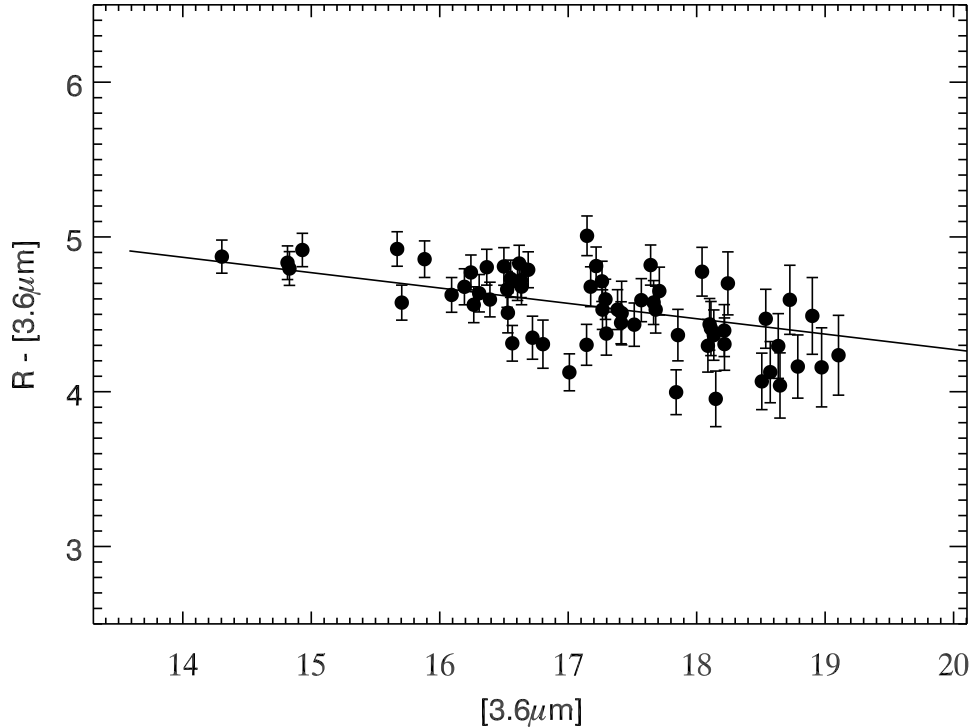
Figure 4.1 Color-Magnitude diagram within a 1 Mpc (2.5 arcmin) diameter of FLS J171648+5838.6 (cluster 44, z_{spec} = 0.573), the richest cluster in the FLS. Several field galaxies with R - [3.6μm] colors > 5.5 have been removed for clarity. The solid line is the best red-sequence model for the cluster (§3.1). The intrinsic scatter in the red-sequence for this cluster is 0.091 mag for galaxies with [3.6μm] > 17 mag, and 0.151 mag for galaxies with [3.6μm] < 17 mag, and is comparable to the scatter in other clusters at this redshift.

fair agreement with typical red-sequence scatters and demonstrates that this simple method for determining colors works well and recovers the expected intrinsic scatter in the color-magnitude relation.

4.3.4 Keck, WIYN, & SDSS Spectroscopic Data

A large number of spectroscopic redshifts are available for galaxies in the FLS field from several spectroscopic campaigns. A sample of 642 redshifts were obtained using the HYDRA spectrograph on the Wisconsin-Illinois-Yale-NOAO (WIYN) 3.6m telescope as part of a program to followup radio sources in the FLS (Marleau et al. 2007). A set of 1373 redshifts in the FLS field were obtained for galaxies selected by their red R - K_s colors using the DEIMOS spectrograph on the 10m KECK II telescope by

Choi et al. (2006). Lastly, 1296 redshifts were obtained using the Hectospec Fiber Spectrograph on the 6.5m MMT by Papovich et al. (2006). The primary target of that survey were galaxies that are detected in the FLS MIPS $24\mu m$ imaging and have R < 21.5 mag. In addition to redshifts from these projects, 1192 redshifts in the FLS field are also available from the Sloan Digital Sky Survey (SDSS) DR5 database (Adelman-McCarthy et al. 2007). In total there are 4503 redshifts at various positions available in the FLS. Of these, 26 are likely to be cluster red-sequence galaxies (see §3.7).

4.3.5   Palomar Spectroscopy

In addition to the spectroscopic catalogues available, we also obtained our own longslit spectroscopy for bright red-sequence galaxies in three clusters with $0.4 < z_{phot} < 0.6$ in the FLS using the Double-Spectrograph (Doublespec) on the 200-inch Hale telescope at Palomar Mountain (P200). We also obtained multi-object spectroscopy using the COSMIC Spectrograph on the P200 for an additional three clusters with $z_{phot} < 0.3$

Double-Spectrograph Data

Spectroscopy of bright red-sequence galaxies in clusters FLS J171241+5855.9, FLS J172122+5922.7, and FLS J171648+5838.6 (clusters 16, 38, and 44 listed in Table 1) was performed on 17, 18, and 19 August 2004 with Doublespec on the P200. The observations were made with the "Red" camera using the 316 l/mm grating blazed at 7150Å and a 0.5″ wide slit, giving a spectral resolution of 2.6Å ($\sim$ 150 km s^{-1}). The Doublespec longslit is $\sim$ 1.5 arcmin long and the angle of the slit on the sky can be rotated. In all 3 clusters we centered the slit on the brightest cluster galaxy (BCG) and then chose a rotation angle so that we could get at least 2 other bright objects (preferentially red-sequence galaxies) on the slit.

For FLS J172122+5922.7 and FLS J171648+5838.6 we obtained spectra of 3 objects in the field, and in FLS J171241+5855.9 we managed 4. We obtained three 20 minute exposures for FLS J172122+5922.7 and FLS J171648+5838.6, which have photometric redshifts of 0.57 and 0.55, respectively, and one 20 minute exposure for FLS J171241+5855.9, which has a photometric redshift of 0.39. We also observed a spectroscopic standard, calibration lamps, dome flats and twilight flats at the beginning of each night. Data reduction and wavelength calibration were performed using the standard IRAF techniques. After 1-d spectra were extracted, 7 of the 10 objects had a signal-to-noise ratio suitable for cross-correlation. One of the spectra in FLS J171241+5855.9 has a strong

emission line at 7056Å and no possible identification that puts it near the photo-z of the cluster. This object was therefore considered a field interloper. The remaining 6 spectra (two per cluster) showed significant absorption features typical of early-type galaxies and redshifts were obtained by cross correlating them with an elliptical galaxy spectrum. The redshifts of the galaxies within each cluster were similar (Δz < 0.01) and are in excellent agreement with the cluster photometric redshift. These spectroscopic redshifts are listed in the cluster catalogue (Table 1).

COSMIC Data

Multi-object spectroscopy of both red-sequence galaxies and MIPS 24μm-detected galaxies in the fields of clusters FLS J171059+5934.2, FLS J171639+5915.2, FLS J171505+5859.6, and FLS J172449+5921.3 (clusters 1, 2, 8, and 10 listed in Table 1) were performed on 26, 27, 28, 29 May 2006, and 15, 16, 17 June 2007 using the COSMIC Spectrograph on the 200″ Hale Telescope at Palomar Mountain. These observations were made with the 300 l/mm grating blazed at 5500Å with 1″ wide slits giving a spectral resolution of 8Å ($\sim$ 450 km s^{-1}). These data are part of a larger campaign to study cluster 24μm sources and full details of the data reduction, calibration and cross-correlation will be presented in a future paper (Muzzin et al. 2007, in preparation). We obtained 17, 16, 12 and 20 good-quality spectra in the fields of FLS J171059+5934.2, FLS J171505+5859.6, and FLS J172449+5921.3 respectively, and redshifts were determined using cross-correlation. Including the data from the other spectroscopic campaigns, the field of FLS J171059+5934.2 has 10 galaxies with $\bar{z}$ = 0.126, the field of FLS J171639+5915.2 has 7 galaxies with $\bar{z}$ = 0.129, the field of FLS J171505+5859.6 has 9 galaxies with $\bar{z}$ = 0.252, and the field of FLS J172449+5921.3 has 12 galaxies with $\bar{z}$ = 0.253. These redshifts are included in the cluster catalogue (Table 1).

4.3.6 Keck/DEIMOS Spectroscopy of FLS J172126+5856.6

Spectroscopy was obtained of the candidate cluster FLS J172126+5856.6 (cluster 93 in Table 1) with the Deep Imaging Multi-Object Spectrograph (DEIMOS, Faber et al. 2003) on the 10 m Keck I telescope. On the night of 1 September 2005, we obtained three 1800s exposures in the same mask in good conditions. The 600ZD grating (λ_{blaze} = 7500 Å; $\Delta\lambda_{\text{FWHM}}$ = 3.7 Å) and a GG455 order-blocking filter were used. The DEIMOS data were processed using a slightly modified version of the pipeline de-

veloped by the DEEP2 team at UC-Berkeley[3]. Relative flux calibration was achieved from observations of standard stars from Massey & Gronwall (1990).

Slits were preferentially placed on candidate red-sequence galaxies. Of the five candidate red-sequence galaxies with sufficient S/N for determining redshifts, four had redshifts $\Delta z < 0.01$ from each other, with the $\bar{z}$ = 1.045. These redshifts are included in the cluster catalogue (Table 1).

4.4 Cluster Finding Algorithm

The cluster finding algorithm employed in this study is essentially the CRS algorithm of Gladders & Yee (2000, 2005) with some minor modifications. Here we outline only the major steps, and refer to those papers for a more detailed explanation of the procedures.

The CRS algorithm is motivated by the observation that early-type galaxies dominate the bright-end of the cluster LF and that these galaxies always follow a tight red-sequence in the color-magnitude plane. At increasing redshift the observed red-sequence color becomes redder[4] and because this change in color follows closely the predictions from a passively evolving stellar population, the color can be used as a robust photometric redshift estimate for a cluster. In order to apply the CRS algorithm, slices are made in the color-magnitude plane of a survey. Galaxies are then assigned weights based on the probability that they belong to a particular slice. This probability is determined by the color and the photometric error in the color. Once color weights for each galaxy in each slice have been assigned, each galaxy is also assigned a magnitude weight. Magnitude weighting is done because bright red-sequence galaxies are more likely to be members of clusters than faint ones, which can be field interlopers.

Once each galaxy is assigned a color and magnitude weight for each slice, the positions of each galaxy are plotted for each slice with their respective weights. The resulting "probability map" for each slice is then smoothed and peaks in these maps represent likely cluster candidates. In the following subsections we discuss in more detail the steps in our algorithm.

---

[3] http://astro.berkeley.edu/ cooper/deep/spec2d/

[4] The observed-frame color of the red-sequence becomes redder with increasing redshift because of band shifting. The rest-frame color change due to passive evolution actually makes galaxies bluer at higher redshift, but is a very small effect for a single-burst population formed at high redshift. Because the change in observed-frame color is dominated by the k-correction from an old stellar population, it can be modeled very well and hence red-sequence photometric redshifts are accurate.

4.4.1 Red-Sequence Models

The first step in finding clusters with the CRS is to model the color and slope of the cluster red-sequence at different redshifts. This was done by making simulated single-burst galaxies using all available metallicities from the Bruzual & Charlot (2003) spectral synthesis code. The models are constructed with 50% of the stars forming in a single-burst at t = 0, and the remainder forming with an exponentially declining star formation rate of τ = 0.l Gyr. Using a range of metallicities causes the color of each galaxy to be slightly different at $z = 0$, with the most metal-rich galaxies being the reddest. The absolute magnitude of each galaxy with a different metallicity is normalized using the U-V, V-I, and J-K red-sequences of Coma (Bower et al. 1992) assuming that a metallicity gradient with magnitude is the primary source of the slope of the red-sequence. Normalizing the absolute magnitude of each galaxy this way allows us to reproduce models with the correct red-sequence color and slope with redshift.

There is increasing evidence that the slope of the red-sequence is not only caused by a metallicity-sequence, but is also the product of an age-sequence, with the less luminous galaxies being both more metal-poor and younger (e.g., Nelan et al. 2005; Gallazzi et al. 2006). Examination of spectroscopically-confirmed clusters in the FLS shows that the pure metallicity-sequence used in our models reproduces the red-sequence slope and color very well at all redshifts, and because we are only interested in determining a fidicial model for detecting clusters and determining photometric redshifts, no further tuning of the ages of galaxies along the sequence is done.

Once the absolute magnitude of each model galaxy is normalized using the Coma red-sequences, linear fits to the R - [3.6µm] vs. [3.6µm] color-magnitude relations of the model galaxies between $0.1 < z < 1.6$ are made. A high-density of redshift models are fit so that there is significant overlap in color space (185 slices between $0.1 < z < 1.6$). This is computationally expensive when doing cluster-finding; however, it assures that no clusters are missed because they have colors between the finite number of models and it also allows for increased precision in the photometric redshifts.

We computed two sets of single-burst models, one with a formation redshift (z_f) = 2.8, and another with z_f = 5.0. These two sets of models produce nearly identical observed red-sequences at $z < 1.1$, but begin to diverge at higher redshifts. There is evidence from previous studies of the fundamental plane (e.g., van Dokkum et al. 1998; van Dokkum & Stanford 2003, and many others), evolution of the color-magnitude diagram (Stanford et al. 1998; Holden et al. 2004), and K-band luminosity function

(De Propris et al. 1999; Lin et al. 2006; Muzzin et al. 2007a) that a $z_f \sim 3$ model is appropriate for cluster early-types; however, the uncertainties in these studies are fairly large. There is also evidence that many of the most massive field early-types formed the majority of their stars at $z > 5$ (McCarthy et al. 2004; Glazebrook et al. 2004), so the possibility remains that a $z_f = 5.0$ is more appropriate. Regardless, the majority of the systems we have discovered are at $z < 1.1$, and therefore the z_f uncertainty does not affect the photometric redshifts of these systems. For systems at $z > 1.1$, the photometric redshift can be considered an upper limit. For example, the photometric redshift for a cluster at $z = 1.3$ in the $z_f = 2.8$ model would be $z \sim 1.2$ in the $z_f = 5.0$ model.

To illustrate the depth of the survey, and the location of the red-sequence models, Figure 2 shows the R - [$3.6\mu m$] vs. [$3.6\mu m$] color-magnitude diagram for all galaxies in the FLS with some of the $z_f = 2.8$ red-sequence models overlaid. The density of galaxies with $M \sim M^*$ begins to drop off significantly for the $z > 1.2$ red-sequence models because of the depth of the R-band data ($M^*([3.6\mu m]) \sim 17.0$ mag at $z = 1.2$) and therefore we consider $z \sim 1.2$ the upper limit at which we can reliably detect clusters.

4.4.2 Color Weights

Once red-sequence models have been made, weights based on the probability that a galaxy belongs within a color slice are computed. The typical 1σ scatter in the local cluster color-magnitude relation is ~ 0.075 mag (e.g., Lopez-Cruz et al. 2004; Bower et al. 1992). The scatter has been measured in clusters to $z \sim 1$ where it remains remarkable consistent (e.g., Stanford et al. 1998; Gladders et al. 1998; Blakeslee et al. 2003). Thereafter, it may become somewhat more scattered (Holden et al. 2004). Assuming that this relation holds to $z \sim 1.3$, color weights (with values ranging from 0 to 1) are assigned by computing the overlapping area of a galaxy's color with the red-sequence assuming a red-sequence intrinsic dispersion of 0.075 mag and assuming the galaxy's color is represented by a Gaussian centered on the measured color with a 1σ dispersion equal to the color error (see e.g. GY00, Figure 3 for an example). Using this method, the weight of a bright galaxy lying directly on the red-sequence with a color error significantly narrower than the width of the red-sequence is 1.0. The same galaxy, with a color error equal to the dispersion in the red-sequence, has a weight of 0.67. Color weights are computed for all galaxies in all 185 color slices.
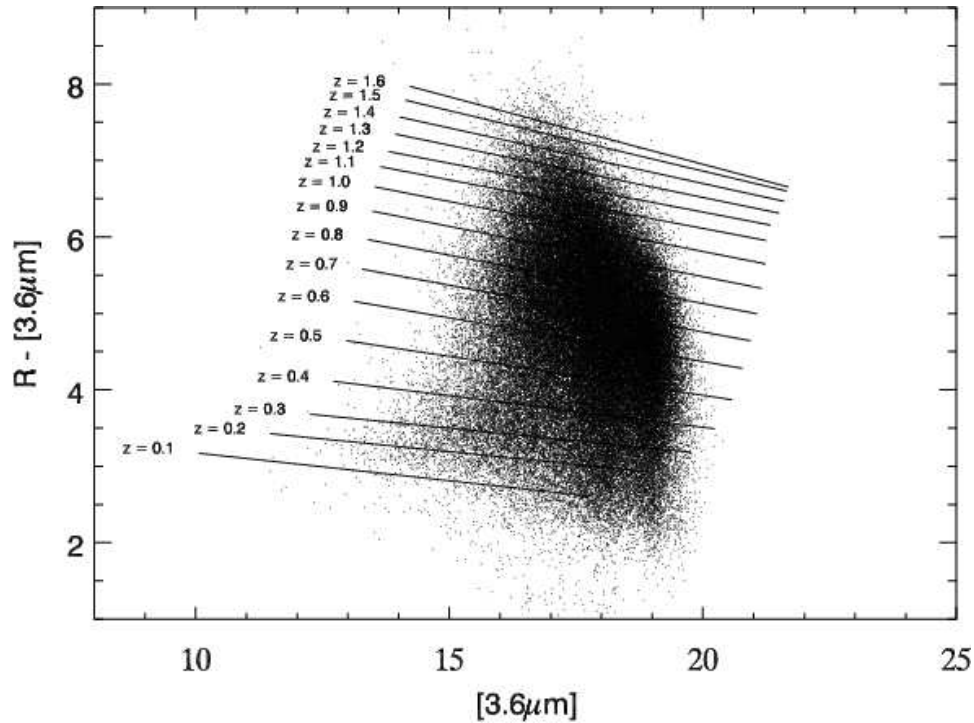
Figure 4.2 Observed color-magnitude diagram for all galaxies in the FLS. The solid lines are fiducial red-sequence models at different redshifts generated using the Bruzual & Charot code. The redshift of each model is labelled in the figure. The bulk of the shift in color with redshift of the models is due to bandpass shifting or "k-correction", not because of evolution in the rest-frame colors of the galaxies.

4.4.3 Magnitude Weights

In addition to the color weights, galaxies are also weighted based on their magnitude relative to a fiducial M* value. Cluster early-types are usually the brightest, reddest galaxies at a given redshift and therefore, the brightest galaxies within a color slice are more likely to be cluster galaxies and should be given extra weight. The distribution of magnitude weights was defined as P(M) by GY00 (see their §4.3). We compute the P(M) using the data themselves, as suggested by those authors, and when doing so we consider objects within the one-percentile highest density regime as "cluster" galaxies. This is a slightly more strict cut than the ten-percentile cut used by GY00; however, the fact that IR-selected galaxies are more strongly clustered than optically-selected galaxies justifies using a more stringent cut.

4.4.4 Probability Maps

Once the magnitude and color weights for all galaxies in each of the individual color slices have been computed, a probablility map of each slice is created. The map is a spatial galaxy density map of the survey within each redshift slice. The map is made using pixels which are 125 kpc in physical size at the redshift of each slice. The probablility flux from each pixel is determined by placing each galaxy on the pixel that corresponds to its location in the survey, weighted by the product of its color and magnitude weights. Once each slice is constructed this way, it is smoothed with the exponential kernel suggested in GY00 (their equation 3).

4.4.5 Noise Maps

The noise properties of the probability maps of different color/redshifts slices can be quite different. In particular, the maps of the highest redshift slices tend to have large noise peaks because the survey is only as deep as $\sim M^*$ in those slices. The lower redshift probability maps have a smoother background because there are numerous $M > M^*$ galaxies which are more evenly distributed spatially and have a low probability of belonging to any slice because of their large color error. The higher redshift maps are shallower, thereby lacking the $M > M^*$ galaxies which provide this smooth background. If peak finding is run on all probability maps using similar detection parameters, it produces very different numbers of detections in different slices. In particular, almost any noise in the highest redshift maps results in the detection of a "cluster".

To circumvent this problem the parameters of the peak finding for each map can be tuned individually in order to produce a reasonable number of detections in each slice; however, the resulting cluster catalogue is clearly biased by what is considered a "real" detection in a given map. It is preferrable to have a cluster catalogue which is as homogenously-selected as possible and based on a quantitative selection. Therefore "noise" maps are constructed and are added to each probability map to homogenize their noise properties.

The noise maps are constructed by adding fake red-sequence galaxies to each pixel of the probability maps. Adding a constant background of fake galaxies does not change the noise properties of a map. Some *variance* in the number of background galaxies must be added. We experimented with a variety of variances to add, but settled that the variance from the photometric color errors of six M^* red-sequence

galaxies per pixel provided the best results. This level of noise removes the spurious detections in the highest redshift slices, but does not add so much noise as to wash-out lower richness clusters in the lower redshift slices.

The noise in each pixel is calculated by first determining the average color error of an M* red-sequence galaxy using the survey data. Once the average color error per slice is tabulated, the weights of six M* red-sequence galaxies are Monte-Carlo simulated for each pixel of a noise map assuming that the colors are normally distributed around the red-sequence with a dispersion equal to the mean color error. These simulated weights are then assigned to each pixel of the noise map and each noise map is added to the appropriate cluster probability map. This approach thereby implictly defines a "cluster" as an overdensity detectable above the noise from six M* background red-sequence galaxies at any redshift. The noise+clusters maps have similar noise properties for every slice and peak finding can be run using identical parameters for all maps.

4.4.6 Cluster Detection

Once the combined noise-probability maps have been made, peaks are detected in each map using SExtractor. The peak-finding is done differently from GY00 in that the individual 2d slices are searched instead of merging the slices into a 3d datacube and searching for 3d peaks. It is unclear how these two methods compare; however, they are likely to be similar and searching the slices individually permits easy visual inspection of the sources on each map which allows us to check any problems that have occured with peak finding or in the generation of the map. Pixels 5σ above the background are flagged and 40 connected pixels are required to make a detection.

The slices are very close in color space and therefore clusters (particularly rich ones) are detected in more than one color slice. The same cluster is identified in multiple color slices by merging the slice catalogues using a matching radius of 8 pixels (1 Mpc). Clusters found across as many as 20 color slices are connected as being the same object. The color slices are not linear in redshift, but 20 slices correspond to $\Delta z \sim \pm 0.06$. These combined spatial and color limits for connecting clusters imply that clusters with separations > 1 Mpc in transverse distance and > 0.06 in redshift space can be resolved into distinct systems. This level of sensitivity is similar to that found by Gladders & Yee (2005) using R - z$'$ colors to select clusters. They also demonstrated that subclumps at redshift spacings much less than this are likely to be associ-

ated subclumps or infalling structures related to the main body of the cluster.

4.4.7 Photometric Redshifts

Each cluster is assigned the photometric redshift of the color slice in which it is most strongly detected. The strength of the detection is determined by using SExtractor to perform aperture photometry of each cluster on each slicemap. This provides a "probability flux", and the cluster is assigned to the slice in which it has the largest probability flux.

The large number of spectroscopic redshifts available for the FLS can be used to verify the accuracy of the red-sequence photometric redshifts. Examining the spectroscopic catalogue for galaxies within a 1 Mpc circle around each cluster shows that there are numerous galaxies with spectroscopic redshifts in the field of many of the clusters. The spectroscopic targets were chosen with a variety of selection criteria (none of which preferentially select early-type galaxies) and therefore the majority of galaxies with redshifts are foreground or background galaxies. We use only the spectroscopic redshifts for galaxies which have a combined magnitude and color weight of > 0.2 in order to preferentially select likely cluster members. This cut in weight is used because it corresponds to the typical combined magnitude and color weight of $M < M^*$ red-sequence galaxies. Once the cut is made there are 21 clusters which have at least one spectroscopic redshift for a likely cluster red-sequence galaxy. Remarkably, there are 26 galaxies which meet this criteria and 24 of these have a spectroscopic redshift < 0.1 from the photometric redshift of the cluster. This illustrates the effectiveness of the red-sequence color at estimating photometric redshifts provided that the galaxy has a high-probability of being a cluster early-type.

In Figure 3 we plot spectroscopic vs. photometric redshift for these 21 clusters plus the additional 9 for which we obtained our own spectroscopic redshifts (§ 2.5). The straight line marks a direct correlation. Large points represent clusters with more than one galaxy with a redshift consistent with the being in the cluster. Small points represent clusters with a single spectroscopic redshift. Excluding the large single outlier with $z_{spec} \sim 0.9$ (which is likely to be a bluer galaxy at high-redshift based on its spectrum and IRAC colors, see §6.3) the rms scatter in the cluster spectroscopic vs. photometric redshift is $\Delta z = 0.04$, demonstrating that the photometric redshifts from the red-sequence algorithm work extremely well.

The accuracy of the photometric redshifts from the FLS sample is comparable to
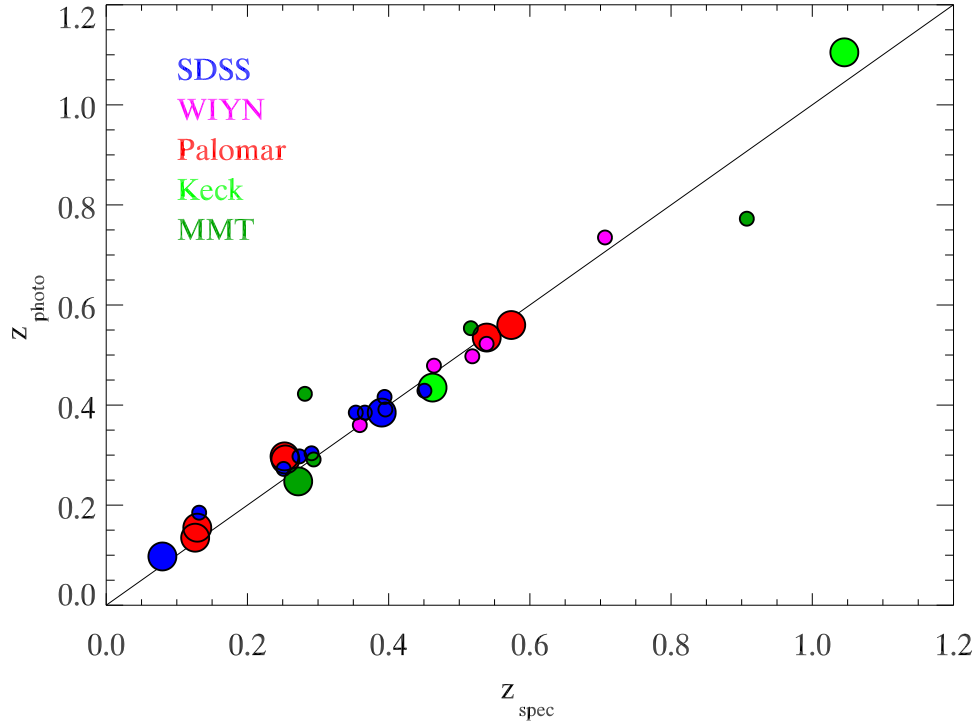
Figure 4.3 Photometric vs. spectroscopic redshift for clusters in the FLS field. The color of the circle corresponds to the telescope/project where the spectroscopic redshifts were obtained (see §2). Large circles denote clusters with more than one spectroscopic redshift, small circles denote clusters with only one spectroscopic redshift. Excluding the one large outlier at $z_{spec} \sim 0.9$, the rms scatter is $\Delta z = 0.04$.

the accuracy of the RCS surveys (Yee et al. 2007; Gladders & Yee 2005) which use R - z' color selection, even though the R - [$3.6\mu m$] colors have larger photometric errors than the R - z' colors. It is likely this is because the model red-sequence colors change more rapidly with redshift in R - [$3.6\mu m$] than in R - z' (R - [$3.6\mu m$] spans 2 magnitudes between $z = 0.5$ and $z = 1.0$, whereas it spans only 1 magnitude in R - z'). The larger change in the R - [$3.6\mu m$] colors with redshift means that photometric measurement errors should correspond to smaller errors in photometric redshift.

4.4.8 B_{gc} Richness Parameter

The final step in the selection of the cluster sample is to cut low-richness spurious detections from the catalogue. We do this using the B_{gc} richness parameter (Longair & Seldner 1979; for a detailed look at the application of B_{gc} to measuring cluster richnesses see Yee & López-Cruz 1999). B_{gc} is the amplitude of the 3-dimensional correla-

tion function between cluster galaxies and the cluster center. B_{gc} is measured within a fixed aperture (typically 500 kpc) and is well-correlated with cluster physical parameters such as velocity disperion (σ), X-ray temperature (T_x), and the radius as which the mean density of the cluster exceeds the critical density by a factor of 200 (R_{200}) (e.g., Yee & Lopez-Cruz 1999; Yee & Ellingson 2003; Gilbank et al. 2004; Muzzin et al 2007b).

Gladders & Yee (2005) introduced a new form of the B_{gc} parameter, counting the overdensity of red-sequence galaxies within a fixed aperture, rather than all galaxies and defined this new parameter as $B_{gc,R}$. This form of richness suffers less from cosmic variance in the background because red-sequence galaxies provide better contrast with the field, and therefore it is likely to be a more robust esimate of the cluster richness. We use $B_{gc,R}$ rather than B_{gc} for determing the richnesses of the FLS clusters. The net number of [$3.6\mu m$] red-sequence galaxies within a fixed aperture of 500 kpc with $M < M^* + 1.0$ (where M^* is determined from the data itself, see §5.1) are counted. The model red-sequences from §3.1 are used and galaxies within ± 0.3 in color are considered to belong to the red-sequence.

Before low-richness systems are cut from the catalogue there are 134 cluster candidates between $0.1 < z < 1.4$ in the FLS field. Removing systems with $B_{gc,R} < 200$ leaves a total of 99 clusters in the sample. Systems that are removed by this cut are typically tight compact groups of 3-4 very bright galaxies that are the same color. They have a strong probability of being detected by the CRS algorithm; however, they are not more than potentially a few bright clustered galaxies, and are unlikely to be clusters or rich groups. Although the majority of these systems are probably bona fide low-richness galaxy groups, at low richness the number of false-positive detections does increase. We prefer to concentrate our study on a reliable sample of galaxy clusters and therefore remove these low richness galaxy groups.

4.4.9   Cluster Centroids

Defining a centroid for clusters can be a challenging task, yet is extremely important because properties determined within some aperture around the cluster (such as richness, or LF) can vary strongly with the choice of centroid. In many cluster studies the location of the BCG is used as the center of the cluster. This is a reasonble definition as frequently the BCG lies at the center of the dark matter halo and X-ray emission; however, there are also many examples where it does not. Furthermore, not all clus-

ters have an obvious BCG, particularly at higher redshift.

Given these issues, two centroids are computed for the FLS clusters, one based on the location of the peak of the red-sequence probability flux in the probability maps, and the other based on the location of the BCG within 500 kpc of this centroid. In order to avoid bright foreground galaxies the brightest galaxy in the field with a red-sequence weight > 0.4 is designated as the BCG. Eye examination of the clusters shows that this criteria is effective at choosing what appears visually to be the correct galaxy; however, because it chooses only a single galaxy this technique is still potentially suseptible to very red low-redshift field interlopers.

When computing the cluster LFs, only one of the centroids can be used. We define an "optimum" centroid for each cluster using the $B_{gc,R}$ parameter. $B_{gc,R}$ is computed at both centroids and the optimum centroid is the centroid which produces the maximum value of $B_{gc,R}$. This approach is simplistic, but because B_{gc} is the correlation amplitude between the cluster center and galaxies, the centroid which produces the largest value should be the best centroid of the galaxy population.

4.5 Properties of the Cluster Catalogue

The final cluster catalogue of 99 clusters and groups is presented in Table 1. Where spectroscopic redshifts are available for high-probability cluster members they are listed in column 3, with the number of redshifts in parenthesis. For each cluster we also compute an estimate of R_{200} and the mass (M_{200}) contained within R_{200}. The M_{200} values are estimated using the correlation between B_{gc} and M_{200} measured by Muzzin et al. (2007b) for 15 X-ray selected clusters at $z \sim 0.3$ in the K-band. The K-band and [3.6 μm] bandpasses sample similar parts of a galaxy's spectrum at $0.1 < z < 1.3$ and therefore it is reasonable to assume that B_{gc} values measured in both these bands will be comparable. The best-fit relation between M_{200} and B_{gc} is

$$Log(M_{200}) = (1.62 \pm 0.24)Log(B_{gc}) + (9.86 \pm 0.77). \qquad (4.1)$$

Muzzin et al. (2007b) did not measure the correlation between B_{gc} and R_{200} in the K-band, although Yee & Ellingson (2003) showed a tight correlation for the same clusters using r-band selected B_{gc}. Using the Muzzin et al. (2007b) K-band data we fit the correlation between these parameters for those clusters and find that the best fit relation is

$$Log(R_{200}) = (0.53 \pm 0.09)Log(B_{gc}) - (1.42 \pm 0.29). \qquad (4.2)$$

The rms scatter in the M_{200} - B_{gc} relation is 35% and for the R_{200} - B_{gc} relation it is 12%. These scatters are similar to that measured between M_{200} and richness (parameterized by N_{200}) at $z \sim 0$ by Lin et al. (2004). The values of M_{200} and R_{200} derived from these equations are listed in columns 9 and 10 of Table 1, respectively.

Using an indirect method such as this to estimate M_{200} and R_{200} means that we cannot compute reliable errors for these values for individual clusters; however, the rms scatters in the correlations are at least indicative of the average uncertainty in the measurement of the parameters for the sample. Therefore, we suggest that the average error in the M_{200} and R_{200} values listed in Table 1 are $\pm$ 35% and 12% respectively, but that the error in a particular cluster can be several times larger or smaller.

In Figure 4 we plot a histogram of the number of clusters as a function of redshift in the FLS. The solid histogram shows the distribution of all clusters and the dot-dashed histogram shows the distribution of clusters with $M_{200} > 3 \times 10^{14}$ $M_\odot$ ($B_{gc,R} > 600$). Similar to the predictions of numerical simulations (e.g., Haiman et al. 2003) the number of clusters peaks at $z \sim 0.6$. Qualitatively, the distribution of clusters is also similar to that found by Gladders & Yee (2005) in comparable size patches; however, the cosmic variance in the number of clusters in ~ 4 deg^2 patches is too large to make a meaningful comparison between the selection of clusters in the R - z' bandpasses versus the R - [3.6μm] bandpasses.

We plot the locations of the clusters superposed on the [3.6μm] image of the FLS field in Figure 5 as open circles. Large and small circles represent clusters with $M_{200} > 3 \times 10^{14}$ $M_\odot$ and $M_{200} < 3 \times 10^{14}$ $M_\odot$, respectively, and clusters with photometric redshifts $0.1 < z < 0.4$, $0.4 < z < 0.8$, $z > 0.8$ are plotted as blue, green, and red circles, respectively. The clusters themselves are clearly clustered; demonstrating the need for wide-field surveys when searching for representative samples of galaxy clusters.

We show a few examples of some of the richest cluster candidates in Figures 6 - 11. The top left panel for each Figure is the R-band image; the top right is the [3.6μm] image, and the bottom left panel is the [8.0μm] image. All images are 1 Mpc across at the cluster redshift. The bottom right panel of each figure shows a histogram of the color distribution of galaxies with M < M* within a 1 Mpc diameter aperture. The color of the red-sequence for the photometric redshift is marked with an arrow. The dashed histogram is the mean color background in that aperture measured from the entire survey. The error bars on the dashed histogram are computed as the 1σ variance in each bin from 200 randomly selected 1 Mpc apertures within the survey. Galaxies are clustered, and therefore assuming the variance is Gaussian-distributed is probably an

overestimate of the true variance (because there will be large wings in the distribution due to clustering); however, it provides a first-order demonstration of the overdensity of the cluster relative to the field.

Overall, the cluster catalogue is qualitatively similar in both redshift, mass, and spatial distributions to catalogues selected with the same technique in different band-passes (e.g. Gladders & Yee 2005, Gilbank et al. 2004), demonstrating that clusters can be reliably selected with the CRS method on IRAC data despite the limited spatial resolution of the instrument.

Table 4.1.   FLS Cluster Catalogue

#	Name	z_{phot}	z_{spec}	R.A. J2000	Decl. J2000	$B_{gc,R}$ Mpc$^{1.8}$	$\epsilon B_{gc,R}$ Mpc$^{1.8}$	M_{200} $M_\odot \times 10^{14}$	R_{200} Mpc	Centr
(1)	(2)	(3)	(4)	(5)	(6)	(7)	(8)	(9)	(10)	(11)
0	FLS J172321+5835.0	0.09	0.079(4)	17:23:21.5	58:35:03.5	237	133	0.64	0.68	BCG
1	FLS J171059+5934.2	0.13	0.126(10)	17:10:59.8	59:34:16.4	521	196	2.30	1.04	BCG
2	FLS J171639+5915.2	0.16	0.129(7)	17:16:39.3	59:15:13.5	326	155	1.07	0.81	BCG
3	FLS J172319+6019.5	0.18	0.131(1)	17:23:19.7	60:19:33.7	358	162	1.24	0.85	BCG
4	FLS J171233+5956.4	0.22	—	17:12:33.0	59:56:28.2	534	199	2.38	1.06	RS-Flu
5	FLS J172207+5943.8	0.24	0.271(2)	17:22:07.9	59:43:52.1	251	132	0.70	0.71	RS-Flu
6	FLS J172618+5934.5	0.27	—	17:26:18.8	59:34:32.3	386	168	1.41	0.89	BCG
7	FLS J171618+5907.8	0.27	0.251(1)	17:16:18.5	59:07:53.0	251	132	0.70	0.71	RS-Flu
8	FLS J171505+5859.6	0.29	0.252(9)	17:15:05.2	58:59:41.4	310	149	0.99	0.79	BCG
9	FLS J171152+6007.7	0.29	0.293(1)	17:11:52.8	60:07:43.7	381	166	1.38	0.88	RS-Flu
10	FLS J172449+5921.3	0.29	0.253(13)	17:24:49.0	59:21:22.9	861	252	5.18	1.36	BCG
11	FLS J172454+5930.5	0.29	0.273(1)	17:24:54.4	59:30:32.8	447	181	1.79	0.96	BCG
12	FLS J171431+5957.8	0.29	—	17:14:31.1	59:57:52.2	378	165	1.36	0.88	RS-Flu
13	FLS J171455+5836.5	0.30	0.291(1)	17:14:55.0	58:36:34.7	791	242	4.51	1.30	BCG
14	FLS J172505+5932.3	0.34	—	17:25:05.8	59:32:22.9	516	195	2.25	1.04	BCG
15	FLS J172008+5949.9	0.36	0.359(2)	17:20:08.7	59:49:54.1	308	148	0.97	0.79	BCG
16	FLS J171241+5855.9	0.38	0.390(2)	17:12:41.6	58:55:58.7	797	243	4.57	1.31	RS-Flu
17	FLS J171537+5849.4	0.38	0.353(1)	17:15:37.0	58:49:24.4	590	209	2.80	1.11	RS-Flu
18	FLS J172541+5929.9	0.38	0.366(1)	17:25:41.7	59:29:59.4	521	196	2.29	1.04	BCG
19	FLS J171720+5920.0	0.39	0.395(1)	17:17:20.3	59:20:05.9	316	150	1.02	0.80	BCG
20	FLS J171204+5855.6	0.41	—	17:12:04.7	58:55:36.1	248	131	0.69	0.70	BCG
21	FLS J172013+5925.4	0.41	—	17:20:13.1	59:25:29.6	456	183	1.85	0.97	BCG
22	FLS J171432+5915.9	0.41	0.394(1)	17:14:32.6	59:15:54.7	525	197	2.32	1.05	BCG
23	FLS J171437+6002.8	0.42	—	17:14:37.8	60:02:53.5	319	151	1.03	0.80	BCG
24	FLS J172028+5922.6	0.42	0.281(1)	17:20:28.9	59:22:38.8	457	183	1.85	0.97	BCG
25	FLS J172546+6011.5	0.43	0.450(1)	17:25:46.3	60:11:30.2	872	253	5.28	1.37	RS-Flu
26	FLS J172026+5916.0	0.43	0.462(2)	17:20:26.9	59:16:05.0	804	243	4.63	1.31	RS-Flu
27	FLS J171103+5839.9	0.43	—	17:11:03.4	58:39:56.3	528	197	2.34	1.05	RS-Flu
28	FLS J172418+5954.6	0.44	—	17:24:18.5	59:54:37.4	391	169	1.44	0.89	BCG
29	FLS J172158+6014.3	0.45	—	17:21:58.3	60:14:20.2	323	152	1.05	0.81	BCG
30	FLS J171153+5905.4	0.45	—	17:11:53.6	59:05:28.2	530	198	2.36	1.05	RS-Flu
31	FLS J171447+6018.9	0.48	0.464(1)	17:14:47.5	60:18:54.7	255	134	0.72	0.71	RS-Flu

Table 4.1 (cont'd)

#	Name	z_{phot}	z_{spec}	R.A. J2000	Decl. J2000	$B_{gc,R}$ Mpc$^{1.8}$	$\epsilon B_{gc,R}$ Mpc$^{1.8}$	M_{200} $M_\odot \times 10^{14}$	R_{200} Mpc	Centroi
(1)	(2)	(3)	(4)	(5)	(6)	(7)	(8)	(9)	(10)	(11)
32	FLS J172540+5909.5	0.48	—	17:25:40.5	59:09:34.5	600	211	2.88	1.12	RS-Flux
33	FLS J172109+5939.2	0.49	—	17:21:09.1	59:39:15.5	878	254	5.34	1.38	BCG
34	FLS J172513+5923.6	0.49	0.518(1)	17:25:13.1	59:23:36.6	807	244	4.66	1.32	RS-Flux
35	FLS J172142+5921.8	0.52	0.538(1)	17:21:42.9	59:21:49.1	597	210	2.86	1.12	BCG
36	FLS J172342+5941.0	0.52	—	17:23:42.2	59:41:03.5	320	152	1.04	0.80	BCG
37	FLS J171622+5915.5	0.53	—	17:16:22.7	59:15:30.7	250	132	0.69	0.70	BCG
38	FLS J172122+5922.7	0.53	0.538(2)	17:21:22.0	59:22:46.3	1287	306	9.94	1.69	BCG
39	FLS J172339+5937.2	0.53	—	17:23:39.5	59:37:12.5	318	151	1.03	0.80	BCG
40	FLS J171459+6016.7	0.55	—	17:14:59.9	60:16:44.5	730	232	3.96	1.25	BCG
41	FLS J171300+5919.4	0.55	—	17:13:00.2	59:19:28.0	591	209	2.81	1.11	RS-Flux
42	FLS J172228+6013.4	0.55	—	17:22:28.8	60:13:24.2	453	182	1.83	0.97	RS-Flux
43	FLS J171405+5900.6	0.55	0.516(1)	17:14:05.0	59:00:41.7	454	183	1.84	0.97	BCG
44	FLS J171648+5838.6	0.56	0.573(2)	17:16:48.2	58:38:37.7	2040	383	20.9	2.15	BCG
45	FLS J172037+5853.4	0.58	—	17:20:37.2	58:53:26.2	518	195	2.27	1.04	RS-Flux
46	FLS J171227+5904.8	0.61	—	17:12:27.6	59:04:53.8	650	219	3.28	1.17	RS-Flux
47	FLS J171452+5917.2	0.61	—	17:14:52.8	59:17:12.9	719	230	3.86	1.24	BCG
48	FLS J171104+5858.5	0.61	—	17:11:04.6	58:58:32.7	926	261	5.83	1.42	BCG
49	FLS J171634+6009.2	0.62	—	17:16:34.4	60:09:15.2	621	214	3.05	1.14	BCG
50	FLS J171420+6005.5	0.63	—	17:14:20.1	60:05:35.3	1131	288	8.06	1.57	BCG
51	FLS J171654+6004.8	0.63	—	17:16:54.0	60:04:48.0	510	194	2.21	1.03	RS-Flux
52	FLS J171628+5836.6	0.66	—	17:16:28.5	58:36:40.9	229	124	0.60	0.67	BCG
53	FLS J171523+5858.7	0.68	—	17:15:23.9	58:58:47.2	916	260	5.73	1.41	BCG
54	FLS J171633+5920.9	0.68	—	17:16:33.9	59:20:54.6	292	143	0.89	0.77	BCG
55	FLS J172601+5945.7	0.69	—	17:26:01.1	59:45:47.0	637	217	3.18	1.16	BCG
56	FLS J172013+5845.4	0.69	—	17:20:13.0	58:45:26.9	1051	278	7.16	1.51	BCG
57	FLS J171836+6006.7	0.70	—	17:18:36.7	60:06:43.3	430	177	1.68	0.94	BCG
58	FLS J171903+5851.8	0.70	—	17:19:03.7	58:51:51.1	430	177	1.68	0.94	RS-Flux
59	FLS J172246+5843.7	0.71	—	17:22:46.3	58:43:43.3	429	176	1.67	0.94	BCG
60	FLS J171703+5857.9	0.72	—	17:17:03.5	58:57:57.8	912	259	5.68	1.40	BCG
61	FLS J172431+5928.3	0.72	—	17:24:31.8	59:28:23.4	220	120	0.56	0.66	BCG
62	FLS J171203+6006.6	0.73	—	17:12:03.9	60:06:38.8	289	142	0.88	0.76	RS-Flux
63	FLS J171430+5901.7	0.73	—	17:14:30.1	59:01:47.1	978	269	6.37	1.46	RS-Flux

Table 4.1 (cont'd)

#	Name	z_{phot}	z_{spec}	R.A. J2000	Decl. J2000	$B_{gc,R}$ Mpc$^{1.8}$	$\epsilon B_{gc,R}$ Mpc$^{1.8}$	M_{200} $M_\odot \times 10^{14}$	R_{200} Mpc	Centroi
(1)	(2)	(3)	(4)	(5)	(6)	(7)	(8)	(9)	(10)	(11)
64	FLS J171834+5844.6	0.73	—	17:18:34.1	58:44:39.4	359	160	1.25	0.85	BCG
65	FLS J172009+6008.0	0.73	0.706(1)	17:20:09.7	60:08:02.6	426	176	1.65	0.94	BCG
66	FLS J172319+5922.2	0.73	—	17:23:19.5	59:22:15.9	356	159	1.23	0.85	BCG
67	FLS J172525+5924.7	0.74	—	17:25:25.8	59:24:46.4	633	216	3.14	1.16	RS-Flux
68	FLS J171508+5845.4	0.75	—	17:15:08.8	58:45:27.2	1116	287	7.89	1.56	BCG
69	FLS J172148+6016.1	0.77	0.907(1)	17:21:48.5	60:16:07.7	774	239	4.36	1.29	BCG
70	FLS J171454+5958.3	0.77	—	17:14:54.6	59:58:18.4	360	160	1.26	0.86	BCG
71	FLS J171511+6028.0	0.77	—	17:15:11.3	60:28:01.4	704	228	3.74	1.22	RS-Flux
72	FLS J172012+5958.3	0.78	—	17:20:12.7	59:58:19.9	705	228	3.74	1.22	RS-Flux
73	FLS J172209+5935.2	0.78	—	17:22:09.4	59:35:16.6	360	160	1.26	0.86	RS-Flux
74	FLS J172035+5928.6	0.78	—	17:20:35.5	59:28:40.4	428	176	1.67	0.94	BCG
75	FLS J171411+6027.7	0.78	—	17:14:11.7	60:27:44.3	705	228	3.74	1.22	BCG
76	FLS J171545+5853.8	0.78	—	17:15:45.9	58:53:48.6	291	142	0.89	0.76	BCG
77	FLS J171556+5859.9	0.79	—	17:15:56.1	58:59:54.3	636	217	3.17	1.16	BCG
78	FLS J171932+5929.3	0.79	—	17:19:32.0	59:29:18.5	499	191	2.14	1.02	RS-Flux
79	FLS J172019+5926.6	0.79	—	17:20:19.8	59:26:41.4	291	142	0.89	0.76	RS-Flux
80	FLS J171828+5836.2	0.79	—	17:18:28.7	58:36:13.8	498	191	2.13	1.02	RS-Flux
81	FLS J172304+5832.3	0.81	—	17:23:04.5	58:32:18.6	363	161	1.27	0.86	BCG
82	FLS J171657+6004.8	0.82	—	17:16:57.9	60:04:49.3	711	229	3.80	1.23	BCG
83	FLS J171945+5909.1	0.84	—	17:19:45.4	59:09:09.1	507	193	2.19	1.03	RS-Flux
84	FLS J171155+6013.1	0.90	—	17:11:55.1	60:13:08.5	522	196	2.30	1.04	RS-Flux
85	FLS J171808+5915.8	0.91	—	17:18:08.7	59:15:50.7	387	168	1.42	0.89	RS-Flux
86	FLS J171223+6015.1	0.95	—	17:12:23.7	60:15:09.4	605	211	2.92	1.13	RS-Flux
87	FLS J171051+5930.8	1.02	—	17:10:51.8	59:30:50.5	760	237	4.23	1.27	BCG
88	FLS J172147+6011.5	1.02	—	17:21:47.3	60:11:35.7	277	141	0.82	0.74	BCG
89	FLS J171852+6009.9	1.02	—	17:18:52.7	60:09:56.9	485	189	2.04	1.00	RS-Flux
90	FLS J171221+6010.6	1.03	—	17:12:21.2	60:10:41.0	349	160	1.20	0.84	BCG
91	FLS J171431+5946.9	1.06	—	17:14:31.9	59:46:59.5	425	177	1.65	0.94	RS-Flux
92	FLS J171117+5902.8	1.06	—	17:11:17.5	59:02:48.6	287	144	0.87	0.76	BCG
93	FLS J172126+5856.6	1.11	1.045(4)	17:21:26.4	58:56:41.7	646	218	3.25	1.17	BCG
94	FLS J171227+6015.2	1.14	—	17:12:27.0	60:15:16.7	448	182	1.80	0.96	BCG
95	FLS J172045+5834.8	1.17	—	17:20:45.3	58:34:50.9	386	169	1.41	0.89	RS-Flux

Table 4.1 (cont'd)

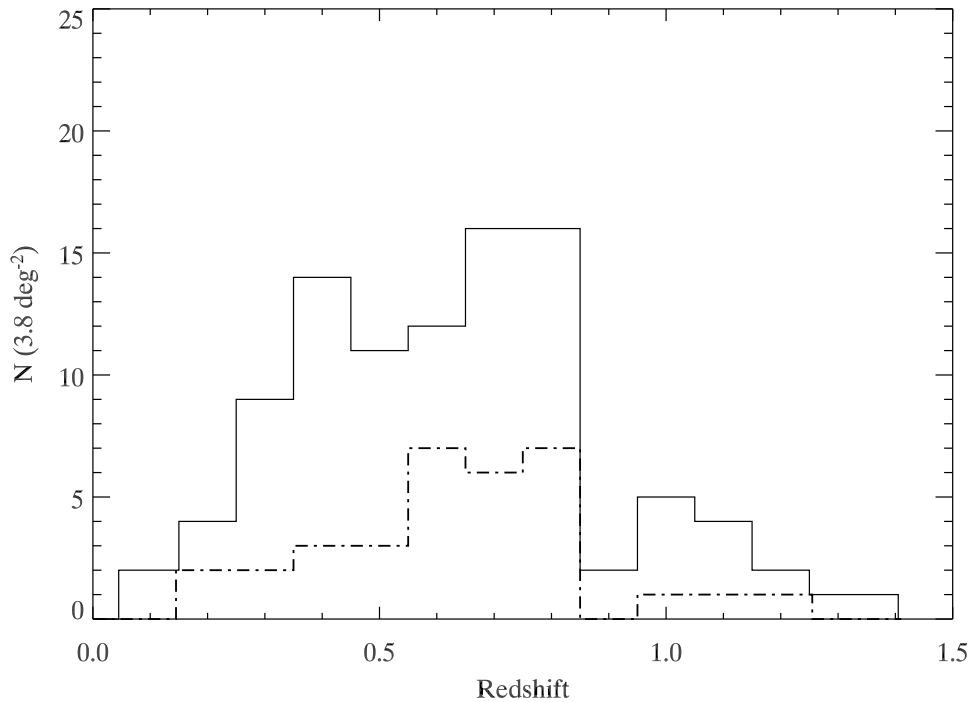| #	Name	z_{phot}	z_{spec}	R.A. J2000	Decl. J2000	$B_{gc,R}$ Mpc$^{1.8}$	$\epsilon B_{gc,R}$ Mpc$^{1.8}$	M_{200} $M_\odot \times 10^{14}$	R_{200} Mpc	Centroid
(1)	(2)	(3)	(4)	(5)	(6)	(7)	(8)	(9)	(10)	(11)
96	FLS J172113+5901.0	1.24	—	17:21:13.8	59:01:05.7	338	158	1.13	0.83	RS-Flux
97	FLS J171223+6006.9	1.27	—	17:12:23.6	60:06:56.4	208	124	0.51	0.64	RS-Flux
98	FLS J171942+5938.3	1.38	—	17:19:42.8	59:38:23.2	374	165	1.34	0.87	RS-Flux

Figure 4.4 Redshift distribution of clusters in the FLS. The solid histogram is for all clusters and the dot-dashed histogram is for clusters with $M_{200} > 3 \times 10^{14}$ $M_\odot$.

4.6 Cluster Luminosity Functions

In this section we measure the IRAC luminosity functions of the FLS cluster sample and use these to study the evolution of stellar mass assembly and dusty star formation in clusters.
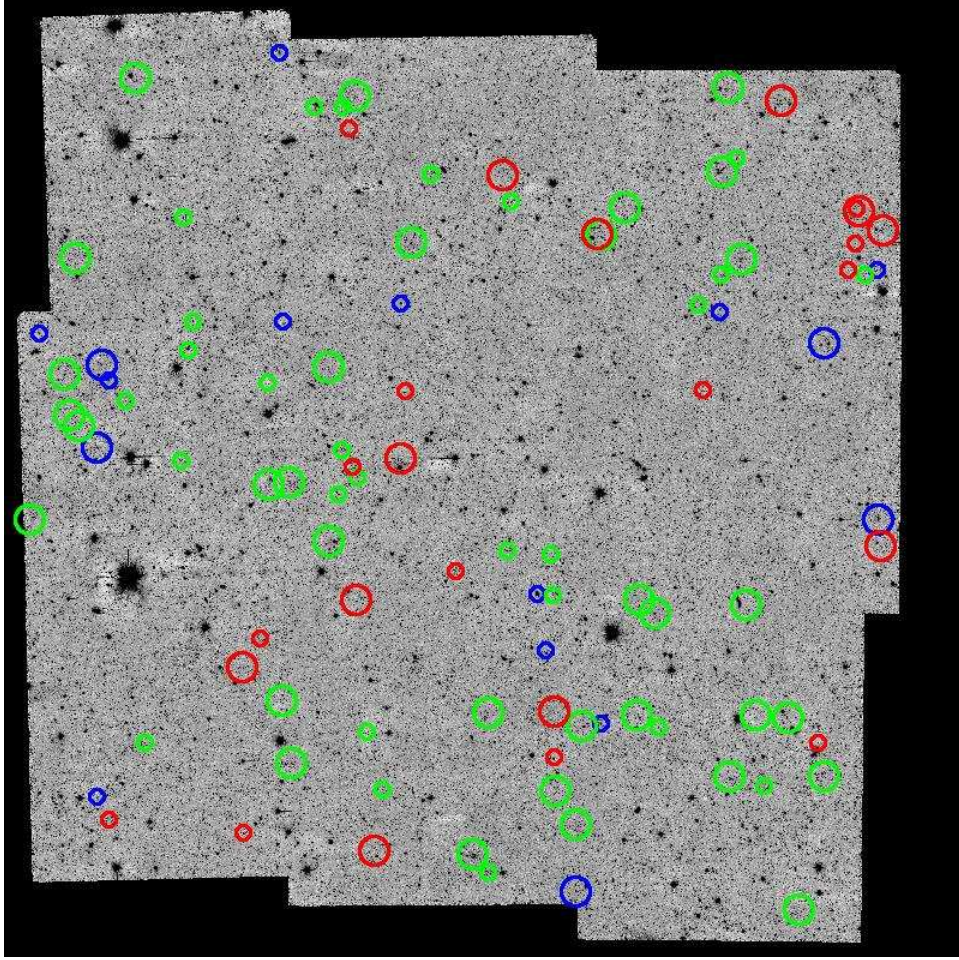
Figure 4.5 The [3.6μm] image of the FLS with the positions of clusters superposed. The blue, green, and red circles denote clusters with $0.1 < z < 0.4$, $0.4 < z < 0.8$, and $z > 0.8$ respectively. Large circles represent clusters with $M_{200} > 3 \times 10^{14}$ $M_{\odot}$ and small circles represent clusters with $M_{200} > 3 \times 10^{14}$ $M_{\odot}$. The size of the circles is arbitrarily chosen for clarity and is not related to the projected size of R_{200} for the clusters.

4.6.1   The [3.6μm] and [4.5μm] Luminosity Functions

The luminosity of galaxies at [3.6μm] and [4.5μm] over the redshift range $0.1 < z < 1.5$ is dominated by emission from low mass stars and is fairly insensitive to ongoing star formation or dust. Although there can be variations in the stellar mass-to-light ratio (M_*/L) of galaxies in similar bandpasses as large as a factor of 5-7 (such as in the K-band, e.g., Brinchmann 1999; Bell & de Jong, 2001; Bell et al. 2003), the luminosity of a galaxy at [3.6μm] and [4.5μm] is still a reasonable proxy for its stellar mass. Therefore, the [3.6μm] and [4.5μm] cluster LFs provide an estimate of the stellar mass function of cluster galaxies, and its evolution can constrain the mass assembly history of cluster
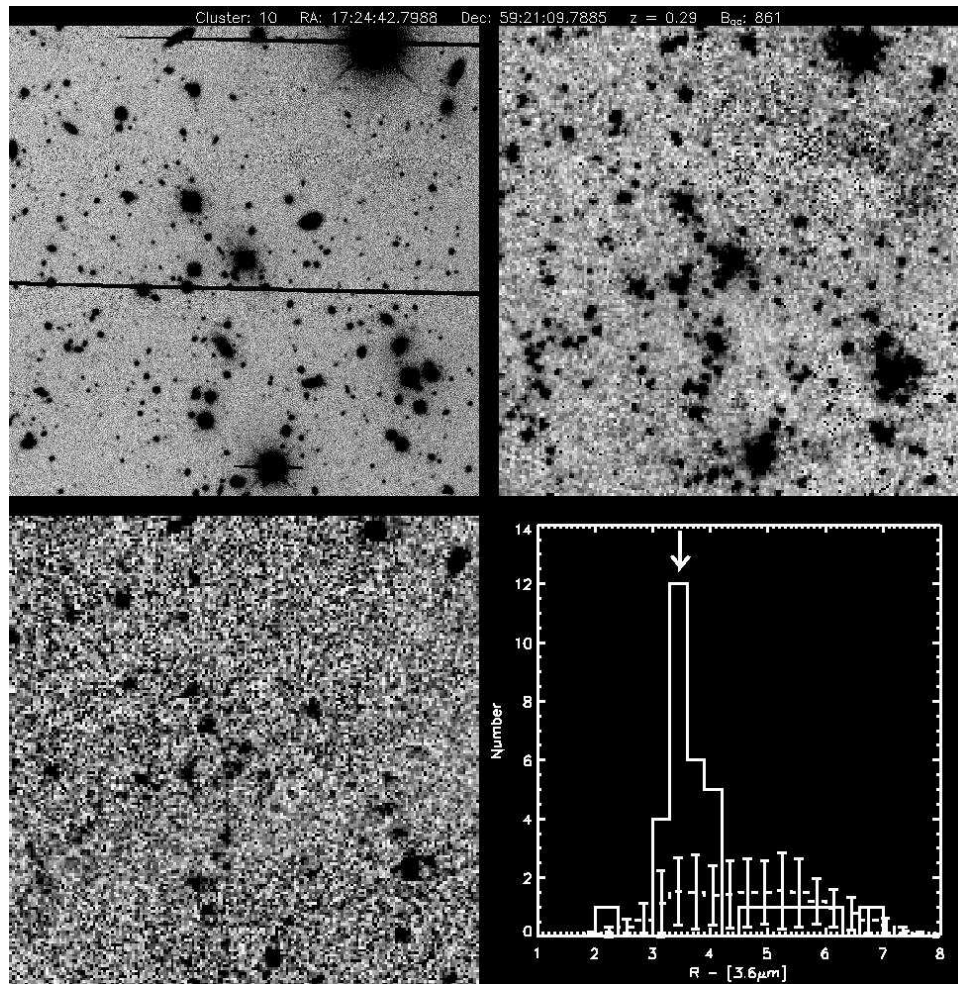
Figure 4.6 Multi-wavelength images of FLS J172449+5921.3 at z_{spec} = 0.252 (Cluster #10 from Table 1). The top left, top right, and bottom left panels are the R-band, IRAC [$3.6\mu m$], and IRAC [$8.0\mu m$] respectively. In each image the field-of-view is 1 Mpc across at the redshift of the cluster. The solid histogram in the bottom right panel shows the color distribution of galaxies with M < M* in the same field. The dashed histogram is the background distribution in the same aperture and the error bars show the average variance in the background. The arrow marks the color of the red-sequence from the color-redshift models. The cluster red-sequence is clearly detected at many sigma above the background.
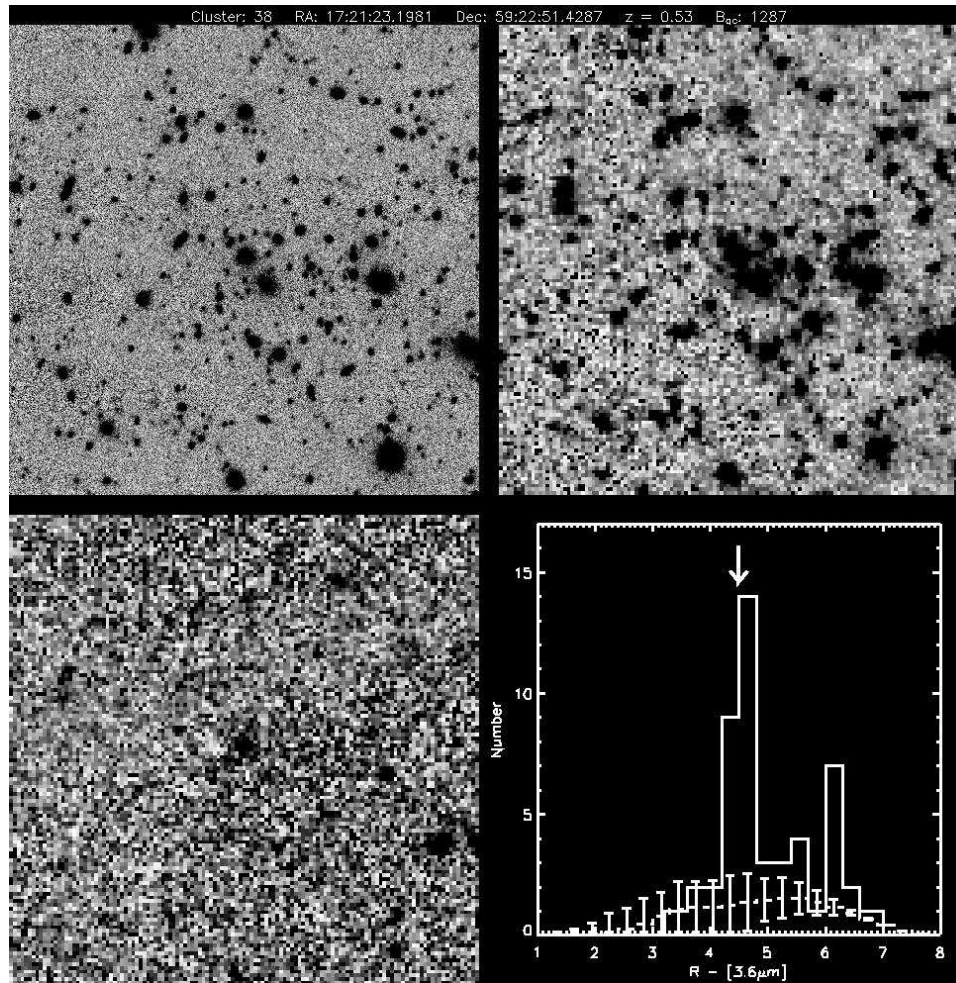
Figure 4.7 Same as for Figure 6, but for FLS J172122+5922.7 at z_{spec} = 0.538 (Cluster #38 from Table 1).

galaxies.

Exhaustive studies of both the K-band (e.g., De Propris et al. 1999, Lin et al. 2006, Muzzin et al. 2007a) and [3.6μm] & [4.5μm] (Andreon 2006, De Propris et al. 2007) LFs of cluster galaxies have shown that the evolution of M* in these bands is consistent with a passively evolving stellar population formed at high-redshift ($z_f > 1.5$), suggesting that the majority of the stellar mass in bright cluster galaxies is already assembled into massive galaxies by at least $z \sim 1$. Here we compute the LFs in the [3.6μm] and [4.5μm] bands for the FLS clusters to confirm that the FLS cluster sample provides similar results, and to demonstrate that these LFs can be used to estimate the stellar contribution to the mid-IR cluster LFs (§5.2).

The LFs are measured by stacking clusters in redshift bins of Δz = 0.1 starting from $z = 0.1$. For each cluster, the number of galaxies within R$_{200}$ in 0.25 mag bins is
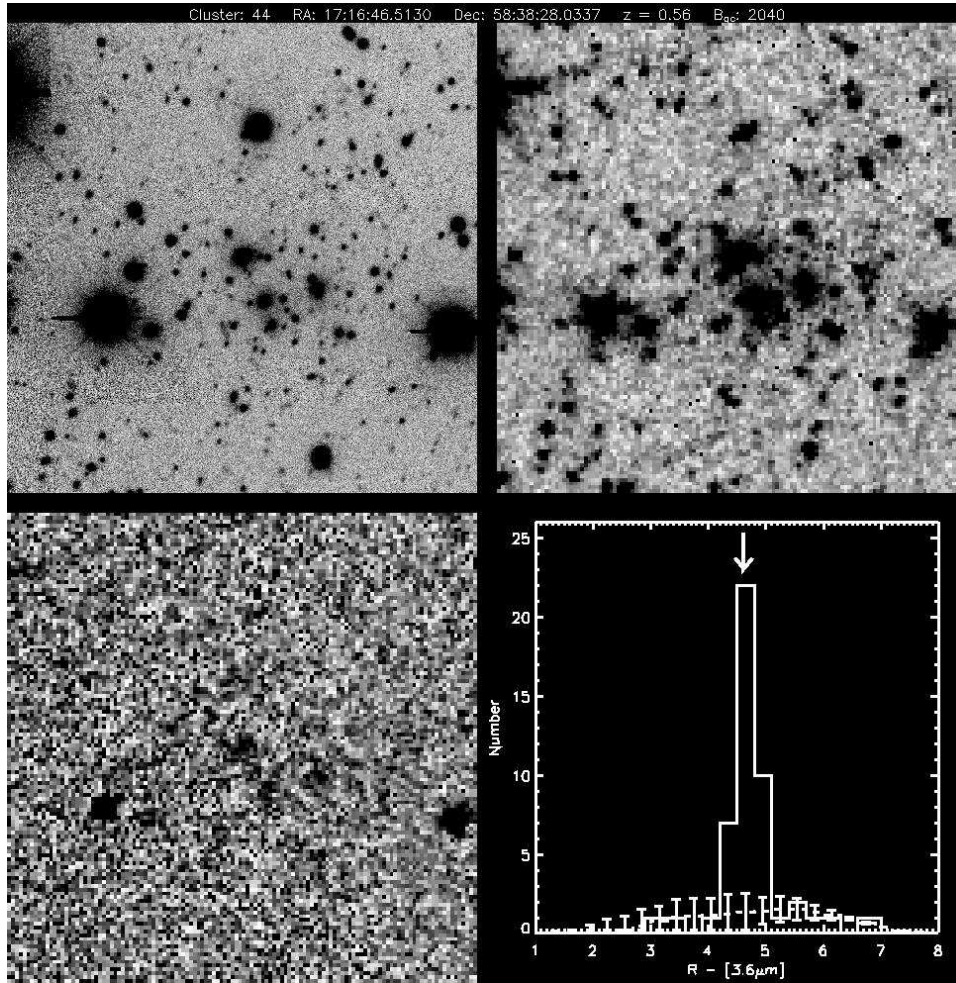
Figure 4.8 Same as for Figure 6, but for FLS J171648+5838.6 at $z_{spec} = 0.573$ (Cluster #44 from Table 1).

tabulated and the expected number of background galaxies within R_{200} is subtracted from these counts. The background counts are determined from the entire 3.8 deg^2 survey area and are very well constrained. Each background-subtracted cluster LF is then "redshifted" to the mean redshift of the bin using a differential distance modulus and a differential k-correction determined from the single-burst model (§3.1). At $[3.6\mu m]$ and $[4.5\mu m]$ the k-corrections for galaxies are almost independent of spectral-type (e.g., Huang et al. 2007a) and therefore using only the single-burst k-correction rather than a k-correction based on spectral-type does not affect the LFs. Furthermore, the differential k-corrections and distance moduli are very small (typically < 0.1 mag) and do not affect the LFs in a significant way.

The final stacked LFs are constructed by summing the individual LFs within each bin. The errors for each magnitude bin of the final LF are computed by adding the
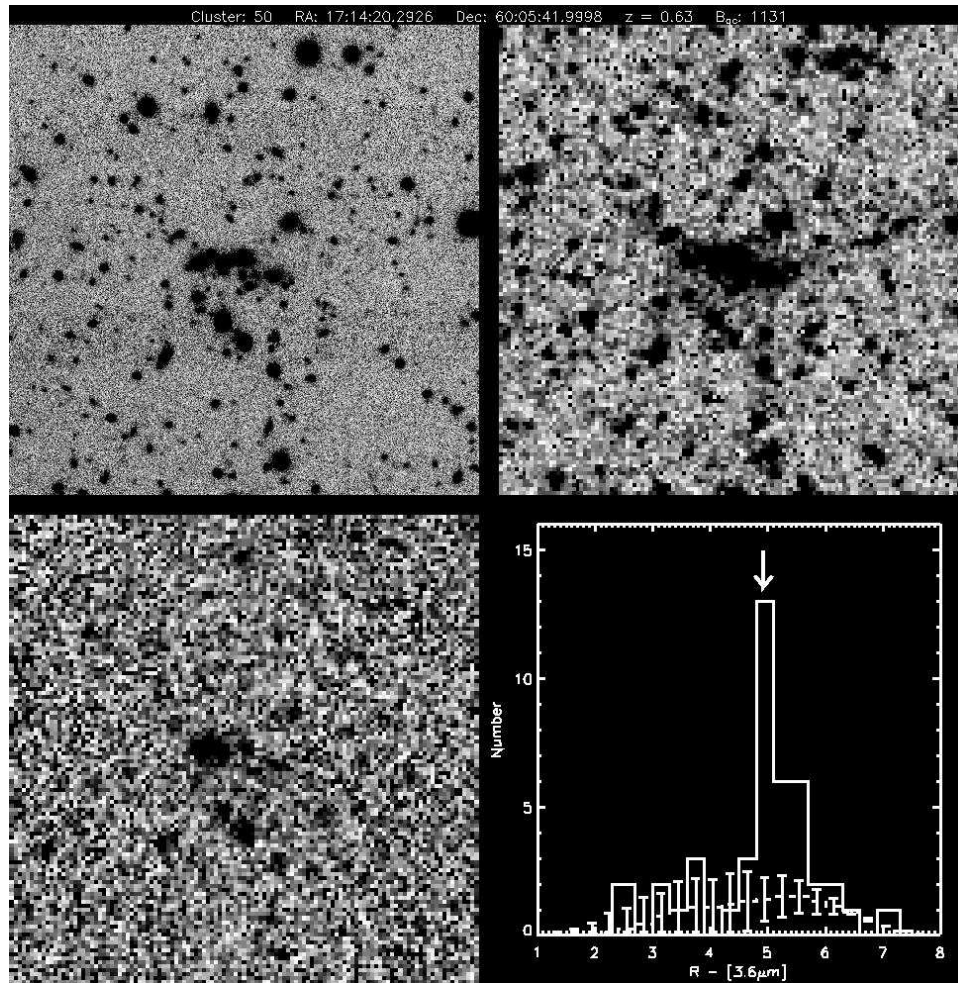
Figure 4.9 Same as for Figure 6, but for FLS J171420+6005.5 at $z_{phot} = 0.63$ (Cluster #50 from Table 1).

Poisson error of the total cluster counts to the Poisson error of the total background counts in quadrature.

In Figure 12 and Figure 13 we plot the [$3.6\mu m$] and [$4.5\mu m$] cluster LFs respectively. The [$3.6\mu m$] LFs are fit to a Schechter (1976) function of the form

$$\phi(\mathrm{M}) = (0.4\ln10)\phi_*(10^{0.4(M^*\text{-}M)})^{1+\alpha}\exp(-10^{0.4(M^*\text{-}M)}), \qquad (4.3)$$

where α is the faint-end slope; ϕ_*, the normalization; and M^* is the "characteristic" magnitude, which indicates the transition between the power-law behavior of the faint-end and the exponential behavior of the bright-end. The functions are fit using the Levenberg-Marquardt algorithm for least-squares (Press et al. 1992) and errors are estimated from the fitting covariance matrix. The data are not deep enough to provide good constraints on α, ϕ^* and M^* simultaneously, and therefore the faint-end
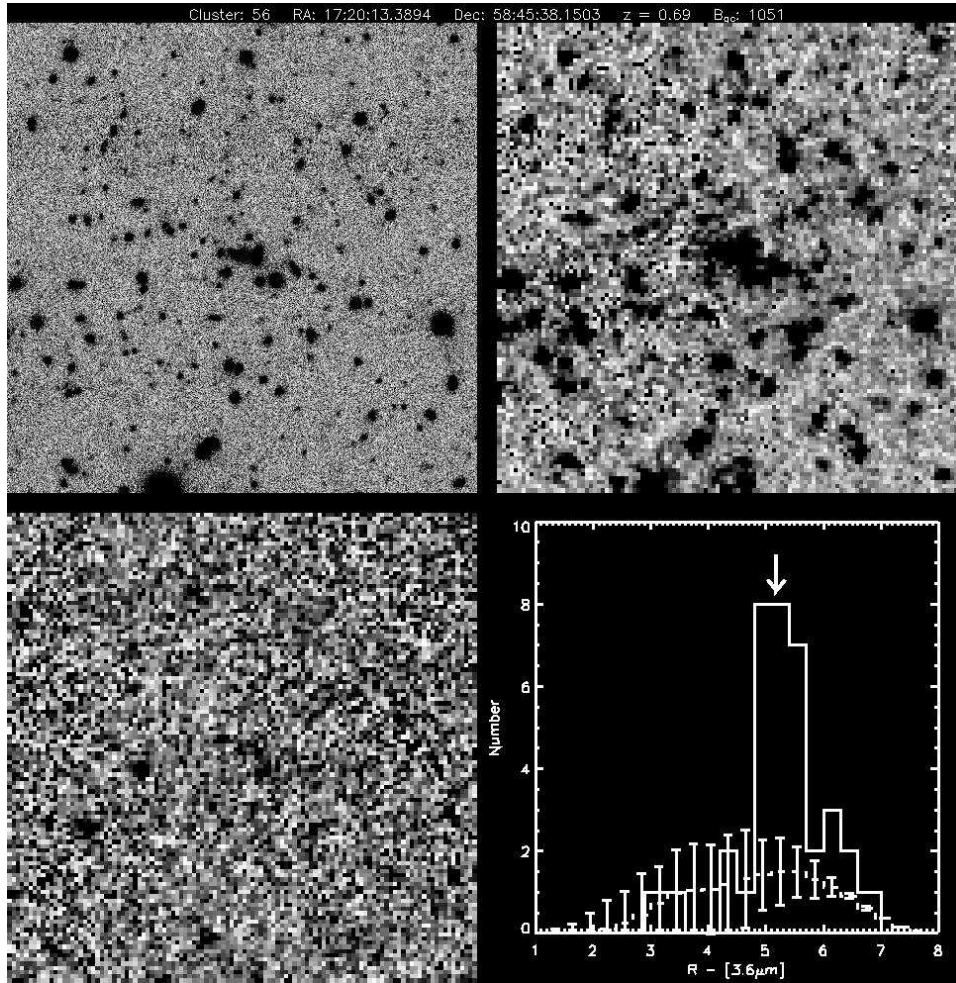
Figure 4.10 Same as for Figure 6, but for FLS J172013+5845.4 at z_{phot} = 0.69 (Cluster #56 from Table 1).

slopes of the LFs are assumed to be fixed at α = -0.8. This value is similar to the α = -0.84 $\pm$ 0.08 measured in the K-band for clusters at $z \sim 0.3$ by Muzzin et al. (2007a) as well as the value measured in the K-band for local clusters (α = -0.84 $\pm$ 0.02) by Lin et al. (2004). Although assuming a fixed value of α precludes measuring any evolution of the faint-end slope of the LFs with redshift, it removes the strong correlation between M^* and α in the fitting and is therefore the best way to measure the luminosity evolution of the cluster galaxies via the evolution of M^*. The fitted values of M^* and the 1σ errors are listed in the upper left of the panels in Figure 12.

We plot the evolution of M^* at $[3.6\mu m]$ as a function of redshift in Figure 14 as filled circles. Figure 14 also shows the predicted evolution of M^* for single-burst models with z_f = 1.0, 1.5, 2.0, 2.8, and 5.0. These models are normalized to M^* = -24.02 at $z =$ 0 in the K-band, the result obtained by Lin et al. (2004) for 93 local clusters. This corre-
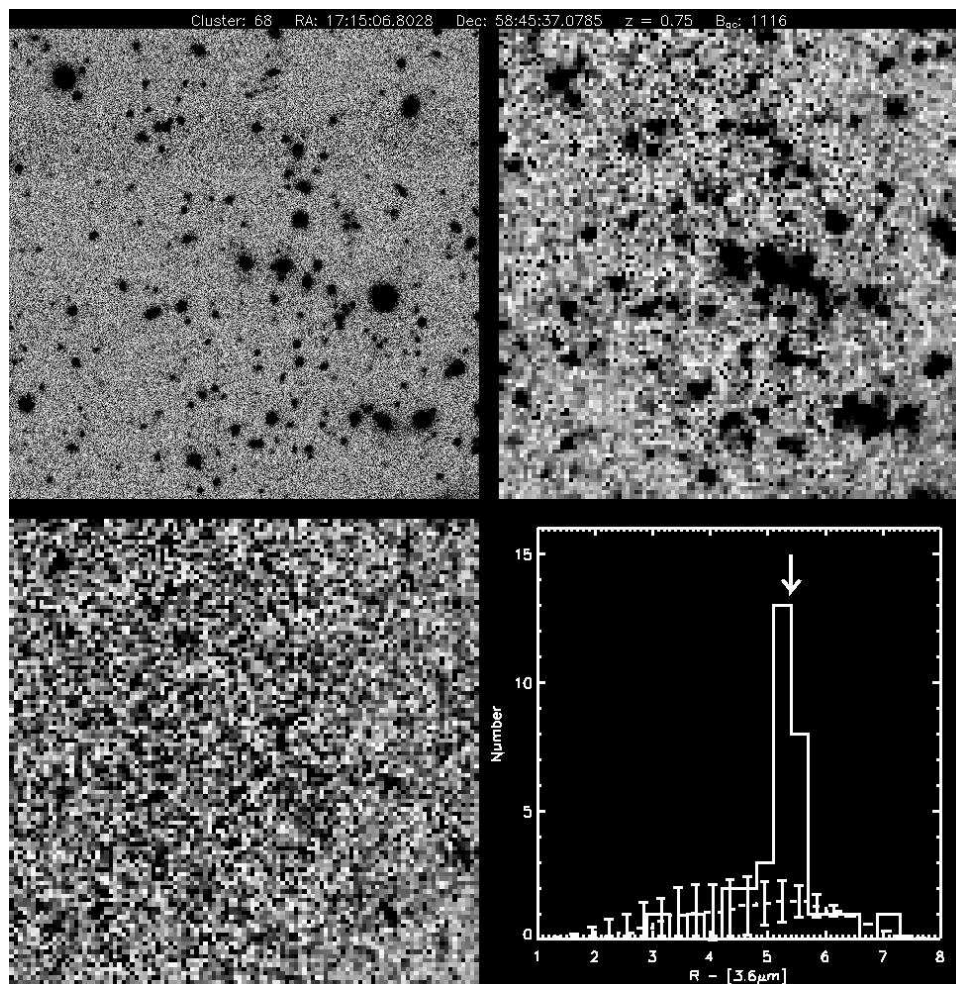
Figure 4.11 Same as for Figure 6, but for FLS J171508+5845.4 at z_{phot} = 0.75 (Cluster #68 from Table 1).

sponds to a normalization of M* = -24.32 at [$3.6\mu m$], assuming a K-[$3.6\mu m$] color from the z_f = 2.8 passive evolution model. The FLS values of M* are consistent with most of these models, except the z_f = 1.0 model, for which they are clearly too faint. Therefore, similar to the majority of previous studies we can conclude that the bulk of the stellar mass in bright cluster galaxies is consistent with having been formed at $z > 1.5$ and has passively evolved since then. As a comparison, the values measured at [$3.6\mu m$] by De Propris et al. (2007) and Andreon (2006) are overplotted as open squares and open diamonds respectively. These values are from spectroscopically confirmed samples of ~ 40 clusters (the majority of which are X-ray detected clusters) and both agree well with the FLS values demonstrating that passive evolution appears to be the ubiquitous conclusion regardless of cluster sample.

Similar to the [$3.6\mu m$] LFs, the [$4.5\mu m$] LFs can be fit using a Schechter function;

Figure 4.12 The [$3.6\mu m$] LFs of clusters in the FLS. The solid line shows the best-fit Schechter function assuming α = -0.8. The redshift, the value of M*, and the number of clusters combined to make the LF are listed in the upper left corner of each panel.

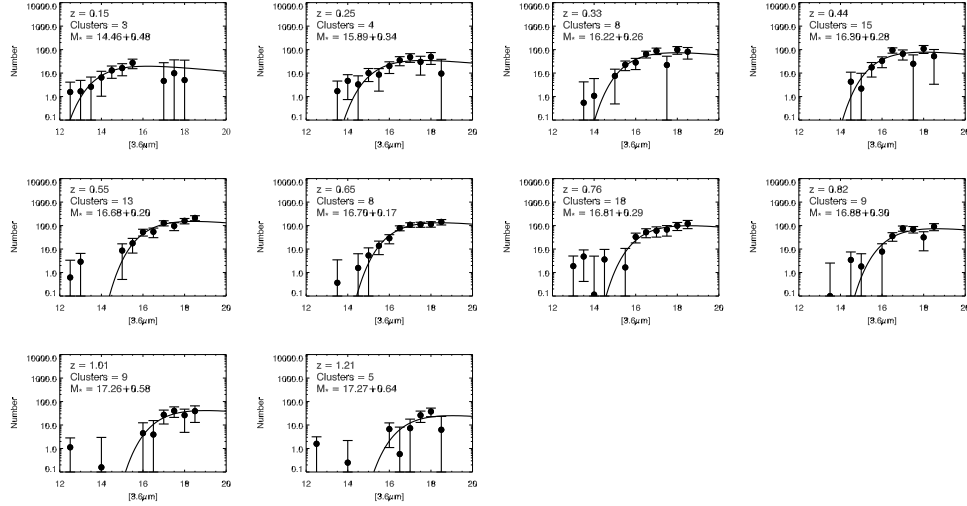however, we do not perform fitting of the [$4.5\mu m$] LFs. Instead, as a demonstration of the technique presented in §5.2.1 and §5.2.2, we use the measured [$3.6\mu m$] LFs to predict the [$4.5\mu m$] LFs. Unlike colors from the redder IRAC channels, the [$3.6\mu m$]-[$4.5\mu m$] colors of galaxies have little dependence on spectral-type over the redshift range $0 < z < 1$. As a consequence, the [$4.5\mu m$] LFs can be predicted from the [$3.6\mu m$] LFs using the [$3.6\mu m$]-[$4.5\mu m$] colors from the passive evolution model. The inferred [$4.5\mu m$] LFs are overplotted as solid lines in Figure 13. The predicted [$4.5\mu m$] LFs agree very well with the measured ones and this demonstrates that the [$3.6\mu m$] LFs, combined with simple models for the color evolution of galaxies, can predict the LFs in other bandpasses very well.

4.6.2 The [$5.8\mu m$] and [$8.0\mu m$] Luminosity Functions

Unlike the [$3.6\mu m$] and [$4.5\mu m$] bandpasses where the dominant emission source in galaxies is almost exclusively from low mass stars, the luminosity of galaxies at [$5.8\mu m$] and [$8.0\mu m$] has contributions from warm dust continuum, PAH emission, and low mass stars. In particular, if warm dust (primarily heated by ongoing star formation or an AGN) or PAH emission is present, it typically dominates the luminosity at these wavelengths. Therefore, the [$5.8\mu m$] and [$8.0\mu m$] LFs can be used to probe the amount of dusty star formation and AGN activity in clusters if the contribution from stellar
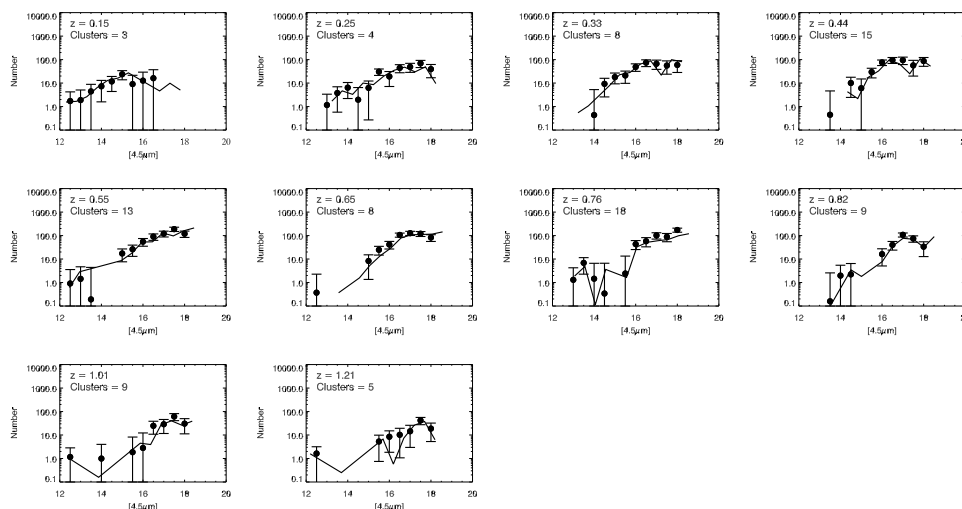
Figure 4.13 The [4.5μm] LFs of clusters in the FLS in the same redshift bins as Figure 12. The solid line is the [4.5μm] LF that is predicted from the [3.6μm] LF assuming that galaxies have the [3.6μm] - [4.5μm] colors of a passively evolving population formed at high redshift.

emission is properly accounted for.

The main challenge in modeling the LFs at these wavelengths is that a massive, dust-free early-type galaxy produces relatively the same flux at [5.8μm] and [8.0μm] from pure stellar emission as a much lower mass dusty starburst galaxy produces from warm dust continuum or PAH emission. These are clearly different populations of galaxies; however, determining the relative abundance of each in a LF is more challenging for a statistically defined sample such as this cluster sample where individual galaxies are not identified as field/cluster or star forming/non-star forming. Despite this challenge, we showed in §5.1 that the [3.6μm] LFs can be used as a diagnostic of the average stellar emission from the cluster galaxies and that even with a relatively simple model for galaxy colors they can predict the [4.5μm] LFs extremely well. The [3.6μm]-[5.8μm] and [3.6μm]-[8.0μm] colors of different spectral-types vary significantly more than the [3.6μm]-[4.5μm] colors; however, if these colors are modeled correctly the same technique can be used to model the LFs in the [5.8μm] and [8.0μm] bandpasses and provide constraints on the number and type of star forming galaxies in clusters.

Put another way, the [3.6μm] LF provides effectively a "stellar mass budget" for predicting the [5.8μm] and [8.0μm] LFs. Subtracting this stellar mass budget at [5.8μm] and [8.0μm] leaves an excess which can be modeled with different populations of star

Figure 4.14 L
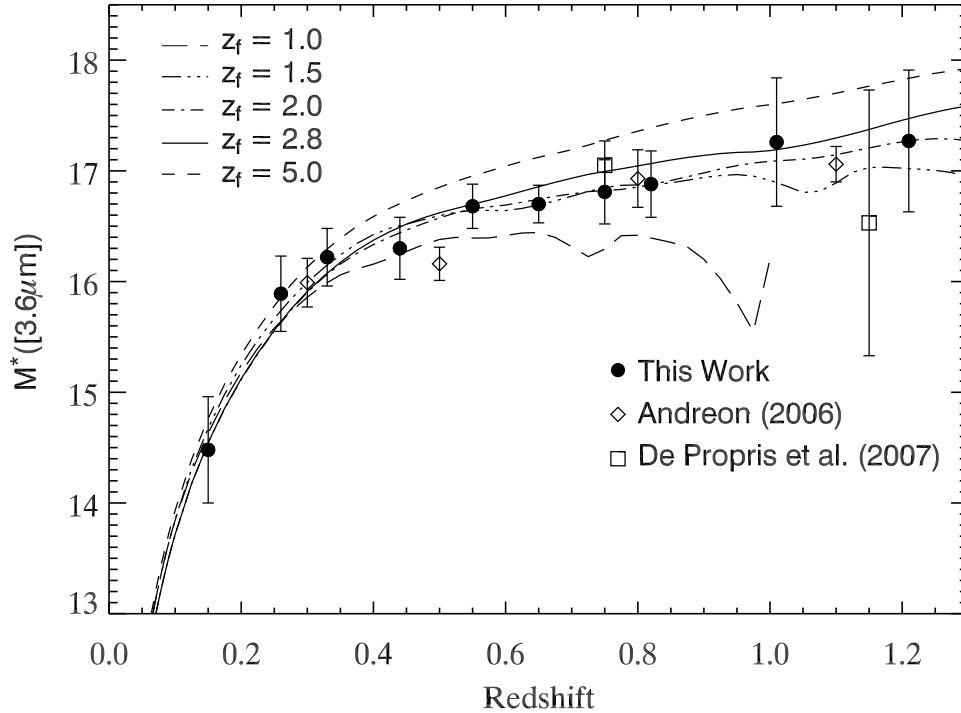
Fs as a function of redshift]Evolution in M* from the [$3.6\mu m$] LFs as a function of redshift. The long dashed, dash-dotted, dash-dot, solid, and dashed lines show models where the stars form in a single burst at $z = 1.0, 1.5, 2.0, 2.8$, and 5.0 respectively. The filled circles are the FLS clusters and the open diamonds and open squares are the M* values from the Andreon (2006) and De Propris et al. (2007) cluster samples.

forming galaxies. Unfortunately, such models are unlikely to be completely unique in the sense that there will be a degeneracy between the *fraction* of star forming galaxies, and the *mode* of star formation (i.e., regular or dusty starburst); however, we will show that using only weak observational constraints on the percentage of star forming/non-star forming galaxies in clusters places constraints on the mode of star formation in cluster galaxies, and the relative percentages of "regular" star forming galaxies and dusty starbursts.

For the sake of simplicity we have not attempted to model an AGN component to the [$5.8\mu m$] and [$8.0\mu m$] LFs in this analysis. Martini et al. (2007) have shown that the AGN fraction in clusters at $z \sim 0.2$ is only 0.1% for AGN with X-ray luminosities (L_X) $> 10^{42}$ erg s^{-1} and $< 0.1\%$ for AGN with $L_X > 10^{43}$ erg s^{-1}. Eastman et al. (2007) showed a large increase in this fraction out to $z \sim 0.6$, but the overall fractions are still

very low, only 3% for AGN with $L_X > 10^{42}$ erg s^{-1} and 2% for AGN with $L_X > 10^{43}$ erg s^{-1}. Although AGN are more luminous at [$5.8\mu m$] and [$8.0\mu m$] than star forming galaxies, in number they are so much less abundant (cluster blue fractions at these redshifts typically range between 10-60%) that they should not contribute significantly to the [$5.8\mu m$] and [$8.0\mu m$] LFs.

Before models of the cluster population are made, we measure the [$5.8\mu m$] and [$8.0\mu m$] LFs from the data. This is performed with the same stacking and background subtraction methods as for the [$3.6\mu m$] and [$4.5\mu m$] LFs and the resulting LFs are plotted in Figures 15 and 16. IRAC is significantly less sensitive at [$5.8\mu m$] and [$8.0\mu m$] than at [$3.6\mu m$] and [$4.5\mu m$] and therefore these LFs are much shallower. Only the bright end of the LF (roughly M < M*, assuming a dust-free, pure stellar emission early-type model) can be measured with these data; however, this shallow depth is still sufficient to be a good diagnostic of the presence of luminous dusty starbursts. For example, at $0.1 < z < 0.4$, an M82-type starburst is roughly 3 magnitudes brighter at [$8.0\mu m$] than an early-type model (e.g., Huang et al. 2007a; Wilson et al. 2007, see §6.3) and therefore, even a galaxy with M $\sim$ M* + 3 from the [$3.6\mu m$] LF would be detected at [$8.0\mu m$] if undergoing an M82-like dusty starburst.

Modeling the $5.8\mu m$ Luminosity Function

The simplest fiducial model that can be made for the mid-IR cluster galaxy population is to assume that the bright-end of the LF is dominated by passive, dust-free, early-type galaxies (i.e., the emission at [$5.8\mu m$] and [$8.0\mu m$] is completely stellar). Although such a model is unrealistic, it provides a baseline for predicting the amount of emission in the mid-IR from stellar emission, and any excess beyond this model is likely to be from dusty star formation in the cluster population. Assuming such a model, the [$5.8\mu m$] LFs can be inferred from the [$3.6\mu m$] LFs using the [$3.6\mu m$]-[$5.8\mu m$] colors from the Bruzual & Charlot passive evolution model. These predicted [$5.8\mu m$] LFs are overplotted on the LFs in Figure 15 as the solid red lines (Figure 15 also has additional models overplotted which are introduced in §5.2.2).

Qualitatively, the [$3.6\mu m$] LFs and the passive evolution model predict the [$5.8\mu m$] LFs reasonably well at all redshifts. This is perhaps not surprising because due to k-corrections, [$5.8\mu m$] is only sensitive to emission from warm dust or PAHs in star forming galaxies at $z < 0.3$ (see §6.3). For galaxies at higher redshift, [$5.8\mu m$] probes rest-frame wavelengths which, similar to the [$3.6\mu m$] LFs, are dominated by stellar

emission. As a result, any dusty star forming cluster galaxies would only be visible as a notable excess in the predicted [$5.8\mu m$] LFs at $z < 0.3$. No such excess is seen; however, the fraction of blue star forming galaxies in clusters evolves rapidly (i.e., the Butcher-Oemler Effect) and clusters at $z < 0.3$ typically have low blue fractions and relatively few star forming galaxies (e.g., Ellingson et al. 2001; Balogh et al. 1999; Margoniner et al. 2001). Our result confirms that not only is the fraction of star forming galaxies in clusters at $z < 0.3$ low, but that there is no significant additional population of mid-IR luminous dusty star forming galaxies in clusters at these redshifts that may have been missed in optically-selected spectroscopic or photometric studies.

Modeling the $8.0\mu m$ Luminosity Function

The shape of the cluster [$8.0\mu m$] LFs is not the same as the [$5.8\mu m$] LFs, and this is illustrated by the solid red lines plotted in Figure 16. These lines represent the predicted [$8.0\mu m$] LFs using the [$3.6\mu m$] LFs and assuming the passive evolution model. Unlike for the [$5.8\mu m$] LFs, this model clearly underpredicts the number of galaxies in the [$8.0\mu m$] LFs at all redshifts. We argue in this section that the excess of galaxies above the passive evolution model is caused by star forming cluster galaxies which are significantly more luminous than early-type galaxies at [$8.0\mu m$].

In order to construct a more useful model for the [$8.0\mu m$] LF that includes the cluster star forming population, we use the [$3.6\mu m$]-[$8.0\mu m$] colors for different types of star forming galaxies from J. Huang et al. (2007b, in preparation). These authors have empirically extended the color/redshift models of Coleman et al. (1980) to $10\mu m$ using local galaxies with *ISO* spectroscopy. Some examples of the colors from these models are presented in Wilson et al. (2007).

Given the large number of permutations possible in the types of star forming galaxies, we are interested in as simple a model as possible which will allow for a straightforward interpretation of the data. For this analysis we divide the cluster star forming population into two basic types: "regular" star forming cluster spirals, and dusty starburst galaxies. Huang et al. (2007b) have models for both Sbc and Scd galaxies; however, the [$3.6\mu m$]-[$8.0\mu m$] colors of these models are indistinguishable, and therefore we adopt their Sbc galaxy as the model for a "regular" star forming cluster spiral. Huang et al. also have colors for several "canonical" dusty starburst galaxies such as M82, Arp220, and NGC 1068. M82 is a moderate-strength dusty starburst, has no AGN component, and is classified as a luminous infrared galaxy (LIRG). By contrast,

Arp220 and NGC 1068 are powerful dusty starbursts with AGN components. The IR luminosity of Arp220 is dominated by star formation from a major merger, while the IR luminosity of NGC 1068 is dominated by a powerful AGN (although both galaxies have AGN and starburst components). Both are classified as ultra-luminous infrared galaxies (ULIRGs). Given that the majority of distant clusters studied thus far in the mid-IR have shown a significant population of LIRGs but no population of ULIRGs (e.g., Coia et al. 2005; Geach et al. 2006; Marcillac et al. 2007), we assume that any cluster dusty starbursts will have colors similar to M82, rather than Arp220 or NGC 1068. In general, replacing M82 as the model for cluster dusty starbursts with either Arp220 or NGC 1068 requires a smaller fraction of dusty starbursts since they are more luminous.

In order to ascertain the dominant mode of star formation present in the cluster population we can construct simple models for the [8.0μm] LFs from the [3.6μm] LFs using various combinations of these populations. The purpose of the models is not to perfectly reproduce the cluster [8.0μm] LFs (this requires a much more detailed knowledge of the populations in each cluster than can be obtained by statistical background subtraction), but to demonstrate how the [8.0μm] LFs should appear given different proportions of these populations and thereby estimate the importance of each's contribution to the [8.0μm] LFs. Hereafter we refer to the Sbc model as "regular", the M82 model as "dusty starburst", and the Bruzual & Charlot passive evolution model as "quiescent".

Beyond assuming that all cluster galaxies are quiescent, which clearly underpredicts the [8.0μm] LFs, the next most simple model that can be made is to assume some fraction of the cluster galaxies are "regular" star forming galaxies (hereafter we refer to this model as regular+quiescent). In order to make such a model we require an approximation of the relative proportions of star forming and quiescent galaxies in clusters as a function of redshift and luminosity. The best spectroscopically-classified data at these redshifts comes from the MORPHS (Dressler et al. 1999; Poggianti et al. 1999) and CNOC1 (Balogh et al. 1999; Ellingson et al. 2001) projects. Unfortunately, the number of cluster spectra per dz is relatively small in these samples and they cover only a modest range in redshift ($0.2 < z < 0.5$) and depth in terms of the cluster M*.

Although spectroscopic classification would be the most reliable, the lack of data motivates the use of cluster blue fractions (f_b) as a function of redshift as a model for the relative fractions of star forming/non-star forming galaxies. Blue fractions for reasonably large samples of clusters at different redshifts have been calculated and

it is fairly straightforward to measure them as a function of magnitude within these clusters. In particular, using f_b as an estimate of the star forming fraction should predict the number of blue star forming galaxies (i.e., those with colors similar to the Sbc model). If a population of red, dust-obscured starburst galaxies exists in clusters they should be evident in the [8.0μm] LFs as an excess of galaxies beyond the regular+quiescent model.

For f_b as a function of redshift we use the data of Ellingson et al. (2001) from the CNOC1 clusters which span the redshift range $z = 0.2$ to $z = 0.4$, and for clusters at $z > 0.4$ we use the data on RCS-1 clusters from D. Gilbank et al. (2007b, in preparation). Rough f_b values for both these samples were recomputed using only galaxies with M < M* (D. Gilbank private communication), because this matches the depth of the [5.8μm] and [8.0μm] LFs. These f_b values as a function of redshift are listed in Table 2.

The scatter in cluster f_b values at a given redshift is large, and therefore different studies find different mean values depending on sample. The values we have adopted are consistent with the majority of work in the field (e.g., Butcher & Oemler 1984; Smail et al. 1998; Margoniner et al. 2001; Andreon et al. 2004), although we have measured them using a brighter luminosity cut. Of course, the best way to infer the f_b of the FLS clusters would be to measure it from the clusters themselves; however, we do not have the proper filter coverage at $z < 0.5$ to make this measurement properly nor a large enough sample to make a measurement that would be statistically different from the adopted values.

The cluster f_b is also a function of limiting magnitude (e.g., Ellingson et al. 2001), and without incorporating some variation in f_b as a function of magnitude, all of the model LFs consistently overpredict the number of bright galaxies in the [8.0μm] LFs, and underpredict the number of faint ones. In order to estimate the variation of f_b as a function of magnitude we use the spectrally-typed LFs of Muzzin et al. (2007a). They measured the K-band LF for cluster galaxies defined spectroscopically as either star forming or quiescent. Comparing those LFs (their Figure 13) and assuming all star forming galaxies are blue, and all quiescent galaxies are red, results in f_b values of 0.19, 0.35, and 0.52 for galaxies with M < M*, M* < M < M* + 1, and M* +1 < M < M* + 2 respectively in clusters at $z \sim 0.3$. Comparing these values shows that f_b is 1.8 times larger at M* < M < M* + 1 than at M < M*, and is 2.7 times larger at M* +1 < M < M* + 2 than at M < M*. We therefore adopt an f_b that varies with magnitude with the following conditions: For galaxies with M < M* in the [3.6μm] LF we use the f_b

values from Table 2. For galaxies with $M^* < M < M^* + 1$, we assume that f_b is twice as large as the values in Table 2, and for galaxies with $M^* + 1 < M < M^* + 2$ we assume that f_b is three times as large as the values in Table 2. In cases where this causes $f_b > 1.0$, it is set equal to 1.0.

Combining the f_b as a function of redshift and magnitude with the [3.6μm] LFs assuming all "blue" galaxies have the color of the Huang et al. Sbc galaxies and all "red" galaxies have the color of the passive evolution model results in the models that are plotted as green dashed lines in Figures 15 and 16. Comparing the data to these models shows that this simple model using only regular+quiescent galaxies predicts the cluster [8.0μm] LFs fairly well. In particular, the z = 0.15, 0.25 and 0.33 LFs are very well described by this model. For the higher redshift LFs this model is clearly better than the purely quiescent model; however, it still does not account for the entire [8.0μm] population.

Most importantly, the regular+quiescent model shows that out to $z \sim 0.65$, where [8.0μm] still probes rest-frame dust emission, *there is no significant population of bright (M < M*) galaxies in clusters that cannot reasonably be accounted for by "regular" star forming cluster spirals*. This is significant because it suggests that whatever processes responsible for transforming the morphology and spectral-type of *bright* cluster galaxies over the same redshift range do not involve an ultra-luminous dusty starburst phase such as those caused by major mergers of gas-rich galaxies (i.e., "wet" mergers). We note that there appears to be an overdensity of very bright galaxies in the $z = 0.82$ LF that cannot be accounted for by the regular+quiescent model and this suggests the possibility of an onset of luminous starbursts (possibly from mergers) or AGN activity in bright galaxies at higher redshift.

Although the regular+quiescent models predict the [8.0μm] LFs fairly well, the LFs still deviate from the models. This is most notable at $z > 0.4$ where the models underpredict the number of [8.0μm] sources, and, in particular, seem to underpredict the number of fainter galaxies in the [8.0μm] LF. This suggests a third component to the cluster [8.0μm] population, possibly a red, dusty starburst population which is not accounted for by the cluster f_b. Such a population was suggested by Wolf et al. (2005) who found that the SEDs of roughly 30% of the red-sequence galaxies in the Abell 901/902 supercluster (z = 0.17) were better described by dusty templates rather than a dust-free, old stellar population. In order to explore this possibility, we construct a new model with the same values of f_b as a function of magnitude and redshift as for the regular+quiescent model, but this time we assume that some of the red qui-

escent galaxies are instead M82-like dusty starbursts. M82 has optical-IR colors that are similar to quiescent galaxies (see Huang et al. 2007b and §6.3) so it is reasonable to assume that any M82-like dusty starbursts would be part of the population of red cluster galaxies rather than the blue cluster galaxies.

If we assume that the dusty starburst population is a constant fraction of the red cluster galaxies, this would result in a varying ratio of dusty starburst to regular star forming galaxies in clusters as a function of redshift. In particular, clusters at low redshift will have the highest fraction of dusty starburst galaxies (because the f_b is low and the red fraction is high). The LFs above have already suggested that there is no need for a dusty starburst population at low redshift, so modeling the dusty starbursts as a fixed fraction of the red galaxies seems inappropriate. Instead, a better way to model the population is to assume that the cluster f_b is a tracer of the total star formation in the cluster and that ratio of dusty starburst to regular star forming galaxies is a constant. Given this assumption we can predict the fraction of dusty starbursts directly from the cluster f_b. This fraction of dusty starbursts is then removed from the fraction of red quiescent galaxies and a model for the LFs can be made. Hereafter we refer to this model as starburst+regular+quiescent. The fractions of the cluster galaxy populations in terms of f_b are defined using the equations,

$$f_{dsb} = f_b \times f_{dsb/reg}, \tag{4.4}$$

$$f_q = 1 - f_b - f_{dsb}, \tag{4.5}$$

where f_{dsb} is the fraction of dusty starburst galaxies, $f_{dsb/reg}$ is the assumed ratio of dusty starburst to regular star forming galaxies, and f_q is the fraction of quiescent galaxies. In cases where $f_{dsb} + f_b > 1$ we set $f_{dsb} = 1 - f_b$ and $f_q = 0$.

As of yet there are no good observational constraints on the parameter $f_{dsb/reg}$. Therefore, as a first-order fiducial value we assume that $f_{dsb/reg} = 0.5$. In general, we find that allowing a range of values between 0.3 - 1.0 provides models that are fairly similar. More importantly, the differences in models that use $f_{sb/reg}$ between 0.3 - 1.0 are much smaller than the difference between any of those models and the regular+quiescent model. Therefore, the interpretation of the data using these models will not depend strongly on the assumed value of $f_{sb/reg}$. The starburst+regular+quiescent model with $f_{sb/reg} = 0.5$ is overplotted on Figures 15 and 16 as the dotted blue line.

This starburst+regular+quiescent model over-predicts the number of bright galaxies in the $z < 0.4$ [8.0μm] LFs but it is better at describing the LFs at $z > 0.4$ than the regular+quiescent or purely quiescent models. This suggests that there is a population
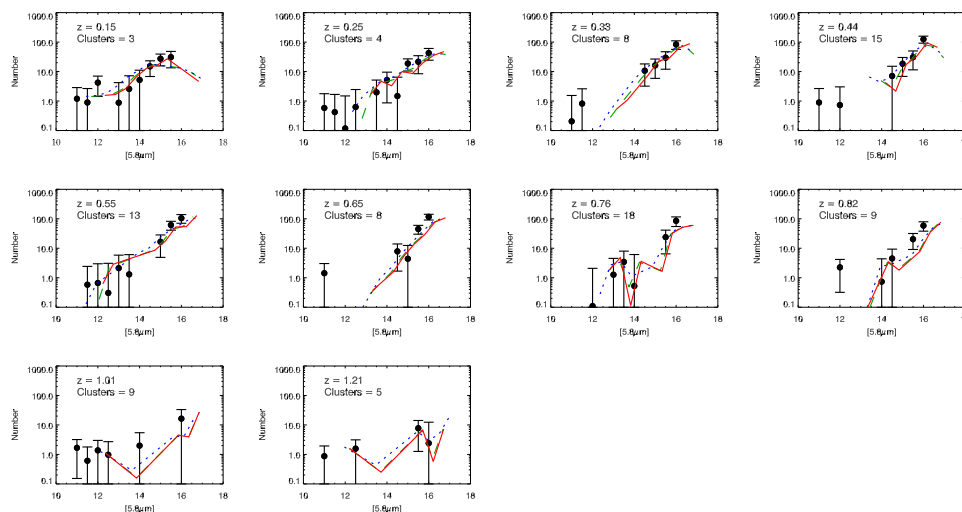
Figure 4.15 The [$5.8\mu m$] LFs of clusters in the FLS. The solid red line shows the [$5.8\mu m$] predicted from the [$3.6\mu m$] LF assuming all galaxies have the colors of the passive evolution model. The dashed green lines and dotted blue lines are the regular+quiescent and starburst+regular+quiescent models described in §5.2.2 respectively; however, [$5.8\mu m$] is not sensitive to warm dust at $z > 0.3$ and therefore these models are not notably different from the passive evolution model.

of dusty starbursts in clusters at $z > 0.4$ that does not exist at $z < 0.4$, and that these starbursts are consistent with being of an M82-type. We discuss this in more detail in §6.1.

4.7 Discussion

4.7.1 Evidence for a Change in Star Formation Properties of Cluster Galaxies?

In order to better illustrate the differences in the model populations described above, we subtract the quiescent model from the [$5.8\mu m$] and [$8.0\mu m$] LFs between $0.15 < z < 0.65$ and plot the residuals in Figures 17 and 18. The residuals from the quiescent+regular model and starburst+regular+quiescent models from §5.2.2 are also plotted in Figures 17 and 18. The solid vertical lines in the plots represent the magnitude of M* inferred from the [$3.6\mu m$] LF assuming the passive evolution model, and give some indication of the depth of the LFs. If we compare the data to the models and take the results at face value, it suggests that the dominant "mode" of star forma-
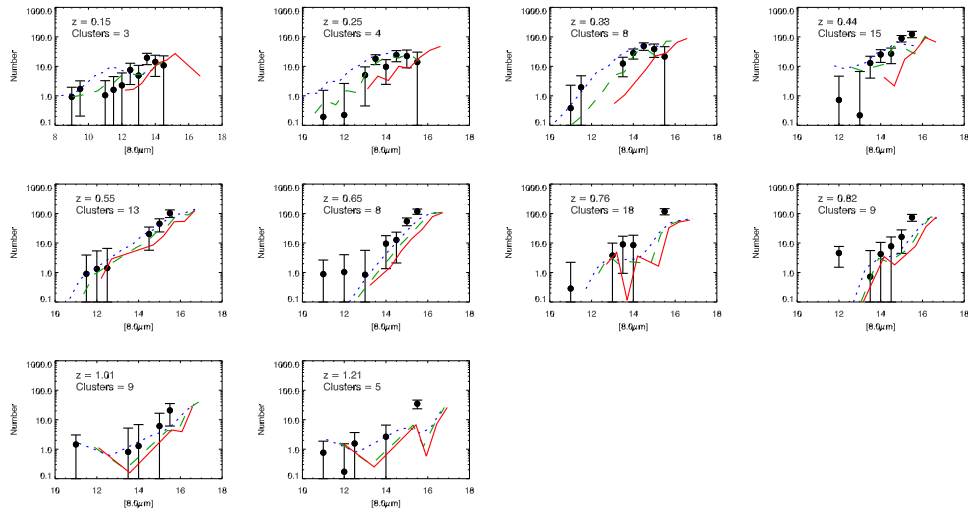
Figure 4.16 The [8.0μm] LFs of clusters in the FLS. The solid red line, dashed green line, and dotted blue line are the [8.0μm] LFs predicted using the [3.6μm] LF and the quiescent, regular+quiescent, and starburst+regular+quiescent models described in §5.2.2. At lower redshift ($z < 0.4$) the LFs are most similar to the predictions from the regular+quiescent model whereas at higher redshift ($z > 0.4$) the LFs are better described by the starburst+regular+quiescent model.

Table 4.2. Assumed Blue Fractions

z	F_b (M < M*)
(1)	(2)
0.15	0.05
0.25	0.15
0.33	0.20
0.44	0.25
0.55	0.30
0.65	0.40
0.76	0.50
0.82	0.50
1.01	0.60
1.21	0.60

tion in clusters is evolving with redshift and that it can be classified into three types. The first mode of star formation is "weak" and best describes the lowest redshift clusters ($z < 0.15$) which are consistent with the colors of an almost exclusively quiescent population in all IRAC bandpasses. This result is consistent with numerous studies of nearby clusters using spectroscopy which show very few star forming galaxies (e.g., Dressler et al. 1985, Popesso et al. 2007; Christlein & Zabludoff 2005; Rines et al. 2005).

Between $0.2 < z < 0.5$ the [$8.0\mu m$] LFs are no longer well-described by the purely quiescent model and the regular+quiescent model is the best model. This shows that the majority of star formation in clusters at this epoch is primarily relegated to galaxies that have mid-IR colors similar to local late-type star forming galaxies (i.e., the Sbc model). This has direct implications for the SFRs of these galaxies because Wu et al. (2005) showed that the dust-obscured SFR of galaxies is proportional to their [$8.0\mu m$] flux. Although other authors have demonstrated that there are caveats when using the [$8.0\mu m$] flux to infer SFRs (i.e., the scatter can be as high as a factor of 20-30, Dale et al. 2005), this still implies that the average SFR or the average SFR per unit stellar mass (the average specific star formation rate, SSFR) of star forming cluster galaxies at $0.2 < z < 0.5$ is similar to those in the local universe (because they have [$3.6\mu m$]-[$8.0\mu m$] colors similar to local Sbc galaxies). This second mode of star formation in clusters is roughly what would be considered "regular" star formation for galaxies in the local universe.

At $z > 0.5$ the starburst+regular+quiescent model becomes the best description of the LFs. Again, assuming that [$8.0\mu m$] flux is an indicator of SFR, the M82 starburst model is approximately a factor 2.5 brighter at [$8.0\mu m$] than the regular Sbc model for the same [$3.6\mu m$] flux. Given that our model suggests that regular star forming galaxies make up $\sim$ 30-40% of the cluster population at this redshift and M82 galaxies make up $\sim$ 15-20%, this implies that not only is the *abundance* of star forming galaxies in clusters higher at higher redshift (i.e., the Butcher-Oemler Effect), but also the average SSFR of cluster galaxies is approximately a factor of 1.5 higher at $z > 0.5$ than it is at $z < 0.5$. This increase in SSFR suggests a third mode of star formation in cluster galaxies that could be considered a "burst" mode, at least relative to local star formation rates. Interestingly, this increase in the SSFR of cluster galaxies at higher redshift is consistent with field studies of the universal star formation density (ρ_*) which show an increase of roughly a factor of 2-5 between $z = 0.2$ and $z = 0.5$ (e.g., Lilly et al. 1996; Madau et al. 1996; Wilson et al. 2002; Schiminovich et al. 2005; Le Floc'h et al. 2005). It suggests that the increasing fraction of the cluster dusty starburst population could be

interpreted as the result of an increase in the universal SSFR of galaxies with redshift and the constant accretion of these galaxies into clusters and is not necessarily because starbursts are triggered by the cluster environment. Furthermore, these galaxies might only be considered "starbursts" relative to the mean SSFR locally, whereas at higher redshift their higher SSFR is simply typical of galaxies at that redshift. We compare the cluster [$5.8\mu m$] and [$8.0\mu m$] LFs to the field LFs in §6.2 and discuss this further in that section.

It is interesting that the cluster star forming population transitions from being best described by regular star forming galaxies to regular and dusty starburst galaxies around a redshift of $z \sim 0.4$. This is notable because of the discrepant abundances of k+a and a+k post-starburst galaxies found in clusters by the MORPHS (Dressler et al. 1999) and CNOC1 (Balogh et al. 1999) projects. Dressler et al. (1999) found that approximately 18% of cluster galaxy spectra could be classified as k+a galaxies based on the equivalent width of the Hδ line, whereas Balogh et al. (1999) found that only 2% of the cluster population could be classified this way. These results obviously lead to very different interpretations of the role of starbursts in the evolution of cluster galaxies. In particular, Dressler et al. found that the number of k+a galaxies was an order of magnitude higher in clusters than the coeval field, suggesting a cluster-related process to the creation of these galaxies, while Balogh et al. found roughly equal numbers, suggesting no environmental role.

Although both Dressler et al. (2004) and Balogh et al. (1999) have pointed out that the different methods of data analysis may be partly responsible for such discrepant results, this study suggests that the slightly different redshift range of the MORPHS and CNOC1 sample may also play some role. Excluding the two highest redshift clusters in the CNOC1 sample (MS 0451-03 and MS 0016+16, both at $z \sim 0.55$) the mean redshift of the other 14/16 (88%) clusters in the sample is $z = 0.28$. By contrast, the mean redshift of the MORPHS sample is $z = 0.46$. Our [$8.0\mu m$] cluster LFs seem to indicate that $z \sim 0.4$ represents a transition redshift above which the dominant mode of star formation in clusters is better described as starburst, as opposed to regular. Given that once star formation ceases, the typical lifetime of the A star component of a starburst galaxy's spectrum is ~ 1.5 Gyr, and that the lookback time between $z = 0.46$ and $z = 0.28$ is also 1.5 Gyr, it is possible that both dusty starbursts, and k+a galaxies that are in clusters at $z = 0.46$ may have evolved to quiescent "k"-type galaxies by $z \sim 0.28$, provided that the dusty star formation is immediately truncated. This would be consistent with the change in the [$8.0\mu m$] LFs around this redshift and may explain why

the MORPHS and CNOC1 samples show very different abundances of post-starburst galaxies. Furthermore, 1.5 Gyr prior to $z = 0.46$ is $z \sim 0.65$. Our $z = 0.65$ cluster LF has the largest abundance of dusty starburst galaxies, and if a significant fraction of these had their star formation truncated, these would be logical progenitors to the large population of k+a galaxies seen at $z = 0.46$ by Dressler et al. (1999).

Our results, which show an increase in the strength of the dominant mode of star formation in cluster galaxies (from quiescent to normal to starburst), as well as an overall increase in the abundance of dusty star forming galaxies are also consistent with mid-IR observations of other clusters at these redshift ranges. In particular, Marcillac et al. (2007), Geach et al. (2006) and Coia et al. (2005) have shown that clusters at higher redshifts have significantly more mid-IR sources than clusters at lower-redshift, and that these sources are typically brighter than the sources in lower-redshift clusters. Taken at face value, our results and their results show the equivalent of a Butcher-Oemler Effect in the mid-IR where both the fraction, and SSFR of star forming galaxies is increasing with increasing redshift. Whether this increase is caused by the increase in the universal SFR with redshift, and the constant infall of such galaxies into the cluster environment, or by the triggering of starbursts by the high-redshift cluster environment is still uncertain. We investigate this point further in §6.2 by comparing the cluster and field IRAC LFs.

4.7.2 Is the Cluster Population Different From the Field Population?

The most obvious way to understand if the cluster environment is responsible for triggering starburst events is to directly compare the field and cluster [$5.8\mu m$] or [$8.0\mu m$] LFs and look for an excess of galaxies in the cluster LFs. For this comparison we use the field LFs measured by Babbedge et al. (2006, hereafter B06). Their LFs are determined using photometric redshifts of $\sim 100\,000$ galaxies from a 6.5 deg^2 patch of the SWIRE survey. The field LFs are measured in 5 redshift bins, and we compare the cluster LFs to the three bins which overlap the redshift range of the clusters ($0.0 < z < 0.25$, $0.25 < z < 0.50$, and $0.5 < z < 1.0$). The corresponding cluster LFs used for comparison are the $z = 0.15$, $z = 0.33$, and $z = 0.65$ LFs respectively.

The B06 field LFs are determined using total luminosities, not apparent magnitudes like for the cluster LFs. Converting the units of the cluster LFs to total luminosities requires distance moduli and full k-corrections. In §5.2.2 we showed that the cluster LFs can be well-described using three basic populations of galaxies: quiescent,
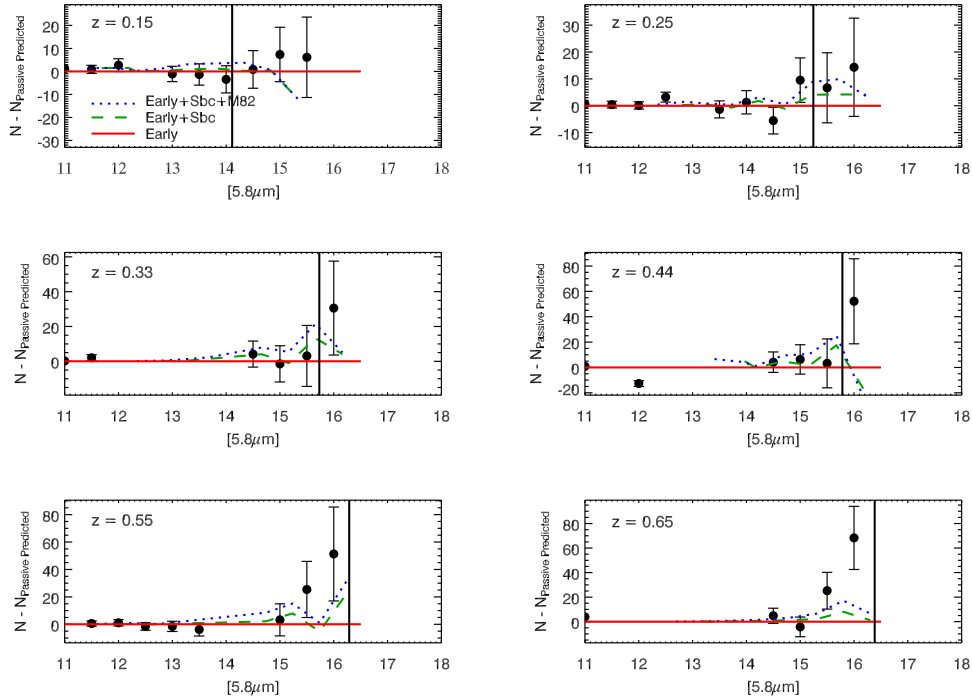
Figure 4.17 Residuals of the cluster $[5.8\mu m]$ LFs once the predictions from the $[3.6\mu m]$ LFs and the passive evolution model have been subtracted. The solid red line shows the passive evolution model, the dashed green line shows the regular+quiescent model and the dotted blue line shows the starburst+regular+quiescent model. The solid vertical line represents the location of M^* from the $[3.6\mu m]$ LFs assuming the $[3.6\mu m]$ - $[5.8\mu m]$ color of the passive evolution model.

regular star forming, and dusty starburst. We use the models of these three spectral types for the k-corrections. The k-corrections for the quiescent galaxies are taken from the single-burst model and the k-corrections for the regular and dusty starburst galaxies are taken from the Huang et al. (2007b) Sbc and M82 models respectively. Each LF is statistically k-corrected using the relative proportions of the galaxies which best described the LFs in §5.2.2. The apparent LF for each redshift is divided into the three components by the fraction of galaxies of that type and are individually k-corrected and shifted by the distance modulus. These LFs are then summed to provide the total cluster LF in terms of absolute luminosities in units of $\nu L_\nu / L_\odot$.

The cluster LFs are normalized by the number of galaxies per virial volume, whereas the field LFs are normalized by their actual number density per Mpc^3. The cluster normalization can be put in the same units as the field LFs by dividing by the virial volume; however, this does not provide a fair comparison because clusters have much
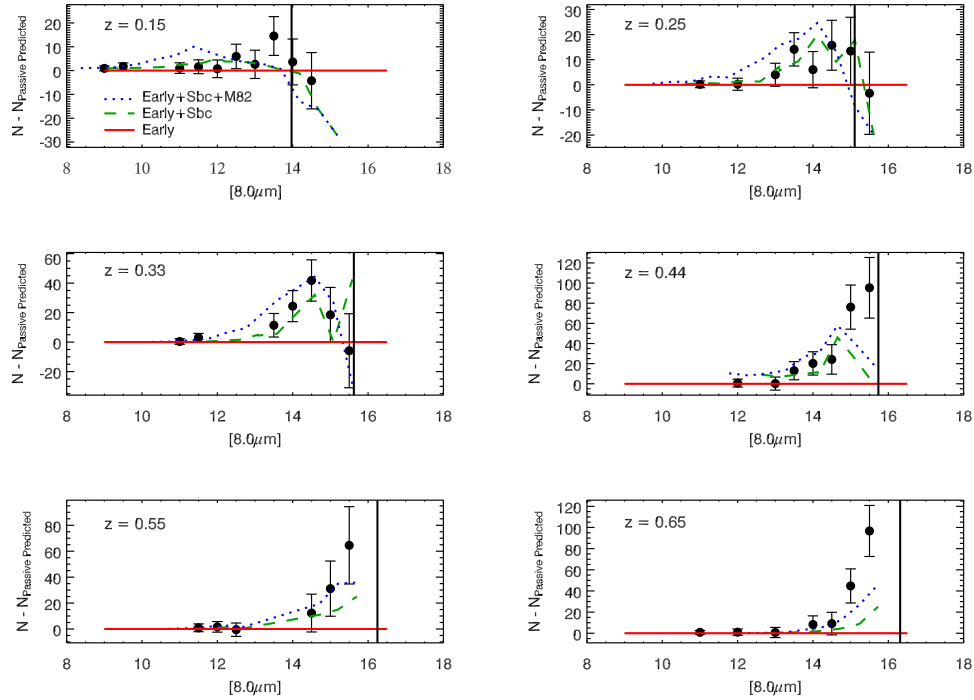
Figure 4.18 Same as Figure 17 but for the [8.0μm] LFs.

higher volume densities of galaxies than the field. The most useful way to compare the cluster and field LFs is on a per unit stellar mass basis. We do not have stellar mass functions for either the field or cluster; however, we can again assume that the [3.6μm] luminosity is roughly a proxy for stellar mass and renormalize the LFs to a common normalization so that they reproduce the same ϕ^* in the Schechter function fits. The renormalized [3.6μm], [4.5μm], [5.8μm], and [8.0μm] cluster LFs are plotted in Figures 19, 20, 21, and 22, respectively as the filled red circles. The field LFs are overplotted as blue squares.

Figures 19 and 20 show that the overall shape of the cluster and field [3.6μm] and [4.5μm] LFs are similar at all redshifts. There is a slight, though not statistically significant, excess in the number of the brightest galaxies in the cluster LFs; however, these are likely to be giant elliptical galaxies which are common in clusters and typically do not follow the distribution of the Schechter function. Other than the giant ellipticals, the shape of the [3.6μm] and [4.5μm] cluster and field LFs are similar which shows that the distribution of galaxies as a function of stellar mass is nearly identical in these environments. This result is consistent with K-band studies which have shown only small differences in M* (< 0.2 mag) between these environments (e.g., Balogh et al. 2001; Lin et al. 2004; Rines et al. 2004; Muzzin et al. 2007a).

Conversely, there are significant differences in the [5.8μm] and [8.0μm] LFs of the cluster and field. Both the [5.8μm] and [8.0μm] LFs follow a sequence where the cluster LF is more abundant in mid-IR galaxies at $z = 0.65$, particularly moderate-luminosity galaxies, and thereafter the abundance of mid-IR galaxies in clusters declines relative to the field with decreasing redshift. At $z = 0.33$, the cluster is slightly deficient in both [5.8μm] and [8.0μm] galaxies relative the field, reduced by a factor of ~ 2 for galaxies with $\nu L_\nu = 5$ x 10^9 - 5 x 10^{10} L$_\odot$. At $z = 0.15$, the cluster LF is significantly depleted compared to the field, reduced by a factor of ~ 5 for galaxies with $\nu L_\nu = 5$ x 10^8 - 5 x 10^{10} L$_\odot$. This suggests that environment does play some role in the evolution of dusty starburst galaxies, but it appears that the environmental effects evolve with redshift.

It is not entirely obvious why starbursts should prefer the cluster environment over the field environment at high ($z > 0.5$) redshift and then reject it at lower redshift ($z <$ 0.5). We suggest that starbursts could preferentially be triggered during the initial formation and collapse of the cluster, and be quenched thereafter by the high-density environment. If this interpretation is correct, it is likely that the parameter most responsible for the change in star formation properties relative to the field is the degree of virialization of the clusters.

Clusters that are unrelaxed, or in the process of collapsing, have two properties that would permit increased numbers of dusty starbursts. Firstly, before virialization, the cluster gas has not yet been shock-heated to its maximum temperature. This hot intracluster gas has long been considered the primary cause for the quenching of star formation in cluster galaxies because it prevents the cooling of gas in the outer halo of a galaxy, thereby "strangling" star formation. Depending on the density/temperature threshold required for quenching, it is possible that starbursts that would normally be quenched in virialized clusters at lower redshifts may survive longer in unvirialized clusters at high redshift. Secondly, the velocity dispersions in unrelaxed systems are lower and therefore mergers and harassments should be more common at higher redshift (e.g., Tran et al. 2005b). It is plausible that this more dynamically "active" environment preferentially triggers star formation. The combination of more triggered dusty starbursts through harassment and mergers as well as a weaker quenching process may be the reason for more dusty starbursts in clusters relative to the field at higher redshift. Once a cluster becomes virialized the interactions between galaxies should become less frequent and the quenching of star formation by the hot cluster gas will be more efficient. In such a scenario the relative abundances of dusty starbursts in clusters should decrease relative to the field.
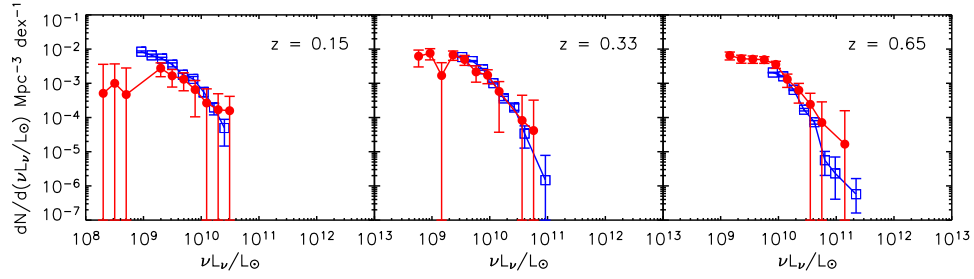
Figure 4.19 Comparison between the cluster and field [3.6μm] LFs at different redshifts. The field LFs are plotted as open blue squares and the cluster LFs are plotted as filled red circles. The cluster LFs are renormalized so that the values of ϕ^* from the Schechter function fits (§5.1) match the ϕ^* values from the Schechter function fits in B06.
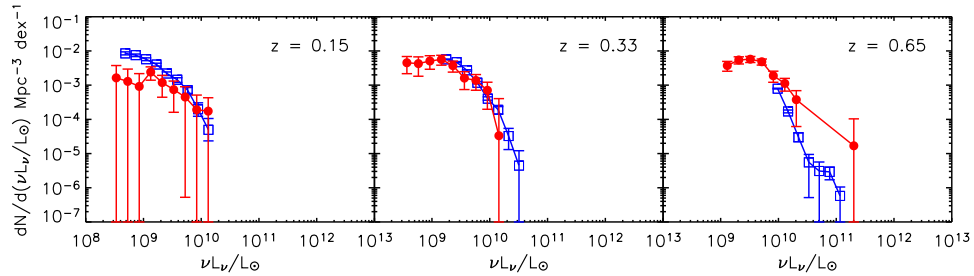
Figure 4.20 Same as Figure 19 but for the [4.5μm] LFs.

If our interpretation is correct we might expect different results from the [8.0μm] LFs of X-ray selected samples of clusters (i.e., those which require a hot virialized cluster gas component) compared to red-sequence selected samples, which, assuming the early-type population is formed prior to cluster collapse, do not require that clusters are fully virialized.
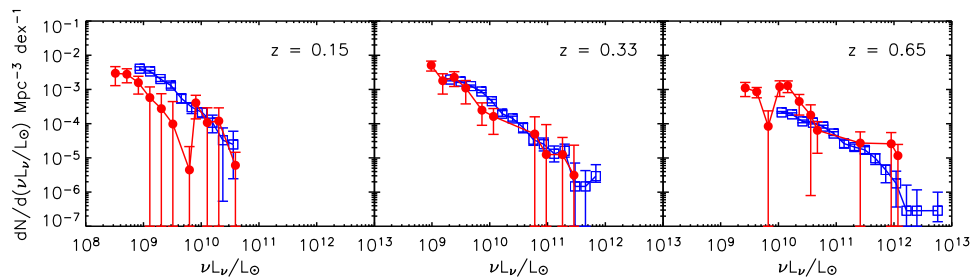
Figure 4.21 Same as Figure 19 but for the [5.8μm] LFs.
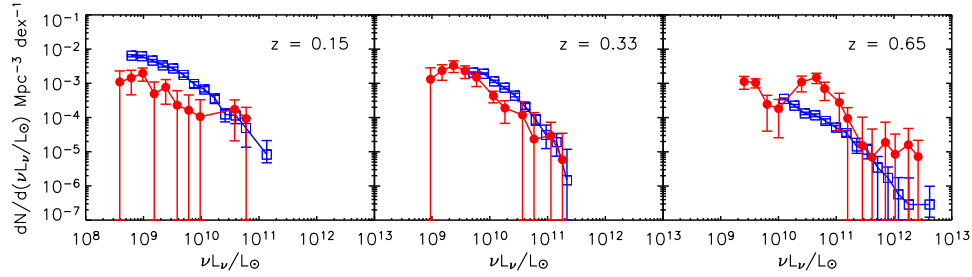
Figure 4.22 Same as Figure 19 but for the [$8.0\mu m$] LFs.

4.7.3 Are the Color Models Correct?

The main conclusions from the cluster LFs presented in this paper depend on interpreting color models that have been primarily calibrated or determined using nearby galaxies. If these models are not applicable at higher redshift then this could cause incorrect conclusions to be drawn from the LFs. Using the spectroscopic redshifts we can examine the colors of confirmed cluster galaxies as a function of redshift to see if the models are reasonable.

There are 55 spectroscopic redshifts available for cluster galaxies (see §2.4 & §2.5). Using the spectra we can classify these galaxies into two basic types, star forming and non-star forming. For the Hectospec, SDSS, and WIYN spectroscopy the best-fitting cross-correlation template is used for the classification. For the remaining galaxies the classification is made by eye-examining the spectra for any evidence of the [OII], [OIII], or Hα emission lines. Galaxies with any of these emission lines are classified as star forming, and those without are classified as non-star forming. Although this is a crude approach to classifying galaxies, we are only interested in a rough classification and taking a more quantitative approach, such as measuring EWs, is unnecessary. Furthermore, in all cases the cluster galaxies had spectra that were very typical of either normal star forming (several emission lines including [OII] and Hα) or quiescent galaxies (strong H and K lines and a 4000Å break), and classification was straightforward. There were no hybrid objects associated with clusters except two AGN from the Hectospec data.

In Figure 23 we plot several of the colors of these galaxies as a function of redshift. Star forming galaxies are plotted as blue points and non-star forming galaxies are plotted as red points. The Bruzual & Charlot single-burst model is overplotted as the solid line, and the Huang et al. (2007b) Sbc and M82 models are overplotted as the dotted and dash dotted lines, respectively. In general, the non-star forming galax-

ies follow the single-burst model well at all redshifts. There are a handful non-star forming galaxies which appear to have some excess $[8.0\mu m]$ emission, and this may be from either very low-level star formation or a low-luminosity AGN.

There are fewer star forming than non-star forming galaxies in the sample; however, their colors follow the Sbc and M82 models very well. At $[8.0\mu m]$, where the colors of the Sbc and M82 models are most different from the single-burst model, it is clear that galaxies with emission lines have colors similar to those models, whereas those without tend to follow the single-burst model. Half of the star-forming galaxies in Figure 23 (8/16) come from our spectroscopy of FLS J172449+5921.3 (cluster #10, $z = 0.252$). These galaxies were selected for spectroscopy because they were detected at $[24\mu m]$. Interestingly, most of these galaxies (7/8) have a $[3.6\mu m]$ - $[8.0\mu m]$ color similar to the Sbc model, yet they show a wide range in R - $[3.6\mu m]$ color. A few have an R - $[3.6\mu m]$ color bluer than the red-sequence, typical of Sbc galaxies, whereas others have an R - $[3.6\mu m]$ color redder than the red-sequence. This illustrates that there are both "red" and "blue" dusty star forming galaxies in clusters, and that our approach of modeling the $[5.8\mu m]$ and $[8.0\mu m]$ LFs with populations of both is reasonable. Furthermore, the fact that these are some of the brightest mid-IR sources in the cluster field, and that most have colors similar to the Sbc model, rather than the M82 model, is consistent with our conclusion that the $[8.0\mu m]$ LF at this redshift is best modeled using the quiescent+regular model, with no need for a luminous dusty starburst component. We defer a more detailed discussion of the spectroscopy, including quantitative measurements of star formation from line widths to a future paper (Muzzin et al. 2007, in preparation).

Overall, Figure 23 demonstrates that the galaxy templates used to model the cluster LFs agree well with the colors of spectroscopically confirmed cluster galaxies, and that they are reasonable descriptions of star forming and non-star forming galaxies between $0 < z < 1$.

4.7.4 Systematic Uncertainties

The data presented in this paper support a self-consistent model of the evolution of stellar mass assembly and dusty star formation in clusters; however, there are several details of this analysis that have not been discussed and could potentially result in inappropriate conclusions being drawn from the data. Although it is difficult to quantify what effect, if any, these details will have on the interpretation of the data,
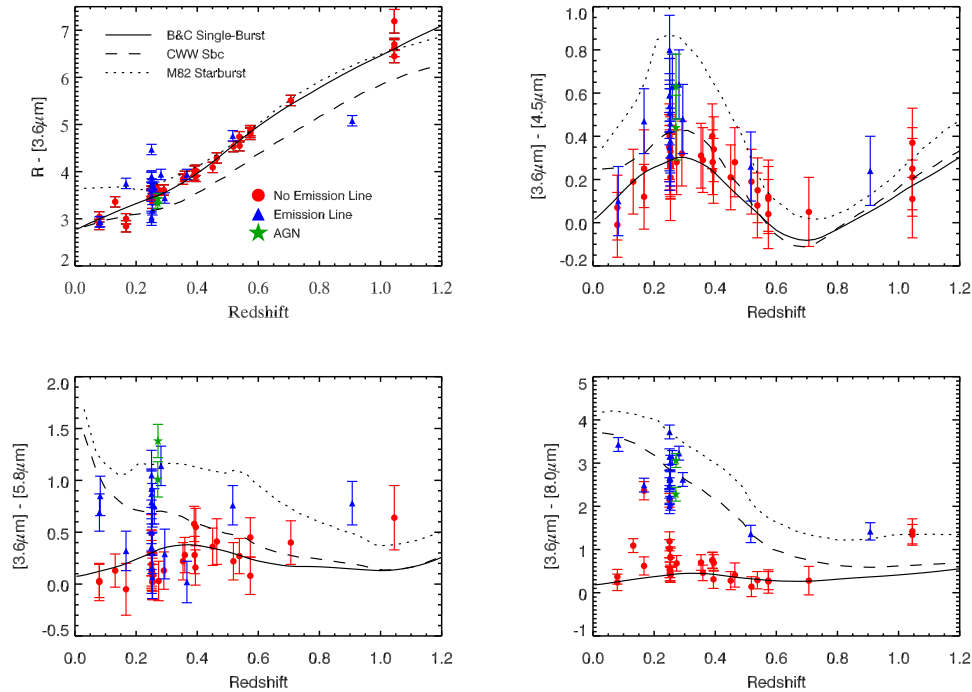
Figure 4.23 Plot of optical - IRAC or IRAC - IRAC colors of galaxies as a function of redshift. The red, blue, and green points are spectroscopic cluster members classified as non-star forming, star forming, and AGN respectively. The solid, dotted, and dashed lines are the model colors from the passive evolution model, the Sbc model, and the M82 model respectively.

we believe it is important to at least note these issues here.

One worthwhile concern is the sample of clusters used in the analysis. Although this sample is much larger than the mere handful of clusters that have been studied in the mid-IR thus far, it is still of modest size and subject to cosmic variance. In particular, given that the clusters come from only 3.8 $\deg^2$, it is unclear whether the higher redshift clusters in the sample are truly the progenitors of the lower redshift clusters. Unfortunately, a cosmologically significant sample of clusters covering of the order 100 degree^2 or more is likely needed to avoid biases that might result from cosmic variance in the sample.

Another potential problem is that there are many more low richness clusters in the sample than high richness clusters, simply because of the nature of the cluster mass function. Any effects that depend on cluster mass will clearly be missed by combining these samples. This could be important because processes that could quench star formation (e.g., ram-pressure stripping, gas strangulation) or incite starbursts (tidal

effects, harassment) will likely depend on cluster mass. Using a much larger sample which can be separated by both mass and redshift would be invaluable for studying this issue further.

Perhaps the most important concern is that there is a degeneracy between the *mode* of star formation in clusters and the fraction of star forming galaxies. We showed in §6.3 that the color models used for the clusters galaxies reproduce the colors of cluster galaxies with spectroscopic redshifts very well; however, even though these colors are correct, the models of the [$5.8\mu m$] and [$8.0\mu m$] LFs still depend on the assumed f_b as a function of magnitude and redshift for the clusters. If the f_b values are overestimated and need to be reduced, then a larger fraction of dusty starburst galaxies than we have assumed will be required to correctly model the cluster [$5.8\mu m$] and [$8.0\mu m$] LFs. Likewise, if the f_b is underestimated, fewer dusty starbursts will be required. The assumed f_b are consistent with most previous studies; however, optimally, if more data were available the f_b should be calculated from the clusters themselves and this would avoid this degeneracy.

Lastly, it is worth mentioning that much of the excess seen in the [$8.0\mu m$] LFs is near the limiting magnitude of the survey. Problems with the background estimation could artificially inflate these values. It is unlikely that this is the case because if the excess of galaxies near the faint limit of the survey were due to an undersubtraction of the background, it should also be seen in the lower redshift LFs, which it is not. Furthermore, undersubtraction of the background should be even more prevalent in the lower redshift LFs because clusters have much larger angular sizes and therefore more total area from which to undersubtract the background. It is unlikely that this is a problem; however, deeper data would be very useful in ensuring there are no errors due to completeness near the survey limit.

4.8 Conclusions

We have presented a catalogue of 99 clusters and groups at $0.1 < z < 1.3$ discovered in the *Spitzer* First Look Survey using the cluster red-sequence technique. Using spectroscopic redshifts from FLS followup campaigns and our own spectroscopic followup of clusters we have shown that the R - [$3.6\mu m$] color of the cluster red-sequence is an accurate photometric redshift estimator at the $\Delta z = 0.04$ level at $z < 1.0$. Furthermore, we demonstrated that the properties of the FLS cluster catalogue are similar to pre-

vious cluster surveys such as the RCS-1. Using this cluster sample we studied the evolution of the cluster [3.6μm], [4.5μm], [5.8μm], and [8.0μm] LFs. The main results from these LFs can be summarized as follows:

- In agreement with previous work, the evolution of the [3.6μm] and [4.5μm] LFs between $0.1 < z < 1.0$ is consistent with a passively evolving population of galaxies formed in a single-burst at $z > 1.5$. Given that the [3.6μm] and [4.5μm] bandpasses are reasonable proxies for stellar mass, this suggests that the majority of stellar mass in clusters is already assembled into massive galaxies by $z \sim 1$.

- The cluster [5.8μm] and [8.0μm] LFs do not look similar to the [3.6μm] and [4.5μm] LFs, and this is due to the presence of the cluster star forming galaxies. Star forming galaxies are much brighter in these bandpasses than early-type galaxies and their varying fractions with redshift cause deviations from the shape of the [3.6μm] and [4.5μm] LFs. The [5.8μm] and [8.0μm] LFs are well-described using different fractions of three basic types of galaxies: quiescent, regular star forming, and dusty starburst by assuming that the fractions of the latter two are proportional to the cluster f_b.

- The [8.0μm] cluster LFs suggest that both the frequency and SSFR of star forming cluster galaxies is increasing with increasing redshift. In particular it appears that the dominant "mode" of star formation in clusters evolves from "quiescent" to "regular" to "starburst" with increasing redshift. Qualitatively, this evolution mimics the evolution in the universal star formation density with redshift suggesting that this evolution is at least in part caused by the accretion of star forming galaxies into the cluster environment.

- Comparing the [3.6μm] and [4.5μm] cluster and field LFs with similar normalization shows that the LFs in these environments are similar, with evidence for a small excess in the brightest galaxies in clusters, likely caused by the cluster giant ellipticals. In agreement with previous K-band studies this suggests that the distribution of galaxies as a function of stellar mass in both environments is roughly equivalent.

- There is a significant differential evolution in the cluster and field [5.8μm] and [8.0μm] LFs with redshift. At $z = 0.65$ the cluster is more abundant in [8.0μm]

galaxies than the field; however, thereafter the relative number of [5.8μm] and [8.0μm] galaxies declines in clusters with decreasing redshift and by $z = 0.15$ the cluster is underdense in these sources by roughly a factor of 5. This differential evolution could be explained if starbursts are preferentially triggered during the early formation stages of the cluster but then preferentially quenched thereafter by the high density environment.

A well-sampled spectroscopic study of several high-redshift clusters with mid-IR data would be extremely valuable for verifying our interpretation of the IRAC cluster LFs because it is always difficult to draw incontrovertible conclusions from LFs alone. Still, the cluster LFs do show a strong increase in the number of [5.8μm] and [8.0μm] sources in clusters with increasing redshift which must almost certainly be attributed to increased amounts of dusty star formation in higher redshift clusters.

One of the strengths of this analysis is that it is based on a relatively large sample of galaxy clusters. It has become clear from the handful of clusters studied thus far by *ISO* and *Spitzer* that the mid-IR properties of cluster galaxies can be quite different from cluster to cluster. They may depend on dynamical state, mass, f_b, or other parameters (e.g., Coia et al. 2005; Geach et al. 2006). The advantage of using many clusters is that it provides a metric of how the "average" cluster is evolving as a function of redshift. Detailed studies of individual clusters with significant ancillary data will pave the way to a better understanding of the physics behind the evolution of dusty star formation in cluster galaxies; however, large statistical studies such as this one will indicate whether the clusters studied in future work are representative of the cluster population as a whole, or are potentially rare, biased clusters with unusual properties caused by an ongoing merger or some other event.

It is worth noting that although the quality of the LFs provided by the 99 clusters in the FLS is good, these LFs would still benefit from a larger statistical sample. In particular, a larger sample would allow for the separation of clusters by other properties such as mass or morphology, and to understand if these properties play a role in shaping the mid-IR cluster galaxy population. We are currently working on a survey to detect clusters in the much larger SWIRE survey: the Spitzer Adaptation of the Red-sequence Cluster Survey (SpARCS). This project has 13 times more area than the FLS and is a factor of 2 deeper in integration time in the IRAC bands. The analysis of that sample should provide a significant improvement in the quality of the cluster LFs.

Acknowledgements

Chapter 5

The Nature and Evolution of Mid-IR Cluster Galaxies

To be submitted as:

"The Nature and Evolution of Mid-IR Cluster Galaxies"

Muzzin, A., Wilson, G., Yee, H.K.C. Lacy, M., & Surace, J., 2007, ApJ, in preparation

5.1   Abstract

We present a spectroscopic study of cluster galaxies detected at [$24\mu m$] in four clusters
in the *Spitzer* First Look Survey at $0.12 < z < 0.26$. There are 177 spectra for galaxies in
the fields of these clusters, of which 117 are [$24\mu m$] sources, 42 are cluster galaxies, and
21 are [$24\mu m$] cluster galaxies. All of the [$24\mu m$] galaxies have at least one emission
line in their spectra and we use line ratios to classify them as either AGN/LINERs or
star forming galaxies. The classification shows the majority of cluster [$24\mu m$] galaxies
($\sim 80\%$) are associated with star forming galaxies, but that their specific types make
them a very heterogeneous subset of galaxies. In general, the brightest [$24\mu m$] clus-
ter galaxies are a mix of starbursts, regular star forming galaxies, and AGN/LINERs,
while lower-luminosity sources are almost exclusively regular star forming galaxies.
Within the total sample, 5% are AGN, 14% are LINERs, 33% are starbursts, and 43%
are regular star forming galaxies. One of the LINERs is clearly the result of a ma-
jor merger near the core of one of the clusters. In the Dressler & Gunn classification
scheme the majority of cluster MIPS galaxies are classified as e(c) galaxies (57%), while
only 10% are classified as e(a) galaxies. Approximately 25% of the [$24\mu m$] cluster

galaxies are classified as k or k+a galaxies based on their [OII] and Hδ EWs; however, these galaxies have Hα in emission, suggesting that they are in fact dusty star forming galaxies misclassified because of dust attenuation of the [OII]-line. The [24μm] sources show a wide range of R - [3.6μm] colors with 25% of the galaxies having colors bluer than the cluster red-sequence, 25% having colors similar to the red-sequence and 50% being redder than the red-sequence. Comparison of the EW([OII])/EW(Hα + [NII]) ratios suggests that the red cluster galaxies are very dusty star forming galaxies and demonstrates that cluster blue fractions provide an incomplete census of the cluster star forming population. Lastly, we use the entire sample of 99 clusters in the FLS to statistically measure the evolution of LIRG and ULIRG-like galaxies in clusters. We find that the number of LIRGs in clusters increases by at least a factor ~ 3 from $z = 0.2$ to $z = 0.3$ at >68% confidence level. ULIRGs are extremely rare in clusters and show no significant increase out to $z = 0.5$. Both these results agree well with the number of LIRGs and ULIRGs predicted from the [8μm] counts in the same clusters. Comparison with field studies shows that the increasing fraction of LIRGs and ULIRGS in clusters may be slightly more rapid than the corresponding increase in the field; however, the uncertainties in this measurement are quite large.

5.2   Introduction

Recent advances in mid-infrared (mid-IR) imaging capabilities from satellites such as *ISO* and *Spitzer* as well as submillimeter observations from SCUBA have led to a revolution in our understanding of galaxy formation and evolution. Studies of field galaxies have shown a two orders of magnitude increase in the average luminosity of mid-IR luminous galaxies with increasing redshift (e.g., Franceschini et al. 2001; Elbaz et al. 2002; Blain et al. 2002; Chapman et al. 2003; Pérez-González et al. 2005; Le Floc'h et al. 2005). Luminous Infrared Galaxies[1] (LIRGs; $L_{IR} > 10^{11}$ $L_{\odot}$), which are rare in the local universe (e.g., Soifer et al. 1987; Sanders et al. 1988) appear to be the major source of the IR luminosity density of galaxies from $z \sim 0.5$ - 1.0 (Pérez-González et al. 2005; Le Floc'h et al. 2005; Huynh et al. 2007). Given that the bulk of the mid-IR emission from these galaxies is expected to come from dusty star forming regions, this shows that the fraction of dust-obscured star formation in the universe is increasing with increasing redshift (e.g., Takeuchi et al. 2005; Papovich et al. 2006a). At $z >$

---

[1]L_{IR} is defined as the integrated IR luminosity of a galaxy between 8 - 1000 μm.

2.0, it is expected that dusty star formation becomes even more vigorous and that the dominant contribution to the IR luminosity density of the universe moves from LIRGs to Ultra Luminous Infrared Galaxies (ULIRGs; $L_{IR} > 10^{12}$ $L_\odot$, e.g., Pérez-González et al. 2005). This remarkable evolution in the fraction of dust-obscured star formation suggests the possibility that we may be missing an increasing fraction of the universal star formation density as a function of redshift in UV-selected samples such as Lyman-break galaxies (e.g., Steidel et al. 1999; Giavalisco et al. 2004a).

Thus far, the majority of our understanding of the evolution of LIRGs and ULIRGs has come from studies of field galaxies in narrow pencil-beam surveys. One question that has not been well-addressed by these data is the role of environment in the evolution of these galaxies. Perhaps the most relevant question with respect to environment is, do high density regions such as galaxy clusters trigger the formation of LIRGs or ULIRGs from mergers, harassment or tidal interactions, or instead do they quench dusty star formation in these galaxies? Early $15\mu m$ *ISO* observations of a few clusters showed that LIRGS are rare in clusters at z < 0.2 (Fadda et al. 2000; Duc et al. 2002; Biviano et al. 2004). Although possibly biased by the fact that these observations were concentrated in the cores of massive, strong-lensing, X-ray luminous galaxy clusters where star formation is usually strongly suppressed, this result is consistent with field studies that also show very few LIRGs at z < 0.2 (e.g., Franceschini et al. 2001; Elbaz et al. 2002; Pérez-González et al. 2005; Le Floc'h et al. 2005). More recent observations from *Spitzer* and *ISO* of higher redshift clusters have suggested that the frequency of LIRGs increases in clusters out to $z \sim 0.8$ (Coia et al. 2005; Geach et al. 2006; Marcillac et al. 2007; Bai et al. 2007), which is qualitatively in agreement with the evolution of LIRGs in the field.

In an earlier paper (Muzzin et al. 2007c; hereafter M07) we examined the [$3.6\mu m$], [$4.5\mu m$], [$5.8\mu m$] and [$8.0\mu m$] IRAC luminosity functions (LFs) of 99 clusters at 0.1 < z < 1.3 in an attempt to better understand the evolution of dusty star formation in the cluster environment. The clusters in that sample were selected by the cluster red-sequence technique (Gladders & Yee 2000) in the 3.8 deg² *Spitzer* First Look Survey (FLS). We modeled the amount of dusty star formation in clusters as a function of redshift using the LFs of the [$5.8\mu m$] and [$8.0\mu m$] IRAC bandpasses because those bandpasses are sensitive to warm dust continuum and Polycyclic Aromatic Hydrocarbon (PAH) emission at z < 0.6, both of which are tracers of dusty star forming regions. The [$3.6\mu m$] and [$4.5\mu m$] LFs were crucial to that analysis because they are good proxies for the stellar mass of galaxies and allowed us to model the non-negligible contri-

bution from stellar emission in the [5.8μm] and [8.0μm] LFs.

The [8.0μm] cluster LFs showed a marked increase in the number of sources with increasing redshift; however, using the cluster blue fraction (f_b) as an estimate of the number of star forming galaxies we showed that the increase in [8.0μm] sources at $z < 0.4$ could be accounted for by the well-known increase in the number of regular star forming cluster spirals (the Butcher-Oemler Effect, e.g., Butcher & Oemler 1984; Ellingson et al. 2001) and that there was no evidence for a significant population of obscured dusty starbursts in clusters. At $z > 0.4$ we showed that the cluster [8.0μm] population increases faster than predicted from the f_b alone, which suggests that a population of dust-obscured starbursts (i.e., those missed in the measurement of f_b) exist in clusters at $z > 0.4$. Interestingly, this is also the redshift range where dust-obscured starbursts start to become more prevalent in the field (Pérez-González et al. 2005; Le Floc'h et al. 2005).

Clearly some fraction of the cluster [8.0μm] population has to be attributed to AGN activity; however, X-ray luminous AGN are rare in clusters at z < 0.6 ($< 3\%$ of the population; e.g., Branchesi et al 2007; Eastman et al. 2007), whereas star forming galaxies can be as much as 50% of the population (e.g., Butcher & Oemler 1984; Dressler et al. 1999; Ellingson et al. 2001), therefore we argued that the majority of excess cluster [8.0μm] sources are likely to be dusty star forming galaxies, and not dusty AGN.

Comparison to the field LFs of Babbedge et al. (2006) showed that clusters are actually more abundant in [8.0μm] galaxies per unit stellar mass than the field at $z > 0.6$, but thereafter the number of sources in clusters rapidly decreases with decreasing redshift and by z ~ 0.15 is approximately a factor of 5 lower than the field. This shows that dusty starbursts may actually *prefer* the high-density cluster environment at higher redshift, but the rapid decrease thereafter suggests that environmental processes may be responsible for quenching these events.

The major complication in the interpretation of the M07 LFs is that [8.0μm] data is not a completely "clean" tracer of dusty star formation because there is still some flux from stellar continuum in that bandpass. Furthermore, at higher redshift ($z > 0.5$) the [8.0μm] bandpasses moves from probing the rest-frame region of a galaxy's spectrum that is dominated by dust and PAHs towards the region dominated by stellar emission, which makes it increasingly harder to attribute the [8.0μm] flux ($F_{8.0}$) to ongoing star formation. In an attempt to account for these issues we used the cluster [3.6μm] LFs and combinations of stellar population models to account for the stellar component in the [8.0μm] LFs. A caveat with the M07 results is that the modeling

depends on assuming that local star forming galaxies are a good representation of star forming galaxies at higher redshift. While this has been demonstrated to be a reasonable assumption by other authors (e.g., Elbaz et al. 2002; Appleton et al. 2004), it is preferable to have as model-independent result as possible. One way to avoid modeling the stellar component of the mid-IR LFs is to observe clusters at longer mid-IR bandpasses such as the $[24\mu m]$ channel of Multiband Imaging Photometer (MIPS) onboard *Spitzer*. Although less sensitive than the IRAC $[8.0\mu m]$ channel, the $[24\mu m]$ bandpass is a much "cleaner" measure of the total amount of dusty star formation or AGN activity because the stellar continuum in this bandpass is negligible until $z \sim 3$. The FLS field was also observed at MIPS $[24\mu m]$ and in this paper we use those data, as well as a large set of spectroscopic redshifts in the fields of 4 clusters, to examine in more detail some of the assumptions made in M07, as well as their conclusions.

The interpretation of the M07 LFs depends mostly on the assumed nature of the cluster $[8.0\mu m]$ galaxies. Namely that 1) they are primarily star forming galaxies, and not AGN, and 2) that some portion of the cluster galaxies are very red, star forming galaxies and that the number of these is roughly proportional to the number of blue star forming galaxies.

We have obtained good-quality optical spectra for 21 cluster $[24\mu m]$ galaxies covering the wavelength range from [OII](3727Å) to [SII](6731Å) and using this data we classify these galaxies as either star forming galaxies or AGN, thus addressing assumption 1). We also test assumption 2) by examining the optical colors and nebular emission lines of these galaxies to demonstrate that there is a significant population of dust-obscured star forming galaxies in clusters. Lastly, we examine the evolution of the frequency of $[24\mu m]$ galaxies in clusters and compare this to the predictions from the $[8.0\mu m]$ LFs as well as the field to understand whether the environment of these galaxies is important in their evolution.

The structure of this paper is as follows. In §2 we give a brief overview of the FLS cluster sample, as well as the MIPS $[24\mu m]$ and spectroscopic data used in the paper. Section 3 examines the spatial distribution of the cluster $[24\mu m]$ population. Section 4 contains a discussion of the spectral classification of the $[24\mu m]$ sources and in §5 we present a discussion of the nature of the cluster $[24\mu m]$ population. In §6 we measure the evolution of the frequency of $[24\mu m]$ sources in cluster and compare this to the predictions from the $[8.0\mu m]$ LFs as well as the field. We conclude with a summary in §7. Throughout this paper we assume an $\Omega_m = 0.3$, $\Omega_\Lambda = 0.7$, $H_0 = 70$ km s^{-1} Mpc^{-1} cosmology. All magnitudes are on the Vega system.

5.3   The Data

5.3.1   The FLS Cluster Sample

In M07 we presented a catalogue of 99 clusters and groups of galaxies at $0.1 < z_{phot} <$ 1.3 in the 3.8 deg^2 FLS. Those clusters were discovered by their R - [3.6μm] color magnitude relations using the cluster red-sequence technique of Gladders & Yee (2000). Estimates of the cluster masses (M_{200}) and sizes (R_{200}) were provided in M07 based on the correlation between cluster richness (parameterized by B_{gc}) and these quantities shown by Muzzin et al. (2007b). The scatter in the Muzzin et al. (2007b) correlations suggests that the estimates of M_{200} and R_{200} are probably good to $\pm$ 35% and $\pm$ 12% on average, respectively. Complete details of the cluster finding, catalogues and the mass estimates are discussed in that paper.

We targeted four clusters in the FLS field for followup spectroscopy of red-sequence cluster galaxies and [24μm] galaxies. Those four clusters are FLS J171059+5934.2, FLS J171639+5915.2, FLS J171505+5859.6, and FLS J172449+5921.3 which correspond to clusters 1, 2, 8, and 10 listed in Table 1 of M07, respectively. Hereafter, for simplicity, we refer to these clusters by their M07 numbers. The clusters have spectroscopic redshifts of z = 0.126, 0.129, 0.252, and 0.253, respectively, and hereafter we refer to the two $z \sim 0.125$ clusters as the "low redshift clusters" and the two $z \sim 0.25$ clusters as the "high redshift clusters". Given the small amount of volume covered at these redshifts in a survey the size of the FLS these four clusters are of fairly modest mass, and not necessarily akin to the massive, X-ray luminous clusters that have thus far been studied in the MIR at similar redshift such as Abell 2218 (Biviano et al. 2004) and Abell 1689 (Fadda et al. 2000; Duc et al. 2002). Based on their richnesses, the average mass of the low and high redshift clusters is approximately 2 x 10^{14} M$_\odot$ and 3 x 10^{14} M$_\odot$ respectively.

5.3.2   FLS 24μm Photometry

The [24μm] data used in this study are part of the publically available *Spitzer* First Look Survey. The main field of the FLS [24μm] data covers an area of $\sim$ 5 deg^2 and has an on-sky integration time of 84 s/pixel. A smaller verification strip in the same field with an area of 0.5 deg^2 was observed to an integration time of 426 s/pixel. Given that the verification strip overlaps with only a few clusters in the FLS fields the main field data are used in this study. Complete details of the FLS [24μm] data acquisition,

data reduction, source extraction and photometry are presented in Fadda et al. (2006). Here we only briefly summarize the main points of the photometric catalogues that are relevant to this paper.

Sources were extracted from the fully reduced and calibrated images using the MOPEX software (Makovoz & Marleau 2005). Several steps were taken to avoid false detections from the Airy rings of point sources as well as to identify extended sources. Photometry was performed by PSF-fitting using a PSF that was determined empirically from bright stars within the FLS data. Simulations of the completeness and reliability of the [24μm] photometry were performed by re-inserting fake sources into the data. The simulations demonstrated that the [24μm] photometry is 100% complete at a flux density of $F_{24} \sim 800$ μJy, and is 80% complete to $F_{24} = 350$ μJy. Fadda et al. (2006) showed that while the catalogue completeness drops rapidly below 350 muJy, the number of spurious sources is still very low. The reliability of sources to $F_{24} = 150$ μJy is still $\sim$ 90%. Therefore, we adopt a faint limit of $F_{24} = 350$ μJy for the survey.

5.3.3   FLS R-band Data

The FLS was also observed in the R-band using the MOSAIC camera on the KPNO 4m Mayall Telescope. The R-band data has a 5σ limiting depth of R = 24.5 mag. Full details of the R-band data reduction and catalogues are presented in Fadda et al. (2004). The R-band data were matched with the [24μm] catalogue using a likelihood ratio technique by Fadda et al. (2006). Approximately 80% of [24μm] sources have an R-band counterpart brighter than 24.5 mag. The R-band data are used for star/galaxy classification and we removed [24μm] sources associated with stars from the catalogue.

5.3.4   Palomar Spectroscopy

Multi-object spectroscopy of red-sequence galaxies and [24μm]-detected galaxies in the fields of Clusters 1, 2, 8, and 10 were performed on 26, 27, 28, 29 May 2006 and 15, 16, 17, June 2007 using the COSMIC Spectrograph on the 200$''$ Hale Telescope at the Palomar Observatory. Conditions were good on all nights and seeing ranged between 0.9$''$ - 1.3$''$. The observations were made with the 300 l/mm grating blazed at 5500Å with 1$''$ wide slits giving a spectral resolution of 8Å ($\sim$ 450 km s^{-1}). With this grating setting the spectra cover the wavelength range 4500Å- 8500Å, which for cluster galax-

ies at $z = 0.12 - 0.25$ permits the measurement of all major spectral features between [OII](3727Å) through [SII](6731Å).

COSMIC has a field-of-view (FOV) of $11' \times 4'$ usable for spectroscopy. Three masks per cluster were observed, one centered on the cluster and two offset $2.5'$ north and south of the cluster center respectively. This results in a area covered by spectroscopy of $11' \times 9'$ around the cluster center which is $\sim 1.5 \times 1.2$ Mpc for the two clusters at $z \sim 0.12$, and $\sim 2.6 \times 2.1$ Mpc for the two clusters at $z \sim 0.25$. This is slightly larger than the estimated R_{200} for the clusters (see M07) and permits spectroscopic confirmation of virialized cluster galaxies as well as galaxies that are likely to be infalling into the cluster. Slits were placed preferentially on galaxies detected at $[24\mu m]$; however, a few slits were reserved for red-sequence cluster galaxies so that the redshift of the clusters could also be confirmed. Including the 5-7 stars required for mask alignment, 18 - 25 slits were positioned on each mask.

We restricted the selection of slits placements to red-sequence and $[24\mu m]$ galaxies with R < 21.5 for the $z \sim 0.12$ clusters and to galaxies with R < 22.5 for the $z \sim 0.25$ clusters. Four 900s exposures were made for the low redshift cluster masks giving a total exposure time of ~ 1 hour, and seven 1200s exposures were made for the high redshift clusters giving a total exposure time of ~ 2.5 hours. Details of the individual mask exposures are presented in Table 1. With these exposure times, absorption line redshifts can be obtained for galaxies with R < 20.5 and 21.5 for the low and high redshift clusters respectively, and emission lines redshifts can be obtained for galaxies roughly one magnitude fainter than this. Given that we expect most $[24\mu m]$ sources to have emission lines we allowed the selection of these galaxies to one magnitude fainter than the absorption line redshift limit.

The spectra were reduced using the standard IRAF[2] procedures contained in the NOAO *twodspec* package. This includes overscan correction, flat fielding and illumination corrections. Relative flux calibration was made using long slit observations of BD+253941, a B1.5V standard star. Wavelength calibration for the June 2007 data was performed using comparison spectra of a FeAr arc lamp. Unfortunately, the FeAr lamp was broken during the May 2006 run and those data had to be wavelength calibrated using bright sky lines. The wavelength calibration for most of those spectra is quite good (with the rms of major spectral features less than the 8 Å spectral resolu-

---

[2]IRAF is distributed by the National Optical Astronomy Observatory, which is operated by the Association of Universities for Research in Astronomy (AURA), Inc., under cooperative agreement with the National Science Foundation

tion); however, at the time of the writing of this thesis, a couple of spectra have poor wavelength calibration on the blue-end of the spectra, which has not been corrected. The poor calibration of the blue end occurs because of a lack of strong sky lines blueward of 5000Å with which to calibrate. The red-end of the calibration should still be reliable, so redshifts for those few spectra are taken from features redward of 5000Å (observed-frame).

After 1d spectra were extracted, redshifts were determined by cross-correlation with a set of 5 standard spectral templates using the IRAF *rvsao* package. Where the S/N of spectra is low and cross-correlation failed, redshifts were obtained manually by looking for well-known spectral features such as the [OII], [OIII], and Hα emission lines, or the H and K calcium absorption features. In total, 64 redshifts were obtained in the fields of these clusters, 13 of which were cluster red-sequence galaxies, 12 of which were cluster [24μm] sources, with the remainder being field [24μm] sources. The list of galaxies with redshifts is presented in Table 2. The quality of the spectroscopic redshifts is denoted with an integer between 2 and 4, with 4 being a high-quality redshift from the identification of several features as well as the continuum shape, and 2 denoting the lowest acceptable quality of redshift, typically from a single feature.

Table 5.1.   COSMIC Masks and Exposure Times

Cluster	Mask	Exptime	N_{exp}	Total Exptime
(1)	(2)	(3)	(4)	(5)
1	1	900s	4	3600s
1	2	900s	4	3600s
1	3	900s	4	3600s
2	1	900s	6	5400s
2	2	900s	5	4500s
2	3	900s	3	3600s
8	1	1200s	6	7200s
8	2	1200s	7	8400s
8	3	1200s	7	8400s
10	1	1200s	7	8400s
10	2	1200s	7	8400s
10	3	1200s	7	8400s

Table 5.2.   COSMIC Spectroscopic Redshifts

Cluster	RA	Dec	R	F_{24}	z	Quality	Name
(1)	(2)	(3)	(4)	(5)	(6)	(7)	(8)
1	257.921500	59.604840	19.78	610	0.2565	4	PAL-E-1-0
1	257.910600	59.596400	21.49	-	0.5609	3	PAL-S-1-1
1	257.878600	59.598610	18.68	-	0.2194	3	PAL-E-1-4
1	257.858700	59.611440	17.91	-	0.1259	4	PAL-E-1-6
1	257.832600	59.598720	18.62	1520	0.1275	4	PAL-S-1-8
1	257.824000	59.564300	19.25	1110	0.1795	4	PAL-S-1-9
1	257.739600	59.575480	19.77	-	0.1236	4	PAL-E-1-14
1	257.723600	59.587110	20.39	480	0.2847	4	PAL-S-1-15
1	257.701500	59.570850	20.81	530	0.4440	3	PAL-S-1-17
1	257.643000	59.627350	20.46	720	0.4735	4	PAL-S-1-19
1	257.631400	59.622240	20.07	-	0.4515	2	PAL-S-1-20
1	257.890900	59.521930	21.16	1070	0.8800	2	PAL-S-2-1
1	257.793900	59.550980	19.53	-	0.1407	4	PAL-S-2-6
1	257.761600	59.577740	18.17	-	0.1220	4	PAL-E-2-9
1	257.742700	59.576160	20.89	660	0.1260	3	PAL-S-2-11
1	257.707300	59.566520	19.27	800	0.1700	4	PAL-S-2-13
1	257.590000	59.556700	19.54	610	0.4681	3	PAL-S-2-20
2	259.340300	59.275810	20.91	-	0.7000	2	PAL-S-1-0
2	259.274900	59.263630	18.18	-	0.1266	4	PAL-S-1-5
2	259.254600	59.252320	20.27	590	0.3288	2	PAL-S-1-7
2	259.242800	59.259550	20.62	340	0.3951	4	PAL-S-1-8
2	259.210900	59.280430	18.95	-	0.1297	4	PAL-E-1-10
2	259.175800	59.265610	19.06	-	0.1621	2	PAL-E-1-13
2	259.165000	59.249290	18.06	-	0.1302	3	PAL-E-1-14
2	259.122900	59.273470	20.84	570	0.4992	3	PAL-S-1-16
2	259.095300	59.281830	20.47	350	0.3969	4	PAL-S-1-17
2	259.001100	59.257200	20.19	670	0.4993	2	PAL-S-1-21
2	259.286400	59.228110	21.05	5420	0.6455	3	PAL-S-2-3
2	259.202100	59.251010	18.82	-	0.1312	4	PAL-E-2-8
2	259.164000	59.253770	17.29	-	0.1282	4	PAL-E-2-10
2	259.124900	59.255570	19.47	1690	0.3546	4	PAL-E-2-14
2	259.047800	59.207620	18.39	-	0.1629	4	PAL-E-2-19
8	258.935000	59.021140	19.50	360	0.2240	4	PAL-S-1-1a

5.3.5 HectoSpec and SDSS Spectroscopic Data

One advantage of studying cluster $[24\mu m]$ galaxies in the FLS is that the FLS field has already been widely surveyed in other spectroscopic campaigns. In particular, Papovich et al. (2006b) performed an extensive survey of $[24\mu m]$-selected galaxies with MMT/Hectospec. The survey preferentially targeted bright $[24\mu m]$ sources with bright i-band counterparts. A total of 1296 redshifts were obtained, 89 of which lie within $1.5R_{200}$ of our four clusters.

In addition to the Papovich et al. (2006b) spectroscopy there are 1192 redshifts available in the FLS field from the Sloan Digital Sky Survey (SDSS, Adelman-McCarthy et al. 2007). Of these, 38 are within $1.5R_{200}$ of our four clusters .

Once duplicate objects are removed, the combined Palomar/HectoSpec/SDSS spectroscopic catalogue have 177 spectra in the cluster fields, 117 of which are $[24\mu m]$ sources, 42 of which are cluster members, 21 of which are cluster members detected at $[24\mu m]$. We list the redshifts and positions of cluster $[24\mu m]$ galaxies from the HectoSpec and SDSS spectroscopy in Table 3.

5.3.6 Spectroscopic Completeness

The spectroscopic completeness for $[24\mu m]$ sources is presented in Figure 1. The open histogram shows the number of $[24\mu m]$ sources as a function of F_{24} within $R < 1.5R_{200}$. The superposed black solid histogram shows the number of these galaxies with spectroscopic redshifts, and the light-blue histogram shows the number of those which are cluster members. Figure 1 demonstrates that the spectroscopic catalogues are reasonably complete for bright ($> 1000\ \mu$Jy) $[24\mu m]$ galaxies. There are 81 $[24\mu m]$ galaxies with $F_{24} > 1000\ \mu$Jy within 1.5 R_{200} of the four clusters. Of these, 35 (43%) have confirmed spectroscopic redshifts. Below 1000 μJy, the spectroscopic completeness drops off rapidly. There are 588 galaxies with 350 μJy $< F_{24} < 1000\ \mu$Jy within 1.5 R_{200}, of these, only 59 (10%) have spectroscopic redshifts.

Even though the cluster fields were observed in multiple spectroscopic campaigns with multiple masks or fibers, obtaining a completeness higher than this is challenging because the high density of objects near clusters limits the number of galaxies that can have slits or fibers placed on them at one time. Furthermore, of the 669 sources in the cluster fields with $[24\mu m] > 350\ \mu$Jy, 259 (39%) have R-band counterparts fainter than 22.0 mag. Given our exposure times and the sensitivity of COSMIC, it is very difficult to get redshifts for these galaxies. Due to the small number of bright sources

Table 5.2 (cont'd)

Cluster	RA	Dec	R	F_{24}	z	Quality	Name
(1)	(2)	(3)	(4)	(5)	(6)	(7)	(8)
8	258.818900	59.029850	20.80	-	0.2526	3	PAL-S-1-9
8	258.776800	59.030980	20.01	600	0.3510	3	PAL-S-1-12
8	258.759200	58.990300	18.39	-	0.2550	4	PAL-E-1-14
8	258.744800	58.992210	19.42	-	0.2520	4	PAL-E-1-15
8	258.685200	58.989880	20.04	3930	0.2130	4	PAL-S-1-19
8	258.771800	58.994840	18.33	-	0.2530	4	PAL-E-2-11
8	258.751900	58.999110	19.36	-	0.2530	4	PAL-E-2-13
8	258.695900	58.939640	20.80	-	0.3830	3	PAL-S-2-16
8	258.618000	58.945610	20.35	-	0.3840	4	PAL-S-2-20
8	258.598300	58.973210	19.35	530	0.2910	4	PAL-S-2-21
10	261.343600	59.374870	20.27	-	0.6840	4	PAL-E-1-2a
10	261.277400	59.391330	20.47	800	0.2817	4	PAL-S-1-4
10	261.204300	59.356360	18.40	-	0.2509	4	PAL-E-1-9
10	261.167700	59.349080	19.65	580	0.2550	4	PAL-E-1-11
10	261.151500	59.381370	19.05	670	0.1468	4	PAL-E-1-12
10	261.141100	59.409270	20.39	950	0.2352	4	PAL-S-1-13
10	261.081200	59.400480	19.75	-	0.2523	4	PAL-E-1-15
10	261.063700	59.410790	19.27	1220	0.2535	4	PAL-S-1-16
10	261.025700	59.398000	19.82	-	0.1570	3	PAL-E-1-18
10	261.267800	59.364280	19.62	430	0.2475	3	PAL-S-2-6
10	261.234600	59.364200	19.83	370	0.2494	2	PAL-S-2-8
10	261.192700	59.334270	19.69	-	0.2551	3	PAL-E-2-11
10	261.150800	59.327130	20.70	370	0.2496	3	PAL-S-2-15
10	261.137200	59.324170	18.85	750	0.2505	4	PAL-E-2-16
10	261.122900	59.345320	20.34	370	0.2542	4	PAL-S-2-17
10	261.109700	59.317860	20.50	1130	0.2535	4	PAL-S-2-18
10	261.067200	59.326010	20.07	-	0.2544	4	PAL-S-2-21
10	261.026300	59.314650	20.26	380	0.3403	3	PAL-S-2-24

Table 5.3. COSMIC Palomar Spectroscopic Redshifts

Cluster	RA	Dec	R	F_{24}	z	Name
(1)	(2)	(3)	(4)	(5)	(6)	(7)
1	257.787750	59.765640	18.57	2550	0.12649	spHect-131-263
2	259.010220	59.376660	18.75	720	0.12740	spHect-134-295
2	259.307710	59.250480	-	720	0.13936	spHect-134-257
8	258.670070	58.946820	19.60	550	0.24152	spHect-134-287
8	258.781950	58.987890	18.29	1010	0.25381	spHect-135-212
8	258.675020	59.004070	19.92	460	0.25387	spHect-134-218
8	258.832790	59.048910	20.17	410	0.24134	spHect-134-213
10	261.112390	59.289248	18.03	930	0.25439	spSpec-52017-0366-468
10	261.171600	59.417600	18.89	2330	0.26643	spHect-135-003

in the catalogue, and the large incompleteness of fainter sources, we do not attempt to apply a spectroscopic weight function to correct for completeness. Instead, we restrict our study to the nature of individual sources assuming that the spectroscopic catalogues are incomplete, but unbiased. This provides a reasonable census of the types of cluster galaxies which are detected at [24μm].

The spectroscopic catalogues are unbiased in the sense that the only selection criteria was that sources be detected at [24μm] and have R-band counterparts bright enough for optical spectroscopy. Given that not a single cluster [24μm] source was detected without at least one emission line, it is unlikely that the spectroscopic catalogue is biased in terms of preferentially getting redshifts for emission-line galaxies. Furthermore, Figure 1 shows that the number of galaxies with redshifts is evenly distributed by F_{24}, which shows that we have probed a subset of galaxies at the full range of F_{24} available at the FLS depth. The only under-represented sample in the catalogues are [24μm] sources that have faint optical counterparts. We note this means that if there was a population of extraordinarily dust-enshrouded star forming galaxies in the clusters that it would most likely be missed in our sample. Many studies have shown that due to the increasing presence of LIRGs and ULIRGs at higher redshift, a significant percentage of [24μm] sources are at $z > 1$ (e.g., Le Floc'h et al. 2005; Pérez-González et al. 2005), and that these galaxies are often very faint in the optical bands due to the

presence of a significant amount of dust extinction (e.g., Choi et al. 2006). Therefore, we expect that the the majority of [24μm]-bright, R-band faint galaxies in the cluster fields are likely to be background galaxies, and not very dusty cluster members.

This is further demonstrated by the solid lines plotted in Figure 1 which represent the expected number of background galaxies in the cluster fields. These curves are obtained using number counts from the entire FLS survey area scaled to the area of the cluster fields. They show that the vast majority of the sources are almost certainly background galaxies. Nonetheless, if they are not, a population of heavily obscured star forming galaxies in clusters at this redshift would be an interesting find. At the time of this writing, we have begun a small pilot campaign with Keck/DEIMOS to get spectroscopic redshifts for a few of these sources to explore the possibility that they are cluster members. That data will be taken in September 2007 and will be included in a future paper.

5.4 Spatial Distribution of 24μm Galaxies

The [24μm] sources in the cluster fields are fairly homogeneously distributed which is consistent with the majority being foreground or background galaxies. In order to better illustrate the distribution of sources by R-band flux, F_{24}, position, and spectroscopic completeness we plot the R-band images of the four clusters in Figures 2 - 5 with the MIPS [24μm] map overplotted as the white contours. Also overplotted are green squares and blue circles which represent galaxies with spectroscopic redshifts. The green squares are confirmed background or foreground galaxies while the blue circles are galaxies considered cluster members or near-field objects. Included with the cluster members are red-sequence galaxies which are not necessarily detected at [24μm].

Figures 2 - 5 reinforce what was already shown in Figure 1, namely that the majority of bright [24μm] sources have spectroscopic redshifts. Most of the remaining bright sources that do not have redshifts have large angular sizes in the R-band image making them almost certainly foreground galaxies. This suggests that at least in terms of bright mid-IR galaxies such as ULIRGs, the spectroscopic catalogues are reasonably complete[3]. Still, a significant number of [24μm] sources remain without redshifts and

---

[3]Assuming an M82 k-correction, a LIRG would have a F_{24} of ~ 400 μJy and 3500 μJy at $z = 0.25$ and 0.12, respectively
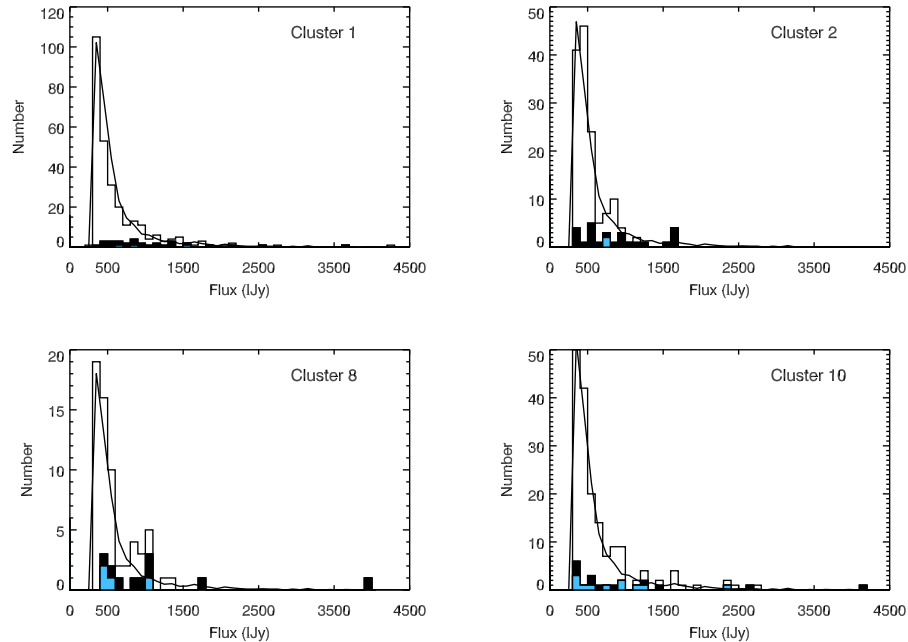
Figure 5.1 Histograms of the number of $[24\mu m]$ sources within $1.5R_{200}$ for the four clusters in our sample. The open histogram represents all MIPS sources, the filled black histogram is sources with spectroscopic redshifts, and the filled blue histogram are sources with spectroscopic redshifts that are cluster members. The solid line is the expected number of background counts estimated using the ~ 5 deg^2 of $[24\mu m]$ data from the FLS and shows that most sources in the fields of the clusters are likely to be background sources. Averaged over the four clusters the spectroscopic completeness for sources with $F_{24} > 1000\mu$Jy is 43%.

therefore additional spectroscopy would likely confirm more $[24\mu m]$ cluster galaxies.

In Figure 6 we plot the surface density of all MIPS sources as a function of R_{200} by combining the four clusters (filled blue circles). The solid blue line represents the expected background surface density of sources calculated from the entire FLS survey area. There is clearly a statistically significant excess of sources around the clusters; however, other than at slight increase around $R \leq 0.3R_{200}$, the surface density of sources is nearly flat.

Overplotted as the filled red circles on Figure 6 is the distribution of $[24\mu m]$ sources with spectroscopic redshifts (both cluster and field). The spectroscopic completeness is reasonably good for the central part of the cluster (~ 30 - 50%) but decreases to $<$ 10% at $R > R_{200}$. We compute the density profile of the cluster $[24\mu m]$ galaxies by scal-

ing their number density by the spectroscopic completeness in each bin (i.e., the ratio of blue to red filled circles). This density profile and 1σ error bar are plotted at the filled grey area in Figure 6. The error in the profile is the Poisson error in the number of spectroscopic members per surface area.

Unfortunately, the low level of completeness, combined with the fact that only $\sim$ 12 % of the [$24\mu m$] sources with redshifts are cluster members, makes computing a reliable density profile difficult. It is not possible to make useful conclusions from Figure 6 other than to say that the radial distribution of cluster MIPS sources is consistent with being flat, or possibly a decreasing power-law out to R $\sim 1.5R_{200}$. The distribution does not appear to be similar to an NFW (Navarro et al. 1997) profile; however, the error bars are large enough that no profile can reasonably be excluded.

Figure 6 demonstrates that a good measurement of the radial distribution of cluster [$24\mu m$] sources will be a challenging prospect for future work. The surface density of [$24\mu m$] sources is fairly high; however, the fraction of these that are cluster members is quite low. This causes the profile to suffer significantly from Poisson noise in the number of cluster members. Future spectroscopic studies will need to be more complete and stack a larger number of clusters in order to significantly improve on this result. Our density profile is based on only 21 cluster members. In order to obtain a good profile it might be expected that a total of $\sim$ 500 cluster [$24\mu m$] sources (which is roughly 25 per $\Delta R = 0.1R_{200}$) might be required, and that not less than 50% completeness in the catalogues would be desirable. For example, Muzzin et al. (2007b) measured the K-band selected number density profile of the CNOC1 clusters using spectroscopic redshifts for $\sim$ 1000 cluster members across 15 clusters and managed to measure the the NFW concentration parameter to $\pm$ 15%.

The mean spectroscopic completeness for the [$24\mu m$] galaxies is 14%. Assuming that the number of cluster members scales the same suggests that improving the completeness to 50% would result in a total of 75 cluster [$24\mu m$] galaxies. Bringing this to a total of 500 galaxies would require stacking an additional 24 clusters. Given that we were only able to achieve spectroscopic completeness of 14% using 3 masks per cluster at Palomar combined with the Hectospec and SDSS fiber spectroscopy suggests that such a sample will be extremely costly in terms of the observational resources required.

A better approach to measuring the radial profile may be to combine an even larger number of clusters and perform statistical background subtraction, but again, the high background level will make this challenging without a very large number of clusters.

Indeed, Geach et al. (2006) could not even find an *overdensity* of [24μm] sources around the very rich clusters MS 0451-03 and CL 0024+16 by pure background subtraction alone and needed to resort to a quasi-photometric redshift method to even detect a statistical overdensity associated with the clusters, let alone measure a density profile.

Perhaps more disconcerting for future work is that stacking clusters to measure the [24μm] density profile implicitly assumes that the objects being stacked are a homologous group. Although this is probably a reasonable assumption for the number density or radial profile of all cluster galaxies, it may not be appropriate for the [24μm] population. If [24μm] sources are the product of infalling groups which contain triggered dusty starbursts, or else are star forming galaxies which are quenched by the cluster on short timescales, then the profile will be stochastic, depending strongly on the location of the infalling groups and the specific dynamics of the cluster.

This concern is probably best demonstrated by the [24μm] maps of Clusters 2 and 10 (Figures 3 and 5 respectively). Cluster 2 appears to be a dynamically relaxed cluster with an overwhelmingly dominant central cD galaxy. Almost all the the [24μm] sources in the field around Cluster 2 are confirmed foreground or background galaxies. By comparison, Cluster 10 has a large number of confirmed cluster [24μm] galaxies which appear roughly in a strip through the cluster from the top left to the bottom right of Figure 5. Interestingly, a low significance cluster was found nearby to Cluster 10 with a similar photometric redshift. The overdensity is visible in Figure 5 as the compact lump of bright galaxies near the green square directly below the very bright star on the lower right of Figure 5. This group was later culled from the cluster catalogue because it did not meet the B$_{gc}$ > 200 richness cut (see M07). The strip of [24μm] galaxies appears to connect cluster 10 and the compact group suggesting that they may be related, and possibly that the abundance of [24μm] sources is caused by the merging of these structures.

Whether or not Cluster 10 is really undergoing a cluster-cluster merger remains to be shown; however, it is clear that Clusters 2 and 10 are very different both dynamically and also in terms of the radial profile of [24μm] sources. It suggests that cluster [24μm] sources may not follow a universal density profile that can be measured by stacking clusters. If a larger subset of clusters are shown to not be homologous, it would suggest that the timescale during which cluster galaxies remain bright at [24μm] is relatively short.
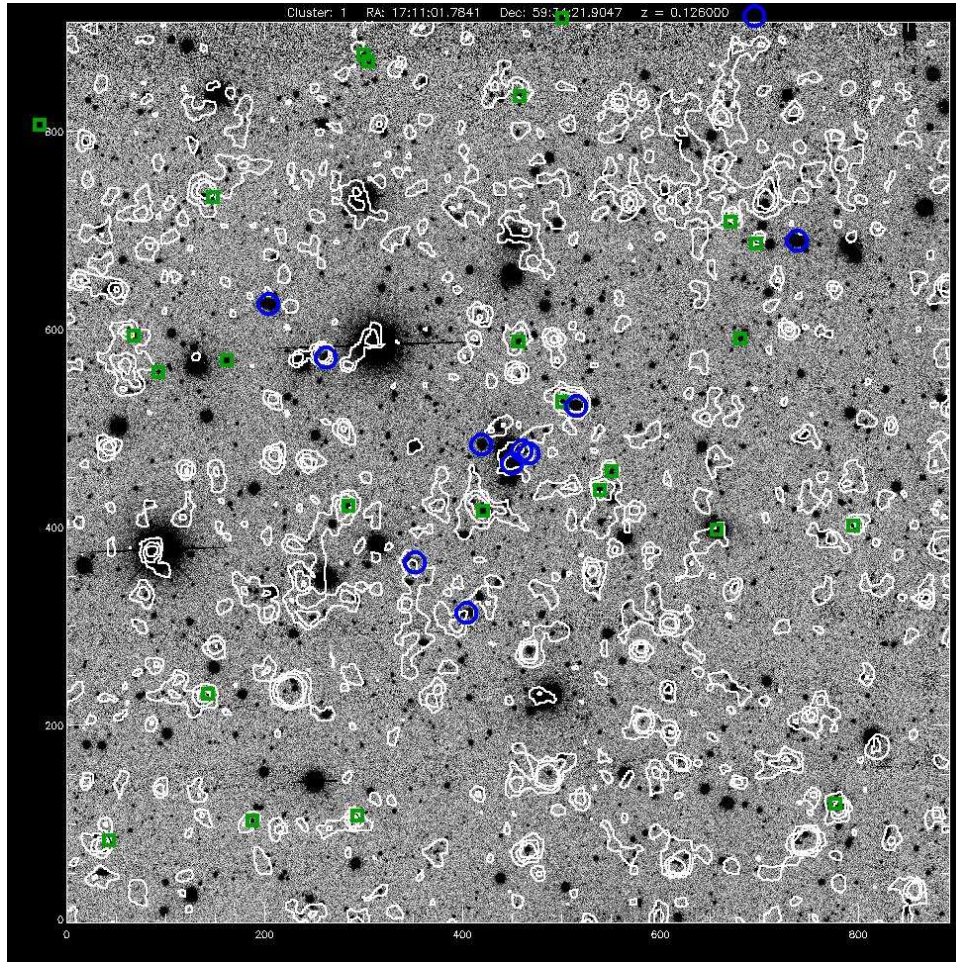
Figure 5.2 R-band image of FLS J171059+5934.2 (Cluster #1). The FOV is ~ 1.5 times the cluster R_{200}. The white overlaid contours are the from the [24μm] map. Galaxies marked with blue circles are confirmed cluster members and include cluster red-sequence members that are not necessarily detected at [24μm]. Galaxies marked with green squares are [24μm] sources which are confirmed to be foreground or background objects. The units along the x and y axes are arbitrary.

5.5   Spectral Classification

In this section we use the spectroscopy of the [24μm] cluster galaxies to classify them as either star forming galaxies or AGN/LINERs. The classification is based on the scheme of Baldwin et al. (1981) who showed that star forming galaxies and AGN can be identified using plots of four emission line ratios: [OIII]/Hβ, [NII]/Hα, [SII]/Hα, and [OI]/Hα. Since that seminal work, plots of these line ratios have typically been called Baldwin-Phillips-Terlevich (BPT) diagrams. In general, star forming galaxies
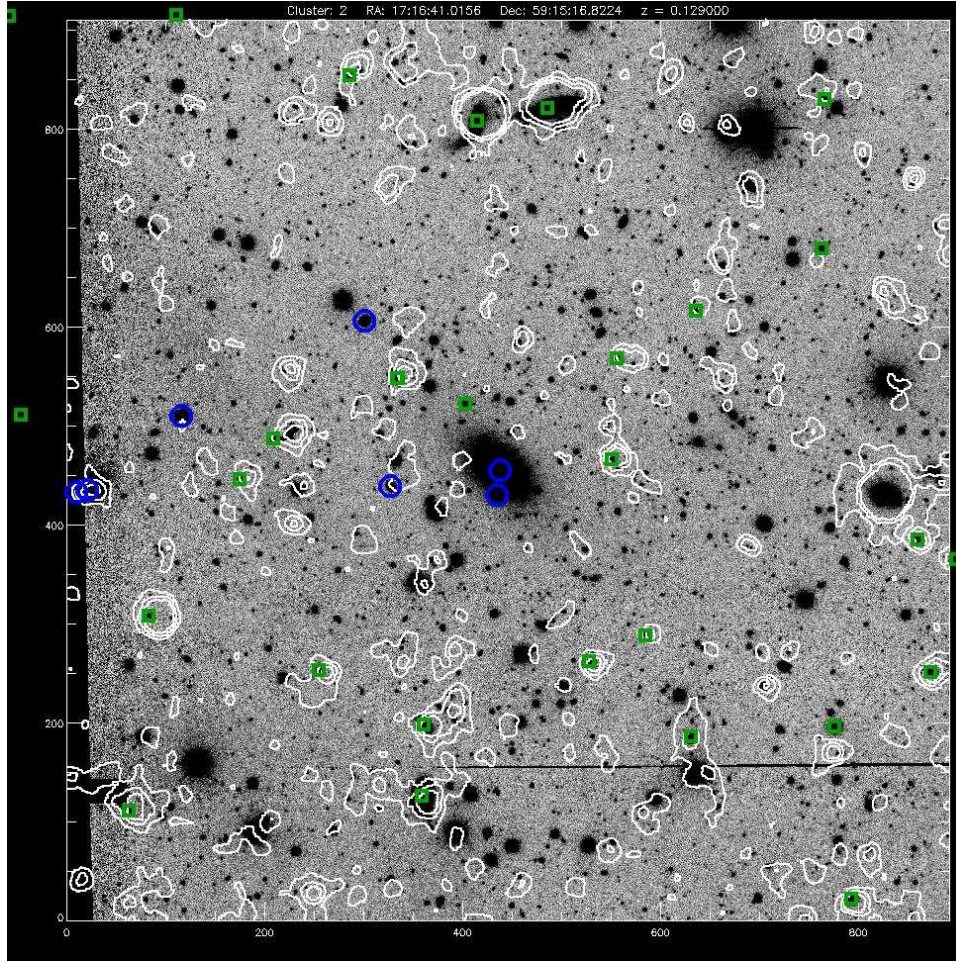
Figure 5.3 As Figure 2, but for FLS J171639+5915.2 (Cluster 2).

follow "star forming main sequences" in the BPT diagrams, where the sequence is caused by the range of metallicities within the subset of galaxies. AGN/LINERs tend to have larger [NII]/Hα and [SII]/Hα at a fixed [OIII]/Hβ than the star forming main sequence which makes them easy to identify in the BPT diagram.

Recently, the classical BPT diagrams were refined by Kewley et al. (2001) who used a combination of spectral synthesis and photoionization models to determine a "maximal starburst line" which denotes the upper limits of the line ratios allowed by pure stellar photoionization models. The maximal starburst lines are defined as

$$Log([OIII]/H\beta) = 0.61/[Log([NII]/H\alpha) - 0.05] + 1.3, \tag{5.1}$$

and

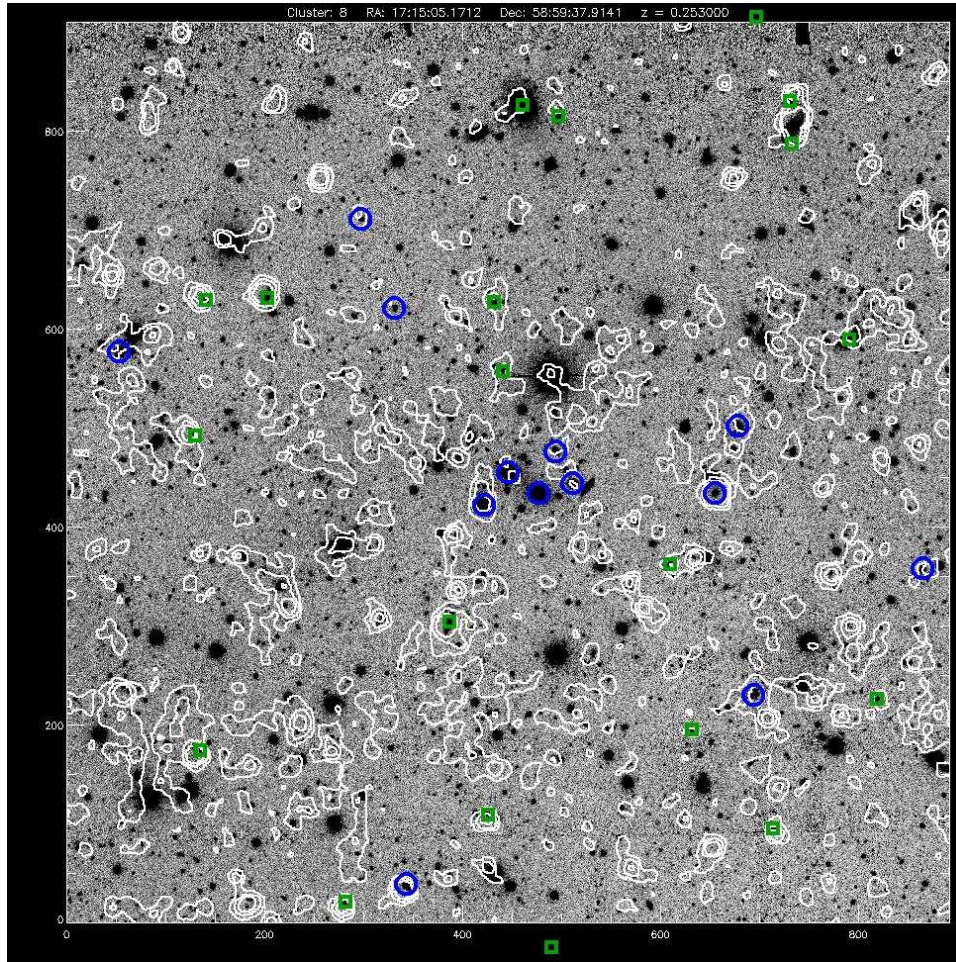$$Log([OIII]/H\beta) = 0.72/[Log([SII]/H\alpha) - 0.32] + 1.3. \tag{5.2}$$

Figure 5.4 As Figure 2, but for FLS J171505+5859.6 (Cluster 8).

Galaxies that lie below these lines are likely to have their emission dominated by star forming galaxies and those that lie above are likely to be dominated by an AGN. This classification scheme was further refined by Kauffmann et al. (2003) who empirically showed with SDSS spectra that some galaxies have spectra with both a star formation component as well as an AGN component. They labeled these "composite" galaxies, and the line denoting composite galaxies is defined as

$$Log([OIII]/H\beta) = 0.61/[Log([NII]/H\alpha) - 0.47] + 1.19. \qquad (5.3)$$

Galaxies which above this line, but below the maximal starburst line are considered to have composite spectra. For illustration, the Kewley et al. (2001) maximal starburst models and the Kauffmann et al. (2003) composite model are plotted in Figure 7 as the solid and dashed lines respectively.

Kewley et al. (2001) also showed that Seyfert-type AGN could be differentiated
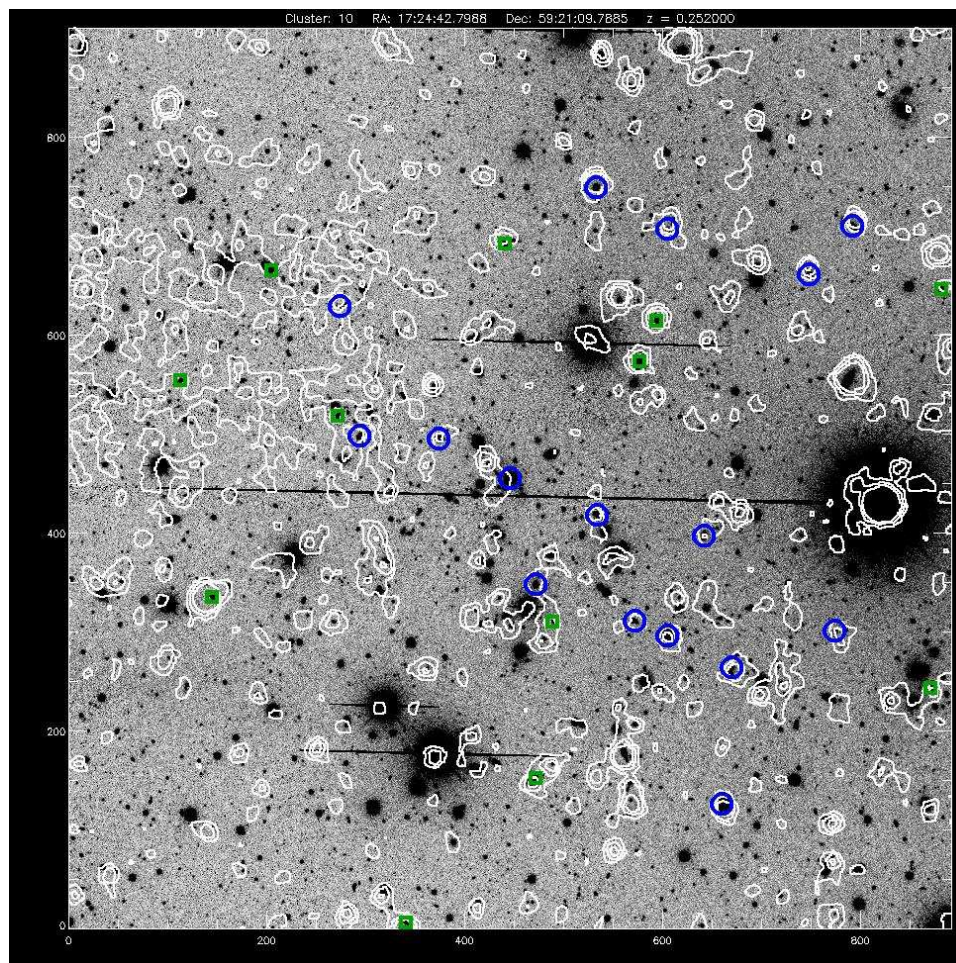
Figure 5.5 As Figure 2, but for FLS J172449+5921.3 (Cluster 10).

from low-ionization narrow emission line regions (LINERs) in the [OIII]/Hβ vs. [SII]/Hα plot using the equation

$$Log([OIII]/H\beta) = 1.89Log([SII]/H\alpha) + 0.76, \tag{5.4}$$

with galaxies lying above this line being Seyferts and those below being LINERs, provided that they already lie above the Kewley et al. (2001) maximal starburst line. Given that our spectra cover the entire range from rest-frame [OII](3727Å) to [SII](6731Å) we can measure all of these line ratios and classify the cluster [24μm] sources as either star forming galaxies or AGN, and furthermore, classify the AGN as either Seyferts or LINERs. Within our sample we make a further distinction, which is to classify star forming galaxies as regular star forming galaxies (SF), or starbursts. Galaxies which have [NII]/Hα line ratios which are > 0.1 dex than predicted from the star forming main sequence (i.e., are outliers in the direction of the maximal starburst line, see
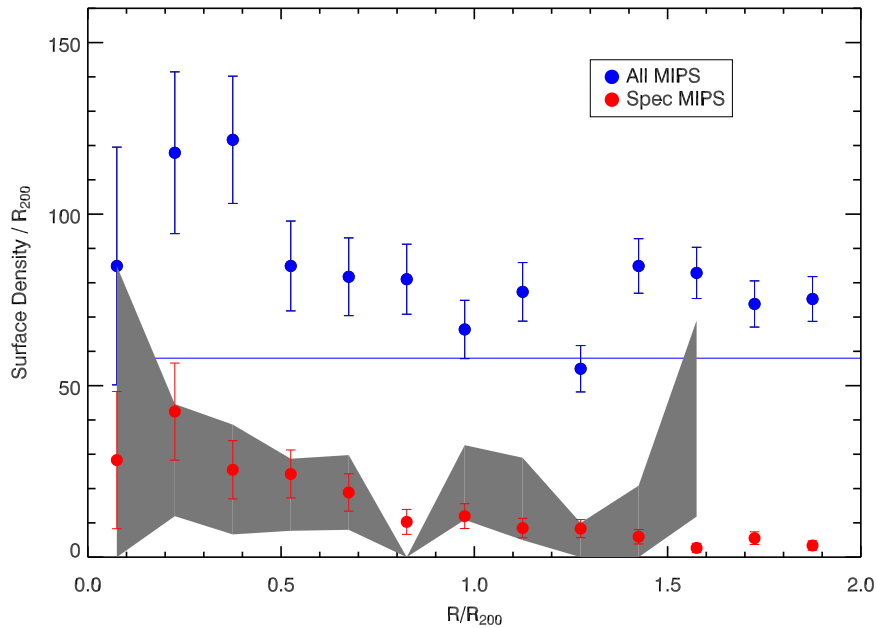
Figure 5.6 Plot of the surface density of $[24\mu m]$ sources as a function of R_{200} in the fields of the four clusters. The blue points are for all $[24\mu m]$ sources and the expected background density is shown by the blue line. The red points are for all galaxies with spectroscopic redshifts and demonstrated the completeness of the spectroscopy as a function of radius. The grey shaded region is the surface density and 1σ error of $[24\mu m]$ sources that are spectroscopic members of the clusters.

Kewley et al. 2001) but have [OIII]/Hβ vs. [SII]/Hα line ratios consistent with being star forming galaxies are considered starbursts. This includes galaxies with normal [OIII]/Hβ vs. [SII]/Hα ratios but with [OIII]/Hβ vs. [NII]/Hα ratios consistent with being "composite" spectra as defined by the Kauffmann et al. (2003) relation. We classify galaxies as "composite" only when they have [OIII]/Hβ vs. [NII]/Hα line ratios in the composite range defined by equation (3) *and* when their [OIII]/Hβ vs. [SII]/Hα ratios diverge from the star forming main sequence.

In addition to the BPT classification, we also classify the cluster galaxy spectra using the classification scheme of Dressler & Gunn (1992) and Dressler et al. (1999). Hereafter, we refer to this classification as the to this as the "DG class". This classification is based on the comparison of equivalent widths (EWs) of the [OII] emission line and the Hδ absorption feature. Although somewhat cruder because it relies on

the [OII] line as measure of current star formation[4], it has been used more extensively in the study of distant cluster galaxy spectra (e.g., Dressler et al. 1999; Poggianti et al. 1999; Balogh et al. 1999; Duc et al. 2002; Dressler et al. 2004) because the Hα-emission line passes out of range of all but the most red-sensitive spectrographs at $z > 0.4$. The DG scheme does not separate weak AGN/LINERs from star forming galaxies; however, it is useful for differentiating between currently star forming galaxies and those which may have had their star formation recently truncated (e.g., the "post-starburst" k+a or a+k galaxies). A brief summary of the DG classes is presented below.

1. *k Galaxies*: These are galaxies devoid of emission lines with EW(Hδ) < 3Å. The "k" designation comes from the fact that their spectra are most similar to that of K stars. This spectral class is most common amongst early-type galaxies.

2. *k+a and a+k Galaxies*: These galaxies have very little or no [OII] emission (EW([OII]) < 3Å) and very strong Hδ absorption (3Å< EW(Hδ) < 8Å for k+a galaxies, and EW(Hδ) > 8Å for a+k galaxies). The Hδ absorption arises from absorption in the atmospheres of A stars. A stars are an indicator of star formation within the last 1.5 Gyr; however, the lack of emission lines suggests that these galaxies are probably "post-starburst", or "post-star formation" galaxies with no currently ongoing star formation.

3. *e Galaxies*: These are galaxies with emission lines. Dressler et al. (1999) subdivided these into several classes. e(c) galaxies are typical of "average" star forming spiral galaxies. They are defined as galaxies with 5Å < EW([OII]) < 40Å and Hδ < 4Å. The "c" in their designation stands for "continuous" star formation. The e(b) galaxies are defined as starburst galaxies, they have the largest [OII] emission (EW([OII]) > 40Å) and are permitted any level of Hδ absorption. Lastly, the e(a) galaxies are defined as emission line galaxies with some A star characteristics. Like e(c) galaxies they have 5Å < EW([OII]) < 40Å; however, they have Hδ > 4Å. Prior to the consideration of dust, these galaxies were considered to be post-starburst galaxies with low levels of residual star formation. It was Poggianti et al. (1999) who first suggested that these galaxies might be strongly star forming systems (hence the large Hδ > 4Å) but that they have strong dust extinction of the [OII] line which is why they are not classified as e(b) galaxies. It was expected that a large fraction of MIR-bright galaxies would have this optical spectrum (e.g., Poggianti & Wu 2000).

---

[4]The strength of the [OII] line is correlated with star formation rate; however, there is a large scatter due to both metallicity and the fact that the line is a UV line which makes it very sensitive to the amount of dust extinction in the host galaxy (e.g., Charot & Longhetti 2001, Jansen et al. 2001).

5.5.1   Measurement of Line Ratios and Equivalent Widths

The line ratios and equivalent widths for the [OII], Hδ, Hβ, [OIII], Hα, [NII], and [SII] lines are measured with the *splot* task in the IRAF NOAO package. The line profiles are fit using a Gaussian, and EWs are measured using the EW algorithm included in this package. This approach is not as sophisticated as the algorithms for measuring EWs employed by Dressler et al. (1999), Balogh et al. (1999) and Moran et al. (2005) which also take into account the pixel-by-pixel variance from the sky subtraction. The primary advantage to those algorithms is not that they provide a better EW measurement than the *splot* task, but that they allow the computation of an error bar for the line ratios and EWs. Poggianti & Wu (2000) compared the EWs measured by the Dressler et al. (1999) algorithm to those measured by the *splot* task and showed that they provide consistent results with an rms scatter of $\sim 20\%$. Error bars on the EWs are useful in studies that measure star formation rates (SFRs) using the [OII] and Hα lines because they provide some metric of the error in that quantity. We use the line ratios and EWs only for classification purposes, and therefore error bars are not important (other than possibly to show that the S/N was insufficient to robustly classify the galaxy). Regardless, even with error bars a galaxy must be assigned to a specific class, and therefore we do not attempt to calculate error bars in our line ratios and EWs.

The relevant line ratios and EWs needed for classifying galaxies in the BPT and DG schemes as well as the classifications are listed in Table 4 for the [$24\mu m$] galaxies in the $z \sim 0.25$ clusters and in Table 5 for the $z \sim 0.12$ clusters. The [OIII]/Hβ vs. [NII]/Hα and [OIII]/Hβ vs. [NII]/Hα line ratios for [$24\mu m$] galaxies in the high and low redshift clusters are plotted in Figure 7 as the solid dots and asterisks, respectively. For illustrative purposes we also plot the individual spectra in the high and low redshift clusters sorted by increasing F$_{24}$ with the the major spectra lines labeled in Figures 8 - 13 and Figures 14 - 15, respectively.

There are a few galaxies that have [OII], Hα, and [NII] in emission, but have no [OIII] line as well as Hβ in absorption (e.g., PAL-10_2_18, spHect-134-257). Most normal star forming galaxies that have [OII], Hα, and [NII] in emission also show Hβ and [OIII] in emission. Often there is some absorption of Hβ due to an underlying old stellar population, but the line usually remains in emission. Most likely the explanation for the spectra of these galaxies is that they have a very dominant old stellar population with a small amount of additional star formation superposed, or else they
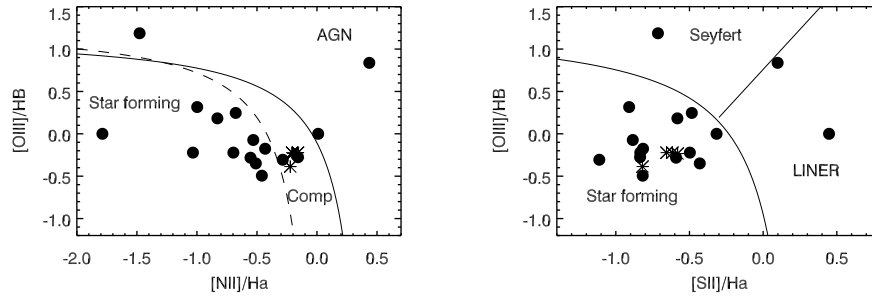
Figure 5.7 BPT diagrams for [24μm] cluster galaxies. The solid lines are the Kewley et al. (2001) "maximum starburst line" that separates star forming galaxies from AGN. The dashed line in the left panel is the empirical model from Kauffmann et al. (2003) used to select composite galaxies that have both star formation and AGN activity. The filled circles and asterisks are galaxies in the high redshift and low redshift clusters, respectively.

were recently star forming and had their star formation truncated, leaving only a small residual.

There are five galaxies in the [24μm] sample with this property, and this makes them difficult to classify in the BPT diagram because the classification depends on the [OIII]/Hβ line ratio which is undefined for Hβ in absorption. So that they can have a classification, these galaxies have been assigned a [OIII]/Hβ ratio of 0.6, which is the well-known mode of this ratio for star forming galaxies. Although assigning a value which is typical of star forming galaxies could potentially bias against classifying these galaxies as AGN/LINERs, we note that the most discriminating ratio for this the [NII]/Hα line ratio. Even if the assigned [OIII]/Hβ is incorrect, AGN/LINERS should still be obvious from their large [NII]/Hα.

Table 5.4.   Spectroscopic Classification of MIPS sources in High Redshift Sample

Name	z	F_{24}	R	[OIII]/Hβ	[NII]/Hα	[SII]/Hα	[OII] EW	Hδ EW	DG-Type	BPT Type
(1)	(2)	(3)	(4)	(5)	(6)	(7)	(8)	(9)	(10)	(11)
spHect-135-003	0.2664	2330	18.89	0.5	0.5	0.1	-9.4	1.0	e(c)	Starburst
PAL-10_1_16	0.2535	1220	19.28	-6.3	0.2	0.3	-19.0	2.9	e(c)	SF
PAL-10_2_18	0.2535	1130	20.50	0.3	0.3	0.2	-22.0	2.1	e(c)	SF
spHect-134-212	0.2538	1010	18.30	1.0	14.7	2.8	-3.6	1.1	k	LINER-(k)
PAL-10_1_13	0.2352	950	20.39	2.1	0.1	0.1	-8.0	3.4	e(c)	SF
SpSpec-0366-468	0.2544	930	18.04	0.5	0.7	0.1	-9.7	1.2	e(c)	Starburst
PAL-10_2_16	0.2505	750	18.86	-0.1	0.1	0.1	-2.4	3.7	k+a	truncated?-(k+a)
PAL-10_1_11	0.2550	580	19.66	6.9	2.7	1.3	-28.4	0.3	e(c)	LINER
spHect-134-287	0.2415	550	19.60	0.7	0.4	0.2	-10.4	1.1	e(c)	Starburst
spHect-134-218	0.2539	460	19.32	1.0	1.0	0.5	-2.5	3.0	k+a	Comp-(k+a)
PAL-10_2_6	0.2475	430	19.63	0.5	0.3	0.3	-36.7	3.7	e(c)	SF
spHect-134-213	0.2413	410	20.18	0.8	0.3	0.1	-42.0	1.3	e(b)	SF-e(b)
PAL-10_2_15	0.2496	370	20.70	15.4	0.0	0.2	-12.2	0.1	e(c)	Seyfert
PAL-10_2_17	0.2542	370	20.35	1.5	0.1	0.3	-20.9	3.3	e(c)	SF
PAL-8_1_1	0.2240	360	19.50	1.0	0.0	0.0	-6.2	2.7	e(c)	truncated?-e(c)
PAL-10_2_21	0.2544	<350	20.07	0.4	0.3	0.2	-27.9	5.5	e(a)	SF
PAL-10_1_15	0.2523	<350	19.76	1.8	0.2	0.3	-4.6	3.2	k+a	SF-(k+a)

Table 5.5.   Spectroscopic Classification of MIPS sources in Low Redshift Sample

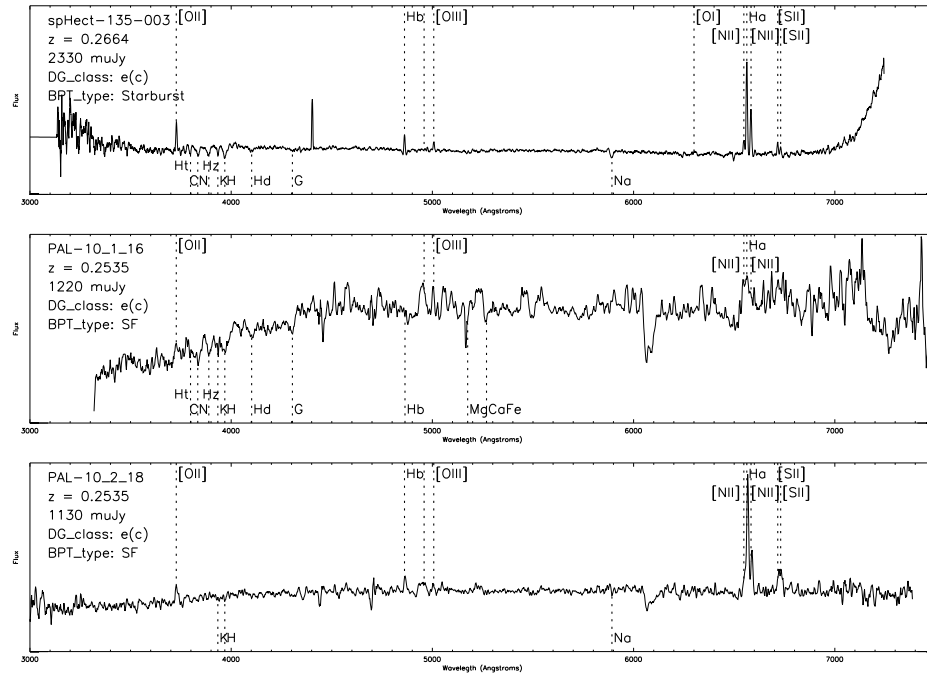| Name	z	F_{24}	R	[OIII]/Hβ	[NII]/Hα	[SII]/Hα	[OII] EW	Hδ EW	DG-Type	BPT Type
(1)	(2)	(3)	(4)	(5)	(6)	(7)	(8)	(9)	(10)	(11)
PAL-1_1_8	0.1275	1520.00	18.62	0.4	0.6	0.2	-5.6	9.5	e(a)	Starburst
spHect-134-295	0.1274	720.00	18.76	-0.1	0.7	0.2	-3.7	1.8	k	Starburst
spHect-131-283	0.1262	2550.00	18.58	0.6	0.6	0.3	-14.0	2.2	e(c)	Starburst
spHect-134-257	0.1394	720.00	-1.00	-0.1	0.6	0.2	-2.0	1.8	k	Starburst

Figure 5.8 Spectra for cluster [24μm] sources in the high redshift clusters ranked in order of increasing F$_{24}$. The spectra are displayed in the rest-frame and spectral features which are detected are labeled using the dotted lines.
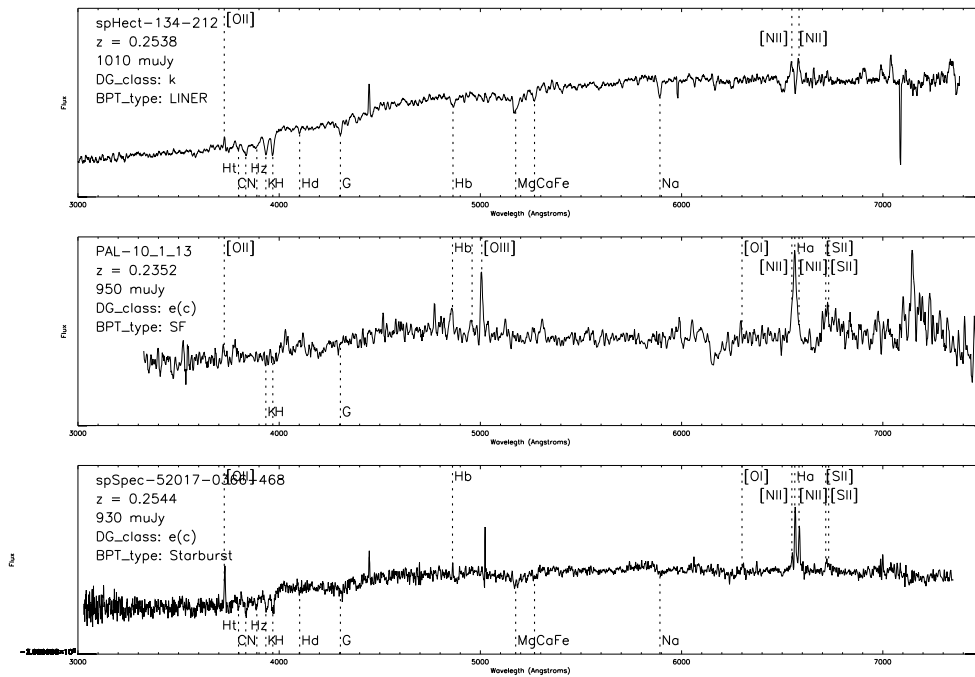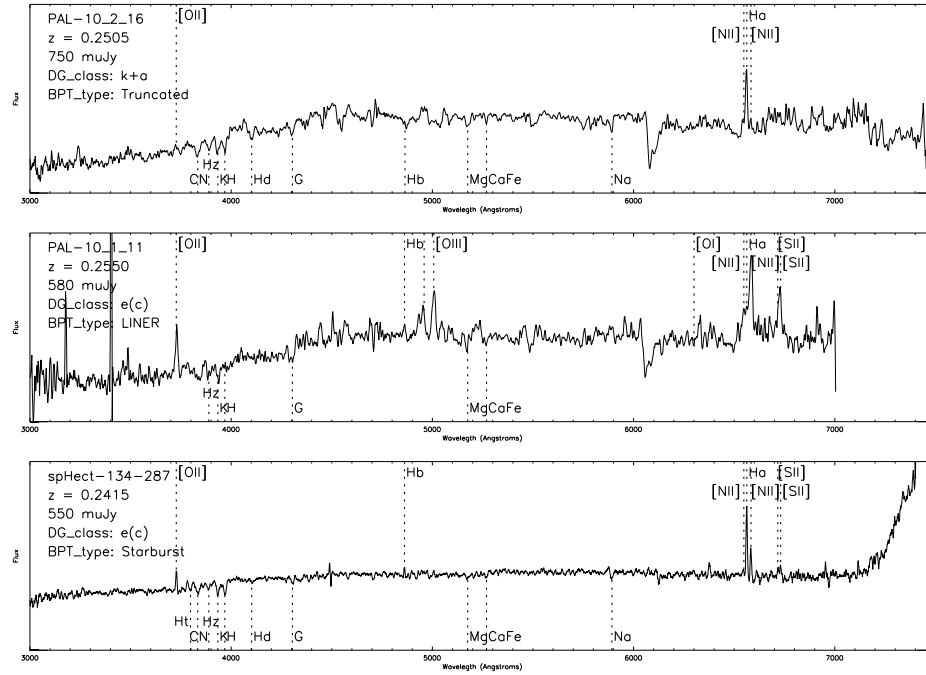
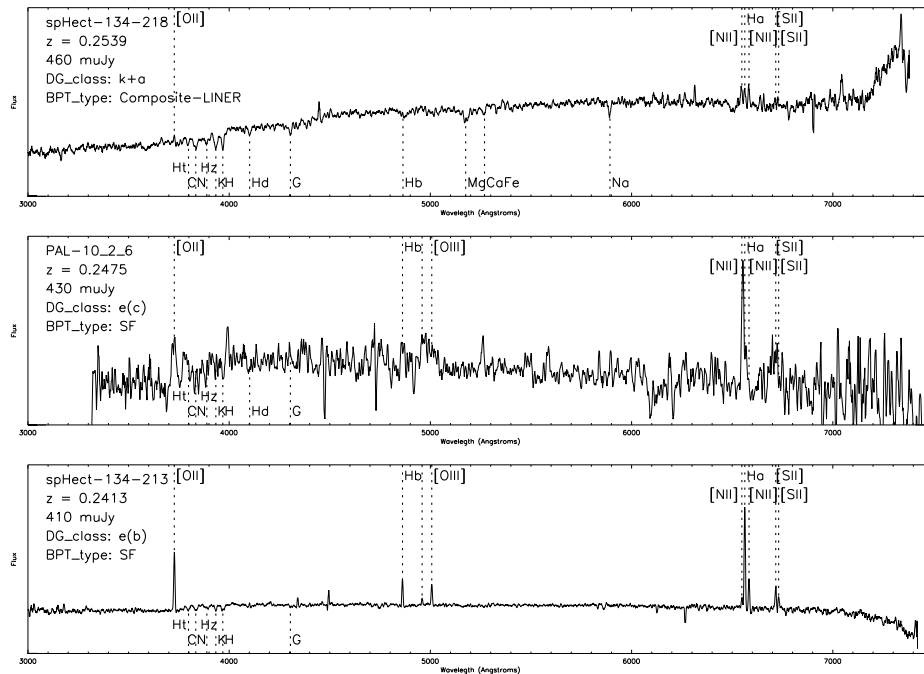

Figure 5.9 As Figure 8.
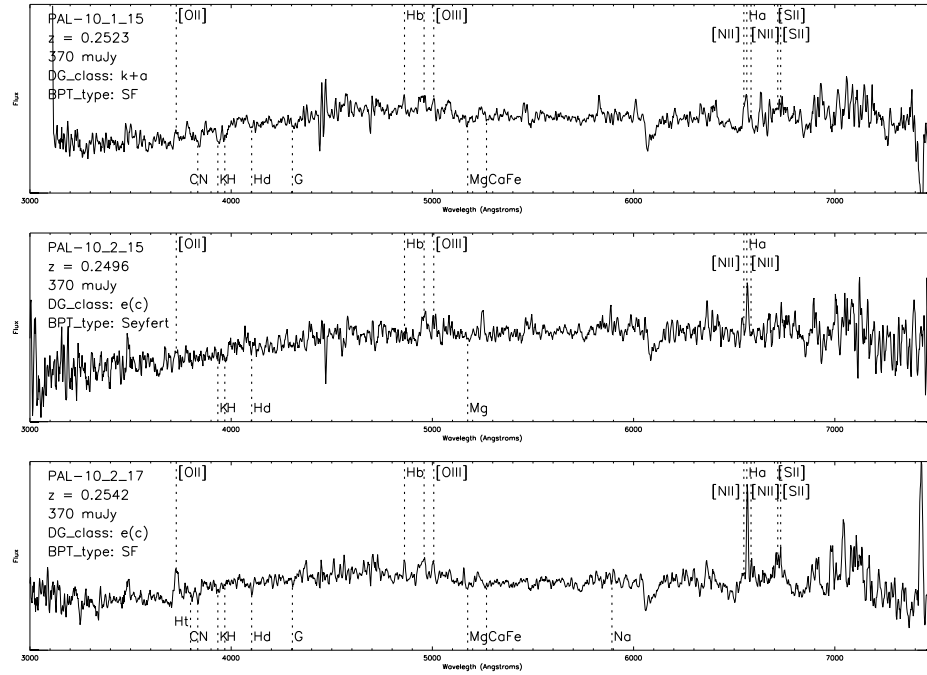
Figure 5.10 As Figure 8.
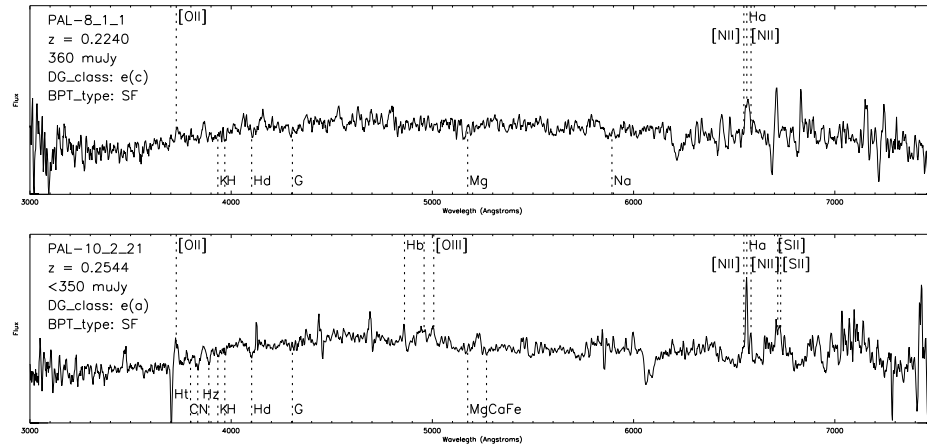

Figure 5.11 As Figure 8.
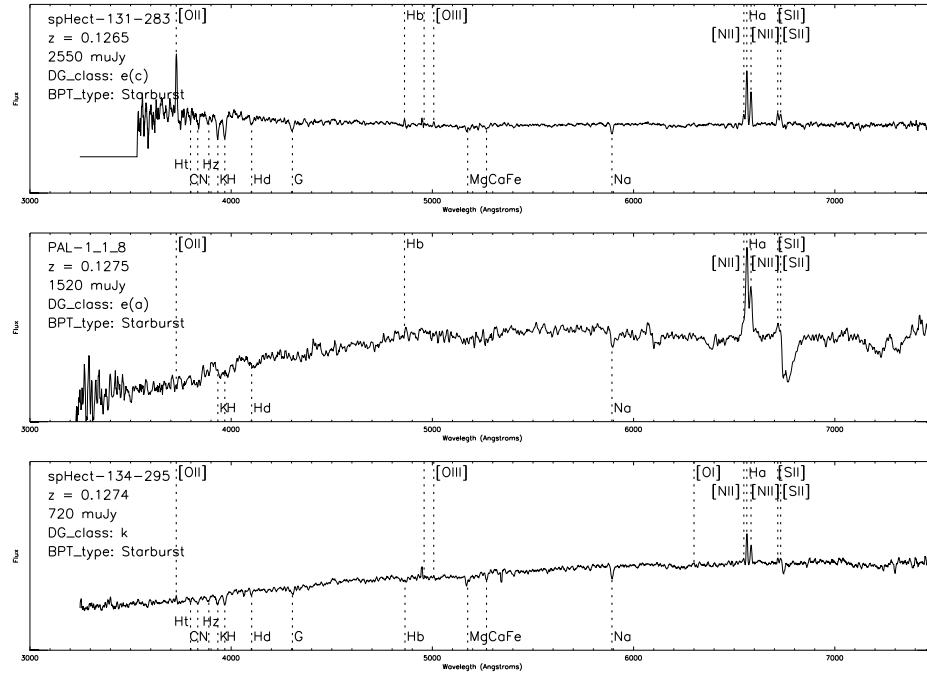
Figure 5.12 As Figure 8.

Figure 5.13 As Figure 8.

Figure 5.14 As Figure 8, but for [24μm] galaxies in the low redshift clusters.
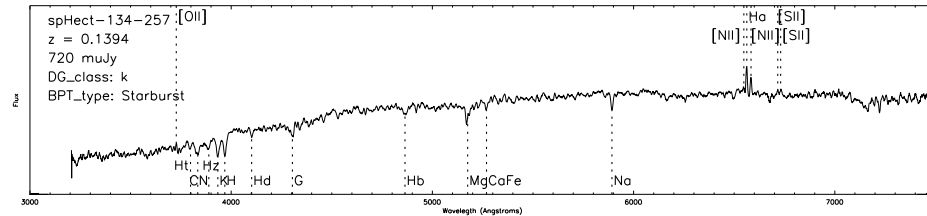

Figure 5.15 As Figure 14.

5.6 Discussion

5.6.1 General Classification

Tables 4 and 5 and Figure 7 show that the cluster [24μm] galaxies are a heterogeneous subset of galaxies. Within our sample of only 21 cluster galaxies there is at least one example of all six of the BPT classifications (starburst, SF, LINER, Seyfert, truncated, composite). Furthermore, there is also at least one example of five of the six DG spectral types (k, k+a, e(a), e(b), e(c)), with the a+k class being the only DG spectral type not found in the sample. That almost all spectral classes are found in such a small sample of galaxies shows that the mid-IR emission in cluster galaxies is coming from a diverse set of physical processes in a variety of intra-galactic environments. The fainter [24μm] sources are more homogeneous than the bright ones. In the high redshift clusters 5/7 (86%) of the faintest [24μm] sources are SF galaxies. Low-luminosity starbursts and AGN/LINERs appear to be rare in our sample; however, it might be expected that low-luminosity starbursts and AGN/LINERs would be found in less-massive galaxies, and therefore their absence may be attributed to the R-band spectroscopic magnitude limit.

The majority of the [24μm] population in our sample is associated with star forming galaxies. Of the cluster members, 17/21 (81%) belong to either the starburst, SF, or truncated class, while only 4/21 (19%) belong to the Seyfert, LINER, or composite classes. The most prevalent classes of [24μm] sources are the SF and starburst classes which comprise 43% and 33% (9/21, 7/21) of the population, respectively. In the DG classification, the dominant class of galaxies is the the e(c) class which comprises 62% (13/21) of the population. This result is consistent with Marcillac et al. (2007) who classified the optical spectra of fifteen [24μm] galaxies in the field of the cluster RX J0152.7-1357 at $z = 0.83$ and also found that the most common class of those galaxies was e(c) (6/15, 40%). Given previous studies, it is somewhat surprising that the e(c) class dominates the cluster [24μm] population in our sample and in RX J0152.7-1357.

Originally, in a study of 10 clusters at $z \sim 0.4$ - 0.5 Poggianti et al. (1999) proposed that galaxies with e(a) spectra were likely to be highly obscured dusty starbursts. Subsequently, Poggianti & Wu (2000) examined the optical spectra of 71 local ($0.02 < z < 0.05$) LIRGs and showed that the majority of their optical spectra (56%) were classified as the e(a) type. Only $\sim 25\%$ of the local LIRGs had spectra classified as e(c), compared to the 62% of [24μm] galaxies in clusters classified as e(c). In the only other published

data on the spectral types of mid-IR cluster galaxies, Duc et al. (2002) did find that the dominant class of galaxies detected at $15\mu m$ by *ISO* in Abell 1689 ($z = 0.17$) was the e(a) class (4/16, 25%), although this was equal to the k class which also had 4/16 cluster members. Interestingly only 1/16 galaxies detected at $15\mu m$ in Abell 1689 was classified as an e(c). This lead us to expect that the majority of the mid-IR sources in distant clusters would be of the e(a) class, and not the e(c) class.

Although our study and the Marcillac et al. (2007) study suffer from small number statistics, the percentages of e(a) galaxies are much lower (10%, and 13% respectively) than for the local LIRGs. This suggests that the local LIRGs in the Poggianti & Wu (2000) sample may not be analogues of the $[24\mu m]$ galaxies found in distant clusters. Poggianti & Wu (2000) showed that the local e(a) LIRGs are dominated by galaxies undergoing mergers or strong interactions (75% of all e(a)'s). They also showed that of all the LIRG spectral types the e(c) galaxies are the most likely to be isolated galaxies (46% of all e(c)'s). They concluded that the very dusty e(a) LIRGs are likely to be triggered by mergers and interactions, while the e(c) LIRGs may be isolated galaxies undergoing vigorous, but not necessarily triggered-from-without, star formation.

That the cluster population is dominated by e(c) galaxies and not e(a) galaxies suggests that they are primarily isolated star forming galaxies and are not the end products of mergers and interactions. We examined the R-band images of the cluster $[24\mu m]$ sources for signs of interactions or close pairs. There are three $[24\mu m]$ galaxies with close ($< 2''$) companions; however, none of those showed signs of obvious asymmetry associated with an interaction, suggesting that they may be projections. Only one galaxy in the sample has signs of a significant interaction. We note that the eye-examination is not completely conclusive because the angular resolution of the R-band images is not particularly good, $\sim 1''$ seeing, which corresponds to ~ 4 kpc at $z = 0.25$; however, it is still sufficient to rule out the possibility that the majority of sources are being caused by interactions.

The only example of an interacting system amongst the cluster $[24\mu m]$ galaxies is spHect-134-212. This galaxy is located near the core of Cluster 8 and has a set of remarkable tidal features (see Figure 16). Ironically, it is one of the few galaxies classified as a LINER, not a star forming galaxy. The tidal features in spHect-134-212 extended as far as $6''$ from the core of the galaxy and the Hectospec fiber aperture is $1.5''$ in diameter. Hence, it is possible that much of the $[24\mu m]$ emission is from star formation, but the optical spectrum comes from the core and is therefore dominated by an AGN-LINER. Regardless of the specifics of spHect-134-212, it is clear that the major-

ity of cluster [24μm] galaxies are classified as e(c) spectra, and that they do not show significant signs for interaction. This supports the idea that they are primarily isolated, vigorously star forming systems that are probably not analogues of local LIRGs. Given the rapid increase in the universal star formation density (e.g., Schiminovich et al. 2005; Pérez-González et al. 2005, and references therein) and IR-inferred specific star formation rate of galaxies (e.g., Pérez-González et al. 2005) with increasing redshift, it is conceivable that LIRG-type star formation in the local universe may be more frequently triggered from mergers, whereas at higher redshift the enhanced level of star formation in LIRGs is simply typical of star formation at that epoch (e.g., Pérez-González et al. 2005; Le Floc'h et al. 2005).

A surprising result from the spectral classification is that 19% of the cluster sample contains AGN or LINER activity. This is larger than the AGN fraction of cluster [24μm] galaxies estimated by Marcillac et al. (2007) and Bai et al. (2007). Those studies used X-ray data as an indicator of AGN activity and both found that only 6% of the mid-IR cluster galaxies were associated with an X-ray AGN. That we find a factor of 3 greater AGN/LINER activity is probably because the X-ray data used in those studies is only sufficiently deep to detect AGN with $L_x > 10^{41}$ erg s^{-1}, which is typical for classical AGN, but much brighter than the average L_x of LINERs which is $\sim 2.5 \times 10^{40}$ erg s^{-1} (Gonzalález-Martín et al. 2006). Given that the optical spectra in Marcillac et al. (2007) and Bai et al. (2007) do not cover the Hα, [NII], and [SII] emission-lines, they cannot unambiguously identify mid-IR sources associated with LINERs. Our results are in better agreement if we consider that only one of the [24μm] sources in our sample is associated with a Seyfert galaxy (PAL-10_2_15). Assuming it would be detected in the X-ray, the AGN fraction in our cluster sample would be 5%. Still, we note that both our data and the Marcillac et al. (2007) and Bai et al. (2007) data suffer from small number statistics. Assuming Poisson errors, our AGN fraction is 19% $\pm$ 9% and their AGN fraction would be 6% $\pm$ 4%, so would be consistent within 1σ. Still, the fact that those studies find no LINERs in a sample of 30 a sample of cluster galaxies suggests they may be missing these objects because their AGN are selected based on X-ray properties.

Overall, the most important result from the classification of the cluster [24μm] galaxy spectra is that star forming galaxies dominate these sources. Similar to previous work it shows that classical AGN are not a major component of the cluster mid-IR sources; however, LINERs may represent a small, but non-negligible (14%) subset of cluster [24μm] sources. If the LINER activity is primarily driven by star formation,
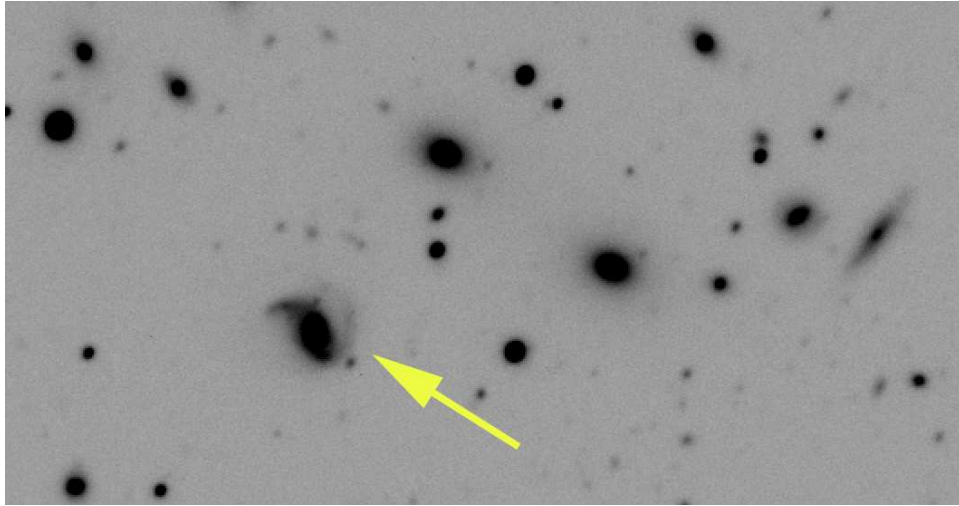
Figure 5.16 A high-contrast image of the central region of Cluster 8. The galaxy spHect-134-212 is marked with the yellow arrow. The galaxy is classified as a LINER and is the only [24μm] cluster galaxy with obvious signs of an ongoing interaction. The two bright galaxies near the center of the image are the two brightest cluster galaxies. The angular size of the tails of spHect-134-212 span a diameter of $\sim 12''$ (~ 48 kpc), which shows that they are too large to be consistent with an amorphous disk.

then 95% of the cluster [24μm] sources can be associated with star forming galaxies. If the LINER activity is primarily from an AGN, then this means only 80% of the [24μm] sources are associated with star formation, and that this AGN component will need to be accounted for in future studies.

5.6.2   The k+a and k 24μm Galaxies

Another interesting result from the spectroscopy is that there are three [24μm] galaxies with spectra classified as k-type and three with spectra classified as k+a type. Excluding spHect-134-212 which is a LINER, the other five galaxies appear to have old stellar populations (i.e., with well-developed Balmer absorption lines and a 4000Å break) but atypical of old stellar populations, they have the Hα line in emission. The strong [24μm] emission from these galaxies coupled with the presence of weak Hα and negligible [OII] suggests that these galaxies do have ongoing star formation, but that the star formation is highly dust-extincted (we discuss this further in § 5.3 and § 5.4).

The origin, nature, and even definition of the k+a class of galaxies has been a widely debated subject. Normally these galaxies have been interpreted as "post-

starburst" galaxies with no ongoing current star formation. It was Poggianti et al. (1999) who first proposed the possibility that k+a galaxies may actually have ongoing star formation but that it is so dusty as to completely obscure the nebular emission lines. Radio observations of low redshift field k+a galaxies have failed to detect radio continuum or 21 cm emission in the majority of these galaxies, demonstrating that it is unlikely that this is the case (Chang et al. 2001; Miller & Owen 2001; Goto 2004). However, in a 1.4GHz radio observation of the cluster Cl 0939+4713 at $z = 0.41$, Smail et al. (1999) detected 10 cluster galaxies, of which 5 were k+a/a+k galaxies, 3 were k galaxies, 1 was e(a) and the last was unclassified. Using these data they argued that the high redshift cluster k+a's may indeed be highly obscured dusty starburst galaxies. Recently, Blake et al. (2004) studied the properties of k+a galaxies in the 2dFGRS. They selected k+a galaxies using two methods, one based on a weighted average of the H$\beta\delta\gamma$ EWs and one based solely on the EW of Hδ. They found that only 8% of the "weighted" sampled had detectable signs of Hα emission, while by stark contrast 58% of those in the purely Hδ sample had Hα emission.

These studies, coupled with our own detection of k and k+a galaxies in the mid-IR, suggest that the k and k+a types are a bimodal group of galaxies with some fraction having ongoing mild, dust-obscured star formation, while the remainder are bona fide post-starburst or post-star formation galaxies. It is possible that the dusty star forming k and k+a galaxies are related to the e(a) galaxies where these galaxies are actually the same type of objects just with varying levels of ongoing dusty star formation or dust extinction.

What is perhaps most surprising about our data, as well as the Smail et al. (1999) data, is that mid-IR or radio emission is detected more frequently in k and k+a galaxies than in e(a) galaxies in distant clusters. Given that the majority of LIRGs in the Poggianti & Wu (2000) were e(a) galaxies, and none were k or k+a galaxies this was not expected. This, coupled with the fact that the majority of cluster [24μm] galaxies are e(c) galaxies suggests a real difference between the cluster mid-IR galaxies and the local LIRG population. Combined the e(c), k+a, and k class constitute 85% of the cluster [24μm] galaxies while they are only 25% of the local LIRG sample. Likewise e(a) galaxies are only 10% of the cluster [24μm] galaxies while they are 56% of the local LIRGs.

We suggest that there are two possible scenarios which may explain why the cluster [24μm] population is different. Both scenarios start with the infall of isolated, dusty star forming galaxies (i.e., [24μm]-detected e(c) galaxies) into the cluster. If those

galaxies have their star formation truncated by the intra-cluster medium, then they would plausibly become k+a and k galaxies. The presence of Hα and [24μm] emission could come from the ignition of a secondary burst of star formation in the galaxy, possibly by tidal forces encountered in the first pass through the central gravitational potential of the cluster. Provided this triggered star formation is dusty and weak it would superpose only mild Hα and no [OII] emission on the spectra; effectively resulting in a k or k+a spectrum with [24μm] emission and weak Hα emission. Conversely, it is possible that if the truncation process is exponentially declining (i.e., most of the star formation is halted upon immediate contact with the ICM, but with a tail of small residual star formation) such that a k+a or k spectrum is created, but with just a small residual amount of star formation superposed.

This evolutionary track for cluster [24μm] sources is speculative, and modeling using stellar synthesis codes will be crucial to proving its plausibility. Such modeling is beyond the scope of the current paper and we leave it to future work. Still, it is clear that the moderate redshift cluster [24μm] population is different from the local LIRG population and that some scenario which involves the environment of cluster galaxies will almost certainly be required to explain this difference.

5.6.3   IRAC/Optical Colors of the 24μm Population

One of the concerns with classifying mid-IR sources using optical spectroscopy is that dust extinction may confuse the classification. One way to test the spectroscopic classifications is to use the mid-IR colors available for these galaxies. Lacy et al. (2004) and Stern et al. (2005) showed that AGN could be differentiated from dusty star forming galaxies based on their IRAC colors. In the top panels of Figure 17 and 18 we plot the [3.6μm] - [4.5μm] vs. [5.8μm] - [8.0μm] colors of all the spectroscopically confirmed cluster galaxies in the high and low redshift samples, respectively. As a comparison, we also include the colors of some of the cluster red-sequence galaxies which are not detected at [24μm] and are classified as k galaxies in the DG scheme. The points are labeled by the spectral types of the galaxies. The galaxy spHect-134-257 does not have an unambiguous IRAC counterpart in our catalogue so it is omitted from this analysis. The dashed region in the top panels of the figure represents the location typically occupied by broad-line AGNs (BLAGNs). Narrow-line AGN (NLAGNs) and dusty starburst galaxies tend to lie to the lower-right of these galaxies (see Stern et al. 2005,

Figure 1), and k-type galaxies have colors similar to stars and are located to the lower-left.

Figures 17 and 18 show that the majority of the cluster [24μm] sources lie in the location of dusty star forming galaxies or NLAGN. Within the color errors there are no galaxies with BLAGN colors suggesting that we are not missing a significant amount of dusty AGN activity in the clusters and that the classification of the [24μm] galaxies from the optical spectra is consistent with their mid-IR colors.

One of the major assumptions by M07 was that a subset of the [8.0μm] cluster galaxy population were dusty starburst galaxies with R - [3.6μm] colors redder than the cluster red-sequence. In the bottom panels of Figures 17 and 18 we plot the R - [3.6μm] vs. [3.6μm] color-magnitude relation of the cluster members. The R - [3.6μm] color of an M* red-sequence galaxy is shown as the dashed line. As expected, the galaxies with k spectra have the color of red-sequence galaxies. Interestingly, the [24μm] sources show a wide array of R - [3.6μm] colors relative to the red-sequence. Of the 20 cluster [24μm] sources plotted in Figures 17 and 18, 5 (25%) have R - [3.6μm] colors within 1σ of the cluster red-sequence, 5/20 (25%) have colors more than 1σ bluer than the red-sequence and 10/20 (50%) have colors more than 1σ redder than the red-sequence. All three AGN/LINERs in the sample are red, and removing those shows that the ratio of star forming [24μm] galaxies with colors bluer than the red-sequence to those with colors as red or redder than the red-sequence is 5/12. Given that the spectroscopy was selected in the R-band, it is likely that more [24μm] cluster members with red R - [3.6μm] colors are missed and that if anything, this ratio is an upper limit on this fraction. Figures 17 and 18 clearly show that there is a significant population of red star-forming cluster galaxies and demonstrates that cluster blue fractions may be far-from-complete metrics of the overall level of star formation in clusters. Such an idea was already suggested by Wolf et al. (2003) who showed using COMBO-17 data that 30% of the red-sequence galaxies in Abell 901/902 were better fit with dusty templates than with early-type templates.

M07 assumed that the ratio of blue to red [8.0μm] star forming galaxies was ~ 2, whereas the above spectroscopy shows that for galaxies selected at [24μm] the ratio is more like 0.5. This suggest that M07 may have *underestimated* the contribution of dusty star forming galaxies by as much as a factor of 4. Still, a [24μm] detection is a cleaner measure of purely star forming galaxies than an [8.0μm] detection (there may be some contamination of "red" [8.0μm] galaxies by massive systems with an all but negligible amount of star formation) and this may increase this factor somewhat for

the [8.0μm] galaxies. Still, M07 showed that using ratios between 1-3 has little effect on their conclusions. We recomputed the models of M07 assuming the blue to red fraction of star forming galaxies was 0.5 instead of 2, and find that this actually produces better models for the $z > 0.4$ [8.0μm] LFs (see their Figure 18).

Another interesting result from the CMR of the high redshift clusters is the apparent segregation on the CMR of starbursts/AGN and SF galaxies. Most frequently, SF galaxies are fainter galaxies and tend to lie in the region of the so-called "blue cloud". None of the starburst galaxies or AGN lie in the blue cloud. The majority of these are bright galaxies that have colors similar to, or redder than the red-sequence. This segregation suggests that there may be three distinct populations of [24μm] cluster galaxies. Normal SF galaxies which inhabit the "blue cloud", dusty starburst galaxies which have colors similar to the red-sequence, and AGN, which may have red colors because they are contained mostly within early-type galaxies.

5.6.4 Dusty Starbursts?

In § 5.3 we showed that $\sim 2/3$ of the star forming cluster galaxies detected at [24μm] had R - [3.6μm] colors as red or redder than the cluster red-sequence. We also showed in § 5.2 that $\sim 20\%$ of the cluster galaxies detected at [24μm] have negligible [OII] emission, but some level of Hα emission. Both of these results are evidence that there is a population of highly extincted dusty star forming galaxies in clusters.

Poggianti et al. (1999) demonstrated that one way to statistically separate dusty star forming galaxies from regular star forming galaxies is to use a plot of the EW of [OII] vs. EW of (Hα + [NII]). They compared their galaxies to the relation of Kennicutt (1992) who showed that local star forming galaxies tend to follow the correlation EW([OII]) = 0.43EW(Hα + [NII]). Poggianti & Wu (2000) showed that many of the local LIRGs had ratios that put them below this line, demonstrating that it is a reasonable diagnostic of dusty star formation[5].

In Figure 19 we plot the EW([OII]) of the cluster [24μm] sources as a function of their EW(Hα + [NII]). Galaxies with R - [3.6μm] colors redder than the cluster red-sequence are plotted with solid circles and those with colors similar to, or bluer than the red-sequence are plotted with open diamonds. The solid line in the diagram is the

---

[5]Again, because the [OII] line is more sensitive to the metallicity and ionization state of the gas in the galaxy than Hα, there is a fairly significant scatter in this correlation. Therefore, EW ratios below the standard correlation does not guarantee that a given galaxy contains dusty star formation; however, an ensemble average below the relation would suggest that dust does play a role.
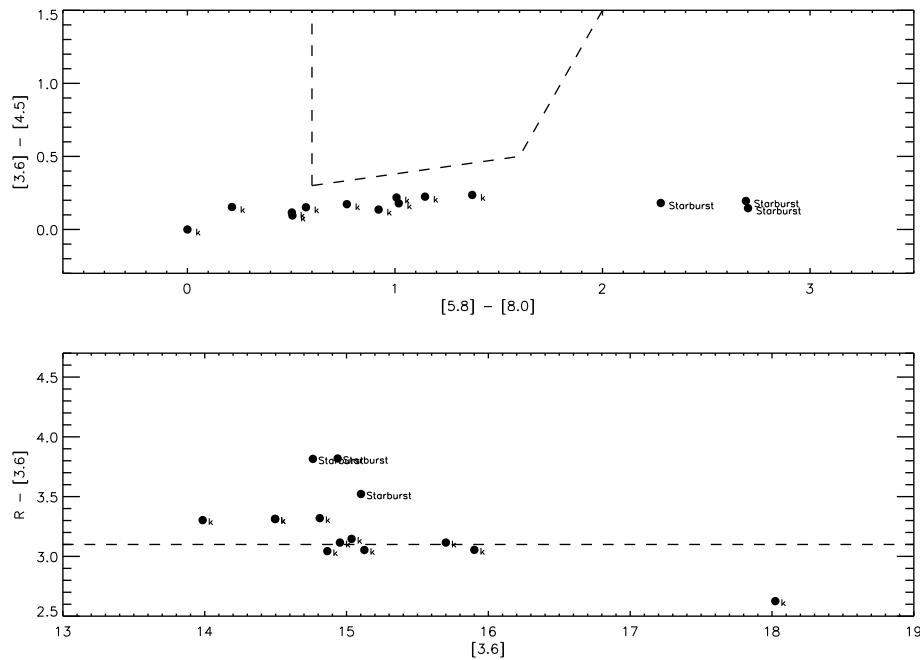
Figure 5.17 Top Panel: plot of the [3.6μm] - [4.5μm] vs. [5.8μm] - [8.0μm] colors of cluster [24μm] galaxies as well as cluster red-sequence members in the low redshift clusters. The spectral type of each point is labeled. The dashed region is the location primarily occupied by BLAGN. The cluster galaxies do no occupy this space and have IRAC colors consistent with star forming galaxies. Bottom Panel: Plot of R - [3.6μm] vs. [3.6μm] for the same galaxies. The dashed line is the color of an M* cluster red-sequence galaxy. This panel and the bottom panel of Figure 17 show that a significant fraction of star forming cluster [24μm] sources are as red, or redder than the red-sequence.

relation EW([OII]) = 0.5EW(Hα + [NII]). The coefficient of 0.5 is slightly steeper that the coefficient of 0.43 reported by Kennicutt (1992); however, it provides a much better fit to the star forming galaxies in the samples of Poggianti et al. (1999) and Poggianti & Wu (2000) (see their Figures 5 and 3, respectively) as well as our own sample. The coefficient of 0.43 from Kennicutt (1992) is a good fit to galaxies with EW([OII]) < 10; however it is clearly too shallow for galaxies with EW([OII]) > 10. This was missed by Kennicutt (1992) because his sample was dominated by low redshift (z < 0.1) galaxies which frequently have EW([OII]) < 10, whereas at higher redshift, galaxies with EW([OII]) > 10 are much more common.

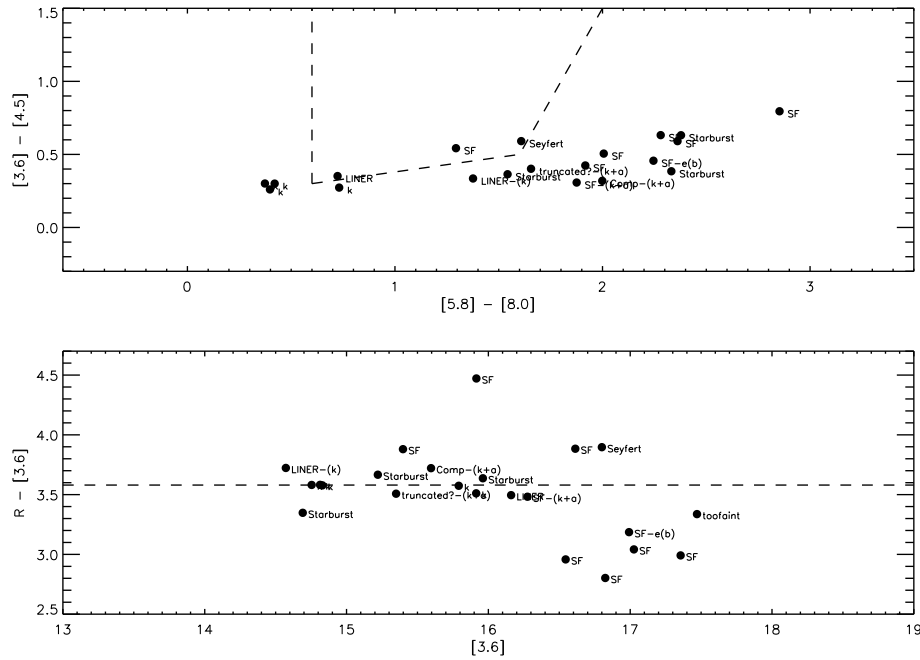Figure 19 demonstrates that the [24μm] galaxies that are redder than the cluster

Figure 5.18 As Figure 17, but for the high redshift clusters.

red-sequence tend to have lower EW([OII]) given their EW(Hα + [NII]) than their blue counterparts, and that they lie below the typical correlation for normal star forming galaxies. The dashed line in Figure 19 is a least-squares fit to these galaxies. The best-fit slope is 0.17 ± 0.03 which is similar to the slope of 0.20 ± 0.03 measured by Poggianti & Wu (2000) for the local LIRGs. The combination of the red R - [3.6μm] colors and the low EW([OII])/EW(Hα + [NII]) ratio shows that these galaxies are undoubtedly extincted dusty star forming galaxies.

Although many of the [24μm] galaxies are highly extincted dusty star forming galaxies, the remainder are not. Figure 19 clearly shows that *a significant detection at [24μm] does not guarantee that there is a strong level of dust extinction within that galaxy.* In fact, it suggests that there is a dichotomy in the cluster [24μm] population with ∼ 50% of the sources being strongly extincted star forming galaxies while the other 50% seems to have the same level of extinction as normal star forming galaxies.

It is unclear what causes this dichotomy in the [24μm] population. It might be reasonable to assume that there are two basic modes of star formation within galaxies, normal (which still has dust, but not a strong screen of dust obscuration) and dusty (which is highly extincted), and that regardless of which type of star formation it has, a galaxy will be detected at [24μm] provided its SFR is high enough. Clearly the op-

tical spectra of these galaxies will have different properties, probably much like the dichotomy seen in Figure 19. While this appears to be a reasonable explanation for the dichotomy in 24$[\mu m]$ sources, it cannot be the entire picture.

Marcillac et al. (2007) showed clearly that not all of the cluster star forming population are detected at $[24\mu m]$. In fact, only 2/15 e(b) galaxies in RX J1052.7-1357 were detected at $[24\mu m]$ and this is notable because e(b) galaxies are the category for the strongest star forming galaxies, being defined as those with EW([OII]) > 40Å. These galaxies show that there can clearly be vigorous star formation without a significant dust presence. The whole picture then shows that both starbursts and normal star forming galaxies can be, but are not necessarily, detected at $[24\mu m]$. Moreover, those detected at $[24\mu m]$ can be highly dust obscured, have almost no dust, or, have a normal level of dust for a star forming galaxy. This suggests there is a large variety in the way that star formation occurs within in these galaxies and it likely that more data will be needed to understand the reasons for the large variation in the dust properties of star forming galaxies (e.g., higher resolution imaging to test if dusty galaxies are perhaps more frequently associated with mergers or harassments which "stir-up" the gas and dust).

Although it hard to interpret the differences in the $[24\mu m]$ population, Figure 19 does show that the R - $[3.6\mu m]$ color of cluster $[24\mu m]$ sources relative to the cluster red-sequence is a good indicator of whether or not they have strongly dust extincted star formation. It also demonstrates that cluster star formation rates measured from [OII] alone will almost certainly underestimate the total amount of star formation. Given that there is already a significant population of these galaxies in clusters at $z \sim$ 0.12 - 0.25, this could be even more severe at higher redshift where galaxies tend to be even more dusty on average. This is an important caveat because at higher redshift Hα is shifted into the IR and cluster SFR are almost exclusively measured from [OII] (e.g., Poggianti et al. 2006). More mid-IR studies of distant clusters will clearly be needed to explore this issue further.

5.7   Redshift Evolution of Cluster 24μm Galaxies

Previous studies of cluster mid-IR galaxies have suggested that the number and average luminosity of mid-IR galaxies in clusters is increasing with increasing redshift (e.g., Coia et al. 2005; Geach et al. 2006; Marcillac et al. 2007; Bai et al. 2007). The evi-
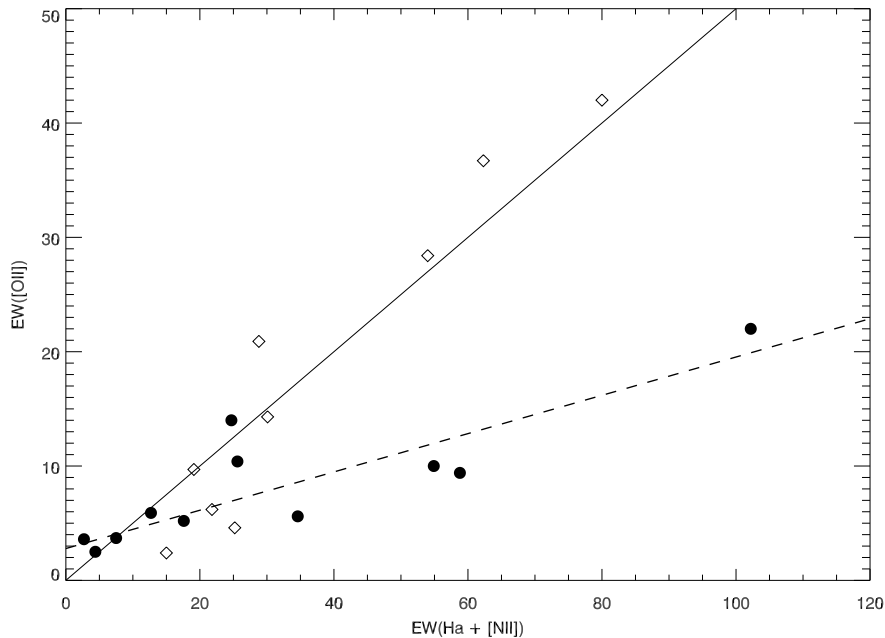
Figure 5.19 Plot of the EW([OII]) vs. the EW(Hα + [NII]) for [24μm] cluster galaxies. Solid circles are galaxies with R - [3.6μm] colors redder than the cluster red-sequence, and open diamonds are for all other galaxies. The solid line is the a slightly modified version of the correlation between these EW in local galaxies (see text). The dashed line is a least-squares fit to the red galaxies and has a slope about a factor of 2 shallower than the correlation for local galaxies. This shows that on average, the solid circles have lower EW([OII]) at a fixed EW(Hα + [NII]) which suggests that they are dust obscured star forming galaxies.

dence for the increase is compelling because spectroscopic redshifts have been used to confirm that the mid-IR sources are cluster galaxies; however, the increase in sources seen in these four studies is based on a combined sample of only 8 clusters. As we demonstrated in § 3, the number of [24μm] sources can vary significantly from cluster-to-cluster, even for objects with relatively similar masses at similar redshifts. The possibility remains that the increase could be caused by the choice of the cluster sample, and may not reflect the evolution in the overall population.

In this section we use the M07 catalogue of 99 clusters at $0.1 < z < 1.3$ to further investigate whether there is an increase in the number of mid-IR galaxies in clusters as a function of redshift. This sample is about an order of magnitude larger than the combined previous work and should give a more robust measurement of the evolu-

tion of mid-IR cluster galaxies. We also compare our results to the number of mid-IR galaxies that would be expected in a field sample with an equivalent number of mass-selected galaxies using the field LFs of Babbedge et al. (2006).

We proceed with a simple procedure which is to stack clusters at similar redshifts and look for a statistical overdensity of galaxies above some flux limit. While the choice of flux limit can be arbitrary, it is sensible to tie the flux limit to objects with familiar luminosities such as LIRGs, ULIRGs, and hyper luminous infrared galaxies (HyLIRGs, $L_{IR} > 10^{13}$ L/L$_\odot$). This requires the conversion of F_{24} in units of νL_ν/L$_\odot$ to L_{IR}[6], which depends on the SEDs of the galaxies. Given that we use statistical background subtraction, we cannot model the SEDs of individual galaxies (nor do we have enough filter coverage that this would be advisable even if redshifts were available). Fortunately, significant effort has already been invested in understanding the conversion of [24μm] fluxes to L_{IR} without proper modeling of the full SED.

In general, it has been shown that even with the large variety of IR SEDs that have been modeled (e.g., Silva et al. 1998; Devriendt et al. 1999; Dale et al. 2001), the vast majority provide the same values of L_{IR} for a given [24μm] flux, with the maximum variance being a factor of $\sim$ 2-3 (e.g., Papovich et al. 2002, Bell et al. 2005; Choi et al. 2006; Papovich et al. 2007). It has also been shown that the local SEDs are a reasonable description of mid-IR luminous galaxies above $z > 0.7$ (e.g., Elbaz et al. 2002; Appleton et al. 2004), with the possible exception of the most luminous galaxies at z > 1.5 (Papovich et al. 2007). Given that these studies show that the choice in SED in not particularly important in determining a rough L_{IR}, we adopt the conversion factor used in Bell et al. (2005), $L_{IR} = 10\nu L_\nu$/L$_\odot$. Bell et al. (2005) determined this conversion factor by averaging over all the Dale et al. (2001) templates. Comparing to the models they showed that this conversion provides L_{IR} estimates which have an rms scatter of a factor $\sim$ 2 around the true values.

We stress that because all overdensity measurements (both cluster and field) are made in units of νL_ν/L$_\odot$, not L_{IR}, the measurement of the overdensity depends in no way on the uncertainty in the conversion to L_{IR}. The uncertainty in this conversion only implies that we may not know if the chosen luminosity limits correspond directly to, for example, the LIRG class (e.g., $10^{10} < \nu L_\nu$/L$_\odot < 10^{11}$ which implies $10^{11} < L_{IR} < 10^{12}$, or a LIRG). It may be that our LIRG luminosity cut corresponds to a slightly brighter or fainter range of luminosities than true LIRGs; however, the luminosity cuts

---

[6]This integral depends on the SED of the galaxy, and therefore, sampling the SED at only one bandpass can potentially lead to large uncertainties in L_{IR}.

are still correct relative to each other. This is not particularly important because the definitions themselves are arbitrary. Galaxies with $L_{IR} = 0.99 \times 10^{12}$ $L_\odot$ are probably not really a different class than those with 1.01×10^{12} $L_\odot$, despite the fact that they are classified as LIRGs and ULIRGs, respectively.

The overdensity of galaxies in the cluster fields is measured by counting the number of background-subtracted galaxies above some apparent flux limit. The apparent flux limits at each redshift are determined by converting the adopted absolute luminosity limits to apparent fluxes using the equation,

$$F_{24,lim} = \frac{\nu L_\nu}{4\pi D_L^2 \cdot \nu \cdot 10^{k/2.512}} \tag{5.5}$$

where D_L is the luminosity distance and the factor k is the adopted k-correction.

Although the choice of L_{IR} conversion factor does not affect the relative overdensities as a function of redshift, the choice of k-correction can have an impact on this measurement. The most significant differences in the [24μm] k-corrections are for star forming galaxies as compared to AGN. This is because the cool dust in the SEDs of star forming galaxies make them steeper in the mid-IR (i.e., more rapidly increasing with increasing λ) than AGN, which have power-law shapes. In order to demonstrate the importance of k-corrections we plot the mid-IR spectra from *ISO* of M82 (Sturm et al. 2000), which is the prototypical dusty starburst galaxy, and NGC 1068 (Lutz et al. 1997), which is an IR-luminous Seyfert galaxy, in the left panels of Figure 20. In the right panels of Figure 20 we plot the [24μm] k-corrections for these galaxies. The k-correction for M82 is about a factor of two larger (in magnitudes) than the NGC 1068 k-correction at most redshifts. Given that the AGN fraction in the subset of clusters studied so far, including our own, is very low ($\sim$ 5%), we adopt the M82 k-correction for this analysis[7]. M82 is a dusty forming galaxy, but is classified as a LIRG, not a ULIRG, so is probably more typical of cluster mid-IR galaxies.

Assuming the Bell et al. (2005) L_{IR} conversion factor, and the M82 k-correction, the 350 μJy flux limit of the FLS corresponds to a LIRG, ULIRG, and HyLIRG at $z \sim$ 0.3, 0.5, and 1.2 respectively. We measure the overdensity of [24μm] galaxies at R < R_{200} above these flux limits as a function of redshift by stacking the clusters below these redshift limits and statistically subtracting the background. The resulting overdensities are plotted in Figure 21. The red, blue and green filled circles represent the

---

[7]We note that using the NGC 1068 k-correction does not significantly affect the overdensity results in this section. As we will discuss, it appears that very bright mid-IR galaxies are rare in clusters, regardless of the choice of k-correction

average number of galaxies per cluster with L > L$_{lim}$ where L$_{lim}$ is a HyLIRG, ULIRG, and LIRG respectively.

Figure 21 clearly demonstrates that both ULIRGs are HyLIRGs are rare in clusters. The average cluster has zero HyLIRGs between $z = 0.2$ and $z = 1.0$, and < 1 ULIRG between $z = 0.2$ and $z = 0.5$. The number of ULIRGs associated with clusters appears to not evolve between $z = 0.1 - 0.5$, and the overall number is consistent with zero per cluster at $<1\sigma$. Although we have a very small redshift range at which we are sensitive LIRGs, there appears to be a rapid evolution in the number of these objects between $z = 0.2$ and $z = 0.3$. The number of LIRGs in clusters at $z = 0.3$ is ~ 50 times larger than at $z = 0.2$. The error bars on both of these data points are large because they comprise only a few clusters (7 per bin); however, using even the 1σ upper limit allowed by $z = 0.2$ bin shows that the number of LIRGs increases by at least a factor of ~ 3 at greater than 68% confidence level (c.l.). This result is in agreement with previous studies which found no LIRGs in clusters at $z < 0.2$ (e.g., Boselli et al. 1998; Fadda et al. 2000; Duc et al. 2002; Biviano et al. 2004) and those which have found LIRGs in every cluster above $z > 0.3$ that has been studied studied thus far (Coia et al. 2005; Geach et al. 2006; Marcillac et al. 2007; Bai et al. 2007). It is also consistent with the M07 results from the [8.0μm] LFs of the same clusters that showed that at $z > 0.4$ the cluster LFs could no longer be described by normal star forming galaxies and that an additional population of dusty star forming galaxies was required.

The increase in the number of LIRGs is also in good agreement with studies of LIRGs in the field. LIRGs are very uncommon in the field until $z \sim 0.2$, whereupon their abundance increases significantly (e.g., Elbaz et al. 2002; Pérez-González et al. 2005; Le Floc'h et al. 2005). The same studies have shown that ULIRGs are uncommon in the field until $z > 1$, which is also consistent with the cluster results.

In order to better illustrate the relative evolution between the cluster and field, the solid red, blue, and green lines in Figure 21 represent the number of HyLIRGs, ULIRGs, and LIRGs that would be expected in the field for an equivalent amount of stellar mass as contained in a 3 x 10^{14} M/M$_\odot$ cluster. The solid lines are computed using the [24μm] LFs of Babbedge et al. (2006). Those LFs are also measured in units of $\nu L_\nu / L_\odot$ and therefore the relative overdensity compared to the clusters is correct. The number of [24μm] galaxies in the field is converted to the number expected for the same stellar mass in clusters using the [3.6μm] LFs of Babbedge et al. (2006) and M07 by assuming that the stellar mass of galaxies is directly proportional to their F$_{3.6}$. We divide the cluster ϕ^* in units of number/cluster/3 x 10^{14}M/M$_\odot$ by the field ϕ^*, which

gives a normalization for the same number of $[3.6\mu m]$ galaxies between the cluster and field LFs. The number of galaxies with $L > L_{lim}$ is then computed from the field $[24\mu m]$ galaxies and scaled by this normalization.

The evolution of the field values demonstrate what was already discussed qualitatively above, namely that the density of HyLIRGs and ULIRGs is very low in the field at $z < 1.0$, and that the slow evolution in clusters is consistent with the slow evolution in the field. The number of LIRGs in the field increases by approximately a factor of 6 between $z = 0.125$ and $z = 0.375$ and appears to slow down thereafter. It is possible that the increase of LIRGs in clusters with increasing redshift may be more rapid than in the field; however, this is based on one data point and is only significant at slightly $> 1\sigma$.

One way to test how robust these statistical results are is to compare them with the number of LIRGs and ULIRGs that have been spectroscopically confirmed in the few clusters studied thus far. The number of confirmed LIRGs and ULIRGs in our clusters as well as MS 0024+16 (Coia et al. 2005) and MS 1054-03 (Bai et al. 2007) and RX J0152.7-1357 (Marcillac et al. 2007) are overplotted in Figure 21 as the green arrows and open blue squares respectively. LIRGs are plotted as lower-limits because spectroscopic redshifts have not been obtained for every galaxy in the fields of the these clusters that has an F_{24} consistent with being a cluster LIRG. ULIRGs are not plotted as lower limits because all galaxies in the cluster fields with F_{24} bright enough to be a cluster ULIRG have been spectroscopically confirmed as a non-cluster member. The masses for CL 0024+16, MS 1054-03 and RX J0152.7-1357 have been taken from the weak lensing studies of Kneib et al. (2003), Jee et al. (2005a), and Jee et al. (2005b) respectively.

Although there is a large scatter, these data points are broadly consistent with the results from the statistical background subtraction of the larger cluster sample, which suggests that it provides a good estimate of these values. The main result from Figure 21 is that the evolution of LIRGs, ULIRGs, and HyLIRGs in clusters is not significantly different in the cluster and field environments. This result is interesting because it appears to conflict with the results of M07 which suggested a significant difference in the evolution of mid-IR galaxies between the cluster in field. In fact, it is completely consistent with the results of M07. The $[24\mu m]$ photometry, while cleaner at selecting purely dusty star formation than $[8.0\mu m]$ photometry, is much shallower. Examining the M07 $[8.0\mu m]$ LFs (their Figure 22) shows that galaxies with $L > 10^{11}$ $\nu L_\nu / L_\odot$ (ULIRGs) show no significant change relative to the relative to the field at

$z = 0.15 - 0.65$. Also, galaxies with $L > 10^{10}$ $\nu L_\nu / L_\odot$ (LIRGs) at $z = 0.15 - 0.33$ show only a mild change relative to the field, and are roughly consistent with the field. This is also consistent with the $[24\mu m]$ data, except that it appears the cluster is slightly more abundant compared to the field when the measurement is made with the $[24\mu m]$ data, but is slightly underabundant compared to the field when the measurement is made with the $[8.0\mu m]$ data. Still, the number of clusters used at these redshifts is relatively small and the Poisson errors are large.

The significant differential evolution between the field and cluster claimed by M07 is based on the galaxies with $L > 10^{10}$ $\nu L_\nu / L_\odot$ in the $z = 0.65$ LFs. Unfortunately, the $[24\mu m]$ data does not reach an equivalent depth so that the same measurement can be made. Still, the steep increase in $[24\mu m]$ sources between $z = 0.2 - 0.3$ suggests that this trend could continue and that deeper $[24\mu m]$ data may be in agreement with the $[8.0\mu m]$ data.

Given that the only notable increase in the cluster mid-IR sources with redshift appears to come at the lowest luminosities observable in the FLS, a deeper study of a large sample of clusters would be worthwhile. Also, given the rarity of ULIRGs and HyLIRGs, a much larger statistical sample would also be worthwhile. The *Spitzer* Wide-area InfraRed Extragalactic Survey (SWIRE; Lonsdale et al. 2003) is a factor of 13 larger in area than the FLS, and the MIPS $[24\mu m]$ data is a factor of 1.4 deeper. A comprehensive look at the overdensity of $[24\mu m]$ sources in clusters in those fields detected in the RCS-2 (Yee et al. 2007) and SpARCS (Wilson et al. 2006) surveys is currently being undertaken (Battaglia et al. 2007, in preparation). Preliminary results of that work using a sample of ~ 900 clusters are in excellent agreement with our results (N. Battaglia, private communication).

5.8   Summary

We have presented a large spectroscopic and statistical study of $[24\mu m]$ cluster galaxies. Statistical background subtraction shows that the majority of $[24\mu m]$ sources ($\sim$ 80%) in the fields of moderate redshift clusters are background galaxies; however, using a large set of spectroscopic redshifts we identified 21 $[24\mu m]$ cluster members in four clusters at $0.12 < z < 0.25$. Using the spectroscopic redshifts we examined the radial profile of the $[24\mu m]$ sources. We find that the radial profile is poorly constrained by our data, but is consistent consistent with being flat out to $R \sim 1.5R_{200}$.
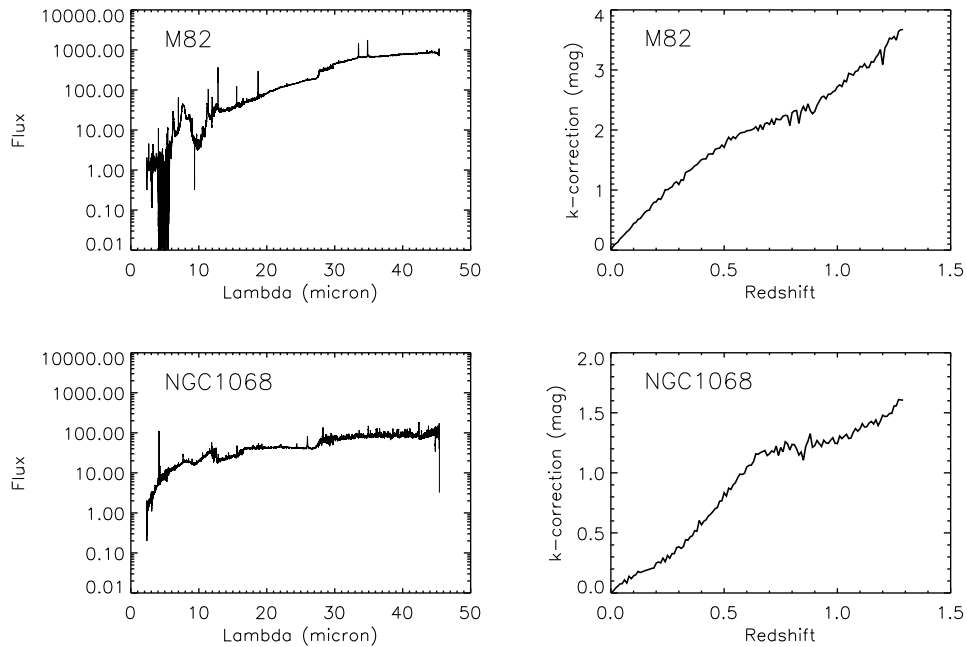
Figure 5.20 Left Panels: *ISO* Mid-IR spectra of the dusty starburst galaxy M82 (from Sturm et al. 2000) and the ULIRG Seyfert galaxy NGC 1068 (from Lutz et al. 1997). Left Panels: [24μm] k-corrections for these spectra in magnitudes. The IR SEDs of starburst galaxies are generally much steeper than AGN due to a cooler dust temperature, and therefore the k-corrections are much larger.

Using the optical spectra we classify the [24μm] galaxies as either star forming galaxies, starbursts, Seyferts, LINERs, or truncated galaxies using BPT diagrams. The classification shows the majority of cluster [24μm] galaxies ($\sim 80\%$) are associated with star forming galaxies, but that the specific types of the [24μm] galaxies make them a very heterogeneous subset of galaxies. The most common types of cluster [24μm] sources are regular star forming galaxies (i.e., consistent with local spirals) and starbursts. These two types make up $\sim 40\%$ and 30%, respectively, of the entire cluster [24μm] population. Approximately 5% of cluster galaxies are associated with AGN in our sample, which agrees well with previous studies. We find that $\sim 15\%$ of cluster [24μm] sources are associated with LINERs. This is the first confirmed detection of mid-IR luminous LINERs in clusters, and shows that although these objects do not make up a large fraction of the overall cluster mid-IR population, they are sufficiently abundant that they will need to be accounted for in future modeling.

We also classify the optical spectra of the [24μm] galaxies using the DG scheme. In

this classification the majority of cluster [$24\mu m$] galaxies are classified as e(c) galaxies ($\sim 60\%$). By contrast, only 10% of cluster galaxies are classified as e(a) galaxies. These percentages are significantly different from the average classification of local LIRGs, which are most frequently found to be interacting systems with e(a) spectra (56%). This suggests that the average cluster LIRG at $0.12 < z < 0.25$ is not an analogue of the average local LIRG. Approximately 25% of local LIRGs are e(c) galaxies with few signs of interactions, and we suggest that the cluster LIRGs are probably more similar to this subpopulation of the local LIRGs.

Approximately 25% of the cluster [$24\mu m$] galaxies are classified as k or k+a galaxies in the DG scheme, yet all of these show Hα in emission. This suggests that they have ongoing dusty star formation that has completely obscured the [OII] emission line. Furthermore, examination of the R - [$3.6\mu m$] colors of the [$24\mu m$] galaxies shows that the majority have colors as red, or redder, than the cluster red-sequence ($\sim 75\%$). This demonstrates that there is a population of red star forming galaxies in clusters and that cluster blue fractions are incomplete estimates of the total star formation within a cluster.

We compare the EW([OII]) to the EW(Hα + [NII]) for the [$24\mu m$] galaxies and find that the population appears to be bimodal. Galaxies with R - [$3.6\mu m$] colors similar to, or bluer than, the red-sequence have EW([OII])/EW(Hα + [NII]) ratios that are consistent with normal blue star forming galaxies, demonstrating that some of the [$24\mu m$] population have dust properties similar to normal star forming galaxies. Galaxies with R - [$3.6\mu m$] colors redder than the red-sequence have a ratios that are about a factor of 2 smaller. This demonstrates that the [$24\mu m$] galaxies with red R - [$3.6\mu m$] colors have red colors because they are obscured dusty star forming galaxies.

Using the entire sample of 99 clusters in the field of the FLS we study the evolution in the abundance of [$24\mu m$] cluster galaxies with redshift. We find that the number of LIRGs in clusters increase by at least a factor of 3 at $> 68\%$ c.l. between $z \sim 0.2$ and $z \sim 0.3$. We find that ULIRGs and HyLIRGs are very rare in clusters. The average cluster has <1 ULIRG and HyLIRG up to $z \sim 0.5$ and 1.2, respectively. Comparing the redshift evolution of the abundance of LIRGs in clusters to the abundance in the field, we find that the number of LIRGs increases slightly faster in clusters; however, this is based on only one data point and is only significant at $<1\sigma$. The abundance of ULIRGs and HyLIRGs in clusters is similar to the field abundance and both are very close to zero. Overall, it appears that mid-IR luminous galaxies are as uncommon in clusters as they are in the field.
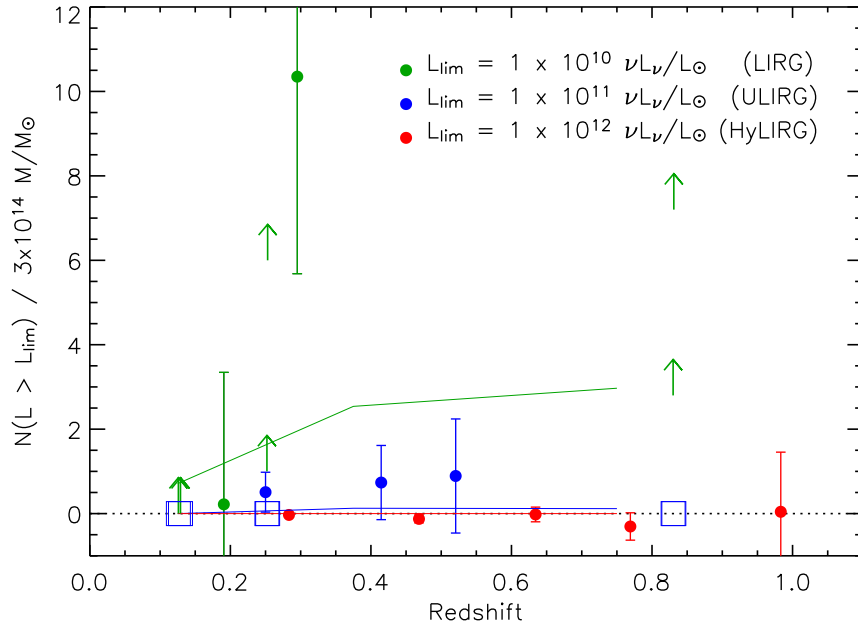
Acknowledgements

Figure 5.21 Plot of the overdensity of [$24\mu m$] galaxies in clusters as a function of red-shift normalized to a cluster mass of 3 x 10^{14} M/M$_\odot$. The green, blue, and red filled circles are ensemble averages of 7-23 clusters and represent the number of galaxies with luminosities brighter than a LIRG, ULIRG, and HyLIRG respectively (see text). The green, blue, and red solid lines represent the expected number of sources in the field from the [$24\mu m$] field LFs of Babbedge et al. (2006), normalized by the equivalent density of cluster galaxies using the LFs of M07. The green arrows at $z < 0.26$ represent lower limits on the number of spectroscopically confirmed members brighter than LIRGs in the four clusters in our spectroscopic sample. The green arrows at $z \sim$ 0.83 are data from MS1054-03 and RX J1052.7-1357 by Bai et al. (2007) and Marcillac et al. (2007) respectively. The open squares are for the same clusters but for spectroscopic members brighter than ULIRGs. The blue squares are not lower limits because all potential cluster ULIRGs in the fields of the clusters are confirmed non-members.

Chapter 6

Conclusions

In the four main chapters of this thesis we have presented results on the evolution of the NIR cluster scaling relations, the NIR cluster LFs, and the evolution and nature of MIR cluster galaxies. The thesis chapters stand alone as separate papers with their own conclusion sections, so it would be repetitious to include an additional summary of those chapters here. Instead, this brief concluding chapter is presented as a discussion connecting the results from the individual chapters into a larger picture of cluster galaxy evolution. We also include a short discussion of future work that can be done.

6.1   The Bigger Picture

Examining this thesis as a whole, one of the more interesting results is the ostensible disconnect between the evolution of the NIR and MIR properties of the cluster galaxies. Specifically, the luminosity evolution of the K-band, $[3.6\mu m]$, and $[4.5\mu m]$ cluster LFs are consistent with the luminosity evolution of a single burst population with a high formation redshift. The NIR cluster LFs are similar to field LFs in terms of the overall shape as well as the values of M^*. Chapter two also showed that the cluster NIR LF looked identical in clusters spanning one order of magnitude in mass. Given that NIR light is a good tracer of stellar mass it suggests that the stellar mass function of galaxies has little dependence on environment.

Contrast this with the evolution seen in the MIR properties of the cluster galaxies. The $[8.0\mu m]$ cluster LF showed a significant differential evolution between the cluster and field. Moreover, even within the cluster environment, the $[8.0\mu m]$ LFs showed the emergence of a new population of dusty starbursts at high redshift. These results suggest a rapid evolution in the star formation properties of the cluster galaxies as well as

a differential evolution in these properties between the cluster and field environments. Although this is the first time this has been seen in the MIR, it is far from a "new" discovery. We already knew from other lines of evidence such as the Butcher-Oemler Effect (e.g., Butcher & Oemler 1984; Ellingson et al. 2001) and spectroscopic studies of star formation in cluster galaxies (e.g., Poggianti et al. 1999; Poggianti et al. 2006) that there is an evolution in the star formation properties of cluster galaxies with redshift. Furthermore, there are additional changes in the cluster population with redshift such as the evolution in the morphology-density relation with redshift (e.g., Dressler et al. 1997; Postman et al. 2005; Smith et al. 2005).

These results present two obvious questions: Firstly, how can we reconcile the rapid change in the star formation properties and morphologies of cluster galaxies with the seemingly passive evolution of the stellar populations seen in the NIR LFs? Secondly, how can the fact that the NIR LFs appear to be similar, regardless of environment be reconciled with the MIR properties which seem to evolve differently in the field and cluster environment?

The first possibility, which was touched on a little in chapter two, is that the transformations in star formation properties and morphology seen in both clusters and field galaxies may be "superficial". This is to say that the majority of the stellar mass in the average galaxy was assembled at high redshift and that the ongoing star formation comprises just a small fraction of that total stellar mass. If this is the case, transformations in the star formation rates or morphologies of galaxies would have little effect on the underlying stellar population, and overall one might expect to see passive evolution in the NIR LFs.

Another possibility is that there are differences between the field and cluster NIR LFs, but they are too subtle to be measured with the current data. We showed in chapter two that the cluster K-band LF was brighter than the field by $\Delta M^* = 0.25 \pm 0.26$ magnitudes at $z \sim 0.3$. The uncertainty in that measurement corresponds to a factor of 1.3 in luminosity and stellar mass. It suggests that the average cluster galaxy could be as much as a factor of 1.3 times more massive than the average field galaxy. This raises the possibility that some of the transformations could come in the form of mergers. Put another way, a difference of a factor of 1.3 in mass would result if one out of every three cluster galaxies experiences one equal mass merger over a Hubble time. If mergers extinguish star formation and change disk galaxies into elliptical galaxies than this could explain how the NIR LFs of the cluster and field are appear similar at the precision of our data, but that the star formation properties and morphologies are

evolving differently.

This interpretation suggests that higher precision LFs for galaxies in both the cluster and field would be a useful endeavor. Even better would be a comparison of the stellar mass functions for both the cluster and field environments. At present, the measurement of stellar mass functions of field galaxies are the key science driver of numerous surveys. Still, what is clear from our analysis is that if we want to be able to measure a difference between the cluster and field LFs or stellar mass functions, we will need significantly more data than presented in this thesis. Assuming that the error in the measurement of M* scales roughly as the Poisson error in the galaxies counts, it suggests a measurement of M* with an uncertainty of $\pm$ 0.05 mag (which would correspond to a factor of 1.05 in mass) would require a sample of clusters with spectroscopic redshifts about a factor of 9 larger than the CNOC1 sample.

A sample of 135 clusters with spectroscopy is still an unfeasible study with current instruments, and therefore other methods such as statistical background subtraction using enormous samples of clusters will need to be employed if we want to look at this issue in more detail. Future projects such as the RCS2 (Yee et al. 2007) and the South Pole Telescope (SPT; Ruhl et al. 2004) promise to return samples of $> 10\,000$ clusters over thousands of square degrees. NIR observations of a large fraction of these clusters may now be feasible using the next generation, wide-format IR cameras such as CFHT/WIRCAM, UKIRT/WFCAM, or KPNO/NEWFIRM.

Another issue that was not explored too deeply in chapter five is the connection between the dusty star forming galaxies selected at $[8.0\mu m]$ in chapter four, and the same type of galaxies selected at $[24\mu m]$ in chapter five. Part of the difficulty in connecting these populations is that the $[24\mu m]$ data is not particularly deep. A flux limit of 350μJy corresponds to a LIRG, ULIRG, HyLIRG at only $z = 0.3, 0.5,$ and 1.2, respectively. In general, the results from the bright galaxies selected using both bandpasses are consistent. The main results being that there are very few ULIRGs and HyLIRGs in clusters, and that this low abundance is consistent with the fraction of these galaxies in the field.

At lower luminosities than ULIRGs it appears that there is an increasing number of cluster $[8.0\mu m]$ sources compared to field sources (see chapter four, Figure 22). It is unfortunate that this increase lies slightly below the flux limit of the $[24\mu m]$ data, because seeing the same evolution from independent bandpasses would be strong evidence for the differential evolution between MIR galaxies in the cluster and field environment.

Of course, when we began this project there was only MIR data on a few clusters at $z < 0.4$, and no data for clusters at $z > 0.4$. The FLS was the first science data obtained with *Spitzer*, so this gave us the opportunity to take a first look at the MIR evolution in cluster galaxies. We were aware that the data was fairly shallow; however, it is cannot be known *apriori* what will be found in new data until the analysis is complete. It is clear from the analysis in this thesis that there is fairly modest number of the brightest MIR galaxies such as ULIRGs and HyLIRGs in clusters out to $z \sim 1.0$, and that the abundance and evolution of these bright galaxies is very similar in both clusters and the field. Our data are just deep enough to hint at a fairly significant population of lower-luminosity star forming sources such as LIRGs. The data is also very suggestive of a strong evolution in these galaxies, as well as a differential evolution between the field and cluster environments. The obvious next step is to obtain deeper MIR data on clusters over the same redshift range, this time reaching the LIRG and sub-LIRG regime. A handful of clusters have been observed with *Spitzer* to such a depth; however, no large study similar to this one exists at deeper flux limits. Given that *Spitzer* is winding down its mission, such work may have to wait until the upcoming launch of the *Herschel* satellite.

6.2   Future Work

As with any thesis there are obvious lines of followup work that can be done. Often students write several paragraphs which could be quickly summarized as "more data, same problem". For this work, using a larger number clusters to measure the mid-IR LFs, as well as the overdensity and classification of [$24\mu m$] sources is an logical place where more data would be useful. As was mentioned in both chapters four and five, there is the SWIRE survey, which is a factor of 13 larger in area than the FLS and this is an obvious place to continue with this work. A study similar to that presented in chapter five on the SWIRE data has already been initiated by a Toronto masters' student (N. Battaglia), and appears to be providing consistent results, albeit with a significant improvement in the uncertainties.

Another obvious place for future work is to look for even more distant clusters using *Spitzer* and the red-sequence method. A large part of my graduate studies were actually devoted to such a project, even though it has only been briefly noted here. That project was the next logical step after the work on the FLS cluster search using

the red-sequence method (chapter four).

At the inception of the FLS project our expectation was that we would be able to discover clusters at much higher redshift using the R - [3.6μm] color as compared to the R - z$'$ color used by the RCS. We believed this would be the case because the R - z$'$ filter combination no longer spans the 4000Å break at $z > 1.1$. Once the filters used to measure colors are blueward of 4000Å (observed frame) the colors of cluster early-types no longer make a red-sequence in the CMR, and the red-sequence technique for selecting clusters breaks down. Given that R - [3.6μm] spans the 4000Å break up to z = 5, this effect should not be a problem for our data, and therefore we might have expected to fare better at higher redshift than the RCS.

Surprisingly, the FLS cluster finding showed that even though the [3.6μm] data was very deep, and the R - [3.6μm] filter combination spanned the 4000Å break, the R - [3.6μm] cluster search was no more efficient at discovering clusters at $z > 1.1$ than the RCS R - z$'$ filter combination. Most likely, this is because at high-redshift the R-band probes the rest-frame UV which is extremely faint in early-type galaxies, and is also susceptible to variations from even small amounts of star-formation. Models constructed with the Bruzual & Charlot (2003) code showed that the optimal filter combination for detecting clusters at $z > 1.1$ would be z$'$ - [3.6μm] (because, as mentioned, z$'$-band moves blueward of 4000Å at $z > 1.1$).

Subsequently, we initiated the Spitzer Adaptation of the Red-sequence Cluster Survey (SpARCS). SpARCS is a deep, z$'$-band imaging survey of the SWIRE Legacy fields. With an area of 50 deg^2, SpARCS is the widest-area of the ongoing optical-NIR searches (e.g., UKIDSS, IRACSS) and probes sufficient volume to return the first significant sample of massive clusters at z > 1.5. As of October 2007, all 50 deg^2 of z$'$ and [3.6μm] imaging data will be in hand. At this time, we have processed the first 23 deg^2 of survey data which has returned hundreds of z > 1 cluster candidates. Of these, approximately 70 are rich clusters with estimated masses greater than 10^{14} M$_\odot$.

There are two main science drivers for the SpARCS survey. Firstly, to discover a large sample of galaxy clusters at $1 < z < 1.5$. At these redshifts red-sequence photometric redshifts still work very well. Given the area of SpARCS, we expect to find $\sim$ 200-300 of these objects (although these predictions are a very strong function of the adopted value of σ_8). Currently there are only a handful of clusters known at this redshift so a large sample with which to perform statistical studies could be revolutionary in our understanding of cluster galaxy evolution. The second science goal of SpARCS is to find the most distant clusters possible in order to try and connect the evolution

of galaxies in proto-clusters, which have already been discovered at $2.2 < z < 6$ using the "radio galaxy signpost" method or blind Lyman-break galaxies surveys, to the lower redshift ($z < 1.4$) massive clusters. Proto-clusters are usually comfirmed using either narrow-band filters, or Lyman-break galaxies, which means they are rich in star forming galaxies. This contrasts with the lower redshift clusters which are dominated by quiescent galaxies. At present, the lowest-redshift confirmed proto-cluster is at $z = 2.16$ (Kurk et al. 2004) and the highest redshift confirmed galaxy cluster is at $z = 1.5$ (McCarthy et al. 2007). Discovering a sample of clusters that connects these objects in redshift space will be critical for understanding how the star forming proto-clusters evolve into their quiescent counterparts.

My postdoctoral position will be at Yale University with Pieter van Dokkum. Pieter is the PI of the Spitzer IRAC-MUSYC Public Legacy in ECDFS Survey (SIMPLE). This project is a very deep IRAC imaging campaign in the Extended Chandra Deep Field South. That data will be excellent for doing studies of the evolution of stellar mass assembly and dusty star formation in field galaxies. This ties obviously to the work done on clusters in chapter four. One thing that has frequently been lacking when comparing the evolution of galaxies in clusters to the evolution of galaxies in the field are homogeneous data sets. Astronomers who study clusters tend to neglect properly defining field comparison samples, and vice-versa for those who study field galaxies. Therefore, comparisons between the field and cluster environments (like was done in this thesis) often involves using different data sets, which can be difficult. Furthermore, it is sometimes unclear whether differences or similarities in the properties being compared are real, or are due to different methods of data analysis. Tying the evolution of field galaxies to the evolution of cluster galaxies to test if environment has a significant role in the evolution of dusty star formation using a consistent method for both the field and cluster sample would be an obvious project for me to work on during my time at Yale.

References

[1] Abell, G. O. 1958, ApJS, 3, 211

[2] Abraham, R. G., et al. 2004, AJ, 127, 2455

[3] Abraham, R. G., Yee, H. K. C., Ellingson, E., Carlberg, R.G., Gravel, P. 1998, ApJS, 116, 231

[4] Abraham, R. G., et al. 1996, AJ, 471, 694

[5] Adelman-McCarthy et al. 2007, AJ, in-prep

[6] Allen, S. W. 1998, MNRAS, 296, 392

[7] Andreon, S. 2006, A&A, 448, 447

[8] Andreon, S., Lobo, C., Iovino, A. 2004, MNRAS, 349, 889

[9] Appleton, P. N. et al. 2004, ApJSS, 154, 147

[10] Aragón-Salamanca, A., Ellis, R. S., Couch, W. J., & Carter, D. 1993, MNRAS, 262, 764

[11] Aragón-Salamanca, A., Ellis, R. S., & Sharples, R. M. 1991, MNRAS, 248, 128

[12] Babbedge, T. S. R., et al. 2006, MNRAS, 370, 1159

[13] Bahcall, N. A., et al. 2003, ApJSS, 148, 243

[14] Bahcall, N. A., & Comerford, J. M. 2002, ApJ, 565, L5

[15] Balogh, M. L., Christlein, D., Zabludoff, A. I., Zaritsky, D. 2001, ApJ, 557, 117

[16] Bai, L., et al. 2007, ApJ, 664, 181

[17] Baldwin, J. A., Phillips, M. M., & Terlevich, R. 1981, PASP, 93, 19

[18] Balogh, M., Morris, S. L., Yee, H. K. C., Carlberg, R. G., Ellingson, E. 1999, ApJ, 527, 54

[19] Barger, A., et al. 1998, ApJ, 501, 522

[20] Barkhouse, W. A. et al. 2006, ApJ, 645, 955

[21] Beers, T. C., Flynn, K., & Gebhardt, K. 1990, AJ, 100, 32

[22] Bekki, K., & Couch, W. J. 2003, ApJ, 596, L13

[23] Bell, E. F., et al. 2005, ApJ, 625, 23

[24] Bell, E., McIntosh, D. H., Katz, N., & Weinberg, M. D. 2003, ApJS, 149, 289

[25] Bell, E., & de Jong, R. S., ApJ, 550, 212

[26] Berlind, A. A., Blanton, M. R., Hogg, D. W., Weinberg, D. H., Davé, R., Eisenstein, D., Katz, N. 2005, ApJ, 629, 625

[27] Berlind, A. A., et al. 2003, ApJ, 593, 1

[28] Berlind, A. A., & Weinberg, D., 2002, ApJ, 575, 587

[29] Bertin, E., & Arnouts, S. 1996, A&AS, 117, 393

[30] Bicay, M. D., & Giovanelli, R. 1987, ApJ, 321, 645

[31] Biviano, A., et al. 2004, A&A, 425, 33

[32] Blain, A., Smail, I., Ivison, R. J., Kneib, J.-P., & Frayer, D. T. 2002, Phys. Rep., 2002, 111

[33] Blake, C. et al. 2004, MNRAS, 355, 713

[36] Blakeslee, J. P., et al. 2003, ApJ, 596, L143

[36] Blanton, M. R., Eisenstien, D., Hogg, D. W., Schlegel, D. J., & Brinkmann, J. 2005, ApJ, 629, 143

[36] Blanton, M. R., et al. 2003, ApJ, 592, 819

[37] Blindert, K., Yee, H. K. C., Gladders, M. D., & Ellingson, E. 2004, in IAU Coll. No. 195, Outskirts of Galaxy Clusters: Intense Life in the Suburbs, ed. A. Diaferio, 215

[38] Borgani, S., Girardi, M., Carlberg, R. G., Yee, H. K. C., Ellingson, E. 1999, ApJ, 527, 561

[39] Boselli, A., et al. 1998, A&A, 335, 53

[40] Boselli, A., Tufts, R. J., Gavazzi, G., Hippelein, H., & Pierini, D. 1997a, A&AS, 121, 507

[41] Boselli, A., et al. 1997b, A&A, 324, L13

[42] Bower, R. G., Lucey, J. R., Ellis, R. S. 1992, MNRAS, 254, 601

[43] Brainerd, T. G., Specian, M. A., 2003, ApJ, 593, L7

[44] Branchesi, M., Gioia, I. M., Fanti, C., & Cappelluti, N. 2007, A&A, 462, 449

[45] Brinchmann, J. 1999, Ph.D. thesis, Cambridge Univ

[46] Brinchmann, J., & Ellis, R. S. 2000, ApJ, 536, 77

[47] Brodwin, M., et al. 2006, ApJ, 651, 791

[48] Bruzual, G., & Charlot, S. 2003, MNRAS, 344, 1000

[49] Bundy, K., et al. 2006, ApJ, 651, 120

[50] Butcher, H., Oemler, A. J. 1984, ApJ, 285, 426

[51] Calzetti, D. et al. 2005, ApJ, 633, 871

[52] Carlberg, R. G., Yee, H. K. C., Ellingson, E., Abraham R., Gravel, P., Morris, S. M., & Pritchet, C.J. 1996, ApJ, 462, 32

[53] Carlberg, R. G., Yee, H. K. C., & Ellingson, E. 1997a, ApJ, 478, 462

[54] Carlberg, R. G.,et al. 1997b, ApJ, 485, L13

[55] Chang, T.-C., van Gorkom, J. H., Zablufoff, A. I., Zaritsky, D., & Mihos, J. C. 2001, AJ, 121, 1965

[56] Chapman, S. C., Blain, A. W., Ivison, R. J., & Smail, I. 2003, Nature, 422, 695

[57] Charlot, S., & Longhetti, M. 2001, MNRAS, 323, 887

[58] Choi, P., et al. 2006, ApJ, 637, 227

[59] Christlein, D. & Zabludoff, A. I. 2005, ApJ, 621, 201

[60] Cimatti, A., et al. 2002, A&A, 392, 395

[62] Coia, D., et al. 2005a, A&A, 431, 433

[62] Coia, D., et al. 2005b, A&A, 430, 59

[63] Cole, S., et al. 2001, MNRAS, 326, 255

[64] Cole, S., Lacey, C. G., Baugh, C. M., Frenk, C. S. 2000, MNRAS, 319, 168

[65] Colín, P., Klypin, A. A., Kravtsov, A. V., Khokhlov, A. M. 1999, ApJ, 523, 32

[66] Colless, M. et al. 2001, MNRAS, 328, 1039

[67] Conroy, C., et al. 2005, ApJ, 635, 982

[68] Contursi, A., Boselli, A., Gavazzi, G., Bertagna, E., Tuffs, R., & Lequeux, J. 2001,
      A&A, 365, 11

[69] Cooper, M. C., et al. 2007, MNRAS, 376, 1445

[70] Cooray, A., & Sheth, R. 2002, Phys. Rep. 372, 1

[71] Cortese, L., et al. 2007, MNRAS, 376, 157

[72] Cowie, L. L., Songaila, A., Hu, E. M., Cohen, J. G. 1996, AJ, 112, 839

[73] Croft, R. A. C., et al. 2002, ApJ, 581, 20

[74] Dahlen, T., et al. 2005, ApJ, 631, 126

[75] Dale, D. A., et al. 2005, ApJ, 633, 857

[76] Dale, D. A., Helou, G., Contursi, A., Silbermann, N. A., & Kolhatkar, S. 2001, ApJ,
      549, 215

[77] Davis, M., et al. 2007, ApJ, 660, L1

[107] Davis, M., et al. 2003, Proc. of the SPIE, 4834, 161, edited by Guhathakurta, Pu-
       rangra.

[79] De Lucia, G., et al. 2004, ApJ, 610, L77

[80] De Propris, R., Stanford, S. A., Eisenhardt, P. R., Holden, B. P., & Rosati, P. 2007, AJ, 133, 2209

[81] De Propris, R., et al. 2003, MNRAS, 342, 745

[82] De Propris, R., Stanford, S. A., Eisenhardt, P. R., Dickinson, M., Elston, R. 1999, AJ, 118, 719

[83] Devriendt, J. E. G., Guiderdoni, B., & Sadat, R. 1999, A&A, 350, 381

[84] Diaferio, A. Kauffman, G., Balogh, M. L., White, S. D. M., Schade, D., Ellinson, E. 2001, MNRAS, 323, 999

[85] Dressler, A., Oemler, A., Poggianti, B., Smail, I., Trager, S., Schectman, S., Couch, W., & Ellis R. S. 2004, ApJ, 617, 867

[86] Dressler, A., Smail, I., Poggianti, B. M., Butcher, H., Couch, W. J., Ellis, R. S., & Oemler, A. 1999, ApJSS, 122, 51

[87] Dressler, A., et al. 1997, Apj, 490, 577

[88] Dressler, A., & Gunn, J. E. 1992, ApJSS, 78, 1

[89] Dressler, A., Thompson, I. B., & Shechtman, S. A. 1985, ApJ, 288, 481

[90] Dressler, A. 1980, ApJ, 236, 351

[91] Drory, N., Bender, R., Feulner, G., Hopp, U., Maraston, C., Snigula, J., Hill, G. J. 2003, ApJ, 595, 698

[92] Drory, N., et al. 2001, MNRAS, 325, 550

[94] Duc, P.-A., et al. 2004, astro-ph#0404183

[94] Duc, P.-A., et al. 2002, A&A, 382, 60

[95] Eastman, J., Martini, P., Sivakoff, G., Kelson, D. D., Mulchaey, J. S., & Tran, K.-V. 2007, ApJ, in-press

[96] Eisenhardt, P. et al. 2004, ApJSS, 154, 48

[97] Eisenstein, D., Blanton, M., Zehavi, I., Bachall, N., Brinkmann, J., Loveday, J., Meiksin, A., Schneider, D. 2005, ApJ, 619, 178

[98] Elbaz, D., Cesarsky, C.J., Chanial, P., Aussel, H., Franceschini, A., Fadda, D., & Chary, R. R. 2002 A&A, 384, 848

[99] Ellingson, E., Lin, H., Yee, H. K. C., & Carlberg, R. G. 2001, ApJ, 547, 609

[100] Ellingson, E., Yee, H. K. C., Abraham, R. G., Morris, S. L., Carlberg, R. G. 1998, ApJS, 116, 247

[102] Ellingson, E., Yee, H. K. C., Abraham, R. G., Morris, S. L., Carlberg, R. G., Smecker-Hane, T. A. 1997, ApJS, 113, 1

[102] Ellis, R. S., Smail, I., Dressler, A., Couch, W. J., Oemler, A., Butcher, H., & Sharples, R. M. 1997, ApJ, 483, 582

[103] Ellis, S., Jones, L. 2004, Proc. IAU Coll #195, astro-ph # 0405043

[104] Ellis, S. C., & Jones, L. R. 2002, MNRAS, 330, 631

[105] Elston, R. J. et al. 2006, ApJ, 639, 816

[106] Faber, S. M., et al. 2005, astro-ph #0506044

[107] Faber, S., et al. 2003, Proc. of the SPIE, 4841, 1657, edited by Iye, Masanori, & Moorwood, Alan F. M.

[108] Fadda, D., et al. 2006, AJ, 131, 2859

[109] Fadda, D., Jannuzi, B. T., Ford, A., & Storrie-Lombardi, L. J. 2004, AJ, 128, 1

[110] Fadda, D., Elbaz, D., Duc, P.-A., Flores, H., Franceschini, A., Cesarsky, C. J., & Moorwood, A. F. M. 2000, A&A, 361, 827

[111] Fahlman, G., Kaiser, N., Squires, G., Woods, D. 1994, ApJ, 437, 56

[112] Feulner, G., Bender, R., Drory, N., Hopp, U., Snigula, J., Hill, G. J. 2003, MNRAS, 342, 605

[113] Franceschini, A., Aussel, H., Cesarsky, C.J., Elbaz, D., & Fadda, D. 2001, A&A, 378, 1

[114] Fukugita, M., Shimasaku, K., Ichikawa, T. 1995, PASP, 107, 945

[115] Gardner, J. P., Cowie, L. L., Wainscoat, R. J. 1993, ApJL, 415, L9

[116] Gallazzi, A., Charlot, S., Brinchmann, J., & White, S. D. M. 2006, MNRAS, 370, 1106

[117] Gavazzi, G., Pierini, D., Boselli, A., Tuffs, R. 1996, A&AS, 120, 489

[118] Geach, J. E., et al. 2006, ApJ, 649, 661

[120] Giavalisco, M. et al. 2004a, ApJ, 600, L93

[120] Giavalisco, M. et al. 2004b, ApJ, 600, L103

[121] Gilbank, D. G., Yee, H. K. C., Ellingson, E., Gladders, M. D., Barrientos, L. F., & Blindert, K. 2007, AJ, 134, 282

[122] Gilbank, D. G., Bower, R. G., Castander, F. J., & Ziegler, B. L. 2004, MNRAS, 348, 551

[123] Gilbank, D. G., Smail, I., Ivison, R. J., Packham, C., 2003, MNRAS, 346, 1125

[124] Gillett, F. C., Forrest, W. J., & Merrill, K. M. 1973, 183, 87

[125] Girardi, M., Manzato, P., Mezzetti, M., Giuricin, G., Limboz, F. 2002, ApJ, 569, 720

[126] Gladders, M. D., Yee, H. K. C., Majumdar, S., Barrientos, L. F., Hoekstra, H., Hall, P. B., Infante, L. 2006, astro-ph # 0603588

[127] Gladders, M. D., & Yee, H. K. C., 2000, AJ, 120, 2148 (GY00)

[128] Gladders, M. D., & Yee, H. K. C. 2005, ApJSS 157, 1

[129] Gladders, M. D., Lopez-Cruz, O., Yee, H. K. C., & Kodama, A. 1998, ApJ, 501, 571

[130] Glazebrook, K., et al. Nat, 430, 181

[131] Gioia, I. M., Maccaraco, T., Schild, R. E., Wolter, A., Stocke, J. T., Morris, S. L., Henry, J. P. 1990, ApJSS, 72, 567

[132] Gomez, P., et al. 2003, ApJ, 584, 210

[133] González-Marín, O., Masegosa, J., Márquez, I., Guerrero, M. A., & Dultzin-Hacyan, D. 2006, A&A, 460, 45

[134] Goto, T. 2004, A&A, 427, 125

[135] Goto, T., Yamauchi, C., Fujita, Y., Okamura, S., Sekiguchi, M., Smail, I., Bernardi, M., Gomez, P. L. 2003a, MNRAS, 346, 601

[136] Goto, T., et al. 2003b, PASJ, 55, 757

[137] Haiman, Z., Mohr, J. J., & Holder, G. P. 2003, ApJ, 553, 545

[138] Halkola, A., Seitz, S., Pannella, M. 2006, astro-ph # 0611078

[139] Hall, P. B., Green, R. F., Cohen, M. 1998, ApJS, 119, 1

[140] Hansen, S. M., McKay, T. A., Wechsler, R. H., Annis, J., Sheldon, E. S., Kimball, A. 2005, ApJ, 633, 122

[141] Henry, J. P. 2000, ApJ, 534, 565

[142] Hicks, A., Ellingson, E., Hoekstra, H., Yee, H. K. C. 2006, ApJ, in-press

[143] Hoekstra, H., Hsieh, B. C., Yee, H. K. C., Lin, H., Gladders, M. D. 2005, ApJ, 635, 73

[144] Hoekstra, H., van Waerbeke, L., Gladders, M. D., Mellier, Y., Yee, H. K. C. 2002, ApJ, 577, 604

[145] Hoekstra, H., Franx, M., Kuijken, K., Squires, G. 1998, 504, 636

[146] Hogg, D., et al. 2004, ApJ, 601, L29

[147] Hogg, D., et al. 2003, ApJ, 585, L5

[148] Hogg, D., et al. 2002, AJ, 124, 646

[149] Holden, B. P., et al. 2005, ApJ, 620, L83

[150] Holden, B. P., Stanford, S. A., Eisenhardt, P., Dickinson, M. 2004, AJ, 127, 2484

[151] Homeier, N. L., et al. 2006, ApJ, 647, 256

[152] Huang, J.-S. et al. 2007, ApJ, in-press

[153] Hubble, E. 1925, ApJ, 62, 409

[154] Huynh, M. T., Frayer, D. T., Mobasher, B., Dickinson, M., Chary, R.-R., & Morrison, G. 2007, arXiv:0707.4505v1

[155] Ilbert, O., et al. 2005, A&A, 439, 863

[156] Jansen, R. A., Franx, M., & Fabricant, D. 2001, ApJ, 551, 825

[157] Jee, M. J., White, R. L., Ford, H. C., Blakeslee, J. P., Illngworth, G. D., Coe, D. A., & Tran K.-V. H. 2005a, arXiv:astro-ph#0508044

[158] Jee, M. J., White, R. L., Benítez, N., Ford, H. C., Blakeslee, J. P., Rosati, P., Demarco, R., Illingworth, G. D. 2005b, ApJ, 618, 46

[159] Juneau, S., et al. 2005, ApJ, 619, L135

[160] Kauffmann, G., et al. 2003, MNRAS, 346, 1055

[161] Kennicutt, R. C. 1998, ApJ, 498, 541

[162] Kennicutt, R. C., 1992, ApJ, 388, 310

[163] Kewley, L. J., Groves, B., Kauffmann, G., Heckman, T. 2006, MNRAS, 372, 961

[164] Kewley, L. J., Dopita, M. A., Sutherland, R. S., Heisler, C. A., & Trevena, J. 2001, AJ, 556, 121

[165] Kim, T.-S., Carswell, R. F., Cristiani, S., D'Odorico, S., Giallongo, E. 2002, MNRAS, 335, 555

[166] Kneib, J.-P. et al. 2003, ApJ, 598, 804

[167] Kochanek, C. S., White, M., Huchra, J., Macri, L., Jarrett, T. H., Schneider, S. E., Mader, J. 2003, ApJ, 585, 161

[168] Kochanek, C. S., et al. 2001, ApJ, 560, 566

[170] Kodama, T., Balogh, M. L., Smail, I., Bower, R. G., & Nakata, F. 2004, MNRAS, 354, 1103

[170] Kodama, T., et al. 2004, MNRAS, 350, 1005

[171] Kodama, T., & Bower, R. 2003, MNRAS, 346, 1

[172] Kodama, T., Arimoto, N., Barger, A. J., Aragon-Salamanaca, A. A. 1998, A&A, 334, 99

[173] Koekemoer, A. M., & Scoville, N. Z. 2005, New Astron. Rev., 49, 461

[174] Koester, B. P., et al. 2007, ApJ, 660, 239

[175] Kosowsky, A. 2006, New Astron. Rev., 50, 969

[176] Kravtsov, A. V., Berlind, A. A., Wechsler, R. H., Klypin, A. A., Gottlöber, S., Allgood, B., Primack, J. R. 2004, 609, 35

[177] Kurk, J. D., et al. 2004, A&A, 428, 817

[178] Lacy, M. et al. 2005, ApJSS, 161, 41

[179] Lacy, M. et et al. 2003, ApJSS, 154, 166

[180] Le Floc'h, E., et al. 2005, ApJ, 632, 169

[181] Lewis, I., et al. 2002, MNRAS, 334, 673

[182] Lewis, A. D., Ellingson, E., Morris, S. L., Carlberg, R. G. 1999, ApJ, 517, 587

[183] Lilly, S. J. 1987, MNRAS, 229, 573

[184] Lilly, S. J., Le Févre, O., Hammer, F., & Crampton, D. 1996, ApJ, 460, L1

[185] Lin, Y.-T., Mohr, J. J., Gonzalez, A. H., & Stanford, S. A. 2006, ApJ, 650, L99

[186] Lin, Y.-T., Mohr, J. J., & Stanford, S. A. 2004, ApJ, 610, 745 (L04)

[187] Lin, Y.-T., Mohr, J. J., & Stanford, S. A. 2003, ApJ, 591, 749

[188] Lokas, E. L., & Mamon, G. A. 2001, MNRAS, 321, 155

[189] Longair, M. S., & Seldner, M. 1979, MNRAS, 189, 433

[190] Lonsdale, C. J., et al. 2003, PASP, 115, 897

[191] Lopez-Cruz, O., Barkhouse, W. A., & Yee, H. K. C. 2004, ApJ, 614, 679

[192] Luppino, G. A., & Gioia, I. M. 1995, 445, 77

[193] Lutz, D., Sturm, E., Genzel, R., Moorwood, A. F. M., & Sternberg, A. 1997, A&SS, 248, 217

[194] Madau, P., Ferguson, H. C., Dickinson, M. E., Giavalisco, M., Steidel, C. C., & Fruchter, A. 1996, MNRAS, 283, 1388

[195] Maihara, T., et al. 2001, PASJ, 53, 25

[196] Makovoz, D., & Marleau, F. R. 2005, PASP, 117, 1113

[197] Mandelbaum, R., Seljak, U., Kauffmann, G., Hirata, C. M., Brinkmann, J. 2006, MNRAS, 368, 715

[198] Mannucci, F., Basile, F., Poggianti, B. M., Cimatti, A., Daddi, E., Pozzetti, L., Vanzi, L. 2001, MNRAS, 326, 745

[203] Marchesini D., & van Dokkum, P. G. 2007, ApJ, 663, L89

[200] Marcillac, D., Rigby, J. R., Rieke, G. H., & Kelly, D. M. 2007, ApJ, 654, 825

[201] Margoniner, V. E., De Carvalho, R. R., Gal, R. R., & Djorgovski, S. G., 2001, ApJ, 548, L143

[203] Marleau, F. R., Fadda, D., Appleton, P. N., Noriega-Crespo, A., Im, M., & Clancy, D. 2007, ApJ, in-press

[203] Martini, P., Mulchaey, J. S., & Kelson, D. D. 2007, ApJ, in-press

[204] Massey, P., & Gronwall, C. 1990, ApJ, 358, 344

[205] McCarth, P. J., et al. 2007, ApJ, 664, L17

[206] McCarthy, D., Ge, J., Hinz, J. L., Finn, R. A., de Jong, R. S. 2001, PASP, 113, 353

[207] McDonald, P., et al. 2006, ApJS, 163, 80

[208] Mei, S., et al. 2006, ApJ, 644, 759

[209] Metcalfe, L., Fadda, D., & Biviano, A. 2005, Space Science Reviews, 119, 425

[210] Metcalfe, L., et al. 2003, A&A, 407, 791

[211] Metevier, A. J., Romer, A. K., & Ulmer, M. P. 2000, AJ, 119, 1090

[212] Miller, C. J., et al. 2005, AJ, 130, 968

[213] Miller, N. A., & Owen, F. N. 2001, ApJ, 554, L25

[214] Moran, S. M., Ellis, R. S., Treu, T., Salim, S., Rich, R. M., Smith, G. P., Kneib, J.-P. 2006, ApJ, 641, L97

[215] Moran, S. M., Ellis, R. S., Treu, T., Smail, I., Dressler, A., Coil, A. L., & Smith, G. P. 2005, ApJ, 634, 977

[216] Moss, C. & Whittle, M. 2000, MNRAS, 317, 667

[217] Mushotzky, R. F., & Scharf, C. A. 1997, ApJL, 482, L13

[218] Muzzin, A., Yee, H. K. C., Hall, P. B., Ellingson, E., & Lin, H. 2007a, ApJ, 659, 1106

[220] Muzzin, A., Yee, H. K. C., Hall, P. B., & Lin, H. 2007b, ApJ, 663, 150

[220] Muzzin, A., Wilson, G., Lacy, M., Yee, H. K. C., & Stanford, S. A. 2007c, ApJ, submitted

[221] Mohr, J. J. 2004, astro-ph # 0408484

[226] Nagai, D., & Kravtsov, A. 2005, ApJ, 618, 557

[223] Nakamura, O., et al. 2003, AJ, 125, 1682

[224] Natarajan, P., Kneib, J.-P., Smail, I. 2002, ApJ, 580, L11

[225] Navarro, J. F., Frenk, C. S., White, S. D. M. 1997, ApJ, 490, 493

[226] Nagai, D., & Kravtsov, A. 2005, ApJ, 618, 557

[227] Nelan, J. E., Smith, R. J., Hudson, M. J., Wegner, G. A., Lucey, J. R., Moore, S. A. W., Quinney, S. J., Suntzeff, N. B. 2005, ApJ, 632, 137

[228] Norberg, P., et al. 2002, MNRAS, 332, 827

[229] Norberg, P., et al. 2001, MNRAS, 328, 64

[230] Oort, J. H., 1958, in La Structure et L'Évolution de L'Univers, Onzieme Conseil de Physique, ed. R. Stoops (Brussels: Solvay Institute), 163

[231] Owen, F. N., Ledlow, M. J., Keel, W. C., Wang, Q. D., & Morrison, G. E. 2005, AJ, 129, 31

[232] Owen, F. N., Ledlow, M. J., Keel, W. C., & Morrison, G. E. 1999, AJ, 118, 633

[233] Papovich, C., et al. 2007, arXiv:0706.2164

[234] Papovich, C., et al. 2006a, AJ, 132, 231

[235] Papovich, C., et al. 2006b, ApJ, 640, 92

[236] Papovich, C., & Bell, E. F. 2002, ApJ, 579, L1

[237] Pearce, F. R., et al. 2001, MNRAS, 326, 649

[238] Pérez-González, P. G., et al. 2005, ApJ, 630, 82

[239] Persson, S. E., Murphy, D. C., Krzeminski, W., Roth, M., Rieke, M. J. 1998, AJ, 116, 2475

[240] Pierre, M., Le Borgne, J. F., Soucail, G., Kneib, J. P. 1996, A&A, 311, 413

[241] Poggianti, B. et al. 2006, ApJ, 642, 188

[242] Poggianti, B., & Wu, H. 2000, ApJ, 529, 157

[243] Poggianti, B. M., Smail, I., Dressler, A., Couch, W. J., Barger, A. J., Butcher, H., Ellis, R. S., Oemler, A. 1999, ApJ, 518, 576

[244] Poggianti, B. M. 1997, A & AS, 122, 399

[245] Popescu, C. C., & Tuffs, R. J. 2002a, MNRAS, 335, 41

[246] Popescu, C. C., Tuffs, R. J., Volk, H. J., Pierini, D., & Madore, B. F. 2002, ApJ, 567, 221

[247] Popesso, P., Biviano, A., Romaniello, M., & Böhringer, H. 2007, A&A, 461, 411

[248] Postman, M., et al. 2005, ApJ, 623, 721

[249] Pozzetti, L., et al. 2003, A&A, 402, 837

[250] Press, W. H., Tuekolsky, S. A., Vetterling, W. T., Flannery, B. P. 1992, Numerical Recipes in Fortran 77, Vol 1; Second Edition; Cambridge, Cambridge University Press

[251] Rakos, K. D., & Schombert, J. M. 1995, ApJ, 439, 47

[252] Ramella, M., Boschin, W., Geller, M. J., Mahdavi, A., Rines, K. 2004, AJ, 128, 2022

[253] Rines, K., Geller, M. J., Kurtz, M. J., & Diaferio, A. 2005, AJ, 130, 1482

[254] Rines, K., Geller, M. J., Diaferio, A., Kurtz, M. J., Jarrett, T. H. 2004, AJ, 128, 1078 (R04)

[255] Rix, H.-W., Rieke, M. J. 1993, ApJ, 418, 123

[256] Ruhl, J. et al. 2004, in Astronomical Structures & Mechanisms Technology. Edited by Antebi, Joseph; Lemke, Dietrich, Proceedings of the SPIE, Volume 5498, pp.11

[257] Sand, D. J., Treu, T., Smith, G. P., & Ellis R. S. 2004, ApJ, 604, 88

[258] Sander, D. B., Soifer, B. T., Elais, J. H., Madore, B. F., Matthews, K., Neugebauer, G., & Scoville, N. 1988, ApJ, 325, 74

[259] Saracco, P., et al. 2001, A&A, 375, 1

[260] Schlegel, D. J., Finkbeiner, D. P., & Davis, M. 1998, ApJ, 500, 525

[261] Schechter, P. 1976, ApJ, 203, 297

[262] Schiminovich, D., et al. 2005, ApJ, 619, L47

[263] Shioya, Y., Bekki, K., & Couch, W. J. 2004, ApJ, 601, 654

[264] Silva, L., Granato, G. L., Bressan, A., & Danese, L. 1998, ApJ, 509, 103

[265] Seljak, U., et al. 2005, Phys. Rev. D., 71, 043511

[266] Shectman, S. A., Landy, S. D., Oemler, A., Tucker, D. L., Lin, H., Kirshner, R. P., Schechter, P. L. 1996, ApJ, 470, 172

[267] Sheldon, E. S., et al. 2004, AJ, 127, 2544

[268] Skrutskie, M. F., et al. 2006, AJ, 131, 1163

[269] Soifer, B. T., Sanders, D. B., Madore, B. F., Neugebauer, G., Danielson, G. E., Elais, J. H., Lonsdale, C. J., & Rice, W. L. 1987, ApJ, 320, 238

[270] Spergel, D. N., et al. 2006, astro-ph # 0603449

[271] Smail, I, Morrison, G., Gray, M. E., Owen, F. N., Ivison, R. J., Kneib, J.-P., & Ellis, R. S. 1999, ApJ, 525, 609

[272] Smail, I., Edge, A., Ellis, R. S., & Blandford, R. D. 1998, MNRAS, 293, 124

[273] Smail, I., Ellis, R. S., Dressler, A., Couch, W. J., Oemler, A., Sharples, R. M., Butcher, H. 1997, ApJ, 479, 70

[274] Smail, I., Ellis, R. S., Fitchett, M. J., Edge, A. C. 1995, MNRAS, 273, 277

[275] Smith, G. P., Treu, T., Ellis, R. S., Moran, S. M., Dressler, A. 2005, ApJ, 620, 78

[276] Stanford, S. A., Eisenhardt, P. R., Dickinson, M., Holden, B. P., de Propris, R. 2002, ApJS, 142, 153

[277] Stanford, S. A., Eisenhardt, P. R., & Dickinson, M. 1998, ApJ, 491, 461

[278] Stanford, S. A., Eisenhardt, P. R., & Dickinson, M., ApJ, 450, 512

[279] Steidel, C. C., Adelberger, K. L., Giavalisco, M., Dickinson, M., & Pettini, M. 1999, ApJ, 519, 1

[280] Stern, D. et al. 2005, ApJ, 631, 163

[281] Strazzullo, V., et al. 2006, A&A, 450, 909

[282] Sturm, E., et al. 2000, A&A, 358, 481

[283] Takeuchi, T. T., Buat, V., & Burgarella, D. 2005, A&A, 440, L17

[284] Tanaka, M., Kodama, T., Arimoto, N., Okamura, S., Umetsu, K., Shimasaki, K., Tanaka, I., Yamada, T. 2005, MNRAS, 362, 268

[285] Tanaka, M., Goto, T., Okamura, S., Shimasaku, K., Brinkmann, J. 2004, AJ, 128, 2677

[286] Tasitsiomi, A., Kravtsov, A. V., Wechsler, R. H., Primack, J. R. 2004, ApJ, 614, 533

[287] Tinker, J. L., Weinberg, D. H., Zheng, Z., Zehavi, I. 2005, ApJ, 631, 41

[288] Toft, S., Mainieri, V., Rosati, P., Lidman, C., Demarco, R., Nonino, M., Stanford, S. A. 2004, A&A, 422, 29

[289] Tokunaga, A. T., Simons, D. A., Vacca, W. D. 2002, PASP, 114, 180

[290] Tran, K.-V. H., Franx, M., Illingworth, G. D., van Dokkum, P., Kelson, D. D., Blakeslee, J. P., & Postman, M. 2007, ApJ, in-press

[291] Tran, K.-V., van Dokkum, P., Illingworth, G. D., Kelson, D., Gonzalez, A., & Franx, M. 2005a, ApJ, 619, 134

[292] Tran, K.-V., van Dokkum, P., Franx, M., Illingworth, G. D., Kelson, D. D., Schreiber, N. M. F. 2005b, ApJ, 627, L25

[293] Treu, T., et al. 2003, ApJ, 591, 53

[294] Tuffs, R.,J., Popescu, C. C., & Pierini, D., et al. 2002, ApJS, 139, 37

[295] Valdes, F. 1982, Proc SPIE, 331, 435

[296] van der Marel, R. P., Magorrian, J., Carlberg, R. G., Yee, H. K. C., Ellingson, E. 2000, AJ, 119, 2038

[297] van Dokkum, P. G., & Stanford, S. A. 2003, ApJ, 585, 78

[298] van Dokkum, P. G., Franx, M., Kelson, D. D., Illingworth, G. D. 2001, ApJ, 553, 39

[299] van Dokkum, P. G., Franx, M., Fabricant, D., Kelson, D. D., Illingworth, G. D. 1999, ApJ, 520, L95

[300] van Dokkum, P. G., Franx, M., Kelson, D. D., Illingworth, G. 1998, ApJ, 504, L17

[301] Wechsler, R. H., Bullock, J. S., Primack, J. R., Kravtsov, A. V., Dekel, A. 2002, ApJ, 568, 52

[302] Weinberg, D. H., Colombi, S., Romeel, D., Katz, N. 2006, astro-ph#0604393

[303] Weinberg, D. H., Davé, R., Katz, N., Hernquist, L. 2004, ApJ, 601, 1

[304] Willner, S. P., Soifer, B. T., Russell, R. W., Joyce, R. R. & Gillett, F. C. 1977, ApJ, 217, L121

[306] Wilson, G., et al. 2007, ApJ, 660, L59

[306] Wilson, G., et al. 2006, astro-ph#0604289

[307] Wilson, G., Cowie, L. L., Barger, A. J., & Burke, D. J. 2002, AJ, 124, 1258

[308] Wolf, C., Meisenheimer, K., Rix, H.-W., Borch, A., Dye, S., Kleinheinrich, M. 2003, A&A, 401, 73

[309] Wu, H., Cao, C., Hao, C.-N., Liu, F.-S., Wang, J.-L., Xia, X.-Y., Deng, Z.-G., & Young, C. K.-S. 2005, ApJ, 632, L79

[310] Wu, X.-P. 2000, MNRAS, 316, 299

[311] Yee, H. K. C., Gladders, M. D., Gilbank, D. G., Majumdar, S., Hoekstra, H., Ellingson, E., 2007, astro-ph#0701839

[312] Yee, H. K. C., & Ellingson, E. 2003, ApJ, 585, 215

[313] Yee, H. K. C., et al. 2000, ApJS, 129, 475

[314] Yee, H. K. C., & Lopez-Cruz, O. 1999, AJ, 117, 1985

[315] Yee, H. K. C., Ellingson, E., Morris, S. L., Abraham, R. G., Carlberg, R. G. 1998, ApJS, 116, 211

[316] Yee, H. K. C., Ellingson, E., & Carlberg, R. G. 1996a, ApJS, 102, 269

[317] Yee, H. K. C., Ellingson, E., Abraham, R. G., Gravel, P., Carlberg, R. G., Smecker-Hane, T. A., Schade, D., Rigler, M. 1996b, ApJS, 102, 289

[318] Yee, H. K. C. 1991, PASP, 103, 662

[319] Yoshikawa, K., Taruya, A., Jing, Y. P., Suto, Y. 2001, ApJ, 558, 520

[320] Zehavi, I., et al. 2005a, ApJ, 630, 1

[321] Zehavi, I., et al. 2005b, ApJ, 621, 22

[322] Zhu, G., Zheng, Z., Lin, W. P., Jing, Y. P., Kang, X., Gao, L. 2006, ApJ, 639, L5

[323] Zwicky, F., Herzog, E., & Wild, P. 1961, Catalogue of Galaxies and Clusters of Galaxies (Pasadena: California Institute of Technology (CIT))